



*Proceedings of International Symposium*



# THUNDERSTORMS & ELEMENTARY PARTICLE ACCELERATION

Nor-Amberd,  
Armenia  
September 9-13



*Edited by A. Chilingarian*  
**COSMIC RAY DIVISION**  
*A. Alikhanyan National Laboratory*  
*Yerevan Physics Institute*





*Proceedings of International Symposium*

# **TEPA 2013**

## **Thunderstorms and Elementary Particle Acceleration**



**Nor-Amberd, Armenia  
September 9 - 13**

**Edited by A. Chilingarian**

**Cosmic Ray Division,  
A. Alikhanyan National Laboratory**



*70 years of YerPhI: 1944-2014*



*SCACRD*



*SCS*

Published by CRD  
Cosmic Ray Division, Alikhanyan National Laboratory,  
Alikhanyan Brothers Street 2, Yerevan, Armenia

©All rights reserved by **CRD**  
<http://crd.yerphi.am>

Printed by **TIGRAN METS**  
2, Arshakouniats Avenue, Yerevan, Armenia  
Tel. (37410) 521 775

**ISBN ?? – ? – ??– ?** March 2014

Copies 150  
Pages 150

## INTERNATIONAL SCIENTIFIC ADVISORY COMMITTEE

- Ashot Chilingarian,  
Yerevan Physics Institute, Armenia, co-chair
- Lev Dorman,  
Israel Cosmic Ray Center and Emilio Segre' Observatory, Israel
- Joe Dwyer,  
Florida Institute of Technology, USA
- Gerald Fishman,  
NASA-Marshall Space Flight Center, Huntsville, USA)
- Hartmut Gemmeke,  
Karlsruhe Institute of Technology, Germany
- Andreas Haungs,  
Karlsruhe Institute of Technology, Germany
- Johannes Knapp,  
Leeds University, UK
- Karel Kudela,  
Institute of Experimental Physics, Slovakia
- Alexandr Lidvanski,  
Nuclear Physics Institute, Russian Academy of Science, Russian Federation
- Jean Lilensten,  
Laboratory of Planetology, Grenoble, France
- Evgeny Mareev,  
Institute of Applied Physics, Nizhny Novgorod, Russian Federation
- Razmik Mirzoyan,  
MPI, Munich, Germany
- Yasushi Muraki,  
STE laboratory, Nagoya University, Japan
- Michail Panasyuk,  
Moscow State University, Russian Federation, co-chair
- Marco Tavani,  
INAF and University of Rome "Tor Vergata", Italy
- Tatsuo Torii,  
Japan Atomic Energy Agency, Tsuruga, Japan (to be confirmed)
- Harufumi Tsuchiya,  
Cosmic Radiation Laboratory, Riken, Japan.
- Lev Zeleny,  
Space Research Institute, Russian Academy of Sciences, Russian Federation (to be confirmed)

# Exploring High-Energy Phenomena in Earth's Atmosphere

## *From editor*

The study of high-energy phenomena in the atmosphere provides unique information about particle acceleration and multiplication in the lower and upper atmosphere during thunderstorms. Generation and propagation of large fluxes of electrons, positrons, gamma rays, and neutrons in the atmosphere and in near space are related to the development of thunderstorms and may be used for monitoring dangerous consequences of extreme weather. Electromagnetic emissions connected with thunderstorms trigger various dynamic processes in the Earth's magnetosphere, causing global geomagnetic storms and changing electrodynamics properties of the ionosphere. The large fluencies of energetic electrons, photons, and neutrons produced by runaway electron avalanches can potentially be a danger to aircraft crews, passengers, and onboard electronic systems.

To discuss these high-energy phenomena, the Thunderstorms and Elementary Particle Acceleration conference were held at the Nor Amberd International Conference Center of the Yerevan Physics Institute (YerPhI) in Armenia. The Cosmic Ray Division of YerPhI and Skobeltsyn Institute of Nuclear Physics of Moscow State University organized the workshop; YerPhI and the Armenian State Science Committee sponsored it. Thirty scientists and students from the United States, Germany, Norway, Russia, and Armenia attended.

Presentations focused on research on thunderstorm ground enhancements (TGEs), terrestrial gamma ray flashes (TGFs), and observations of atmospheric high-energy phenomena by facilities and instrumentation. Discussions on the most intriguing problems of the new emerging topic of high-energy physics in atmosphere covered questions such as the following: What can scientists learn from comparisons of TGEs and TGFs? Is there a causal relation between particle fluxes and atmospheric discharges? Are databases of TGEs and TGFs available for the community? Can a single theoretical framework explain all of the transient energetic events in the Earth's atmosphere (TGE, TGF, and particle precipitation)?

The workshop participants agreed that research on high-energy phenomena in thunderclouds is entering an intensive development stage. New satellite and balloon missions are being prepared exclusively for the detection of optical, radio, and gamma ray emissions from thunderclouds. New research groups from several countries worldwide are installing surface based particle detectors for TGE detection. New models to explain TGF and TGE events are currently being developed and tested. A vast amount of experimental evidence on TGE and TGF is available for tuning the models and for consistency checks on individual observations. Direct measurements of intense particle fluxes on the Earth's surface may be used for tuning the parameters of TGF models. The spatial and energetic characteristics of extensive cloud showers and the measured energy spectra of the TGE gamma rays and electrons may be used for checking characteristics of the particle fluxes obtained by the TGF simulations.

The presentation slides and discussion videos are available on the conference website, <http://crd.yerphi.am/Conferences/tepa2013/home>. More details on the discussions can be found in the supplemental information in the online version of this meeting report.

Some of the reports to TEPA 2013 were published after the symposium and we include them in the proceedings. Also, we include 4 papers on new exciting TGE events detected (or analyzed) after TEPA 2013:

- A.Chilingarian, G.Hovsepyan, E.Mnatsakanyan, A.Reymers, "Preliminary analysis of the unusual TGE event detected by ASEC monitors at 19 October 2013";
- A.Chilingarian, E. Mnatsakanyan, K. Avakyan, A. Reymers, L. Vanyan, T. Karapetyan, "Low energy threshold (0.1-2MeV) detector for registration of the Thunderstorm ground enhancements";
- A.Chilingarian, G.Hovsepyan, L.Vanyan, "On the origin of the particle fluxes from the thunderclouds:Energy spectra analysis";
- A.Chilingarian, "Meteorological conditions during TGEs and estimation of the size of emitting region in the thundercloud".

These and the new expected in 2014 TGE events will be presented on planned on September 22-26 TEPA 2014 Symposium. We will be very happy to welcome you in Nor Amberd International Conference Centre of the Yerevan Physics Institute,

# Table of Contents

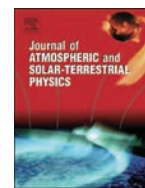
|  |     |
|--|-----|
| Thunderstorm ground enhancements—Model and relation to lightning flashes.....  | 1   |
| <i>A. Chilingarian.</i>  |     |
| Statistical analysis of the Thunderstorm Ground Enhancements (TGEs)<br>detected on Mt. Aragats .....                 | 10  |
| <i>A. Chilingarian, T. Karapetyan and L. Melkumyan</i>   |     |
| Observation of Thunderstorm Ground Enhancements<br>with intense fluxes of high-energy electrons.....                 | 25  |
| <i>A.Chilingarian, L. Vanyan, B. Mailyan</i>   |     |
| Thunderstorm ground enhancements: Gamma ray differential energy spectra.....   | 32  |
| <i>A. Chilingarian, G. Hovsepyan, and L. Kozliner</i>  |     |
| Role of the Lower Positive Charge Region (LPCR) in initiation<br>of the Thunderstorm Ground Enhancements (TGEs)..... | 42  |
| <i>A. Chilingarian, H. Mkrtchyan</i>   |     |
| Remarks on recent results on neutron production during thunderstorms.....  | 53  |
| <i>A. Chilingarian, N. Bostanjyan, T. Karapetyan, L. Vanyan</i>  |     |
| Preliminary analysis of the unusual TGE event detected by<br>ASEC monitors at 19 October 2013.....                   | 60  |
| <i>A.Chilingarian, G.Hovsepyan, E.Mnatsakanyan, A.Reymers, L.Vanyan</i>  |     |
| On the origin of the particle fluxes from the thunderclouds: energy spectra analysis.....                            | 70  |
| <i>A. Chilingarian, G. Hovsepyan, L. Vanyan</i>  |     |
| Meteorological conditions during TGEs and estimation of the<br>size of emitting region in the thundercloud.....      | 75  |
| <i>A. Chilingarian</i>   |     |
| RELEC Mission: TLE amd Relativistic Electron Precipitations.....   | 80  |
| <i>M. Panasyuk, S. Svertilov, V. Bogomolov, G. Garipov, N. Veden'kin</i>   |     |
| Observation of the compact intercloud discharges onboard of microsatellite Chibis-M.....                             | 83  |
| <i>M. Dolgonosov, V. Gotlib, L. Zelenyi , V. Rakov</i>   |     |
| Observing terrestrial gamma flashes at ground level and Balloon altitudes.....                                       | 88  |
| <i>M. Cherry, R. Ringuette, G. Case, D. Granger, G. Guzik, M. Stewart and J. Wefel</i>                               |     |
| Low energy threshold (0.1-2MeV) detector for registration of<br>Thunderstorm ground enhancements .....               | 96  |
| <i>A.Chilingarian, E. Mnatsakanyan, K. Avakyan, A. Reymers, L. Vanyan, T. Karapetyan</i>                             |     |
| Development of a Transportable LIDAR System for the Measuring<br>Electric Field inside the clouds.....               | 102 |
| <i>A. Ghalumyan, R. Hakhumyan, H. Hakhumyan</i>  |     |
| Multi-purpose Pulse Analyzer for Cosmic Ray Research.....  | 105 |
| <i>K. Arakelyan, A. Avetisyan, V. Danielyan, A. Daryan, D. Pokhsranyan</i>   |     |
| Photogallery.....  | 113 |





Contents lists available at ScienceDirect

## Journal of Atmospheric and Solar-Terrestrial Physics

journal homepage: [www.elsevier.com/locate/jastp](http://www.elsevier.com/locate/jastp)

## Thunderstorm ground enhancements—Model and relation to lightning flashes

A. Chilingarian\*

Yerevan Physics Institute, Armenia

## ARTICLE INFO

## Article history:

Received 16 March 2013

Received in revised form

6 November 2013

Accepted 7 November 2013

Available online 15 November 2013

## Keywords:

Atmospheric electricity

Thunderstorms

Electron acceleration

Lightning initiation

## ABSTRACT

In the beginning of last century C.T.R. Wilson proposed that strong electric field of the thunderclouds might accelerate electrons to very high energies. However, this and many other electromagnetic processes in our atmosphere are poorly understood till now; the key questions about the thundercloud electrification and lightning initiation remain unanswered. During recent decades several observations of gamma ray, electron and neutron fluxes correlated with thunderstorms were reported. Nonetheless, the origin of these fluxes is under debate till now. The direct registration of the particle showers initiated by the runaway electrons (the most popular theory) was missing. We present the experimental evidence of the microsecond duration electron bursts originated from runaway electrons accelerated in thunderclouds. The electron acceleration downward becomes possible after creation of the Lower Positive Charged Region below the main negative charged layer in the middle of the thundercloud. Our analysis is based on the vast thunderstorm data from the Aragats Mountain in Armenia, 3200 m above sea level. Varieties of particle detectors located at Aragats Space Environmental Center are registering neutral and charged particle fluxes correlated with thunderstorms, so-called Thunderstorm Ground Enhancements. Simultaneously the electric mills and lightning detectors are monitoring the near-surface electric field and lightning flashes. In the paper we present the model of TGE initiation. We demonstrate the necessity of the Lower positive charge region development for the lower dipole operation and TGE initiation. Our observations establish direct relationship of the negative electric field strength and rain rate with TGE.

© 2013 Elsevier Ltd. All rights reserved.

### 1. Introduction

One of the first particle physicists and researchers of the atmospheric electricity Nobel award winner sir C.T.R. Wilson in the beginning of last century recognized that “the occurrence of exceptional electron encounters has no important effect in preventing the acquisition of large kinetic energy by particles in a strong accelerating field” (Wilson, 1925a). It was the first publication introducing an enigmatic physical phenomenon of electron acceleration by the strong electric fields in thunderclouds called “runaway” electrons by the astronomer Eddington (1926).

Of course, in 1925 the particle cascade theory was not yet established, the measurements of the electric field in thunderclouds were not done and C.T.R. Wilson overestimated the scale of electron acceleration. He thought that electrons could gain unlimited energy from the electric field: “The general effect of an accelerating field is that a beta-particle, instead of dying as it were a natural death by gradual loss of energy, is continually acquiring more and more energy and increasing its chance of surviving all accidents other than direct encounters with the nuclei of atoms” (Wilson, 1925a) and

“A particle may thus acquire energy corresponding to the greater part of the whole potential difference between the poles of the thundercloud, which may be of the order of  $10^9$  V” (Wilson, 1925b). However, that is not possible, due to abundant radiation losses of electrons with energies greater than 50 MeV traversing the atmosphere. The first measured runaway electron spectrum in thunderstorm ground enhancements faded around 50 MeV (Chilingarian et al., 2010). The potential difference as large as  $10^9$  V also seems to be not feasible according to direct measurements of the intracloud electric fields with the balloon experiments (Stolzenburg and Marshall, 2008).

The first model of the structure of the electric field in thunderclouds anticipates a dipole between negative charged layer in the middle of the thundercloud and positive layer on the top. This, so called, main negative dipole<sup>1</sup> accelerated electrons upward. Wilson wrote: “In the central dipole region, where the downward-directed electric field is greatest, the electrons are accelerated upward to the positive layer but once above the positive layer, their motions are retarded by the electrostatic field

\* Tel.: +37 435 2041; fax: +374 135 2041.

E-mail address: [chili@aragats.am](mailto:chili@aragats.am)<sup>1</sup> We adopt the “atmospheric electricity” sign convention: the positive field (E kV/m) accelerates electrons downward in the direction of the Earth; the negative field (−E kV/m) vice-versa accelerates electrons upward in the direction of space.

and their trajectories bend downward again (Wilson's notebooks, cited by Williams (2009)) and "Fast beta rays can then reach the atmosphere or be bent around by magnetic field to reach Earth at varying distances according to energy and initial directions" (letter to B.F.J. Schonland, cited by Williams (2009)).

The more realistic tripole structure of the thundercloud electric field introducing the short leaving Lower positive charged region (LPCR) below the main negative was established only recently and till now its origin is not fully understood. The LPCR on the base of cloud with middle negatively charged layer constitute lower negatively charged dipole, which accelerates electrons downwards. Electrons accelerated by the lower dipole produce, so-called, thunderstorm ground enhancements—TGEs, intense fluxes of electrons, gamma radiation and secondary neutrons (Chilingarian et al., 2011). The idea of Wilson that accelerated electrons can reach the atmosphere find proof after launching of the orbiting gamma ray observatories. Numerous terrestrial gamma flashes (TGFs) are routinely observed at ~500 km above Earth in correlation with strong equatorial thunderstorms (Fishman et al., 1994). The origin of TGFs is believed to be the electrons accelerated by the upper dipole as Wilson suggested in 1925.

The first attempts to observe the runaway electrons on the earth surface were carried out by Wilson's co-workers Schonland, Viljoen and Halliday in South Africa with the cloud chambers. However, due to low sensitivity of cloud chambers to low energy gamma rays (the majority of particles reaching the earth surface from the electron-photon avalanches unleashed by runaway electrons in the thunderclouds are gamma rays) the results of these experiments were discouraging. Looking for the electrons with energies up to 5 GeV incident to the earth surface following the force lines of geomagnetic field surely could not give a positive outcome (see Halliday, 1941). The observation of the runaway electron phenomena turns to be rather difficult. "In summary and as introduction to the present set of experiments, after 70 years of repeated theoretical and experimental investigations, it is still not clear whether or not the runaway electron acceleration mechanisms operates in a significant manner in either thunderstorms or lightning" (Suszcynsky et al., 1996). In last 2 decades there was significant progress in detection of the particles (mostly gamma rays) from thunderclouds (Parks et al., 1981; McCarthy and Parks, 1985; Aglietta et al., 1989; Eack et al., 2000; Brunetti et al., 2000; Alexeenko et al., 2002; Torii et al., 2002; Tsuchiya et al., 2007). However, till now there are numerous unsolved problems concern complicated TGE phenomena. Some of these problems, i.e., the model of TGE; the nature of emerging LPCR; TGE relation to atmospheric discharges will be presented and discussed in the paper.

## 2. Research made on Aragats Space Environmental Center (ASEC)

Cosmic Ray Division (CRD) of the A. Alikhanyan National lab (Yerevan Physics Institute) during recent 20 years commissioned and operated on the research station Aragats and Nor Amberd numerous particle detectors uninterruptedly registering fluxes of charged and neutral cosmic rays. The main topic of research was physics of the high-energy cosmic rays accelerated in our Galaxy and beyond. Surface arrays consisting of hundreds of plastic scintillator were measuring Extensive air showers (EASs), the cascades of particles born in interactions of primary high-energy proton or fully stripped nuclei with atoms of terrestrial atmosphere. Aragats physicists investigate the, so-called, knee region, where energy spectrum of protons and nuclei suddenly change the spectral index from  $-2.7$  to  $-3$ . A new developed method of distinguishing between showers initiated by primary particles lead to possibility of measuring partial spectra and the exploration of the particle acceleration mechanism by the shock waves in

vicinity of exploding super-novae stars. MAKET-ANI experiment proves very sharp knee in light nuclei energy spectrum at energies of 2–3 PeV and absence of knee in heavy nuclei energy spectrum up to 20 PeV (Chilingarian et al., 2004). This finding of charge dependent position of the knee was later confirmed by the KASCADE experiment (Antoni et al., 2005).

After finishing EAS experiments on Aragats was started a new excited topic—Solar physics and Space Weather. The neutron monitors located at 3200 and 2000 m and numerous new particle detectors measuring charged and neutral components of secondary cosmic rays making Aragats one of the largest centers for researching of solar-terrestrial connections. During 23-rd solar activity cycle were measured many important Solar energetic events, including largest series of GLEs (Ground level enhancements) and Forbush decreases in November 2003 (so-called Halloween events) and discovery of the highest energy solar protons at 20 January 2005 (Chilingarian, 2009). Culmination of the solar physics research was creation of the SEVAN (Space Environmental Viewing and Analysis Network) a network of particle detectors located at middle and low latitudes, which aims to improve fundamental research of space weather conditions and to provide short and long-term forecasts of dangerous consequences of space storms (Chilingarian and Reymers, 2008). The SEVAN network consists of hybrid detectors registering charged and neutral components of secondary cosmic rays. The network detects changing fluxes of different species of secondary cosmic rays at different altitudes, longitudes and latitudes, thus turning into a powerful integrated device used to explore solar modulation effects.

Starting from 2008 during very quiet 24-th solar activity cycle the CRD turns to investigations of the high-energy phenomena in the atmosphere. Existing and new designed particle detectors and unique geographical location of Aragats station allow to observe in 5 years more than 300 particle bursts, which were called TGEs—thunderstorm ground enhancements. TGEs observed on Aragats are not only gamma rays, but also sizable enhancements of electrons (Chilingarian et al., 2013b) and rarely also neutrons, usually lasting 10 min or more. Aragats physicists enlarge the possibilities for TGE research by coherent detection of the electrical and geomagnetic fields, rain rate, temperature, relative humidity and other meteorological parameters, as well as by detection of the lightning. Adopted multivariate approach of investigations allows connecting different fluxes, fields and lightning occurrences and finally establishing comprehensive model of the TGE.

The same approach allows unambiguously proving the existence of the neutron fluxes linked to the TGEs and well correlated with the gamma ray fluxes. The mechanism of the neutron generation by the photonuclear reaction of the gamma rays born in thunderclouds was suggested in Babich and Roussel-Dupré (2007) and observed at Aragats during the strongest TGEs (Chilingarian et al., 2012a). A new realistic simulation of the RREA process in the thunderstorm atmosphere helps to clarify contribution of the direct gamma ray production in a lead absorber to the Neutron monitor counts (NM, Tsuchiya et al., 2012). At any offset of the "emitting region" relative to the detector location the "direct neutron production" quickly diminished and the "atmospheric" neutron contribution enlarged (Chilingarian et al., 2012b). Therefore, both photonuclear processes in the air and in the lead absorber of NM should be considered to explain the neutron fluxes correlated with thunderstorms.

## 3. Extensive cloud showers—Experimental proof of the runaway process

Gurevich et al. (1992) developed a theory of the runaway process. They showed that when Møller scattering (electron–electron elastic scattering) is included, the runaway electrons described by Wilson will undergo avalanche multiplication, resulting in a large number of

relativistic runaway electrons and gamma rays for each energetic seed electron injected into the strong electrical field region. Further development of the theoretic knowledge on the runaway process continued with intensive implementation of the Monte Carlo simulation. Sophisticated codes were used to model the propagation of energetic electrons in electric field; codes include energy losses from ionization and atomic excitation, Møller scattering and angular diffusion from elastic scattering with atomic nuclei and other (Lehtinen et al., 1999; Babich et al., 2001; Dwyer, 2003, 2007).

Recently the CERN based GEANT 4 code (Agnostelli et al., 2003) is widely used for study of the propagation of the runaway electron avalanches in the atmosphere (Carlson et al., 2010; Chilingarian et al., 2012c). It is interesting to note that the runaway process is naturally embedded from the GEANT4 simulations: when you switch on appropriate electrical field and use incident cosmic ray electron flux as seeds; the electrons gain energy from field, knock-out atomic electrons and cascade process unleashed; it is another proof that simulation is a creative tool to discover new physical phenomena. The initial name of the cascade released by the runaway electron—the Runaway breakdown (RB, given by Gurevich et al. (1992)), pointed on the relation with lightning occurrence (not proven yet), is recently often replaced by the term RREA (Relativistic Runaway electron avalanches) without any relation to discharge process.

The first observation of the avalanches initiated by the runaway electrons was made at Aragats in 2009 (Chilingarian et al., 2010, 2011). An array of 16 plastic scintillators (Fig. 1, see details of experimental facility in Chilingarian et al. (2004)) was used for detection of extended atmospheric particle showers.

If signals from the first 8 scintillators covering  $\sim 400 \text{ m}^2$  area coincide within the trigger window time of 400 ns the amplitudes of all photomultiplier signals (proportional to the number of particles hitting each scintillator) are stored. At fair weather the surface array registered EASes initiated by the primary protons with energies above  $\sim 50 \text{ TeV}$  ( $\sim 25 \text{ EAS}$  per minute, 8-fold coincidences) and  $100 \text{ TeV}$  ( $\sim 8 \text{ EAS}$  per minute, 16-fold coincidences).

In Fig. 2 we demonstrate the detection of the largest TGE ever measured at Aragats. The significance of detection at energies above  $7 \text{ MeV}$  exceeds  $350\sigma$ . Measuring electron flux with different thresholds allows recovering for the first time the electron integral energy spectrum (see details in Chilingarian et al. (2010)).

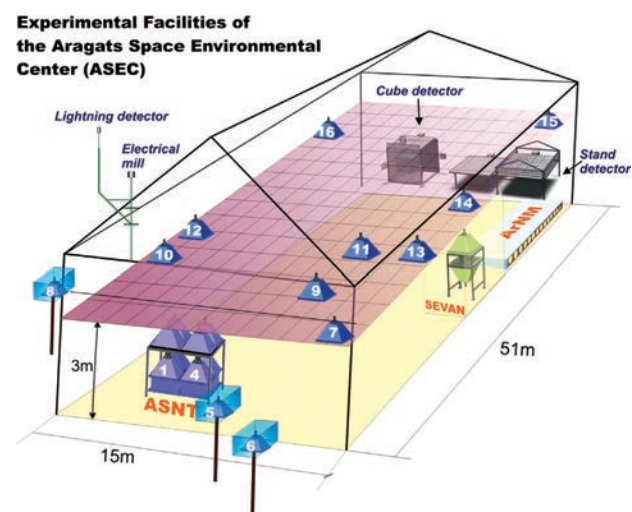


**Fig. 1.** Experimental facilities of the ASEC; 5 cm thick and  $1 \text{ m}^2$  area plastic scintillators belonging to the MAKET surface array are denoted by numbers from 1 to 16. On the roof of building are located Electrical mill EFM 100 and lightning detector LD-250 of BOLTEK firm.

The time series of the surface array triggers also demonstrate huge enhancement, see Fig. 3. During 7 min of the TGE  $\sim 200$  additional triggers were registered; the count rate at 22:47, 19 September 2009 was enhanced  $\sim 8$  times for the 16-fold coincidences and 5 times for the 8-fold coincidences.

The minute of the maximal count of triggers coincides with maximal flux of particles registered by other detectors sensitive to electrons, gamma rays and neutrons. The statistical analysis of detected showers reveals their systematic difference from the EAS events (see for details Chilingarian et al. (2011)): the density of shower particles hitting the scintillators was much lower and spatial spread was much more uniform (spatial distributions of the EASes has characteristic bell-like form). Therefore, the showers of electrons and gamma rays from the thunderclouds constitute different from EAS physical phenomena—extensive cloud showers (ECSs, Chilingarian and Hovsepian (2013)). ECS phenomenon is very rare: only 3 TGEs from 300 observed were accompanied by ECSes. ECSes originated from individual runaway electrons accelerated in the cloud just above the detector. Duration of ECS is expected to be very short: the arrival time of the shower particles from the thundercloud located not higher than few hundreds of meters above the detector could not be large. We do not measure shower particle arrival on microsecond scale; however the statistical analysis of particle second-by-second distribution within the minutes of maximal flux allows estimating the upper limit of ECS duration to be 50 ms (see for details Chilingarian et al. (2011)).

Like multiple EASs from the primary cosmic rays are sustaining stable flux of secondary cosmic rays, multiple ECSes provide transient enhancement of the TGEs lasting minutes. ECS phenomenon is very local and depends on the height of cloud above detector and on the strength of electric field in it. Both parameters are fast changing and only during several minutes cascades from runaway electrons can develop enough to cover several thousand square meters of surface. Only very suitable location and large sizes of the scintillators allow detecting ECSes on Aragats and for the first time directly proving existence of RREA phenomena.

The variety of particle detectors on Aragats allows also measuring the integral spectrum of TGE electrons and differential energy spectrum of gamma rays up to  $100 \text{ MeV}$  (before the gamma ray energy spectrum was measured only till  $20 \text{ MeV}$ ). The energy spectra of the electrons have an exponential shape and extend up to  $40\text{--}50 \text{ MeV}$ . Recovered energy spectra of the gamma rays are power law and extend up to  $100 \text{ MeV}$ .

Prolonged up to  $100 \text{ MeV}$  gamma ray spectrum also was obtained by gamma ray observatory onboard of AGILE satellite (Tavani et al., 2011). Summed over 130 events fluence spectrum does not exhibit the exponential decay at  $50\text{--}60 \text{ MeV}$  as expected from the “pure” RREA mechanism.

Energy spectra of largest TGE events detected in 2009 and 2010 were recovered by the solving inverse problem of cosmic rays—fitting trial energy spectra by simulating the energy response of  $60 \text{ cm}$  thick plastic scintillator (see details in Chilingarian et al. (2012c)). After installing the network of large NaI crystals in 2011 the energy spectra of gamma rays were measured directly (Chilingarian et al., 2013).

Maximal flux of gamma rays exceeds background of secondary cosmic rays by  $\sim 1000\%$  in the energy range of  $2\text{--}20 \text{ MeV}$  and by  $1\text{--}10\%$  in the energy range up to  $100 \text{ MeV}$ . Very large enhancements can be explained only by invoking the RREA process. Ambient population of secondary cosmic ray electrons in the electric fields with strength greater than the critical value unleashes the electron-gamma ray avalanches and total number of particles on the exit from cloud can be multiplied by several orders of magnitude. A GEANT4 simulation helps to estimate characteristics of the thunderclouds

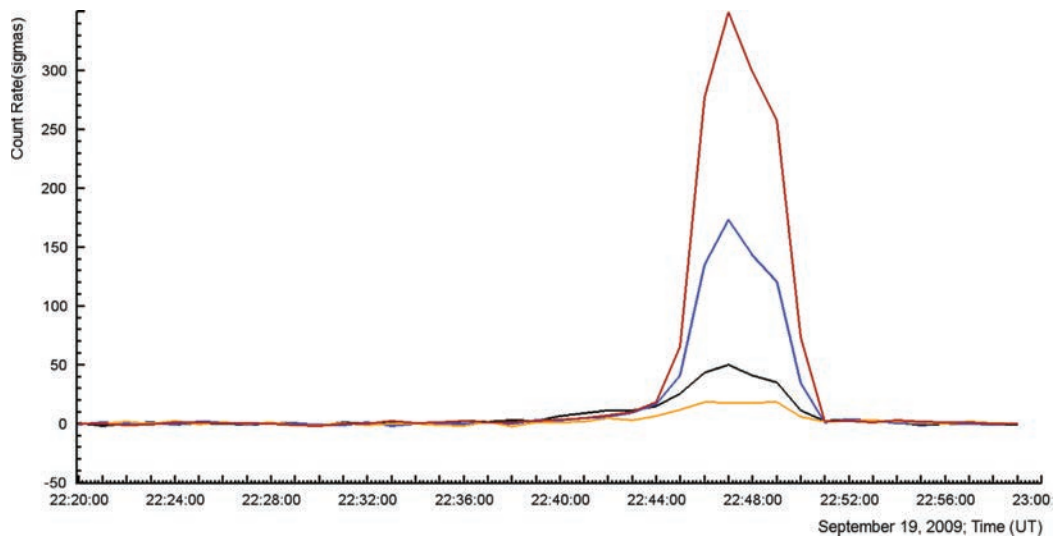


**Fig. 2.** The enhancements of ASEC detectors measured on 19 September 2009 (the maximum of flux at 22:47 UT) in numbers of standard deviations (number of  $\sigma$ ). The 1 m<sup>2</sup> area 5 cm thick outdoor and indoor plastic scintillators measure electron flux with energies above 7 and 10 MeV (2 upper curves); the same type plastic scintillators of SEVAN – with energies larger than 15 MeV (next curve) and coincidence of 5 and 60 cm scintillators of ASNT – with energies above 30 MeV (lowest curve). Corresponding significance of peaks are 350, 170, 50 and 20 standard deviation.

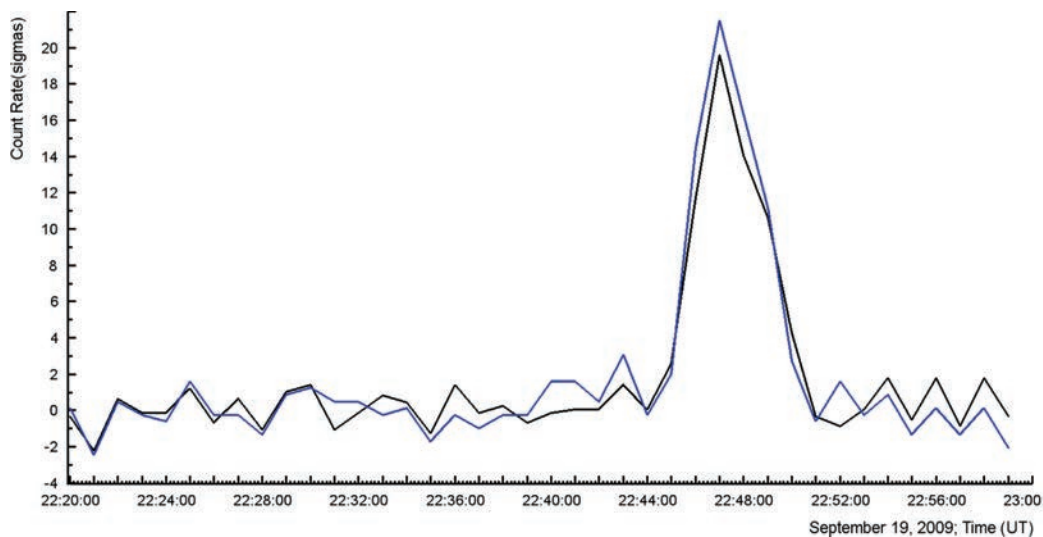


**Fig. 3.** Largest TGE event occurred on 19 September 2009; Minute time series of the triggers of MAKET surface array (16-fold – upper curve – and 8-fold – lower curve – coincidences).

responsible for TGE initiation (the strength of the electrical field and potential drop in the thundercloud, height of thundercloud above detector site). Estimated values of 1.8 kV/cm with elongation of 1–1.5 km and cloud height of 50–150 m for largest events are in good agreement with available measurements (Torii et al., 2011; Tsuchiya et al., 2011). However, the energy spectrum of gamma rays prolonged up to 100 MeV cannot be explained in the framework of the RREA process, as for assumed realistic parameters of the thundercloud maximal energy of the runaway electrons does not exceed 40–50 MeV. GEANT4 simulations demonstrate that these high-energy photons can be explained by the Modification of the energy Spectra (MOS) of charged particles in the electric field of thunderclouds (Muraki et al., 2004; Dorman and Dorman, 2005). The CR relativistic electrons entering prolonged electric field in thundercloud live longer and radiate more gamma rays thus enlarging the gamma ray flux from the thundercloud. The strength of the electric field not necessarily should exceed the RREA initiation threshold.

MOS process has no threshold and amplitude of TGE events may be very small if field is weak or/and its elongation is short (see statistics of TGE events in Chilingarian et al. (2013a)).

#### 4. The model of TGE; TGE amplitude and near-surface electric field

During milliards years of its evolution Earth was bombarded by the protons and fully stripped ions accelerated in Galaxy in tremendous explosions of the supernovas and by other exotic stellar sources. This flux was changed during the passage of sun through the four galactic arms in its course around the center of Galaxy and, may be, was affected several times by huge explosions of nearby stars. Nonetheless, on the shorter time scales the galactic cosmic ray flux is rather stable. High-energy protons and fully stripped nuclei entering the terrestrial atmosphere and colliding

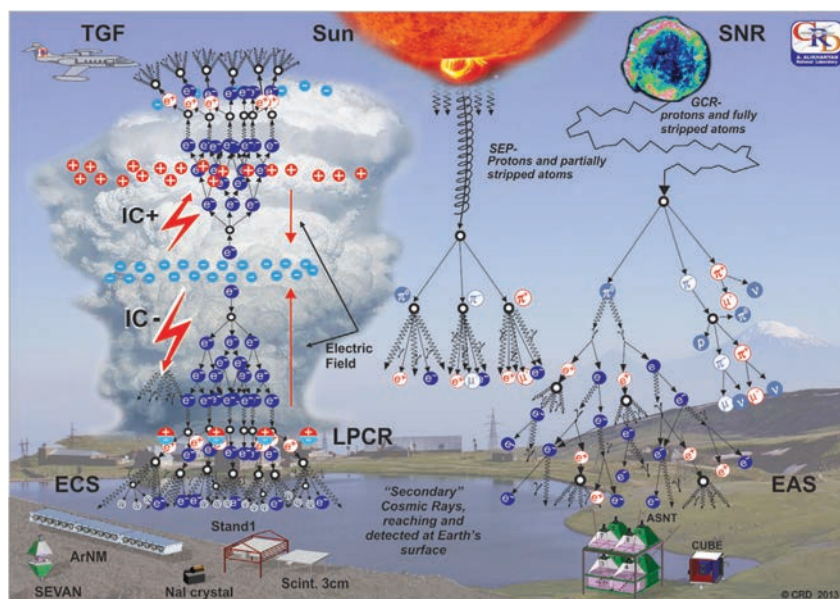


Fig. 4. Sources of the secondary cosmic rays detected on the Earth's surface.

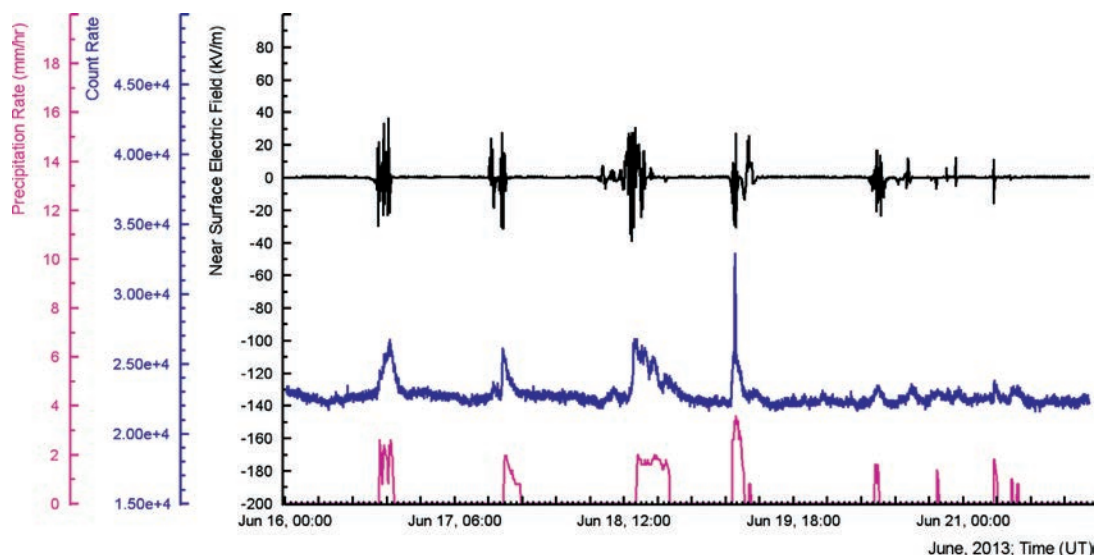


Fig. 5. Time series of the rain rate (bottom); time series of the count rate of outdoor plastic scintillator with energy threshold 1.5 MeV (middle); time series of the disturbances of near surface electric field. (Time series of numerous particle detectors, field meters and weather stations are available from the site of Cosmic ray division of Yerevan physics institute <http://crd.yerphi.am>).

with nitrogen and oxygen atoms generate extensive air showers—cascades of particles developing in atmosphere comprising secondary cosmic rays, see right side of Fig. 4.

Sun influences earth in different ways by emission of radiation, plasma clouds and high-energy particles and ions. Although the overall energy fraction of the high-energy particles is very small compared with visible light energy, nonetheless, on several occasions' solar particles if energetic enough can generate cascades contaminating stable flux of the secondary cosmic rays initiated by galactic primaries. Influence of sun on the secondary cosmic ray flux can be described as modulation of the stable cosmic ray "background" by the sun activity. The most energetic in the solar system flaring process releases up to  $10^{33}$  erg of energy during few minutes. Along with broadband electromagnetic radiation the explosive flaring process

results in ejection of huge amounts of solar plasma and in acceleration of the copious electrons and ions (so called solar energetic phenomena—SEP). Particles can be generated either directly in the coronal flare site with subsequent escape into interplanetary space, or they can be accelerated in the shocks that propagate through corona and interplanetary space (Aschwanden, 2004). These particles, along with neutrons, produced by protons and ions within the flare, constitute Solar cosmic rays (SCR). Only few of SEP events (usually not more than a dozen during solar activity cycle of  $\sim 1$  years) can be detected by surface monitors, see middle sketch in Fig. 4. Such events comprise, so called Ground Level Enhancement (GLE).

Another, newly discovered phenomenon modulated flux of secondary cosmic rays is the high-energy phenomena in thunderclouds. The identified drivers of the TGE are the Relativistic runaway electron

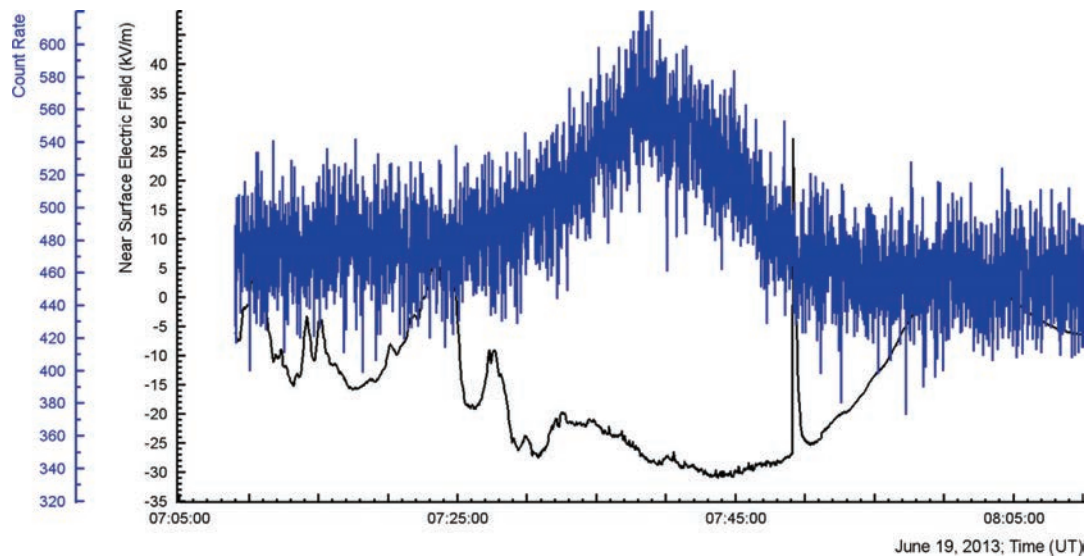


Fig. 6. The 2013 largest TGE of 19 June. Prolonged negative electric field initiates large TGE measured by 1-s time series of 3 cm thick outdoor scintillator.

avalanches (RREA) and Modification of energy spectra (MOS) processes (Chilingarian et al., 2012c).

The Lower positive charge region (LPCR, see left bottom of Fig. 4) with main negative layer in the middle of the cloud forms lower dipole, responsible for the downward electron acceleration and TGE origination. Many researchers outline the dominant role that LCPR plays in initiating/triggering an intracloud and cloud-to-ground lightning discharges (Pawar and Kamra, 2004; Nag and Rakov, 2009; Qie et al., 2005, 2009). The size of LPCR is much smaller than the size of the main negative charge layer. The transient character of LPCR can explain the duration of the TGE. LPCR's are short-lived because, being composed of precipitation, they fall out of the cloud and carry their charge to the ground (Holden et al., 1980). As one can see in Fig. 5, the all TGEs observed in June 2013 was accompanied by rain.

Rain started during TGE in progress and after it stops TGE fast declines. The TGE amplitude is approximately proportional to the rain rate.<sup>2</sup> Consequently, we can deduce that charge is resided on the rain droplets. The positive and negative ions can be separated in the droplet under the action of the ambient electric field, thus forming two residual stretched charged clusters (Gurevich and Karashtin, 2013, see left bottom side of Fig. 4). Therefore, the upper part of droplet forms with main negative layer of the thundercloud the lower dipole accelerated electrons downward; and the negatively charged bottom of the droplet is responsible for the large negative near surface electric field measured by the EFM-100 electrical mill.<sup>3</sup> The TGE amplitude should be proportional to the total positive charge in LPCR; and, therefore—to the amount of rain droplets (water) in the bottom of cloud. An estimate of amount of water in cloud is the rain rate. For the TGEs on June 20–21 (right side of Fig. 5) the charge accumulated in the droplets was not sufficient to provide strong electric field to unleash RREA process and we detect only modest enhancements of particle fluxes due to MOS process. On June 16–19 the rain rate was sufficient to stipulate large and prolonged TGEs. Zooming Fig. 5 we can investigate each TGE in more details. In Fig. 6 we post the 2013 largest TGE of 19 June.

<sup>2</sup> Measured by Professional Davis Instruments Vantage Pro2, <http://www.davisnet.com/>.

<sup>3</sup> Boltek firm electrical mill EFM100, measurement accuracy 5%, <http://www.boltek.com/efm100.html>.

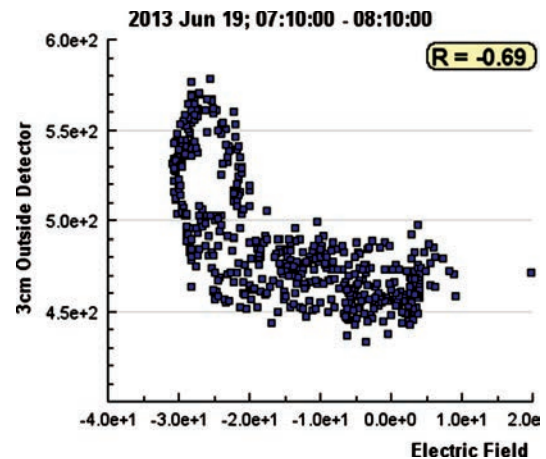


Fig. 7. The scatter plot of particle flux and near surface electric.

As we can see in Fig. 6 as electric field dipping to negative domain at  $\sim 7:25$  the particle flux gradually enhanced, peaking at 7:36 when near surface electric field get the value of  $-30$  KV/m. Rain consequently washed out the LPCR and particle flux started to decay, fully stopping at 7:50.

In Fig. 7 we can see the typical for the large TGEs pattern showing inverse dependence of the particle flux on near surface electric field strength. Apparent anti-correlation of 2 variables can be explained by enhancement of the positive charge of LPCR (resided on the rain droplets) and consecutive increase of negative charge (resided on the bottom of droplets and measured by the field mills located on Earth's surface). The larger is electric field of lower dipole—more electrons are accelerated and unleashing avalanches and more boost get TGE.

## 5. TGEs and lightning occurrences

TGE particle flux was often accompanied with intracloud lightning occurrences (IC–) and suppression of cloud-to-ground lightning occurrences (CG–). This structure of lightning occurrences supports creation of developed lower positive charge region as a fundamental

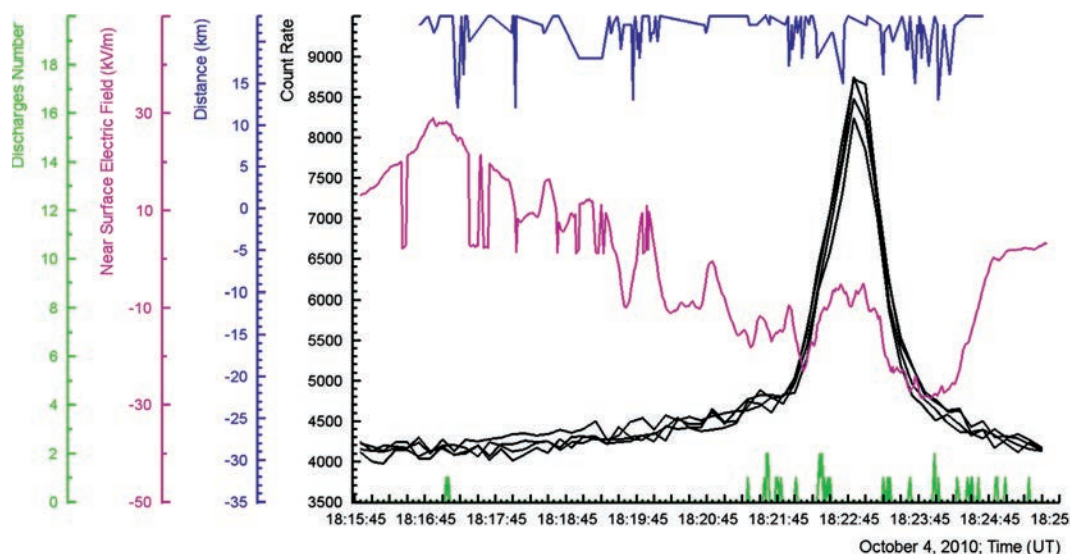


**Fig. 8.** The large TGE of October 4, 2010 measured by 41 m<sup>2</sup> area scintillators; electric field, distance to lightning and lightning occurrences registered by EFM 100 and Storm tracker.

condition of TGE origination (Chilingarian and Mkrtchyan, 2012). Large fluxes of electrons and gamma rays detected on the Earth's surface are only possible when LPCR is well developed and, consequently, lower dipole is accelerated electrons downward. Lower dipole as well can initiate negative intracloud lightning<sup>4</sup>; however TGEs and lightning are not obligatory correlated. Simultaneous measurements of the particle fluxes, electrical field disturbances and lightning occurrences at Aragats in the seasons of 2011–2013 do not give any evidence on causative relation of lightning occurrences to TGEs.

Lightning flashes are detected by 2 devices both produced by Boltek company. The electrical mill EFM-100 traced short-range (30 km) lightning flashes by the abrupt change of the near surface electrical field monitored by electric mill (only CG, cloud-to-ground lightnings are registered by EFM-100). Boltek's StormTracker<sup>5</sup> for each lightning stroke analyzes a signal waveform in real time. The discrimination between IC and CG is based on the shape and amplitude of the waveform, i.e., the rise and decline times. The direction is determined by looking at the magnetic field ratios for each stroke. The initial distance is determined by looking at the signal strength.

In Fig. 8 we present the large TGE event of 4 October 2010. The TGE amplitude measured by the four identical 1 m<sup>2</sup>, 5 cm thick plastic scintillators belonged to ASNT detectors reached 150%. The duration of the TGE peak on the half-maximum (FDHM) was only 40 s, from 18:22:25 till 18:23:05. Lightning activity was modest during this event. In 5 km range Storm Tracker detects 12 IC– lightning flashes at 18:21:20–18:22:30; 8 IC– lightnings at 18:23:15–18:25:15; 2 IC+ lightning flashes at 18:24–18:25:20 and CG– lightning flash at 18:24:51 and CG± at 18:25:35. Only 1 lightning flash was detecting during FDHM of TGE. Distance to cloud-ground lightning flashes measured by EFM-100 was rather far—above 12 km.<sup>6</sup>

<sup>4</sup> Large LPCR prevents negative CG– flashes from occurrence because abundant lower positive charges make an IC– discharge with negative charge region preferable, see for instance Qie et al., 2009.

<sup>5</sup> Boltek's stormTracker lightning detection system, powered by the software from Astrogenic systems, <http://www.boltek.com/stormtracker>.

<sup>6</sup> The EFM-100 detects near lightning flashes much more precise than Storm Tracker. Therefore, if any discrepancy on short distances EFM-100 detection is preferable.

We do not expect that lightning flashes on the distances larger than 10 km can influence TGE. Based on the detection of the winter thunderstorms Tsuchiya et al. (2011) estimate the radii of the circle of intense RREA radiation to be 600 m. Another Japanese group (Torii et al., 2011) detects moving at the speed of 7 m/s energetic radiation source at the height of 300 m; the radiation was emitted from a downward hemispherical surface with radii of 700 m. Intracloud lightning flashes also are too rare to explain minutes long TGE.

Additionally, hundreds of nearby intracloud discharges and numerous cloud-to-ground lightning flashes was registered during the same thunderstorm at 22:00–22:10, October 4, 2010. Nonetheless, this very strong lightning activity was not accompanied by any significant enhancement of particle flux as it is demonstrated in Fig. 9.

From discussed above TGE event we may deduce that a causative relation does not connect large particle fluxes and lightning occurrences. Reported correlation of lightning signals and TGFs can be induced by the one and the same origin of TGFs and lightnings—strong electric fields in the thundercloud. Recently FERMI group infers that the detected VLF signals are from the relativistic electron avalanches that are responsible for the flash of gamma rays rather than are related to intracloud lightning (Connaughton et al., 2013). However, as we can see in Fig. 8 after the maximum of the particle flux enhancement on the stage of LPCR decaying few discharges occurred. Therefore, we cannot reject that the high-energy TGE electrons may create a conductive channel and “assist” lightning flashes to occur. The opposite hypothesis that lightning discharges themselves produce the observed particle flux seem not reasonable because the rise of TGE started far before the lightning occurrences.

## 6. Conclusion

Early in the last century Wilson made ingenious predictions, which still represent the frontiers of the new field of high-energy atmospheric physics (Dwyer et al., 2012a; Williams, 2010); some of them are still under debate. For instance: “By its accelerating action on particles the electric field of a thundercloud may produce extremely penetrating corpuscular radiation and this

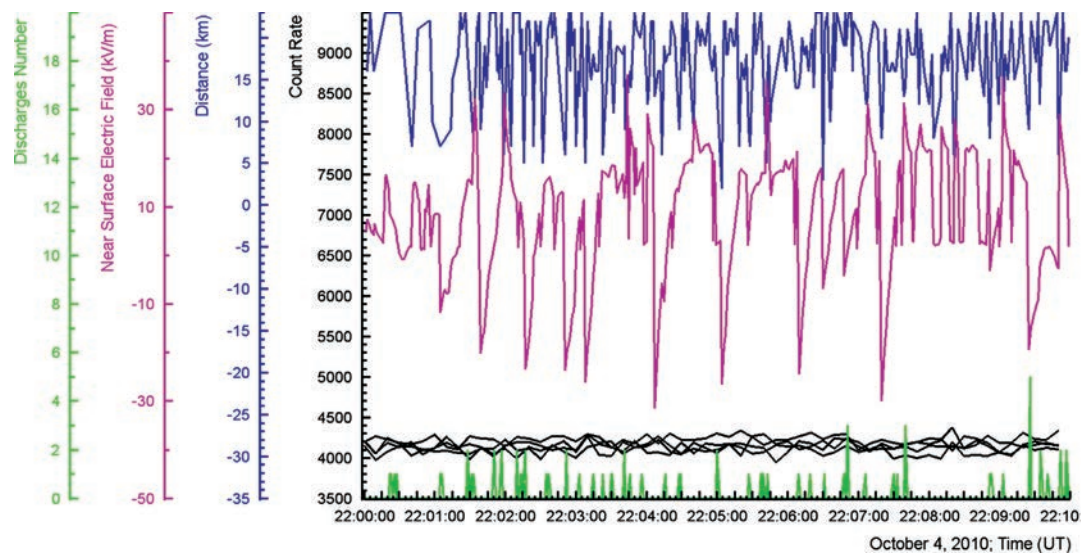


Fig. 9. Huge thunderstorm on October 4, 2010 along with electric field disturbances and lightning occurrences; no significant TGE is detected.

may occur even when there is no thunder” (Wilson, 1925b). This statement concerns one of the hottest topics of the modern research. Are the particles from the clouds due to electric field only (Torii et al., 2011; Chilingarian and Mkrtchyan, 2012) or lightning occurrence is mandatory for emerging particle fluxes (Gurevich et al., 2012)?

Our observations support first hypothesis. Although lightning itself can produce electrons and gamma rays (Dwyer et al., 2012b), the TGE observations prove that lightning is not necessary condition for the particle fluxes initiation. Residing on the rain droplets in the bottom of thundercloud LPCR with main negatively charged layer form a lower dipole. Electrical field of lower dipole effectively transfer field energy to electrons; electrons generate gamma rays and gamma rates by photonuclear reaction born neutrons. Runaway electrons generate secondary electron bursts of microsecond duration; overall duration of TGE is usually  $\sim 10$  min and more; during tens of minutes large amount of short bursts happen. Large TGEs occur during large negative near surface electric field. Amplitude of TGE is proportional to the absolute value of the electric field strength. Atmospheric discharges and TGEs are competitive processes and at maximal TGE flux usually no discharges are detected. However, ECSes provide ionization of atmosphere continuously on the minute time-scale and intracloud negative lightning (IC $-$ ) may use the conductive path opened by multiple ECSs. Only when the LPCR is degraded the lightning leader can propagate till the earth surface and classical negative cloud-to-ground lightning flashes (CG $-$ ) can occur.

## References

- Aglietta, M., EAS-TOP Collaboration, 1989. The EAS-TOP array at  $E_0=1014-1016$  eV: stability and resolutions. Nucl. Instrum. Methods Phys. Res., Sect. A 277, 23–28.
- Antoni, T., Apel, W.D., Badea, F., et al., 2005. KASCADE measurements of elemental groups of cosmic rays: results and open problems. Astropart. Phys. 24, 1–25.
- Aschwanden M.J., In: N. Gopalswamy et al. (Eds.), AGU Monograph of AGU Chapman Conference “Solar Energetic Plasmas and Particles”. 2–6 August 2004, Turku, Finland.
- Agnostelli, S., Allison, J., Amako, K., et al., 2003. GEANT4—a simulation toolkit. Nucl. Instrum. Methods Phys. Res., Sect. A 506, 250–303.
- Alexeenko, V.V., Khaerdinov, N.S., Lidvansky, A.S., Petkov, V.B., 2002. Transient variations of secondary cosmic rays due to atmospheric electric field and evidence for pre-lightning particle acceleration. Phys. Lett. A 301, 299–306, [http://dx.doi.org/10.1016/qS0375-9601\(02\)00981-7](http://dx.doi.org/10.1016/qS0375-9601(02)00981-7).
- Babich, L.P., et al., 2001. Comparison of relativistic runaway electron avalanche rates obtained from Monte Carlo simulations and kinetic equation solution. IEEE Trans. Plasma Sci. 29 (3), 430–438, <http://dx.doi.org/10.1109/27.928940>.
- Babich, L.P., Roussel-Dupré, R.A., 2007. Origin of neutron flux increases observed in correlation with lightning. J. Geophys. Res. 112, D13303.
- Brunetti, M., Cecchini, S., Galli, M., Giovannini, G., Pagliarini, A., 2000. Gamma-ray bursts of atmospheric origin in the MeV energy range. Geophys. Res. Lett. 27 (11), 1599–1602. (art. no. 2000, GL003750).
- Carlson, B.E., Lehtinen, N.G., Inan, U.S., 2010. Terrestrial gamma ray flash production by active lightning leader channels. J. Geophys. Res. 115, A10324, <http://dx.doi.org/10.1029/2010JA015647>.
- Chilingarian, A., Gharagyozyan, G., Hovsepyan, G., Ghazaryan, S., Melkumyan, L., Vardanyan, A., 2004. Light and heavy cosmic-ray mass group energy spectra as measured by the MAKET-ANI detector. Astrophys. J. 603, L29–L32.
- Chilingarian, A., Reymers, A., 2008. Investigations of the response of hybrid particle detectors for the space environmental viewing and analysis network (SEVAN). Ann. Geophys. 26, 249–257.
- Chilingarian, A., 2009. Statistical study of the detection of solar protons of highest energies at 20 January 2005. Adv. Space Res. 43, 702–707.
- Chilingarian, A., Daryan, A., Arakelyan, K., Hovhannisyanyan, A., Mailyan, B., Melkumyan, L., Hovsepyan, G., Chilingaryan, S., Reymers, A., Vanyan, L., 2010. Ground-based observations of thunderstorm-correlated fluxes of high-energy electrons, gamma rays, and neutrons. Phys. Rev. D: Part. Fields 82 (4), 043009.
- Chilingarian, A., Hovsepyan, G., Hovhannisyanyan, A., 2011. Particle bursts from thunderclouds: natural particle accelerators above our heads. Phys. Rev. D: Part. Fields 83 (6), 062001.
- Chilingarian, B., Mailyan, Vanyan, L., 2012c. Recovering of the energy spectra of electrons and gamma rays coming from the thunderclouds. Atmos. Res. 114–115, 1–16.
- Chilingarian, A., Mkrtchyan, H., 2012. Role of the lower positive charge region (LPCR) in initiation of the thunderstorm ground enhancements (TGEs). Phys. Rev. D: Part. Fields 86, 072003.
- Chilingarian, A., Bostanjyan, N., Vanyan, L., 2012a. Neutron bursts associated with thunderstorms. Phys. Rev. D: Part. Fields 85, 085017.
- Chilingarian, A., Bostanjyan, N., Karapetyan, T., Vanyan, L., 2012b. Remarks on recent results on neutron production during thunderstorms. Phys. Rev. D: Part. Fields 86, 093017.
- Chilingarian, A., Hovsepyan, G., 2013. Extensive cloud showers (ECS)—new high-energy phenomena resulting from the thunderstorm atmospheres. J. Phys. Conf. Ser. 409, 012221.
- Chilingarian, A., Karapetyan, T., Melkumyan, L., 2013a. Statistical analysis of the thunderstorm ground enhancements (TGEs) detected on Mt. Aragats. J. Adv. Space Res. 52, 1178.
- Chilingarian, A., Vanyan, L., Mailyan, B., 2013b. Observation of thunderstorm ground enhancements with intense fluxes of high-energy electrons. Astropart. Phys. 48, 1.
- Chilingarian, Hovsepyan, Kozliner, 2013. Thunderstorm ground enhancements gamma ray differential energy spectra. Phys. Rev. D: Part. Fields 88, 073001.

- Connaughton, V., et al., 2013. Radio signals from electron beams in terrestrial gamma ray flashes. *J. Geophys. Res. Space Phys.* 118, 2313–2320, <http://dx.doi.org/10.1029/2012JA018288>.
- Dorman, L.I., Dorman, I.V., 2005. Possible influence of cosmic rays on climate through thunderstorm clouds. *Adv. Space Res.* 35, 476–483.
- Dwyer, J.R., 2007. Relativistic breakdown in planetary atmospheres. *Phys. Plasmas* 14 (4), 042901, <http://dx.doi.org/10.1063/1.2709652>.
- Dwyer, J.R., 2003. A fundamental limit on electric fields in air. *Geophys. Res. Lett.* 30 (20), 2055, <http://dx.doi.org/10.1029/2003GL017781>.
- Dwyer, J.R., Smith, D.M., Cummer, S.A., 2012a. High-energy atmospheric physics: terrestrial gamma-ray flashes and related phenomena. *Space Sci. Rev.* <http://dx.doi.org/10.1007/s11214-012-9894-0>.
- Dwyer, J.R., Schaal, M.M., Cramer, E., Arabshahi, S., Liu, N., Rassoul, H.K., Hill, J.D., Jordan, D.M., Uman, M.A., 2012b. Observation of a gamma-ray flash at ground level in association with a cloud-to-ground lightning return stroke. *J. Geophys. Res.* 117, A10303.
- Eack, K.B., Suszcynsky, D.M., Beasley, W.H., Roussel-Dupre, R., Symbalisty, E.M.D., 2000. Gamma-ray emissions observed in a thunderstorm anvil. *Geophys. Res. Lett.* 27, 185–188, <http://dx.doi.org/10.1029/1999GL010849>.
- Eddington, A.S., 1926. The source of stellar energy. *Nature* 117, 25–32, <http://dx.doi.org/10.1038/117025a0>.
- Fishman, G.J., Bhat, P.N., Mallozzi, R., Horack, J.M., Koshut, T., Kouveliotou, C., Pendleton, G.N., Meegan, C.A., Wilson, R.B., Paciesas, W.S., Goodman, S.J., Christian, H.J., 1994. Discovery of intense gamma ray flashes of atmospheric origin. *Science* 264 (5163), 1313–1316.
- Gurevich, A., Antonova, V.P., Chubenko, A.P., et al., 2012. Strong flux of low-energy neutrons produced by thunderstorms. *Phys. Rev. Lett.* 108, 125001.
- Gurevich, A.V., Milikh, G.M., Roussel-Dupre, R., 1992. Runaway electron mechanism of air breakdown and preconditioning during a thunderstorm. *Phys. Lett. A* 165 (5–6), 463–468.
- Gurevich, A.V., Karashtin, A.N., 2013. Runaway breakdown and hydrometeors in lightning initiation. *Phys. Rev. Lett.* 110, 185005, <http://dx.doi.org/10.1103/PhysRevLett.110.185005>.
- Halliday, E.C., 1941. The thundercloud as a source of penetrating particles. *Phys. Rev.* 60, 101–106, <http://dx.doi.org/10.1103/PhysRev.60.101>.
- Holden D.N., C.R. Holmes, C.B. Moore, W.P. Winn, J.W. Cobb, J.E. Griswold, D.M., Lytle, Local charge concentration in thunderclouds. In: Sixth International Conference on Atmospheric Electricity (University of Manchester, Manchester, England, 1980).
- Lehtinen, N.G., Bell, T.F., Inan, U.S., 1999. Monte Carlo simulation of runaway MeV electron breakdown with application to red sprites and terrestrial gamma ray flashes. *J. Geophys. Res.* 104, 24,699–24,712, <http://dx.doi.org/10.1029/1999JA900335>.
- McCarthy, M., Parks, G.K., 1985. Further observations of X-rays inside thunderstorms. *Geophys. Res. Lett.* 12, 393–396, <http://dx.doi.org/10.1029/GL012i006p00393>.
- Muraki, Y., Axford, W.I., Matsubara, Y., et al., 2004. Effects of atmospheric electric fields on cosmic rays. *Phys. Rev. D: Part. Fields* 69, 123010.
- Nag, A., Rakov, V.A., 2009. Some inferences on the role of lower positive charge region in facilitating different types of lightning. *Geophys. Res. Lett.* 36, L05815, <http://dx.doi.org/10.1029/2008GL036783>.
- Parks, G.K., Mauk, B.H., Spiger, R., Chin, J., 1981. X-ray enhancements detected during thunderstorm and lightning activities. *Geophys. Res. Lett.* 8, 1176–1179, <http://dx.doi.org/10.1029/GL008i011p01176>.
- Pawar, S.D., Kamra, A.K., 2004. *J. Geophys. Res.* 109, D02205.
- Qie, X., Zhang, T., Chen, C., Zhang, G., Zhang, T., Wei, W., 2005. The lower positive charge center and its effect on lightning discharges on the Tibetan Plateau. *Geophys. Res. Lett.* 32, L05814, <http://dx.doi.org/10.1029/2004GL022162>.
- Qie, X., Zhang, T., Chen, C., Zhang, G., Zhang, T., Kong, X., 2009. *Atmos. Res.* 91, 244.
- Stolzenburg, M., Marshall, T.C., 2008. Series profiles of electrostatic potential in five New Mexico thunderstorms. *J. Geophys. Res.* 113, D13207, <http://dx.doi.org/10.1029/2007JD009495>.
- Suszcynsky, D.M., Roussel-Dupre, R., Shaw, G., 1996. Ground-based search for X-rays generated by thunderstorms and lightning. *J. Geophys. Res.* 101, 23,505–23,516, <http://dx.doi.org/10.1029/96JD02134>.
- Tavani, M., et al., 2011. Terrestrial gamma-ray flashes as powerful particle accelerators. *Phys. Rev. Lett.* 106, 018501.
- Torii, T., Takeishi, M., Hosono, T., 2002. Observation of gamma-ray dose increase associated with winter thunderstorm and lightning activity. *J. Geophys. Res.* 107, 4324, <http://dx.doi.org/10.1029/2001JD000938>.
- Torii, T., Sugita, T., Kamogawa, M., et al., 2011. Migrating source of energetic radiation generated by thunderstorm activity. *Geophys. Res. Lett.* 38, L24801.
- Tsuchiya, H., Enoto, T., Yamada, S., et al., 2007. Detection of high-energy gamma rays from winter thunderclouds. *Phys. Rev. Lett.* 99, 165002.
- Tsuchiya, H., Enoto, T., Yamada, S., et al., 2011. Long-duration gamma ray emissions from 2007 to 2008 winter thunderstorms. *J. Geophys. Res.* 116, D09113.
- Tsuchiya, H., Hibino, K., Kawata, K., et al., 2012. Observation of thundercloud-related gamma rays and neutrons in Tibet. *Phys. Rev. D: Part. Fields* 85, 092006.
- Williams, E.R., 2010. Origin and context of C. T. R. Wilson's ideas on electron runaway in thunderclouds. *J. Geophys. Res.* 115, A00E50, <http://dx.doi.org/10.1029/2009JA014581>.
- Wilson, C.T.R., 1925a. The acceleration of b-particles in strong electric fields such as those of thunderclouds. *Proc. Cambridge Philos. Soc.* 22, 534–538, <http://dx.doi.org/10.1017/S0305004100003236>.
- Wilson, C.T.R., 1925b. The electric field of a thundercloud and some of its effects. *Proc. R. Soc. London, Ser. A* 37, 32D–37D.



# Statistical analysis of the Thunderstorm Ground Enhancements (TGEs) detected on Mt. Aragats

A. Chilingarian, T. Karapetyan\*, L. Melkumyan

*Yerevan Physics Institute, Alikhanyan Brothers 2, Yerevan 0036, Armenia*

Received 6 April 2013; received in revised form 4 June 2013; accepted 7 June 2013

Available online 17 June 2013

## Abstract

Starting from 2008 experimental facilities of the Aragats Space Environmental Center (ASEC) routinely measure time series of secondary cosmic ray fluxes. At these years of the minimum of solar activity we analyze the new high-energy phenomena in the terrestrial atmosphere. Namely, Thunderstorm Ground Enhancements (TGEs) and Extensive Cloud Showers (ECSs). Several new particle detectors were designed and fabricated having lower energy threshold to detect particle fluxes from the thunderclouds; some of them have possibility to distinguish charged and neutral fluxes. During 2008–2012 years ASEC detectors located at Aragats, Nor Amberd and Yerevan were detected ~300 TGE enhancements. Amplitude of majority of them is less than 5%; however, 13 TGEs have amplitude exceeding 20%. The maximal value of observed enhancement was 271% (September 19, 2009). The paper summarizes five-years study of the TGEs on Aragats. The statistical analysis revealing the month and day-of-time distributions of TGE events, as well as the amplitude and event duration diagrams are presented.

© 2013 COSPAR. Published by Elsevier Ltd. All rights reserved.

*Keywords:* Cosmic rays; Thunderstorm activity; TGE

## 1. Introduction

Sudden boost of the secondary cosmic ray flux correlated with thunderstorm activity, so called Thunderstorm Ground Enhancements (TGEs, Chilingarian et al., 2010, 2011) is the manifestation of the high-energy processes in the terrestrial atmosphere (Dwyer et al., 2012a) Origin of TGE is strong electrical field in the thundercloud, giving rise to rather complicated physical phenomenon, including several physical processes:

1. Relativistic Runaway Electron Avalanches (RREA, Wilson, 1925; Gurevich et al., 1992; Babich et al., 1998; Dwyer, 2003; Khaerdinov et al., 2005);

2. Modification of the Secondary cosmic ray (electrons, muons, protons and charged mesons) energy spectra (MOS, Dorman and Dorman, 2005; Muraki et al., 2004);
3. Photonuclear reactions of the RREA gamma rays (Chilingarian et al., 2012a,b; Tsuchiya et al., 2012; Babich et al., 2013);
4. Roentgen and gamma radiation from the lightning (Dwyer et al., 2012b);

Surface detections of the TGE process, although have long history, are discrepant and rare. The first attempts to observe the runaway electrons on the earth surface were carried out by Wilson's co-workers Schonland, Viljoen and Halliday in South Africa with cloud chambers. However, due to low sensitivity of cloud chambers to low energy gamma rays (the majority of particles reaching the earth surface from the electron–photon avalanches unleashed by runaway electrons in the thunderclouds are few MeV gamma rays) the results of these experiments were

\* Corresponding author. Tel.: +374 98102505.

E-mail address: [ktigran79@yepphi.am](mailto:ktigran79@yepphi.am) (T. Karapetyan).

discouraging. Looking for the electrons with energies up to 5 GeV subsequently returning to the earth surface following the force lines of geomagnetic field (at the great distance from the thundercloud which had produced them) surely could not give positive outcome (see Halliday, 1941). However, the observation of the runaway electron phenomena and distinguishing it from the modification of energy spectra turns to be rather difficult. “In summary and as introduction to the present set of experiments, after 70 years of repeated theoretical and experimental investigations, it is still not clear whether or not the runaway electron acceleration mechanisms operates in a significant manner in either thunderstorms or lightning” (Suszcynsky et al., 1996). In last 2 decades there were significant progress in detection of the particles (mostly gamma rays) from thunderclouds (Aglietta et al., 1989; Eack et al., 2000; Brunetti et al., 2000; Alexeenko et al., 2002; Torii et al., 2002, 2011; Lidvansky, 2003; Tsuchiya et al., 2007, 2011). Detailed historical reviews of TGE detection are presented in Chilingarian et al. (2010), Dwyer et al. (2012a,b). The idea of C.T.R. Wilson that accelerated in the thunderclouds electrons can reach the atmosphere found its proof after the launch of the orbiting gamma ray observatories. Numerous Terrestrial Gamma Flashes (TGFs) are routinely observed at 500 km above the Earth in correlation with strong equatorial thunderstorms (Fishman et al., 1994; Smith et al., 2005; Bucik et al., 2006). The origin of TGFs is believed to be the runaway electrons accelerated by the upper dipole as Wilson suggested in 1925.

Starting from 2008 experimental facilities of the Aragats Space Environmental Center (ASEC) (Chilingarian et al., 2003, 2005a,b) routinely measure time series of secondary cosmic ray fluxes. During these years several new particle detectors were designed and fabricated having lower energy threshold and possibility to distinguish charged and neutral fluxes (Arakelyan et al., 2013; Chilingarian et al., 2013). Variety of ASEC particle detectors allows for the first time detect RREA process in the atmosphere (Chilingarian et al., 2011), recover both the electron and gamma ray energy spectra of largest TGEs (the sum of multiple RREA) and develop the model of the TGE phenomena (Chilingarian, Mailyan et al., 2012).

16 by 1 m<sup>2</sup> area scintillators previously belonging to the stopped in 2007 MAKET surface array (Chilingarian et al., 2007), registering Extensive Air Showers (EAS) were distributed on the surface of ~1000 m<sup>2</sup>. If signals from the first 8 scintillators covering ~400 m<sup>2</sup> area coincide within the trigger time of 400 nanoseconds the amplitudes of all photomultiplier pulses (proportional to the number of particles hitting each scintillator) are stored. At fair weather the surface array registered EAS events initiated mostly by the primary protons with energies above ~50 TeV (25 EAS per minute, 8-fold coincidences) and 100 TeV (8 EAS per minute, 16-fold coincidences).

At 19 September 2009 the ASEC detectors measure the largest TGE ever measured at Aragats. The significance of

detection at energies of 10 MeV exceeds 200 $\sigma$ . Measuring electron flux with different thresholds allows recovering for the first time the electron integral energy and estimate the height of thundercloud above detectors. The time series of the surface array triggers also demonstrate huge enhancement. During 7 min of the TGE ~200 additional triggers were registered; the count rate at 22:47, 19 September 2009 was enhanced ~8 times for the 16-fold coincidences and 5 times for the 8-fold coincidences. The statistical analysis of detected showers reveals their systematic difference from the EAS events (see for details Chilingarian et al., 2011): the density was much lower and spatial spread of the electrons was much more uniform (EAS spatial distribution have characteristic bell-like form). Therefore, the particle showers from the thunderclouds constitute different from EAS physical phenomena and were named – Cloud Extensive Showers (CESs). A CES phenomenon is very rare: only 3 largest TGEs from 300 were accompanied by CES observation. CESs originated from individual runaway electrons accelerated in the cloud just above the detector. Like multiple EASs from the primary cosmic rays are sustaining stable flux of secondary cosmic rays, multiple CESs are sustaining transient enhancement of the TGEs lasting minutes. Due to global character of primary cosmic ray flux the secondary cosmic ray flux did not change significantly; CES phenomenon is very local and depends on the height of cloud above detector and on the strength of electric field in it. Both parameters are fast changing and only during several minutes cascades from runaway electrons can be developed enough to cover several thousand square meters of surface. Only very suitable location and large sizes of the scintillators allows detect CES on Aragats and for the first time prove existence of RREA phenomena.

During 2008–2012 ASEC detectors at Aragats (3200 m above sea level, geographical coordinates 40°28'N, 44°10'E) were operated 24 h, 12 months uninterruptedly, gathering rich harvest of TGE events (totally 277 TGE events in 5 years, see Tables 1–5). Much less TGE events (20, see Table 6) were detected in the same period at Nor Amberd station, on the slopes of Aragats (2000 m above sea level, geographical coordinates 40°22'N, 44°15'E). And only one TGE by 3.8% amplitude was detected in Yerevan (1000 m above sea level, geographical coordinates 40°20'N, 44°49'E), (see Table 7, measurements in Yerevan started in 2011).

34 of 277 TGE events were registered in 2008, 46 TGEs in 2009, 88 TGEs in 2010, 67 TGEs in 2011 and 42 TGEs in 2012 years. 190 TGEs from 277 have amplitude less than 5%, 55 TGEs have amplitude between 5% and 10% and 32 TGEs have amplitude greater than 10%. Only 13 TGEs have amplitude exceeding 20%. The maximal value of observed enhancements was 271% (September 19, 2009) and the minimal registered –0.8%. In the observed years the most productive months were: May and June in 2008, May–July in 2009. The maximum number of TGE events was detected in October 2010.

Table 1  
Characteristics of TGEs registered at Aragats in 2008.

| Date, time 2008     | Detector | Duration (min) | Number of peaks | Percent of enhancement (%) |
|---------------------|----------|----------------|-----------------|----------------------------|
| 1 May, 12:23        | MAKET    | 10             | 1               | 6.2                        |
| 2 May, 17:31        | MAKET    | 10             | 1               | 3.1                        |
| 3 May, 15:13        | MAKET    | 20             | 1               | 3.4                        |
| 4 May, 10:32        | MAKET    | 24             | 1               | 12                         |
| 5 May, 21:34        | MAKET    | 5              | 1               | 4.6                        |
| 9 May, 5:38         | MAKET    | 4              | 1               | 2.7                        |
| 11 May, 10:10       | MAKET    | 13             | 2               | 5.5                        |
| 13:02               |          | 16             |                 | 4.2                        |
| 12 May, 13:23       | MAKET    | 26             | 2               | 5.4                        |
| 21:57               |          | 6              |                 | 5.5                        |
| 16 May, 7:05        | MAKET    | 15             | 4               | 5.9                        |
| 11:56               |          | 18             |                 | 3.5                        |
| 12:18               |          | 7              |                 | 2.8                        |
| 15:27               |          | 18             |                 | 2                          |
| 17 May, 17:30       | MAKET    | 12             | 1               | 3                          |
| 29 May, 11:43       | MAKET    | 11             | 2               | 7.8                        |
| 15:13               |          | 6              |                 | 10                         |
| 9 June, 1:39        | MAKET    | 8              | 2               | 4.3                        |
| 3:33                |          | 4              |                 | 22.3                       |
| 10 June, 17:16      | MAKET    | 3              | 1               | 2.1                        |
| 12 June, 11:05      | MAKET    | 3              | 1               | 1.9                        |
| 16 June, 13:35      | MAKET    | 15             | 1               | 2.6                        |
| 17 June, 23:38      | MAKET    | 14             | 1               | 5.1                        |
| 21 June, 17:30      | MAKET    | 12             | 3               | 3.8                        |
| 20:19               |          | 15             |                 | 3.5                        |
| 21:43               |          | 3              |                 | 2.3                        |
| 22 June, 3:18       | MAKET    | 14             | 1               | 4.7                        |
| 7 July, 14:46       | MAKET    | 9              | 1               | 4.8                        |
| 8 July, 11:05       | MAKET    | 21             | 1               | 5.5                        |
| 9 July, 23:52       | MAKET    | 4              | 1               | 2.9                        |
| 10 September, 15:53 | MAKET    | 5              | 1               | 2.1                        |
| 16 September, 21:41 | MAKET    | 9              | 1               | 2.9                        |
| 9 October, 12:29    | MAKET    | 6              | 1               | 2.8                        |
| 21 October, 20:44   | MAKET    | 9              | 1               | 11.5                       |

Detailed information about all events, as well as, description of detectors and forewarning/alert services are available from the site of Cosmic Ray Division (CRD) of Yerevan physics institute <http://crd.yerphi.am>. On-line access to database containing multiyear monitoring of secondary cosmic rays with more than 200 measuring channels is enabled by the multivariate visualization program ADEI (<http://adei.crd.yerphi.am/adei/>).

The paper presents statistics of the five-years study of the TGEs on Aragats. The analysis considers the number of TGEs as function of time of a day, month, duration, size of enhancement and other.

## 2. Brief description of ASEC particle detectors

The Aragats Space-Environmental Center provides monitoring of different species of secondary cosmic rays at three altitudes. The ASEC consists of two high altitude stations located on the slope of Mt. Aragats (3200 m, 2000 m) and a detector assembly in Yerevan headquarters of Cosmic Ray Division of Yerevan Physics Institute (1000 m). Two detectors, MAKET (Chilingarian et al.,

2007) and Aragats Multidirectional Muon Monitor (AMMM, Chilingarian and Reymers, 2007) are in operation from late 90-ths with main goal to investigate the energy spectra of the primary cosmic rays in the “knee” region. Both detectors uses the same particle detection techniques to determine the density of electrons belonging to Extensive Air Showers (EAS) and infer the energy and type of a primary particle.

MAKET array consists of four 60 cm thick scintillators and 12 of 5 cm thick ones from which 3 are located outside of the main building. Maket array provides following information:

- 1 min count rates of all 16 channels independently;
- Coincidences of signals from 8 channels from 16, within 400 nanoseconds.

Count rate of the 60 cm detectors is  $\sim 34,000$  counts per minute and variance  $\sim 240$ . Count rate of each 5 cm scintillators is  $\sim 22,000$  counts per minute and variance  $\sim 190$ . The energy threshold of 5cm scintillators is  $\sim 9$  MeV and 60 cm  $\sim 15$  MeV.

Table 2  
Characteristics of TGEs registered at Aragats in 2009.

| Date, time 2009     | Detector | Duration (min) | Number of peaks | Percent of enhancement (%) |
|---------------------|----------|----------------|-----------------|----------------------------|
| 30 April, 22:19     | AMMM     | 5              | 1               | 7.2                        |
| 1 May, 0:22         | AMMM     | 7              | 1               | 6                          |
| 3 May, 9:37         | AMMM     | 12             | 2               | 7.2                        |
| 9:43                |          |                |                 | 7.6                        |
| 8 May, 16:52        | AMMM     | 13             | 1               | 14.9                       |
| 21 May, 17:09       | AMMM     | 20             | 2               | 19.3                       |
| 17:15               |          |                |                 | 30.7                       |
| 26 May, 0:13        | AMMM     | 21             | 4               | 9                          |
| 8:26                |          | 11             |                 | 4.3                        |
| 12:16               |          | 11             |                 | 3.5                        |
| 12:45               |          | 12             |                 | 11.5                       |
| 27 May, 22:53       | AMMM     | 6              | 1               | 8                          |
| 2 June, 14:16       | AMMM     | 7              | 1               | 4.7                        |
| 3 June, 16:14       | AMMM     | 10             | 2               | 10.5                       |
| 17:07               | AMMM     | 5              |                 | 4.1                        |
| 6 June, 16:04       | SEVAN    | 13             | 1               | 2.1                        |
| 8 June, 8:00        | SEVAN    | 20             | 1               | 2.6                        |
| 17 June, 19:22      | SEVAN    | 23             | 1               | 1.8                        |
| 20 June, 10:43      | SEVAN    | 13             | 2               | 2.5                        |
| 10:56               |          | 13             |                 | 2.3                        |
| 26 June, 17:00      | MAKET    | 7              | 1               | 4.8                        |
| 28 June, 11:56      | MAKET    | 2              | 1               | 2.8                        |
| 3 July, 18:21       | MAKET    | 10             | 1               | 2.7                        |
| 9 July, 3:54        | MAKET    | 4              | 3               | 28.7                       |
| 3:56                |          | 4              |                 | 44.7                       |
| 21:26               |          | 4              |                 | 2.3                        |
| 23 July, 19:06      | MAKET    | 11             | 1               | 4                          |
| 27 July, 10:05      | MAKET    | 23             | 1               | 3.6                        |
| 28 July, 16:55      | MAKET    | 21             | 1               | 4.8                        |
| 1 August, 17:34     | MAKET    | 6              | 1               | 2                          |
| 2 August, 13:13     | MAKET    | 11             | 2               | 2.6                        |
| 13:33               |          | 6              |                 | 3.3                        |
| 8 August, 16:39     | MAKET    | 8              | 2               | 2.1                        |
| 17:16               |          | 6              |                 | 2.1                        |
| 8 September, 4:48   | MAKET    | 7              | 1               | 7.7                        |
| September, 11:59    | MAKET    | 4              | 3               | 3.3                        |
| 12:43               |          | 11             |                 | 5.8                        |
| 13:25               |          | 4              |                 | 4.4                        |
| 19 September, 22:47 | MAKET    | 6              | 1               | 270.9                      |
| 22 September, 3:18  | MAKET    | 13             | 1               | 5.2                        |
| 7 October, 9:58     | MAKET    | 12             | 2               | 2.6                        |
| 11:15               |          | 17             |                 | 5.5                        |
| 9 October, 20:43    | MAKET    | 14             | 1               | 3.1                        |
| 2 November, 13:27   | MAKET    | 7              | 1               | 5.8                        |
| 3 November, 2:27    | MAKET    | 3              | 1               | 2.5                        |
| 15 November, 22:31  | MAKET    | 10             | 1               | 4.1                        |

The AMMM detector consists of 5 cm thick 1 m<sup>2</sup> area plastic scintillators located outdoors and in underground hall beneath 14 m of concrete and soil. Upper layer is composed of 29 scintillators; underground detector consists of 90 scintillators of the same type. Count rate of the upper detectors is ~28,000 counts per minute and variance ~170. Count rate of each of 1 m<sup>2</sup> scintillator in the underground hall (for registering high energy muons with energy threshold 5 GeV) is ~3000 counts per minute and variance ~55.

Two standard neutron monitor (NM) of 18NM-64 type consisting of 18 boron-filled proportional chambers,

located below 5 cm of lead (producer) and 10 cm of polyethylene (moderator) are operating at Aragats and Nor Amberd research stations.

The new particle detector system, named SEVAN (Space Environmental Viewing and Analysis Network, Chilingarian et al., 2009), simultaneously measures fluxes of most species of secondary cosmic rays, thus representing an integrated device used for the exploration of the solar modulation effects. In Armenia SEVAN modules are installed at all 3 locations, in Yerevan, Nor-Amberd and top of Aragats. The basic detecting unit of the SEVAN module consists from a “sandwich” of two plastic scintilla-

Table 3.1  
Characteristics of TGEs registered at Aragats in 2010.

| Date, time 2010     | Detector | Duration (min) | Number of peaks | Percent of enhancement (%) |
|---------------------|----------|----------------|-----------------|----------------------------|
| 16 January, 7:43    | MAKET    | 10             | 2               | 6.3                        |
| 9:56                |          | 16             |                 | 9                          |
| 19 January, 2:32    | MAKET    | 20             | 1               | 6.3                        |
| 21 January, 9:04    | MAKET    | 21             | 2               | 5.3                        |
| 9:27                |          | 16             |                 | 5.4                        |
| 16 February, 21:57  | MAKET    | 6              | 1               | 8.8                        |
| 14 March, 22:00     | MAKET    | 3              | 2               | 6.2                        |
| 22:10               |          | 3              |                 | 11                         |
| 8 April, 9:41       | MAKET    | 2              | 2               | 2.7                        |
| 9:45                |          | 2              |                 | 2.8                        |
| 13 April, 7:23      | MAKET    | 13             | 1               | 3.6                        |
| 21 April, 16:26     | MAKET    | 11             | 2               | 3.5                        |
| 20:05               |          | 12             |                 | 5.9                        |
| 22 April, 15:11     | MAKET    | 13             | 2               | 3.3                        |
| 16:21               |          | 30             |                 | 5.8                        |
| 26 April, 12:19     | MAKET    | 10             | 2               | 2.6                        |
| 12:35               |          | 9              |                 | 3.6                        |
| 8 May, 17:28        | MAKET    | 5              | 1               | 2.5                        |
| 21 May, 4:15        | MAKET    | 8              | 2               | 3.1                        |
| 13:15               |          | 12             |                 | 4.2                        |
| 22 May, 6:07        | MAKET    | 9              | 3               | 4.8                        |
| 8:30                |          | 6              |                 | 14.1                       |
| 11:26               |          | 5              |                 | 2.5                        |
| 23 May, 0:50        | MAKET    | 26             | 1               | 7                          |
| 25 May, 6:43        | MAKET    | 7              | 2               | 3.4                        |
| 10:55               |          | 22             |                 | 2.5                        |
| 28 May, 4:45        | MAKET    | 8              | 1               | 3.4                        |
| 7 June, 1:04        | MAKET    | 13             | 3               | 3.6                        |
| 5:20                |          | 10             |                 | 2.5                        |
| 10:29               |          | 15             |                 | 3                          |
| 8 June, 14:35       | MAKET    | 14             | 1               | 3                          |
| 19 June, 8:34       | MAKET    | 4              | 1               | 4.2                        |
| 15 July, 16:42      | MAKET    | 19             | 1               | 2.4                        |
| 19 July, 14:02      | MAKET    | 18             | 1               | 2.4                        |
| 22 July, 18:28      | MAKET    | 12             | 1               | 3.1                        |
| 23 July, 14:06      | MAKET    | 10             | 6               | 3.7                        |
| 14:16               |          | 10             |                 | 2.5                        |
| 16:28               |          | 7              |                 | 3.1                        |
| 16:44               |          | 7              |                 | 2.4                        |
| 17:54               |          | 10             |                 | 3.1                        |
| 18:11               |          | 2              |                 | 2                          |
| 24 July, 17:37      | MAKET    | 19             | 3               | 2.1                        |
| 17:59               |          | 12             |                 | 1.1                        |
| 18:32               |          | 11             |                 | 2.5                        |
| 16 August, 7:00     | MAKET    | 5              | 2               | 2                          |
| 8:47                |          | 6              |                 | 1.7                        |
| 23 August, 17:13    | MAKET    | 10             | 2               | 1.7                        |
| 17:39               | MAKET    | 3              |                 | 3.1                        |
| 24 August, 15:34    | MAKET    | 8              | 1               | 2.1                        |
| 26 August, 9:55     | MAKET    | 10             | 2               | 2.8                        |
| 10:50               |          | 7              |                 | 6.3                        |
| 18 September, 10:53 | MAKET    | 6              | 3               | 2                          |
| 11:15               |          | 9              |                 | 2.8                        |
| 11:33               |          | 17             |                 | 3.1                        |
| 25 September, 19:11 | MAKET    | 9              | 1               | 2.1                        |

tors of 1 m<sup>2</sup> area and 5 cm thick with a 20 cm thick and 0.25 m<sup>2</sup> area scintillator in between. A scintillator light capture cone and photomultiplier tubes are located on the top, bottom, and inter-mediate layers of the detector. Incoming neutral particles undergo nuclear reactions in the thick

20 cm plastic scintillator and produce protons and other charged particles. In the upper 5-cm thick scintillator, charged particles are registered very effectively; however, for the nuclear or photonuclear interactions of neutral particles there is not enough substance. When a neutral

Table 3.2  
Characteristics of TGEs registered at Aragats in 2010.

| Date, time 2010    | Detector | Duration (min) | Number of peaks | Percent of enhancement (%) |   |     |
|--------------------|----------|----------------|-----------------|----------------------------|---|-----|
| 1 October, 0:54    | MAKET    | 8              | 2               | 2.3                        |   |     |
| 12:31              |          | 3              |                 | 1.9                        |   |     |
| 3 October, 4:17    | MAKET    | 7              | 3               | 2.3                        |   |     |
| 4:28               |          | 11             |                 | 3.7                        |   |     |
| 4:41               |          | 11             |                 | 3.4                        |   |     |
| 4 October, 5:50    | MAKET    | 11             | 9               | 2.1                        |   |     |
| 6:32               |          | 5              |                 | 3.9                        |   |     |
| 8:33               |          | 5              |                 | 2                          |   |     |
| 11:48              |          | 13             |                 | 2.7                        |   |     |
| 11:57              |          | 5              |                 | 2.3                        |   |     |
| 18:22              |          | 7              |                 | 98.1                       |   |     |
| 20:28              |          | 12             |                 | 2.3                        |   |     |
| 22:23              |          | 3              |                 | 1.2                        |   |     |
| 22:45              |          | 13             |                 | 4.9                        |   |     |
| 5 October, 1:18    |          | MAKET          |                 | 8                          | 8 | 2.3 |
| 3:07               |          |                |                 | 8                          |   | 3.3 |
| 8:26               | 6        |                | 3.5             |                            |   |     |
| 13:34              | 11       |                | 4.9             |                            |   |     |
| 14:57              | 4        |                | 2.4             |                            |   |     |
| 16:04              | 10       |                | 2.3             |                            |   |     |
| 16:14              | 10       |                | 3.1             |                            |   |     |
| 16:39              | 5        |                | 2.6             |                            |   |     |
| 6 October, 7:48    | MAKET    | 23             | 3               | 5.8                        |   |     |
| 9:46               |          | 6              |                 | 3.9                        |   |     |
| 14:34              |          | 8              |                 | 3.2                        |   |     |
| 10 October, 10:19  | MAKET    | 10             | 1               | 14.3                       |   |     |
| 15 October, 12:07  | MAKET    | 12             | 2               | 3.6                        |   |     |
| 13:40              |          | 11             |                 | 4.7                        |   |     |
| 16 October, 8:42   | MAKET    | 8              | 1               | 2.7                        |   |     |
| 17 October, 14:26  | MAKET    | 12             | 3               | 5                          |   |     |
| 14:40              |          | 6              |                 | 5.2                        |   |     |
| 14:45              |          | 10             |                 | 4.2                        |   |     |
| 12 December, 16:08 | MAKET    | 12             | 1               | 10.2                       |   |     |

particle traverses the top thin (5 cm) scintillator, usually no signal is produced. The absence of the signal in the upper scintillators, coinciding with the signal in the middle scintillator, points to neutral particle detection (gamma ray or neutron). The coincidence of signals from the top and bottom scintillators indicates the traversal of high-energy muons, traversing 10 cm of lead (minimal energy is about 250 MeV).

“STAND” detector (Arakelyan et al., 2013), exclusively designed for the TGE research comprise of three-layer assembly of 1 cm thick 1 m<sup>2</sup> sensitive area molded plastic scintillators one above the other and one 3 cm thick scintillator located aside. Outdoors location, 1-cm thickness and three-layer design allow to measure flux of TGE electrons with 3 different energy thresholds starting from 1.5 MeV and to recover integral spectrum of TGE electrons. Proper tuning of the detector provides 98-99% signal detection efficiency simultaneously suppressing electronic noise down to 1–2%. The DAQ electronics allows measuring and storing all coincidences of the detector channel operation. For instance, coincidence “111” means that all 3 layers register particle, minimal energy of charged particles giving signal

in all 3 layers should be above 10 MeV; coincidence “100” means that only upper detector register particle – the energy threshold of this coincidence is equal ~1.5 MeV. The energy threshold of 3 cm thick scintillators is ~5 MeV.

The Nor Amberd multidirectional muon monitor (NAMMM) consists of two layers of plastic scintillators above and below two of the three sections of the Nor Amberd Neutron Monitor (NANM) 18NM64 (Carmichael, 1964). The lead (Pb) filter of NANM absorbs electrons and low energy muons. The distance between layers is ~1 m. Each layer consists of six detectors of 0.81 m<sup>2</sup> area. NAMMM is hybrid detector measuring neutral and charged CR fluxes. Upper layer of detector measures low energy charged particles, mostly electrons and muons. The energy threshold of the upper scintillators is approximately equal to 7 MeV. Neutron monitor is measuring the secondary neutrons of the cosmic ray flux. The lower layer of the scintillators of NAMMM is sensitive to high-energy muons, since the lead filter absorbs low energy muons and electrons. The energy threshold of the lower scintillators is equal approximately to 250 MeV.

The amplitude of TGE was measured at maximal flux minute relative to the mean value of detector minutely count rate before TGE event started. The enhancement was accepted as genuine TGE only if it was observed by as minimum with 3 independent detectors and the amplitude of signal in each of detectors exceeds 3 standard deviations. Additional necessary condition is large disturbance of the near-surface electrical field.

However, as was discussed in Dwyer et al. (2012a), measurements based solely upon count rates of signals above some discriminator threshold should be viewed with caution, since it is not obvious what is being counted, pulses from energetic particles or, for instance, RF noise from atmospheric discharge processes. To answer if the enhancements in particle detector count rates (peaks in minutely time series) can be due to electromagnetic inferences, we performed in-depth analysis of the enhancements of the ASEC detectors and for each TGE collect evidence demonstrating the existence of the indisputable additional particle fluxes responsible for the detected peaks (see details in the appendix of Chilingarian et al., 2011):

- The distance between AMMM and MAKET detectors is 400 m, detectors operate with fully independent cabling and data acquisition electronics (DAQ), and demonstrate very similar time-coherent patterns of flux enhancements;
- Along with count rates the ASNT DAQ electronics also register energy deposit spectra of PM signals. The TGEs are concentrated only in the region of the small energy deposits. The large energy deposits due to cosmic rays remain unchanged;
- The ASNT detector measures also the incoming directions of the detected particles. The count rates of the near vertical and inclined particles are dramatically dif-

Table 4.1  
Characteristics of TGEs registered at Aragats in 2011.

| Date, Time2011      | Detector | Duration (min) | Number of peaks | Percent of enhancement (%) |
|---------------------|----------|----------------|-----------------|----------------------------|
| 4 May, 14:27        | MAKET    | 5              | 2               | 4.3                        |
| 14:34               |          | 6              |                 | 4.5                        |
| 5 May, 4:43         | MAKET    | 20             | 1               | 2.1                        |
| 7 May, 15:1821:12   | MAKET    | 20             | 2               | 4.2                        |
|                     |          | 10             |                 | 4.1                        |
| 8 May, 1:47         | MAKET    | 18             | 3               | 6.8                        |
| 10:06               |          | 22             |                 | 6.3                        |
| 12:50               |          | 6              |                 | 4.9                        |
| 9 May, 7:44         | MAKET    | 10             | 2               | 2.5                        |
| 9:31                |          | 12             |                 | 5.7                        |
| 13 May, 10:10       | MAKET    | 11             | 3               | 4.5                        |
| 10:22               |          | 1              |                 | 3.9                        |
| 10:27               |          | 11             |                 | 5.1                        |
| 18 May, 22:11       | MAKET    | 16             | 1               | 5.3                        |
| 21 May, 11:57       | MAKET    | 8              | 5               | 8.4                        |
| 12:03               |          | 9              |                 | 9.8                        |
| 14:36               |          | 10             |                 | 5                          |
| 15:06               |          | 12             |                 | 3.4                        |
| 20:38               |          | 10             |                 | 2.6                        |
| 22 May, 15:15       | MAKET    | 9              | 1               | 4.2                        |
| 24 May, 13:31       | MAKET    | 13             | 2               | 3.2                        |
| 13:45               |          | 7              |                 | 2.3                        |
| 25 May, 19:07       | MAKET    | 19             | 1               | 1.4                        |
| 27 May, 13:14       | MAKET    | 12             | 1               | 21                         |
| 4 June, 1:45        | MAKET    | 4              | 1               | 6.5                        |
| 7 June, 14:24       | MAKET    | 3              | 1               | 2.5                        |
| 8 June, 11:55       | MAKET    | 14             | 1               | 2                          |
| 9 June, 15:49       | MAKET    | 3              | 2               | 1.7                        |
| 16:08               |          | 2              |                 | 1.5                        |
| 11 June, 11:54      | MAKET    | 6              | 1               | 2.7                        |
| 12 June, 10:03      | MAKET    | 27             | 1               | 4.3                        |
| 10 July, 22:12      | MAKET    | 9              | 1               | 2.5                        |
| 11 July, 7:46       | MAKET    | 10             | 3               | 2.4                        |
| 8:29                |          | 3              |                 | 2.2                        |
| 9:53                |          | 6              |                 | 2.3                        |
| 13 July, 1:09       | MAKET    | 9              | 2               | 3.7                        |
| 6:29                |          | 16             |                 | 2.6                        |
| 15 July, 21:29      | MAKET    | 9              | 1               | 2.4                        |
| 19 July, 20:11      | MAKET    | 11             | 1               | 3.5                        |
| 22 July, 6:37       | MAKET    | 3              | 1               | 2.4                        |
| 23 July, 13:31      | MAKET    | 8              | 2               | 4.3                        |
| 13:50               |          | 13             |                 | 2.9                        |
| 16 August, 15:49    | MAKET    | 12             | 1               | 1.5                        |
| 18 August, 15:20    | MAKET    | 19             | 2               | 3.9                        |
| 17:34               |          | 8              |                 | 2.1                        |
| 19 August, 12:20    | MAKET    | 8              | 1               | 3.1                        |
| 21 August, 11:31    | MAKET    | 3              | 1               | 2.6                        |
| 22 August, 22:19    | MAKET    | 15             | 1               | 8.4                        |
| 3 September, 15:52  | MAKET    | 15             | 3               | 2.6                        |
| 16:57               |          | 17             |                 | 2.2                        |
| 17:16               |          | 6              |                 | 0.8                        |
| 15 September, 16:01 | MAKET    | 16             | 1               | 3.1                        |

ferent. If we observe huge enhancement in the near vertical direction (expected arrival direction of the TGE particles), in the same time the same detector using the same DAQ electronics and analysis software do not measure any enhancement in the inclined particle flux;

- SEVAN particle detector measures 3 types of particle fluxes: low energy charged particles, neutral particles and high-energy muons ( $E_\mu > 250$  MeV). During several

TGEs we measure deficit of muons and huge peaks in time series of neutral particles and low energy charged particles. All 3 types of particle fluxes are detected by SEVAN detector with one and the same cabling and DAQ electronics.

Nonetheless, we detect some induced signals in a few from hundreds channels of the ASEC detectors. Some of

Table 4.2  
Characteristics of TGEs registered at Aragats in 2011.

| Date, time 2011     | Detector    | Duration (min) | Number of peaks | Percent of enhancement (%) |
|---------------------|-------------|----------------|-----------------|----------------------------|
| 20 September, 9:08  | STAND1 3 cm | 15             | 3               | 2.9                        |
| 10:28               |             | 11             |                 | 3                          |
| 13:58               |             | 22             |                 | 5                          |
| 24 September, 16:14 | STAND1 3 cm | 35             | 1               | 25.7                       |
| 25 September, 11:37 | STAND1 3 cm | 24             | 1               | 8                          |
| 28 September, 3:50  | STAND1 3 cm | 7              | 1               | 4.7                        |
| 30 September, 13:00 | STAND1 3 cm | 15             | 2               | 6.6                        |
| 13:26               |             | 8              |                 | 5.7                        |
| 3 October, 8:48     | STAND1 3 cm | 8              | 1               | 3.5                        |
| 13 October, 5:24    | STAND1 3 cm | 4              | 3               | 2.7                        |
| 5:30                |             | 6              |                 | 2.5                        |
| 11:37               |             | 16             |                 | 22.4                       |
| 16 October, 0:12    | STAND1 3 cm | 8              | 1               | 14.9                       |
| 17 October, 13:55   | STAND1 3 cm | 20             | 1               | 6.9                        |
| 19 October, 7:18    | STAND1 3 cm | 10             | 1               | 10.1                       |

Table 5  
Characteristics of TGEs registered at Aragats in 2012.

| Date, time 2012  | Detector    | Duration (min) | Number of peaks | Percent of enhancement (%) |
|------------------|-------------|----------------|-----------------|----------------------------|
| 5 April, 20:53   | MAKET       | 15             | 1               | 1.7                        |
| 8 April, 0:51    | STEND1 3 cm | 12             | 1               | 2.6                        |
| 9 April, 2:32    | MAKET       | 15             | 2               | 2                          |
| 3:01             |             | 22             |                 | 1.6                        |
| 19 April, 11:52  | MAKET       | 16             | 4               | 3.1                        |
| 11:56            |             | 5              |                 | 2.1                        |
| 13:00            |             | 11             |                 | 1.3                        |
| 13:16            |             | 9              |                 | 2.3                        |
| 28 April, 11:33  | MAKET       | 20             | 2               | 1.6                        |
| 12:16            |             | 8              |                 | 1.3                        |
| 29 April, 12:58  | MAKET       | 15             | 2               | 5.2                        |
| 14:02            |             | 12             |                 | 1.5                        |
| 11 May, 3:02     | STEND1 3 cm | 17             | 1               | 46.4                       |
| 12 May, 18:33    | STAND1 3 cm | 8              | 1               | 17.1                       |
| 13 May, 19:22    | STAND1 3 cm | 22             | 1               | 19.1                       |
| 20 May, 22:22    | STAND1 3 cm | 10             | 1               | 3.2                        |
| 22 May, 7:26     | STAND1 3 cm | 13             | 2               | 8.3                        |
| 7:36             |             | 9              |                 | 2.8                        |
| 25 May, 2:32     | STAND1 3 cm | 11             | 1               | 30.3                       |
| 26 May, 10:22    | STAND1 3 cm | 9              | 1               | 13.2                       |
| 29 May, 13:56    | STEND1 3 cm | 9              | 2               | 1.9                        |
| 14:03            |             | 7              |                 | 3                          |
| 29 June, 15:19   | AMMM        | 14             | 1               | 2.6                        |
| 30 June, 9:22    | STAND1 3 cm | 19             | 3               | 4.3                        |
| 9:56             |             | 11             |                 | 6                          |
| 10:10            |             | 10             |                 | 3.6                        |
| 3 July, 16:44    | STAND1 3 cm | 32             | 1               | 12.8                       |
| 8 July, 19:03    | STAND1 3 cm | 4              | 3               | 5.2                        |
| 19:30            |             | 17             |                 | 37.4                       |
| 20:04            |             | 20             |                 | 9.2                        |
| 10 July, 1:43    | STAND1 3 cm | 17             | 2               | 3                          |
| 2:59             |             | 9              |                 | 4.2                        |
| 4 October, 18:12 | STAND1 3 cm | 18             | 3               | 4.7                        |
| 18:48            |             | 10             |                 | 4.3                        |
| 19:33            |             | 3              |                 | 3.4                        |
| 7 October, 14:12 | STAND1 3 cm | 17             | 2               | 10.8                       |
| 15:09            |             | 15             |                 | 27.7                       |
| 8 October, 14:37 | STAND1 3 cm | 14             | 4               | 6.9                        |
| 16:56            |             | 11             |                 | 16                         |
| 17:35            |             | 17             |                 | 1.8                        |
| 21:20            |             | 19             |                 | 7.1                        |
| 9 October, 11:36 | STAND1 3 cm | 11             | 1               | 4.6                        |

Table 6  
Characteristics of TGEs registered at Nor Amberd in 2008–2012.

| Date, time (2008–2012)    | Detector | Duration (min) | Number of peaks | Percent of enhancement |
|---------------------------|----------|----------------|-----------------|------------------------|
| 14 March, 2008, 12:42     | NAMMM    | 4              | 1               | 2.97                   |
| 09 May, 2008, 11:40       | NAMMM    | 12             | 1               | 2.47                   |
| 11 May, 2008, 13:08       | NAMMM    | 4              | 1               | 1.33                   |
| 24 February, 2009, 17:35  | NAMMM    | 10             | 1               | 3.89                   |
| 24 March, 2009, 10:40     | NAMMM    | 2              | 1               | 3.25                   |
| 28 March, 2009, 13:41     | NAMMM    | 9              | 4               | 5.94                   |
| 14:55                     |          | 11             |                 | 2.17                   |
| 17:16                     |          | 7              |                 | 3.13                   |
| 17:50                     |          | 8              |                 | 5.5                    |
| 25 May, 2009, 12:15       | NAMMM    | 13             | 1               | 3.57                   |
| 09 June, 2009, 11:34      | NAMMM    | 7              | 1               | 1.74                   |
| 27 September, 2009, 22:30 | NAMMM    | 7              | 2               | 1.76                   |
| 23:00                     |          | 17             |                 | 2.59                   |
| 25 January, 2010, 13:19   | NAMMM    | 14             | 1               | 6.47                   |
| 16 February, 2010, 22:15  | NAMMM    | 8              | 1               | 5.35                   |
| 22 February, 2010, 3:00   | NAMMM    | 10             | 1               | 7.35                   |
| 30 March, 2010, 19:41     | NAMMM    | 23             | 1               | 5.24                   |
| 20 May, 2010, 17:34       | NAMMM    | 16             | 1               | 2.7                    |
| 11 March, 2011, 15:50     | NAMMM    | 12             | 1               | 3.28                   |
| 10 June, 2011, 22:28      | NAMMM    | 1              | 1               | 1.69                   |

Table 7  
Characteristics of TGE registered at Yerevan in 2013.

| Date, time 2013        | Detector | Duration (min) | Number of peaks | Percent of enhancement |
|------------------------|----------|----------------|-----------------|------------------------|
| 8 January, 2013, 04:14 | SEVAN    | 14             | 1               | 3.8                    |

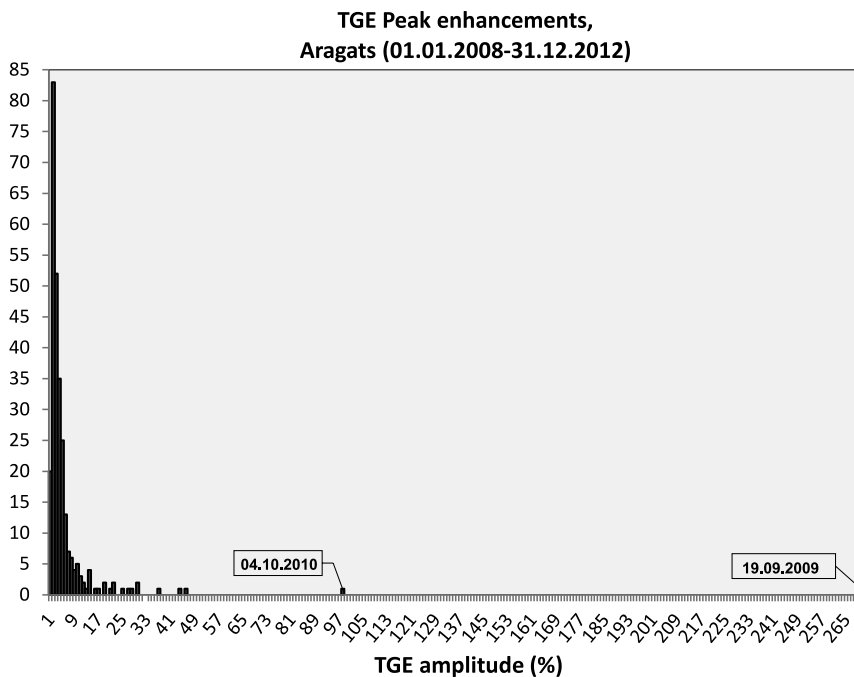


Fig. 1. The histogram of TGE amplitudes registered at Aragats in 2008–2012.

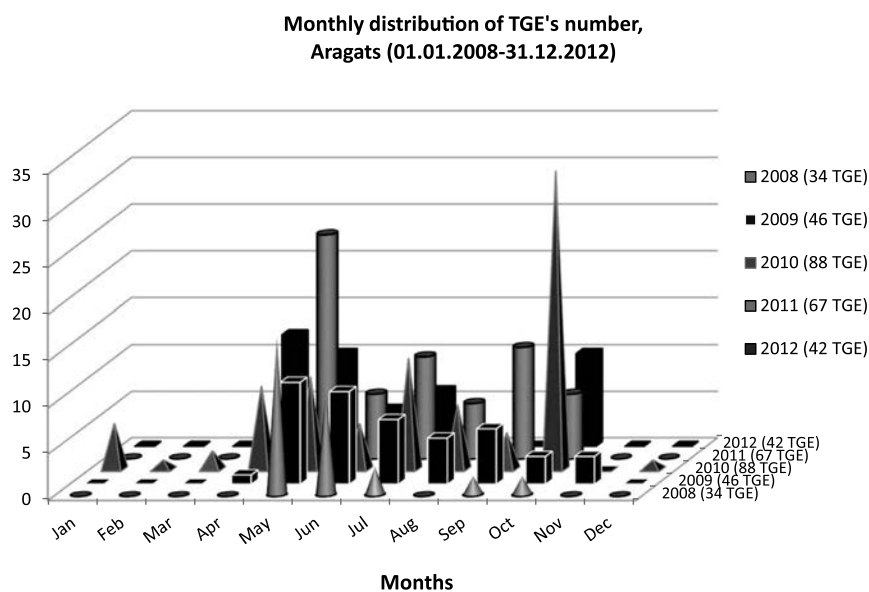


Fig. 2. The monthly distribution of TGE events registered at Aragats in 2008–2012.

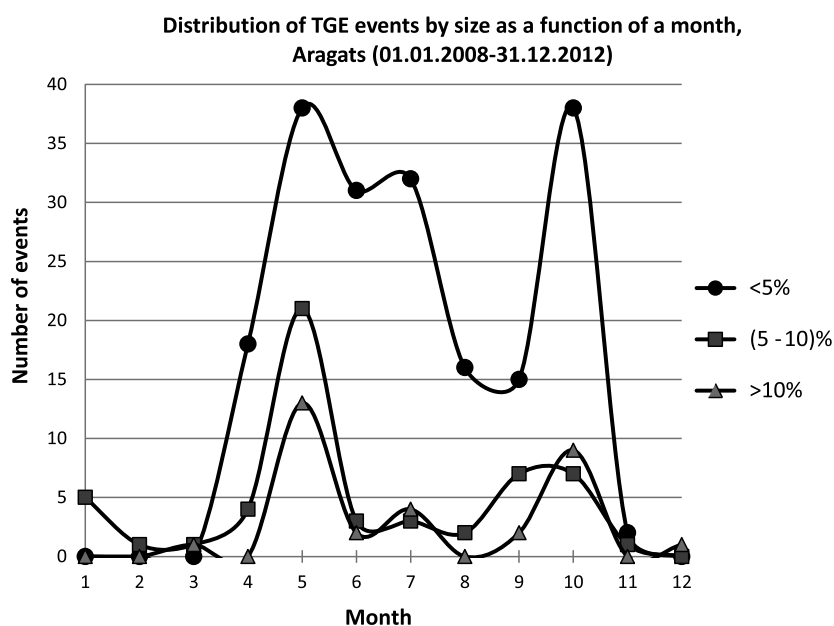


Fig. 3. Distribution of TGE events by enhancement size at Aragats in 2008–2012.

detectors were bad grounded, or some of cables had bad isolation and the radio signals from atmospheric discharges induced peaks in these channels. Lightning induced signals have very specific shape and follow the pattern of the lightning activity, now also monitored by the BOLTEK company lightning detectors. Due to strictly different duration of TGEs (tens of minutes) and atmospheric discharges (hundreds of milliseconds) it is very easy to outline fake peaks in the time series of particle detectors. Moreover during TGEs the lightning activity strictly decreases and

most powerful cloud-to-ground lightnings are suppressed (Chilingarian and Mkrtychyan, 2012).

### 3. Statistical analysis of the registered TGEs

In 2008–2012 at Aragats were registered 277 TGEs. For estimating the amplitude of TGEs we use identical 5 cm thick 1 m<sup>2</sup> area outdoor plastic scintillators of MAKET and AMMM detectors. In 2012 the data from 3 cm thick outdoor plastic scintillator was used due to failure of

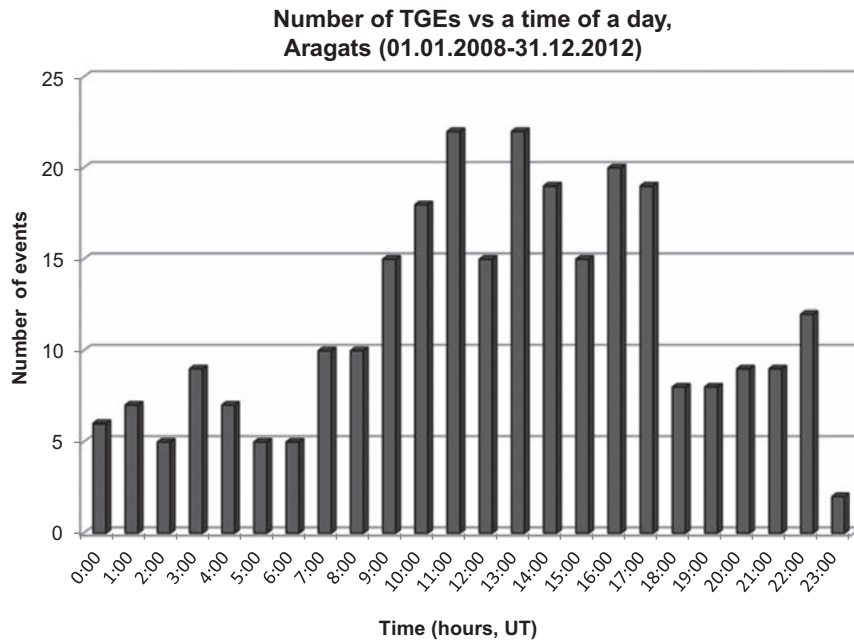


Fig. 4. Distribution of TGE events as a function of a time of a day at Aragats in 2008–2012.

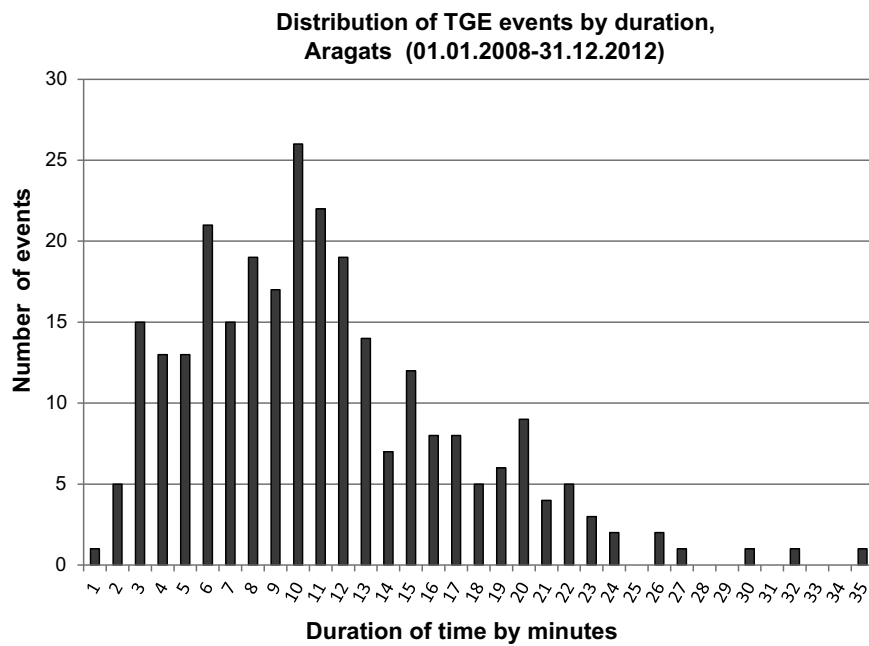


Fig. 5. Distribution of TGE events by duration at Aragats in 2008–2012.

MAKET and AMMM detectors after strong lightning. The flux enhancement is presented by percent relative to rather stable background of secondary cosmic rays. As we can see from Fig. 1 the majority of TGEs have amplitudes less than 10%. The dates of 2 largest TGE events are displayed as boxed text. The amplitude of TGE depends on many factors that are very difficult to measure or estimate. First of all it is structure and strength of elec-

tric field in the thundercloud. Starting from 2011 at all 3 sites the monitoring of the near surface electric field is performed with electric mills produced by the BOLTEK Company.<sup>1</sup> It allows outlining 4 patterns of electric field giving rise to TGEs (Chilingarian and Mkrtychyan, 2012). How-

<sup>1</sup> BOLTEK's electrical mill EFM-100, measurement accuracy 5%, details in <http://www.boltek.com/efm100.html>.

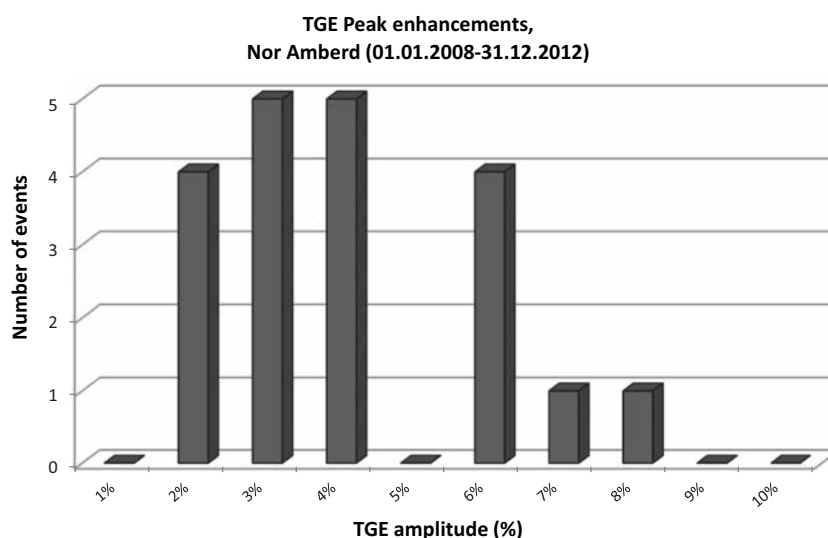


Fig. 6. The histogram of TGE amplitudes registered at Nor Amberd in 2008–2012.

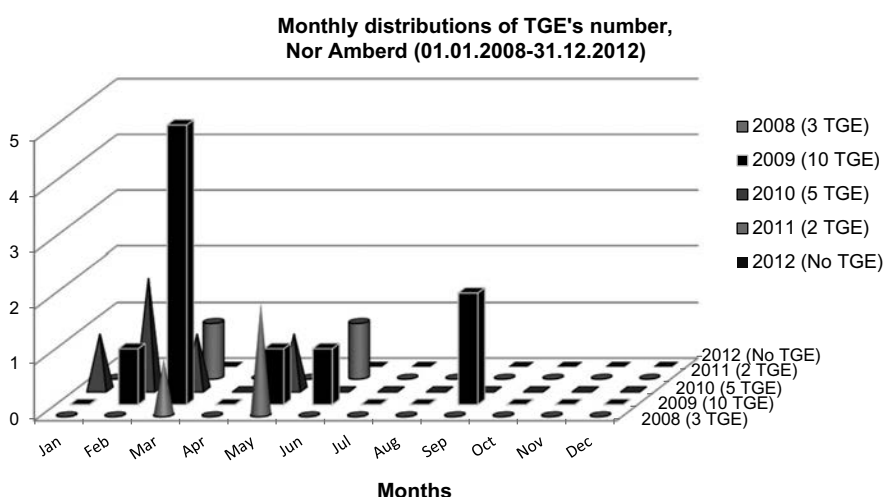


Fig. 7. The monthly distribution of TGE events registered at Nor Amberd in 2008–2012.

ever, although there should be a correlation between measured near-surface electric field and electric field in the thundercloud it is not possible to recover intracloud electric field by measurements of near surface field. Unknown parameters affecting the near surface electric field are the topology of electric field in the thundercloud and location of the cloud relative to detectors. We adopt the tripole structure of electric field with positive dipole between main negative charged layer in the middle of the thundercloud and smaller Lower Positive Charge Region (LPCR) sitting in the bottom of thundercloud. Lower dipole accelerates electrons downward, runaway electrons initiate cascades, and, if thundercloud low above the Earth's surface the particle detectors register enhancement of secondary cosmic

rays above stable background initiated by the ambient flux of galactic cosmic rays incident on the terrestrial atmosphere.

In the Fig. 2 we can observe 2 high frequency clusters of events on April–May and October (especially in 2010). These months coincide with maximum of thunderstorm activity at Aragats. However, even in January there were detected particle fluxes from thunderclouds. The distribution of TGEs by amplitude also demonstrates maximums in April–May and October (see Fig. 3); however, the largest events were detected in September 2009 and October 2010.

In the Fig. 4 we can see that TGEs mostly happen in day-evening time: from 9 till 17 UT (13–22 local time).

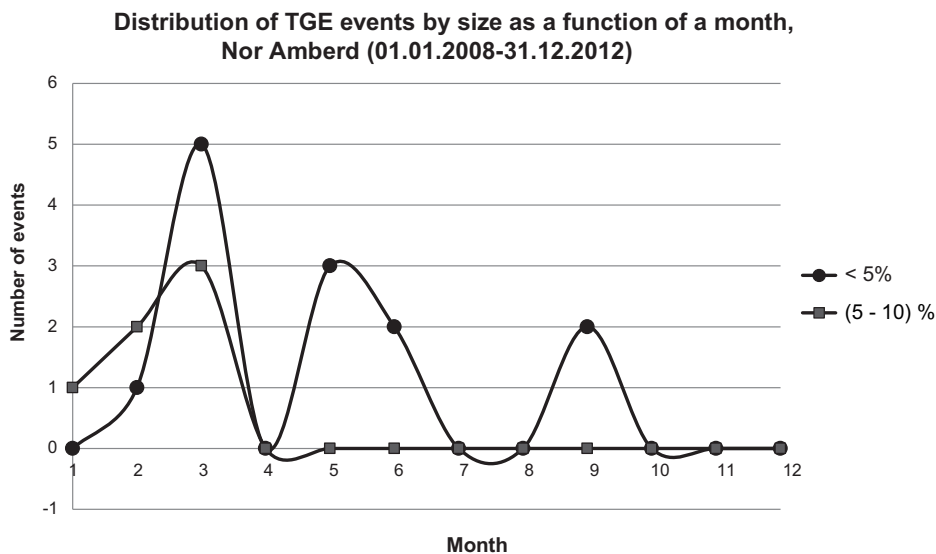


Fig. 8. Distribution of TGE events by enhancement size at Nor Amberd in 2008–2012.

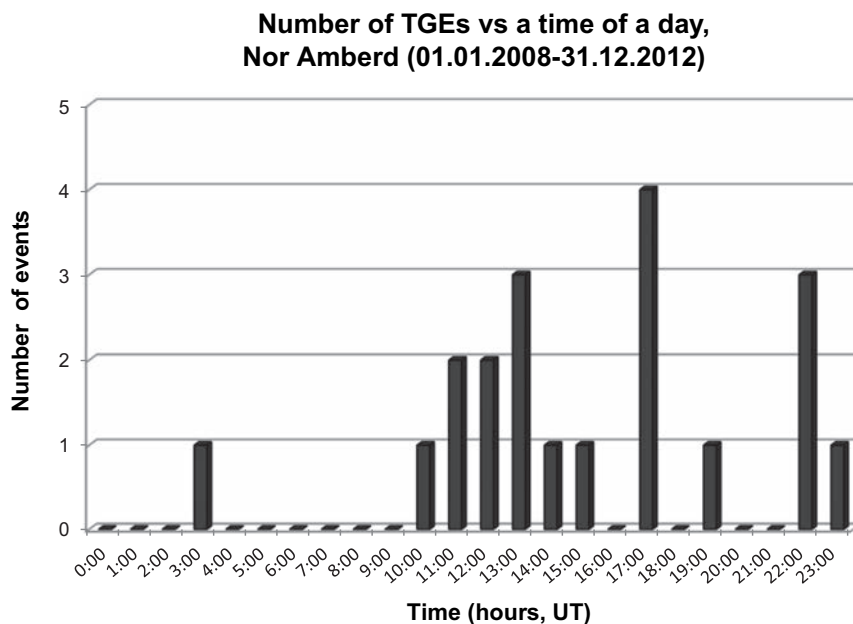


Fig. 9. Distribution of TGE events as a function of a time of a day at Nor Amberd in 2008–2012.

The mean duration of TGEs is ~10 min (see Fig. 5); sometimes it prolonged up to half-an-hour and more.

There are much less TGEs detected in Nor Amberd, comparing with Aragats. Although the thunderstorm activity in both locations is about the same, the topography of Nor Amberd destination doesn't allow thunderclouds to descend down near to detectors. Unlike Aragats station located on broad highland near large lake, Nor Amberd station is located near sharp uprising of mountain preventing low location of clouds.

At Nor Amberd by 5 cm thick scintillators detected only 20 TGEs in 2008–2012 (compare with 277 at Aragats in the same years). 14 events have amplitude lower than <5%, and 6 events – amplitude of above 5%. The maximal value of observed enhancements was 8.6%. In the observed years the most productive months were March and May. The maximum number of TGE events was detected in March 2009. In the Fig. 6 is presented the histogram of 20 TGEs' registered by 5 cm thick scintillators of NAMMM in 2008–2012.

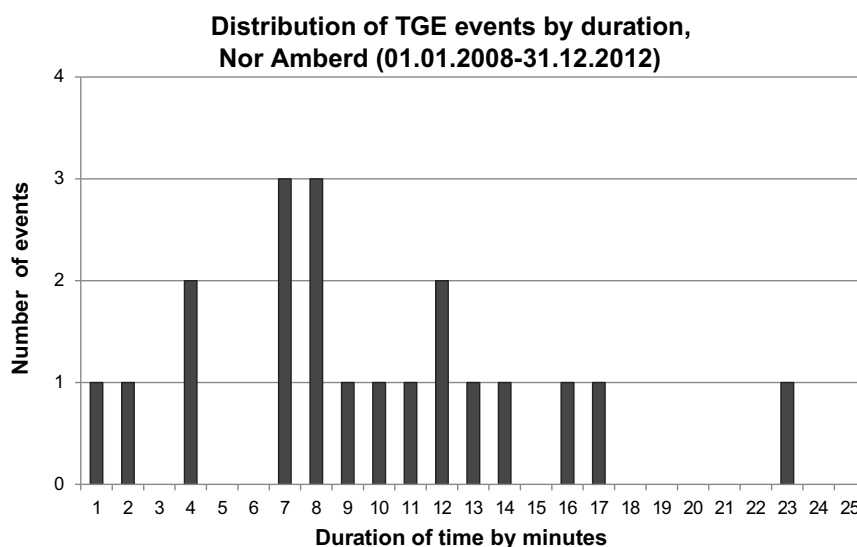


Fig. 10. Distribution of TGE events by duration at Nor Amberd in 2008–2012.

In the Fig. 7 we can detect high frequency of TGE events on March 2009. This month coincide with strong thunderstorm activity at Nor Amberd. However, even in January there were detected particle fluxes from thunderclouds.

The distribution of TGEs by amplitude demonstrates maximum in March (see Fig. 8).

The distribution of the daytime of Nor Amberd TGEs presented in Fig. 9, demonstrates that the most probable time is shifted to evening–night local times comparing with Aragats TGEs. The Fig. 10 demonstrates that mean duration of TGEs is  $\sim 10$  min compatible with duration of Aragats TGEs.

#### 4. Conclusion

In years of low solar activity 2008–2012 Aragats Space Environmental Center particle detectors located at Aragats, Nor Amberd and Yerevan have measured  $\sim 300$  Thunderstorm Ground Enhancements (TGEs), thus proving existence of the new high-energy phenomena in the terrestrial atmosphere.

Several papers were published based on the collected TGEs' exploring characteristics of emerging in thunderclouds electron, gamma ray and neutron fluxes (Chilingarian et al., 2010, 2011, 2012a,b; Chilingarian, Mailyan et al., 2012; Chilingarian and Mkrtchyan, 2012).

190 events from 277 at Aragats, have amplitude less than 5%, 55 events have amplitude between 5% and 10% and 32 events have amplitude greater than 10%. Only 13 TGEs have amplitude exceeding 20%. The maximal value of observed enhancement was 271% (September 19, 2009) and the minimal registered – 0.8%. In the observed years the most productive months were: May and June in 2008, May–July in 2009. The maximum number of TGE events

was detected in October 2010. TGEs at Aragats mostly happen in day-evening time: from 9 till 17 UT (13–22 local time). The mean duration of TGE is  $\sim 10$  min; sometimes it prolonged up to half-an-hour and more. 14 events from 20 at Nor-Amberd, have amplitude lower than  $<5\%$ , and 6 events – amplitude of  $5 \div 10\%$ . The maximal value of observed enhancement was 8.6% and minimal value was 1.33%. In the observed years the most productive months were March and May. The maximum number of TGE events was detected in March 2009. The most probable time is evening–night by local time and the mean duration of TGE is  $\sim 10$  minutes compatible with duration of Aragats TGEs. Amplitude of only one event registered at Yerevan is 3.8%. The duration of TGE was 14 min.

#### References

- Aglietta, M., Collaboration, E.A.S.-T.O.P., et al. The EAS-TOP array at  $E_0 = 1014\text{--}1016$  eV: stability and resolutions. Nucl. Instrum. Methods Phys. Res. Sect. A 277, 23–28, 1989.
- Alexeenko, V.V., Khaerdinov, N.S., Lidvansky, A.S., Petkov, V.B. Transient variations of secondary cosmic rays due to atmospheric electric field and evidence for pre-lightning particle acceleration. Phys. Lett. A 301, 299–306, [http://dx.doi.org/10.1016/S0375-9601\(02\)00981-7](http://dx.doi.org/10.1016/S0375-9601(02)00981-7), 2002.
- Arakelyan, K., et al. New low threshold detectors for measuring electron and gamma ray fluxes from thunderclouds. J. Phys.: Conf. Ser. 409, 012223, 2013.
- Babich, L.P., Donskoi, E.N., Kutsyk, I.M., Kudryavtsev, A.Y. New data on space and time scales of relativistic runaway electron avalanche for thunderstorm environment: Monte Carlo calculations. Phys. Lett. A 245, 460–470, 1998.
- Babich, E.I., Bochkov, I.M., Kutsyk, A.N., Zalyalov, Published in Pis'ma v Zhurnal Eksperimental'noi i Teoreticheskoi Fiziki 2013, 97(6), pp. 333–339; JETP Lett. 2013, 97(6), pp. 291–296. © Pleiades Publishing, Inc., 2013.
- Brunetti, M., Cecchini, S., Galli, M., Giovannini, G., Pagliarini, A. Gamma-ray bursts of atmospheric origin in the MeV energy range.

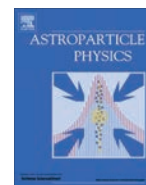
- Geophys. Res. Lett. 27 (11), 1599–1602. Article No. 2000GL003750, 2000.
- Bucik, R., Kudela, K., Kuznetsov, S.N. Satellite observations of lightning-induced hard X-ray flux enhancements in the conjugate region. *Ann. Geophys.* 24, 1969–1976, 2006.
- Carmichael, H., “Cosmic Rays”, (IQSY Instruction manual, #7) London, 1964.
- Chilingarian, A., Mkrtchyan, H. Role of the lower positive charge region (LPCR) in initiation of the thunderstorm ground enhancements (TGEs). *Phys. Rev. D* 86, 072003, 2012.
- Chilingarian, A., Reymers, A. Particle detectors in solar physics and space weather research. *Astropart. Phys.* 27, 465–472, 2007.
- Chilingarian, A. et al. *J. Phys. G* 29, 939, 2003.
- Chilingarian, A., Arakelyan, K., et al., Nor-Amberd multidirectional muon monitor: new detector for the world-wide network, in: *Proceedings of the 29th International Cosmic Ray Conference*, vol. 2. August 3–10, 2005a, Pune, India, p. 445, 2005a.
- Chilingarian, A. et al. *Nucl. Instrum. Methods Phys. Res. Sect. A* 543, 483, 2005b.
- Chilingarian, A., Hovsepyan, G., Garagezyan, G., et al. Study of extensive air showers and primary energy spectra by MAKET-ANI detector on mountain Aragats. *Astropart. Phys.* 28, 58–71, 2007.
- Chilingarian, A., Hovsepyan, G., Arakelyan, K., Chilingarian, S., Danielyan, V., Avakyan, K., Yeghikyan, A., Reymers, A., Tserunyan, S. Space environmental viewing and analysis network (SEVAN). *Earth Moon Planets* 104–1, 195, 2009.
- Chilingarian, A., Daryan, A., et al. Ground-based observations of thunderstorm-correlated fluxes of high-energy electrons, gamma rays, and neutrons. *Phys. Rev. D* 82, 043009, 2010.
- Chilingarian, A., Hovsepyan, G., Hovhannisyanyan, A. Particle bursts from thunderclouds: natural particle accelerators above our heads. *Phys. Rev. D* 83, 062001, 2011.
- Chilingarian, A., Bostanjyan, N., Vanyan, L. Neutron bursts associated with thunderstorms. *Phys. Rev. D* 85, 085017, 2012a.
- Chilingarian, A., Bostanjyan, N., Karapetyan, T., Vanyan, L. Remarks on recent results on neutron production during thunderstorms. *Phys. Rev. D* 86, 093017, 2012b.
- Chilingarian, A., Mailyan, B., Vanyan, L. *Atmos. Res.* 114–115, 1–16, 2012c.
- Chilingarian, A., Arakelyan, K., et al. Thunderstorm Ground Enhancements (TGEs) - New High- Energy Phenomenon Originated in the Terrestrial Atmosphere Correlated measurements of secondary cosmic ray fluxes by the Aragats Space Environmental Center monitors. *J. Phys.: Conf. Ser.* 409, 012222, 2013.
- Dorman, L.I., Dorman, I.V. Possible influence of cosmic rays on climate through thunderstorm clouds. *Adv. Space Res.* 35, 476–483, 2005.
- Dwyer, J.R. A fundamental limit on electric fields in air. *Geophys. Res. Lett.* 30 (20), 2055, 2003.
- Dwyer, J.R., Smith, D.M., Cummer, S.A. High-energy atmospheric physics: terrestrial gamma-ray flashes and related phenomena. *Space Sci. Rev.*, <http://dx.doi.org/10.1007/s11214-012-9894-0>, 2012a.
- Dwyer, J.R., Schaal, M.M., Cramer, E., Arabshahi, S., Liu, N., Rassoul, H.K., Hill, J.D., Jordan, D.M., Uman, M.A. Observation of a gamma-ray flash at ground level in association with a cloud-to-ground lightning return stroke. *J. Geophys. Res.* 117, A10303, <http://dx.doi.org/10.1029/2012JA017810>, 2012b.
- Eack, K.B., Suszcynsky, D.M., Beasley, W.H., Roussel-Dupre, R., Symbalisty, E.M.D. Gamma-ray emissions observed in a thunderstorm anvil. *Geophys. Res. Lett.* 27, 185–188, <http://dx.doi.org/10.1029/1999GL010849>, 2000.
- Fishman, G.J., Bhat, P.N., Mallozzi, R., Horack, J.M., Koshut, T., Kouveliotou, C., Pendleton, G.N., Meegan, C.A., Wilson, R.B., Paciasas, W.S., Goodman, S.J., Christian, H.J. Discovery of intense gamma ray flashes of atmospheric origin. *Science* 264 (5163), 1313–1316, 1994.
- Gurevich, A.V., Milikh, G.M., Roussel-Dupre, R.A. Runaway electron mechanism of air breakdown and preconditioning during a thunderstorm. *Phys. Lett. A* 165, 463, 1992.
- Halliday, E.C. The thundercloud as a source of penetrating particles. *Phys. Rev.* 60, 101–106, <http://dx.doi.org/10.1103/PhysRev.60.101.1941>.
- Khaerdinov, N.S., Lidvansky, A.S., Petkov, V.B. Cosmic rays and electric field of thunderclouds: evidence for acceleration of particles (runaway electrons). *Atmos. Res.* 76, 346–354, 2005.
- Lidvansky, A.S. The effect of the electric field of the atmosphere on cosmic rays. *J. Phys. G: Nucl. Part Phys.* 29, 925–937, 2003.
- Muraki, Y. et al. Effects of atmospheric electric fields on cosmic rays. *Phys. Rev. D* 69, 123010, 2004.
- Smith, D.M., Lopez, L.I., Lin, R.P., Barrington-Leigh, C.P. Terrestrial 492 gamma-ray flashes observed up to 20 MeV. *Science* 307, 1085–1088, 2005.
- Suszcynsky, D.M., Roussel-Dupre, R., Shaw, G. Ground-based search for X-rays generated by thunderstorms and lightning. *J. Geophys. Res.* 101, 23,505–23,516, <http://dx.doi.org/10.1029/96JD02134>, 1996.
- Torii, T., Takeishi, M., Hosono, T. Observation of gamma-ray dose increase associated with winter thunderstorm and lightning activity. *J. Geophys. Res.* 107, 4324, <http://dx.doi.org/10.1029/2001JD000938>, 2002.
- Torii, T., Sugita, T., Kamogawa, M., et al. Migrating source of energetic radiation generated by thunderstorm activity. *Geophys. Res. Lett.* 38, L24801, 2011.
- Tsuchiya, H., Enoto, T., Yamada, S., et al. Detection of high-energy gamma rays from winter thunderclouds. *Phys. Rev. Lett.* 99, 165002, 2007.
- Tsuchiya, H., Enoto, T., Yamada, S., et al. Long-duration gamma ray emissions from 2007 and 2008 winter thunderstorms. *J. Geophys. Res.* 116, D09113, 2011.
- Tsuchiya, H., Hibino, K., Kawata, K., et al. Observation of thundercloud-related gamma rays and neutrons in Tibet. *Phys. Rev. D* 85, 092006, 2012.
- Wilson, C.T.R. The acceleration of b-particles in strong electric fields such as those of thunderclouds. *Proc. Cambridge Philos. Soc.* 22, 534, 1925.



Contents lists available at SciVerse ScienceDirect

## Astroparticle Physics

journal homepage: [www.elsevier.com/locate/astropart](http://www.elsevier.com/locate/astropart)



# Observation of Thunderstorm Ground Enhancements with intense fluxes of high-energy electrons



Ashot Chilingarian, Levon Vanyan, Bagrat Mailyan\*

Yerevan Physics Institute, Cosmic Ray Division, Yerevan, Armenia

### ARTICLE INFO

#### Article history:

Received 1 April 2013  
 Received in revised form 4 June 2013  
 Accepted 17 June 2013  
 Available online 27 June 2013

#### Keywords:

Secondary cosmic rays  
 Atmospheric electricity  
 Particle detectors

### ABSTRACT

The high altitude (~3200 m above sea level) of Aragats Space Environmental Center (ASEC) and low elevation of the thunderclouds provides a good opportunity to detect Thunderstorm Ground Enhancements (TGEs), particles of which rapidly attenuate in the atmosphere. In 2012, we have estimated the energy spectra of several TGEs and revealed significant electron fluxes extended till 30–40 MeV. Measured in the one and the same event gamma ray and electron fluxes allow to estimate the height of the thundercloud above the detector. Proceeding from the energy spectra and the height of the cloud we estimate the electron spectra on the exit from the electric field of the thundercloud, the number of excess electrons in the cloud and avalanche multiplication rate.

© 2013 Elsevier B.V. All rights reserved.

## 1. Introduction

Thunderstorm Ground Enhancements (TGEs) are direct proof of the high-energy phenomena in the terrestrial atmosphere; see review by Dwyer et al. [15] and references therein.

The origin of a TGE is a strong electrical field in a thundercloud, giving rise to rather complicated physical processes, including the following phenomena:

- Relativistic Runaway Electron Avalanches (RREA, [25,17,3,14,18]);
- Modification of the Secondary cosmic ray (electrons, muons, protons and charged mesons) energy spectra (MOS, [13,20]);
- Photonuclear reactions of the RREA gamma rays [10,11,24,4];
- Roentgen and gamma radiation from the lightning [16].

The direct measurement of the RREA by extended surface array of plastic scintillators was performed at Aragats in 2009 [8]. Largest TGEs consist of multiple individual electron/gamma ray avalanches. However, the electron fluxes are very difficult to study due to fast attenuation in the lower atmosphere, till now only for one TGE event it was possible to estimate the electron energy spectrum and calculate avalanche multiplication rate [7,9].

On October 7, 2012 a TGE consisting of two peaks at 14:11 and 15:08 was detected at Aragats Space Environmental Center (ASEC; [5,19]). Different types of the detector assembly operating on Ara-

gats, quipped with sophisticated coincidences techniques, allowed performing electron/gamma ray separation and proving the existence of the large fraction of the high-energy electron flux at 15:08. At 14:11 TGE mainly consists of enhanced gamma ray flux, as the most of TGEs detected at ASEC and worldwide. Because of very fast attenuation of electrons in the atmosphere, usually TGE gamma ray flux significantly exceeds the electron flux; only for very low thunderclouds it is possible to detect electron flux. Thus, even for very low efficiencies of gamma ray registration the gamma ray contamination can be sizable in the overall TGE. To overcome this difficulty, we use in our analysis data from numerous ASEC particle detectors. Among these detectors are STAND3 layered detector and hybrid<sup>1</sup> ASNT (Aragats Solar Neutron Telescope, [6] and Cube detectors [2]. First we will analyze the STAND3 data, for distinguishing the high-energy electrons. Thereafter, we double check for the presence of significant electron fluxes using ASNT data. ASNT data also allows estimating the gamma ray flux. Based on these measurements and assumed spectral shape of the gamma ray flux we decide if the high-energy electrons were detected or only large fluxes of TGE gamma rays are responsible for the detector count rate enhancement. Finally, the estimated flux will be checked with Cube detector data, which allows selecting the neutral component of TGE flux. If the results from these 3 different detectors are consistent, we apply procedures of energy spectra recovery (see details in [9] and get gamma ray and electron energy spectra.

\* Corresponding author. Tel./fax: +374 10 34 47 36.  
 E-mail address: [mbagrat@gmail.com](mailto:mbagrat@gmail.com) (B. Mailyan).

<sup>1</sup> Hybrid detectors consist from thick and thin plastic scintillators and due to sophisticated DAQ electronics are sensitive to both charged and neutral fluxes.

## 2. Experimental data of the October 7, 2012 TGE

The new generation of ASEC detectors comprises from 1 and 3 cm thick molded plastic scintillators arranged in stacks (STAND1 and STAND3 detectors) and in cubical structures surrounding thick scintillators and NaI crystals for purification of detected neutral flux (Cube1 and Cube3 detectors). Light from the scintillators is reradiated by optical spectrum-shifter fibers to the long-wavelength region and passed to the FEU-115 M type photomultiplier (PM). Maximum of luminescence is on about 420 nm wavelength and luminescence time is about 2.3 ns [27]. The tuning of STAND detectors consists in selections of PM high voltage and signal discrimination threshold. The threshold is chosen to guarantee both high efficiency of signal detection and maximal suppression of the electronics noise. Tuning of STAND was made by means of the 8-channel signal analyzer developed at ASEC for online data processing [1]. Proper tuning of the detector provides 98–99% signal detection efficiency simultaneously suppressing electronic noise down to 1–2%. The data acquisition (DAQ) electronics measures and stores all coincidences of the signal appearance in the detector channels. Coincidence “1000” corresponds to signal registration only from upper scintillator, “1100” – from the first two upper scintillators, and so on. GEANT4 simulations demonstrate that STAND3 detector (see Fig. 1), can measure count rate of incident electrons with energy thresholds 5, 15, 25, 35 MeV (combinations “1000”, “1100”, “1110” and “1111”). The 5 MeV electrons can give signal above the discrimination level only in the upper scintillator, to be absorbed then in the scintillator body, or in the metallic tilts of scintillator housing; the 15 MeV electrons can penetrate and be registered also in the second scintillator, and so on. In this way, measuring the enhancements of count rates of above mentioned 4 combinations of detector layer operation we can recover the integral energy spectra of TGE electrons, of course, after subtracting the gamma ray contamination. The peaks of October 7, 2012 TGE measured by the layers of STAND3 detector are shown in the Fig. 2. The increases of the maximal minute count rate corresponding to various coincidences of STAND3 are shown in Table 1 in standard deviations of the measurements (number of  $\sigma$ ).

As we can see in Table 1, at 15:08 October 7 2012, STAND3 detector registered high-energy electron TGE. Electrons with energies above 35 MeV can reach and be registered by the 1111 combination of STAND3 with efficiency dependent on energy. The efficiencies for electron detection by STAND3 detector are shown in Fig. 3. The electronics signal threshold<sup>2</sup> is  $\sim 3$  MeV, thus, all 4 STAND3 layers can detect gamma rays with energies greater than  $\sim 3$  MeV, although with much smaller registration efficiencies comparing with electron detection efficiencies. In Fig. 4, the gamma ray detection efficiencies by coincidences of STAND3 detector layers are shown. Gamma rays should have high enough energy to create high-energy charged particles, which can reach bottom layer (the gamma ray energy should be above 40 MeV to generate signal in all 4 layers with probability 1%).

Electrons with energies greater than 35 MeV will contribute to “1111” combination. In contrast, only a small fraction of high-energy gamma rays will be detected as “1111” combination. Therefore, we conclude that STAND3 data of “1111” combination proves the existence of the high-energy particles above 25 MeV at 15:08. Using GEANT 4 simulations and data from ASNT and Cube detectors we will find if there is a sizeable contamination from gamma rays.

In Fig. 5, ASNT detector consisting of upper 5 cm and lower 60 cm thick scintillator layers is depicted. Each layer consists of 4 scintillators and each scintillator has an area of  $1 \text{ m}^2$ . In Fig. 6,

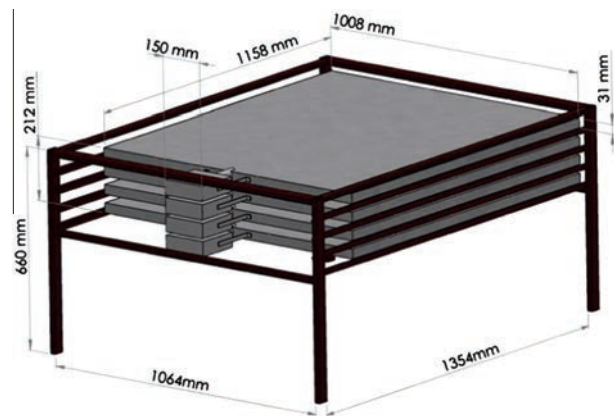


Fig. 1. STAND3 detector; each of 4 stacked horizontally plastic scintillators is 3 cm thick and  $1 \text{ m}^2$  area.

the gamma ray detection efficiencies of 5 cm and 60 cm scintillators are presented. Thicker is the scintillator more is the probability of gamma rays to interact and create charged particles, which will deposit their energy in the scintillator.

During October 7, 2012 TGE at 15:08, the increase detected by 5 cm scintillators of the ASNT detector was twice larger than that of 60 cm scintillators (see Table 2). However, the neutral particle detection efficiency of the thick scintillator is much higher; especially for the gamma rays with energies above 30 MeV (see Fig. 6). Taking into account energy losses in the material of the roof and the electronics threshold, the minimal energy of electrons should be  $\sim 15$  MeV to be measured by the 5 cm detector. Only electrons having energies above  $\sim 30$  MeV can pass through the roof and the upper 5 cm scintillator layer and be detected also by 60 cm scintillator (“11” coincidence).

Detected at 15:08 small increase was measured by ASNT vertical “11” coincidence – a simultaneous signal in both scintillators (see Table 2), the probability of gamma ray detection by this coincidence is vanishingly small (the efficiency of gamma ray detection is near zero at energies  $< 20$  MeV). The increase observed by ASNT vertical coincidence confirms the “electron” nature of TGE of 15:08.

In [9], we discussed and analyzed two largest TGEs of September 19, 2009 and October 4, 2010. The September 19, 2009 TGE has the largest ever detected electron intensity. The October 4, 2010 TGE has the largest ever detected gamma ray intensity, with small electron contamination. The ratio of the enhancements in 5 cm and 60 cm thick scintillators of ASNT on September 19 was  $\sim 4$  and on October 4  $\sim 2$ ; i.e. the largest “electron” TGE has 2 times larger ratio of thin/thick scintillator counts comparing with largest “gamma-ray” TGE. In this concern, it is worth mentioning that for the first peak detected at 14:11 October 7, 2012 the ratio of thin/thick is  $\sim 1.21$ , see Table 2; two times less than at 15:08. Therefore, greater is the ratio, larger is the fraction of electrons reaching the Earth’s surface.

Recovered electron/gamma ray ratios above the roof of the laboratory building for the energies above 10 MeV were estimated to be 0.6 and 0.007 for September 19, 2009 and October 4, 2010 TGEs respectively (see details in [9]).

The Cube assembly (Fig. 7) consists of two 20 cm thick scintillation detectors of  $0.25 \text{ m}^2$  area each surrounded by 1 cm thick  $1 \text{ m}^2$  area scintillators. This design ensures that no particle can hit the inside 20 cm detectors without passing through one of 1 cm scintillators. Both 20 cm thick plastic scintillators are overviewed by the PM FEU- 49 with large cathode, operating in low-noise mode.

<sup>2</sup> The threshold of the shaper-discriminator feed by the PM output.

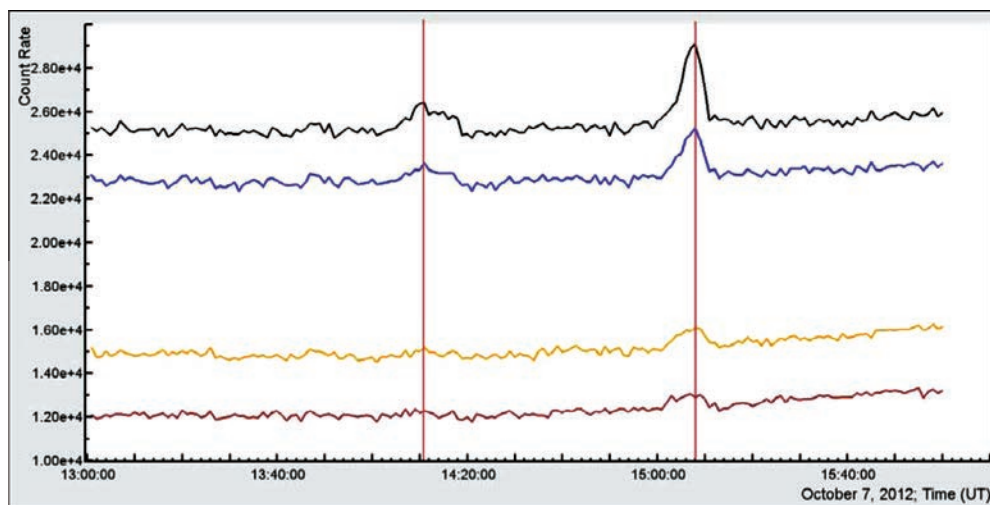


**Fig. 2.** Thunderstorm Ground Enhancements of October 7, 2012 measured by STAND3 detector; the higher count rate corresponds to the upper position of scintillator in the stack. Vertical lines show the minutes of maximal TGE flux, namely 14:11 and 15:08 UT.

**Table 1**

Count rate enhancements (or deficit) detected by STAND3 on October 7, 2012 in standard deviations.

| STAND3 Combinations | [1000] Number of $\sigma$ | [1100] Number of $\sigma$ | [1110] Number of $\sigma$ | [1111] Number of $\sigma$ |
|---------------------|---------------------------|---------------------------|---------------------------|---------------------------|
| 14:11               | 10                        | 4                         | 1                         | 0                         |
| 15:08               | 27                        | 9                         | 5                         | 4                         |

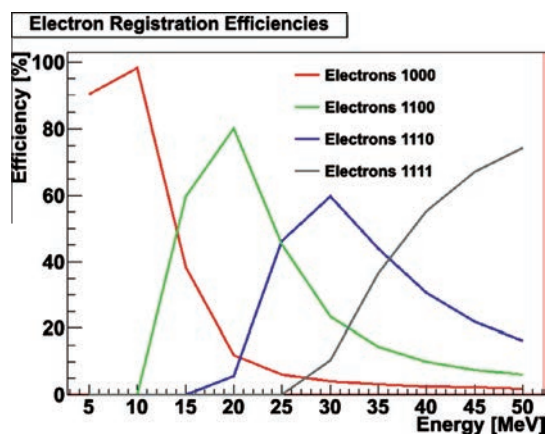


**Fig. 3.** Efficiencies of detection of the electrons by the STAND3 coincidences.

Surrounding detectors (6 units) are 1 cm thick molded plastic scintillators.

Unfortunately, the upper veto scintillator fails on October 7, 2012. Nonetheless, we have used the lower 20 cm Cube scintillator to check for the gamma ray intensity, since electrons with energies less than 50 MeV attenuate till reaching the bottom scintillator. There is no evidence of the presence of such high-energy electrons in the detected at Aragats TGEs and simulations of the RREA also demonstrate that maximal electron energy reaching ASEC detectors is 40–50 MeV [9]. On October 7 2012, Cube lower 20 cm thick scintillator detects a small increase. The increase was  $\sim 150$  and  $\sim 250$  particles at 14:11 and 15:08 respectively. We suppose that particles giving these enhancements are gamma rays with energies

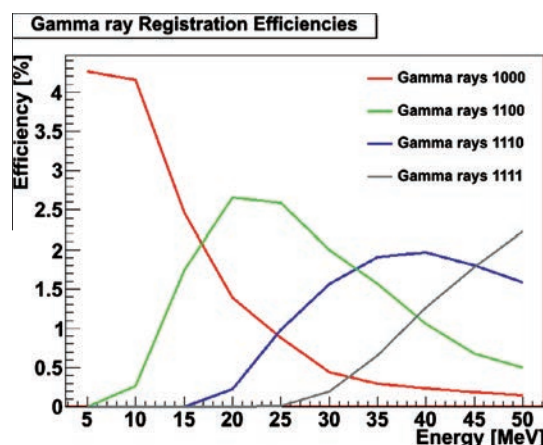


**Fig. 4.** Efficiencies of detection of the gamma rays by the STAND3 coincidences.

above 15 MeV<sup>3</sup>, since electrons attenuate in detector substance. This data along with ASNT data helps to check for the gamma ray spectrum of the TGE and consequently to disentangle the electron and gamma ray fractions of the detected TGE.

### 3. Recovered energy spectra of electrons and gamma rays

After demonstrating that the 15:11 TGE contains high energy electrons, we shall investigate the enhancements measured by above mentioned 3 particle detectors in more details having the goal to recover the energy spectra of gamma rays and electrons.

We use the multiple spectra testing method [7] to reproduce in simulations of gamma ray fluxes the observed by STAND3 detector peaks. Dependent on the simulated gamma ray spectrum index, more or less gamma rays have to be generated to fit the measurements: hard  $E^{-1}$  spectrum requires simulation of only  $\sim 20,000$  gamma rays above 10 MeV to get the measured number of STAND3 “1111” coincidence additional counts, softer  $E^{-3}$  needs more

<sup>3</sup> On October 7, 2012, due to the high electronics threshold (all energy thresholds along with count rates are registered and stored), the particles depositing less than 15 MeV were not detected by PM.

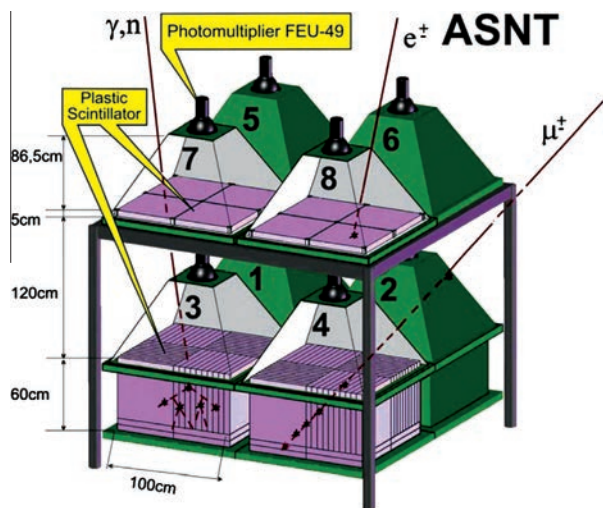


Fig. 5. Aragats Solar Neutron Telescope (ASNT).

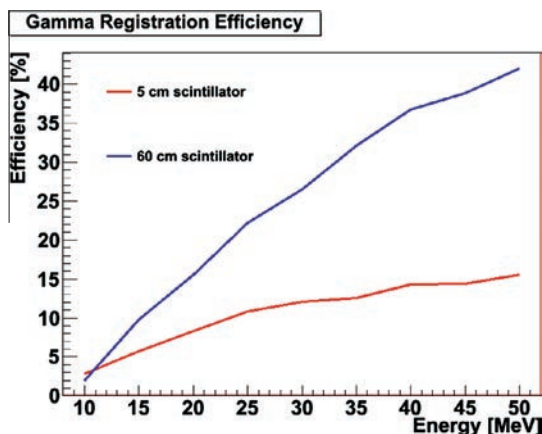


Fig. 6. The efficiency of gamma ray registration by ASNT 5 cm and 60 cm thick plastic scintillators.

Table 2  
The enhancements of ASNT upper and lower layers on 7 October, 2012.

| ASNT                  | 60 cm | 5 cm | 5 cm/60 cm | "11" coincidence |
|-----------------------|-------|------|------------|------------------|
| The first peak 14:11  | 919   | 1110 | 1.21       | 99               |
| The second peak 15:08 | 1018  | 2357 | 2.31       | 135              |

particles,  $\sim 150,000$  to reproduce the observed peaks. Bottom 20 cm scintillator of Cube and ASNT "01" coincidence registers mostly TGE gamma rays. The anticoincidence scheme of ASNT rejects charged particles and electrons should have energy above 50 MeV to be detected by lower scintillator of Cube. In Table 3, we post required in the simulation amounts of gamma rays to reproduce the enhancement measured by the "1111" combination of STAND3 and corresponding counts of ASNT 01 and Cube bottom 20 cm scintillator along with actually measured by these detectors enhancements.

As we can see, if we assume that enhancement in "1111" coincidence of STAND3 is due to gamma rays, Cube and ASNT should measure much more particles than they do.

If we assume  $E^{-2}$  spectrum, and decrease simulated intensity 4 times, we will correctly reproduce intensities measured by ASNT

and Cube. Thus, only quarter of the STAND3 "1111" combination increase can be due to gamma rays. In Table 4 we depict the intensities of measured TGE particles, along with estimated gamma ray and electron intensities, assuming  $E^{-2}$  shape of the gamma ray spectrum. First supposing that the enhancements measured by STAND3 detector are due to gamma rays only, using Geant4 simulations, we estimate expected count rates of all 4 coincidences of layered detector (third row of Table 4). Then, subtracting the estimated gamma ray flux from the experimentally measured increase we obtain the residual increase, which we relay to the electron flux incident on the detector (the fourth row of Table 4). In this way we determine the fractions of electron and gamma ray fluxes in the total TGE flux from the thundercloud reaching the detector assembly. The intensities presented in Table 4 are in a good agreement with ASNT and Cube data for the high-energy electrons and gamma rays.

From the data of Table 4, we can recover electron energy spectra. The electron integral spectrum is very flat and can be fitted by the  $\sim E^{-1}$  function, see Fig. 8, where the background electron spectrum at 3200 m a.s.l. and electron spectra of the largest TGEs on September 19, 2009 and October 4, 2010 are shown as well. Although at high energies the background significantly enhanced the TGE electron flux, nonetheless the relative error of the ASEC detectors is rather small (see [12]) and 2–3% enhancement of the detector count rate can be reliably identified and enumerated. The increases detected by STAND3 at 15:08, October 7, 2012 are 23%, 10%, 10% and 7% for "1000", "1100", "1110" and "1111" combinations respectively. The October 2012 TGE significantly differs from the largest TGEs on September 19, 2009 and October 4, 2010 not only by electron/gamma ray ratios, but also by spectral shapes. On September 19, 2009 TGE electron spectrum was best fitted by the exponential function  $\sim \exp(-0.3 \cdot E)$  and gamma ray spectrum by the power law  $\sim E^{-3}$ . We have supposed that the reason of the flat spectra can be the shorter electric field lengths, since the RREA spectra will be less modified and closer to the background secondary cosmic ray electron spectra. RREA simulations show that if the length of the electric field is near 500 m, the RREA electron and gamma ray spectra's shapes are close to the seed particle (cosmic ray electron) spectra. While the field length is larger

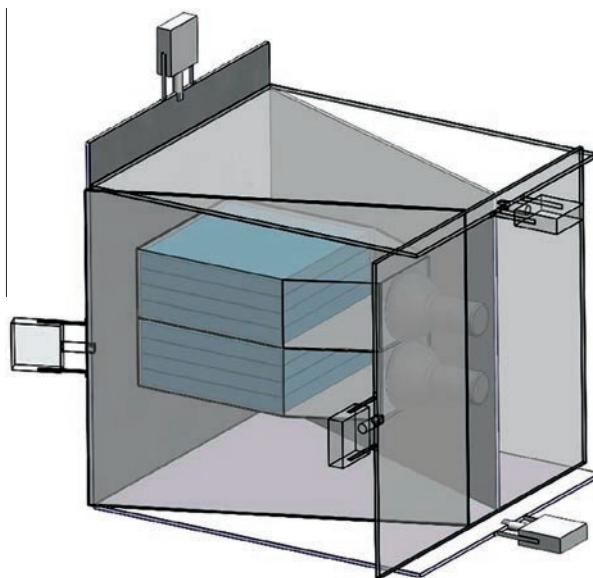


Fig. 7. Cube detector assembly; two 20 cm thick plastic scintillators are fully surrounded by the 1 cm thick molded plastic scintillators (veto system).

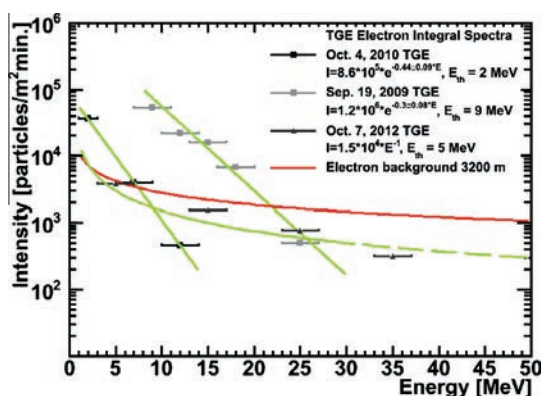
**Table 3**

Simulated gamma ray flux and corresponding ASNT 01 and Cube bottom 20 cm thick scintillator intensities along with experimentally measured values at 15:11, 7 October 2012.

|                           | Simulated intensity of required Gamma ray flux reproducing measured enhancement by “1111” combination of STAND3 | The same as in second column for the ASNT “01” combination | The same as in second column for the Cube bottom 20 cm thick scintillator |
|---------------------------|---|--|---|
| $E^{-1}$                  | 20,000  | 3900   | 884   |
| $E^{-2}$                  | 50,000  | 3500   | 1288  |
| $E^{-3}$                  | 150,000   | 3400   | 2213  |
| Experimental measurements |   | ~900   | ~250  |

**Table 4**Count rates of the STAND3 and estimated numbers of electrons and gamma rays, assuming  $E^{-2}$  gamma ray spectrum and electron threshold corresponding to 30% efficiency; 15:11, 7 October 2012.

| STAND3    | >5 MeV (1000) | >15 MeV (1100) | >25 MeV (1110) | >35 MeV (1111) |
|-----------|---------------|----------------|----------------|----------------|
| Total     | 3821 ± 86     | 1531 ± 84      | 763 ± 89       | 319 ± 76       |
| Gamma ray | 2682          | 197            | 85             | 84             |
| Electron  | 1139          | 1334           | 678            | 235            |

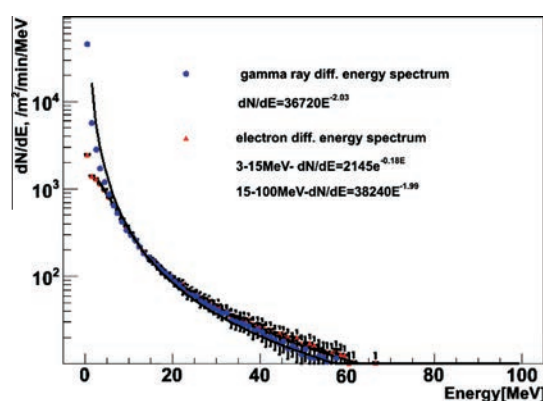
**Fig. 8.** October 7, 2012 TGE electron integral spectrum along with the largest TGE and background cosmic ray electron spectra.

(1500 m), the TGE spectra differ significantly from the background spectra, due to the greater influence of unleashed runaway avalanches. Shorter electric field length could explain the spectra of 15:08, October 7, 2012 TGE, which are close to the background secondary cosmic ray electron and gamma ray spectra [21].

The results of simulations of RREA process in 500 m of 1.8 kV/cm strength uniform electric field are presented in Fig. 9. As we can see, the spectra of electrons and gamma rays are flatter in comparison to those presented in Chilingarian et al. [9] for the 1500 m of electric field length. The differential spectrum of the electrons after 500 m is well described by power function  $\sim E^{-2}$  at energies >15 MeV (smaller energies do not reach the observational level, see [9]). The corresponding electron integral spectrum is fitted by function  $\sim E^{-1}$ , which coincides with the recovered energy spectrum rather well. The gamma ray spectrum obtained in simulation is also in a good agreement with the estimated spectrum presented in Fig. 10.

Because of the short electric field length, gamma ray maximal energy does not reach  $\sim 100$  MeV [9] as for the longer field lengths and ends near 60 MeV. Electron intensity and path length are smaller and less is the probability to emit high-energy gamma rays.

The estimated gamma ray spectrum fitted by the power function  $E^{-2}$  is presented in Fig. 10 along with background gamma ray spectrum at 3200 m and spectra of the largest TGEs on September 19, 2009 and October 4, 2010. The enhancements against background are 16, 8, 5 and 4% for >10, >20, >30 and >40 MeV gamma rays respectively.

**Fig. 9.** The electron and gamma ray differential energy spectra after the electric field in thundercloud obtained from the simulations of RREA process in 500 m of 1.8 kV/cm electric field.

#### 4. The “gamma ray” TGE at 14:11, October 7, 2012

The TGEs like occurring at 15:08 October 7, 2012 with high electron/gamma ray ratio and large maximal energy are rather rare events. The TGE occurred earlier on October 7, 2012 at 14:11 belongs to the class of more frequent events with predominant portion of gamma rays. At 14:11 the thin scintillators of ASNT have detected near the same amount of excess particles as thick scintillators; ratio of thin/thick is 1.21 see Table 2. Moreover, thick scintillators have detected near the same number of excess particles at 14:11 and 15:08. This points on the smaller electron contamination at 14:11 in comparison to the 15:08 peak (see Fig. 6). The reason of the absence of electrons can be the higher thundercloud height at 14:11. Abrupt changes in wind speed, atmospheric pressure (0.5 mbar change in half an hour) and rain rate (reaching 3 mm/h at 14:30, October 7, 2012) measured by Davis Vantage Pro weather station [26], point on the highly variable weather conditions.

Using STAND3, ASNT and Cube data, we estimate the gamma ray intensity at 14:11. From the measurements of STAND3 it is obvious that there are no electrons with energies greater than 15 MeV, since the coincidences “1111” and “1110” do not show any boost.

We have performed simulations of STAND3 detector response using the multiple spectra selection method to reproduce the ob-

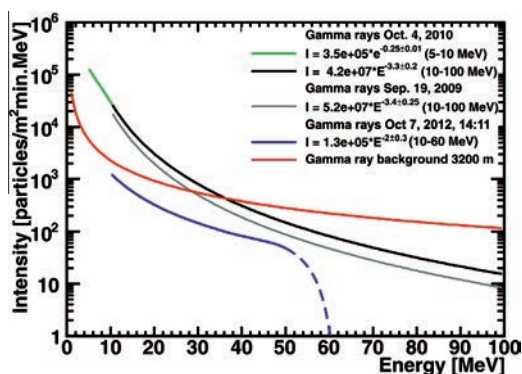


Fig. 10. The gamma ray spectrum of October 7, 2012 TGE along with largest TGE spectra and background gamma ray spectrum at 3200 m.

Table 5

STAND3 detector response simulations and measurements at 14:11, October 7, 2012.

| STAND3                   | [1000] | [1100] | [1110] | [1111] |
|--------------------------|--------|--------|--------|--------|
| 14:11                    | 819    | 334    | 56     | –35    |
| Simulation $\sim E^{-1}$ | 680    | 331    | 226    | 342    |
| Simulation $\sim E^{-2}$ | 906    | 136    | 44     | 63     |
| Simulation $\sim E^{-3}$ | 689    | 34     | 6      | 4      |

Table 6

ASNT 01 and Cube lower 20 cm scintillator data and simulation values.

|          | ASNT 01    | Cube       |
|----------|------------|------------|
| $E^{-1}$ | 5529       | 872        |
| $E^{-2}$ | 1402       | 232        |
| $E^{-3}$ | 267        | 47         |
| 14:11    | $\sim 900$ | $\sim 150$ |

served peaks in the “1000” and “1100” combinations. Again the power law spectral shape was used with spectral indexes of  $-1$ ,  $-2$ ,  $-3$  and spectral coefficient of 20,000/sq m. The gamma ray energy interval in simulation was 3–100 MeV. In Table 5, the simulation results along with the experimental measurements are presented.

As we can see from Table 5, the small enhancement detected by “1110” coincidence can be explained assuming a pure gamma ray flux using  $\sim E^{-2}$  spectrum, or other spectra with diminished or increased intensities. However, the data of various coincidences do not agree with each other without involving low energy electron flux (at energies less than 15 MeV). No test spectrum supports the pure gamma ray flux and absence of electrons at all energy ranges. Again, as for the previous analyzed TGE, we use ASNT and Cube lower 20 cm detector data to estimate the number of gamma rays on October 7, 2012 at 14:11. In Table 6, the measurements and simulations are presented. As we can see, the spectrum  $\sim E^{-2}$  agrees with experiment after diminishing the intensity  $\sim 1.5$  times. The spectrum  $\sim E^{-3}$  also may provide a good agreement with the measurements after enlarging the incident spectrum 3.5 times; however, the STAND3 data do not support this hypothesis.

Assuming the gamma ray spectrum  $\sim E^{-2}$  and diminishing the intensity in a way to fit the Cube lower 20 cm scintillator and ASNT 01 count, we obtain the electron and gamma ray fraction presented in Table 7. As we can see, the estimated  $>5$  MeV electron number is very small in comparison to the largest TGEs and  $\sim 4$  times smaller than at 15:08.

Table 7

STAND3 measurements of 14:11, October 7, 2012 TGE.

| STAND3 coincidence  | [1000]       | [1100]       | [1110]      | [1111]       |
|---------------------|--------------|--------------|-------------|--------------|
| Total               | 819 $\pm$ 86 | 334 $\pm$ 84 | 56 $\pm$ 89 | –35 $\pm$ 76 |
| Gamma ray simulated | 604          | 91           | 29          | 42           |
| Electron simulated  | 215          | 243          | –           | –            |

## 5. Possible systematic errors

We do not estimate the exact length of the electric field in the thundercloud and strength of electric field; however, the obtained spectra are closer to the simulation results for 500 m rather than 1500 m field length. Additional simulation should be performed to find the relation between the field length, strength and the TGE particle spectra. Moreover, in our simulations we assume that seed electrons enter the field region at a definite height; meanwhile, secondary cosmic ray seed particles are distributed in the whole volume of the electric field in the thundercloud and are continuously accelerated from. Also different instrumentation were used to recover the TGE spectra of the largest events and the new events in 2012, which may cause uncertainties connected with the energy threshold estimation, while comparing various TGEs.

## 6. Discussion and conclusions

We have estimated the electron and gamma ray spectra of the TGE observed at 15:08 on October 7, 2013, and the gamma ray spectrum of the preceding TGE at 14:11.

The intensities and spectral indices of gamma ray fluxes are near the same for both TGEs, the difference is due to the more intense electron flux at 15:08. The gamma ray intensities at energy range  $>10$  MeV are  $\sim 13,000$  particles/min  $m^2$ ,  $\sim 10$  times less than for the largest gamma ray TGE on October 4, 2010.

Both gamma ray spectra have power law shape at energies above 10 MeV, with a spectral index about  $-2$ , which is harder than the spectra for the largest observed TGEs on September 19, 2009 and October 4, 2010. The electron spectrum is also harder than the previously measured spectra [7]. Since the obtained spectra shapes are closer to the background secondary cosmic ray electron spectrum, we proposed that the electric field length for October 7, 2012 TGE at 15:08 UT is shorter in comparison with the largest TGEs. We have checked the hypothesis on the short field lengths using GEANT4 simulations. The results of the simulation also support the hypothesis on short field lengths, based on the rather hard recovered spectra.

After estimating the electron and gamma ray energy spectra at the observational level (3200 m a.s.l), based on the electron/gamma ray ratio, we have estimated the thundercloud height to be  $\sim 100$  m (we assume electric field strength 1.8 kV/cm and 500 m field length). Thereafter, we have estimated the electron energy spectrum at 3300 m, i.e.  $\sim 100$  m above the observational level to be  $\sim 130,000$  per minute per  $m^2$ . Consequently, the multiplication rate is  $\sim 33$  and taking into account that the field length is 500 m, we can estimate the e-folding length as  $\sim 150$  m.

The maximal energy of TGE electrons and gamma rays obtained in simulations is approximately 50 MeV for the field length 500 m, i.e. gamma ray maximal energy is smaller than that obtained for longer field lengths [9]. Thundercloud height was low enough at 15:11, allowing electrons to be observed at 3200 m. We have also calculated the total number of RREA electrons assuming the electric field region having a radius 1 km, after estimating the TGE particle intensities just below the electric field in thundercloud to be  $\sim 4.2 \cdot 10^{11}$ , which is  $\sim 10^2$  times less than for September 19, 2009

TGE and  $\sim 10^4$  less than for October 4, 2010 TGE. This is another argument supporting the hypothesis of the short electric field.

Tsuchiya et al. [23] had measured the fluence of gamma rays at sea level for energies above 1 MeV to be  $\sim 2 \cdot 10^4 \text{ m}^{-2}$ , which is comparable to our results. However intensities obtained for Aragats are higher, because of lower thundercloud height.

Experiments carried by the Japanese group [24] are in a good agreement with our results. The estimated gamma ray spectrum index was also  $\sim 2$ , however the thundercloud height was 600–900 m, which did not allow to measure the electron spectrum.

Tsuchiya et al. [24] have measured TGE gamma ray spectra, whereas, till now only Chilingarian et al. [7] had reported on the TGE electron spectra. The indices of estimated gamma ray spectra are in good agreement also with the measurements of TGF spectrum reported by Tavani et al. [22].

## References

- [1] K. Arakelyan et al., New electronics for the Aragats Space-Environmental Center (ASEC) Detectors, in: Proc. of FORGES 2008 international symposium, Tigran Mets, 2009, pp. 105–116.
- [2] K. Avakyan, K. Arakelyan, A. Chilingarian, A. Daryan, L. Melkumyan, D. Pokhsranyan, D. Sargsyan, New low threshold detectors for measuring electron and gamma ray fluxes from thunderclouds, *J. Phys. Conf. Ser.* 409 (2013) 012223.
- [3] L.P. Babich, I.M. Kutsyk, E.N. Donskoy, A.Yu. Kudryavtsev, New data on space and time scales of relativistic runaway electron avalanche for thunderstorm environment: Monte Carlo calculations, *Phys. Lett. A* 24A (1998) 460.
- [4] L.P. Babich, E.I. Bochkov, I.M. Kutsyk, A.N. Zalyalov, On amplifications of photonuclear neutron flux in thunderstorm atmosphere and possibility of detecting them 2013, published in *Pis'ma v Zhurnal Eksperimental'noi i Teoreticheskoi Fiziki*, 97(6), 2013, pp. 333–339, *JETP Lett.* 97 (6) (2013) 291–296. © Pleiades Publishing, Inc..
- [5] A. Chilingarian, K. Arakelyan, K. Avakyan, et al., Correlated measurements of secondary cosmic ray fluxes by the Aragats Space-Environmental Center monitors, *Nucl. Instrum. Methods Phys. Res. Sect. A* 543 (2–3) (2005) 483–496.
- [6] A. Chilingarian, L. Melkumyan, G. Hovsepyan, A. Reymers, The response function of the Aragats Solar Neutron Telescope, *Nucl. Instrum. Methods Phys. Res. Sect. A* 574 (2007) 255–263.
- [7] A. Chilingarian, A. Daryan, K. Arakelyan, et al., Ground-based observations of thunderstorm-correlated fluxes of high-energy electrons, gamma rays, and neutrons, *Phys. Rev. D* 82 (2010) 043009.
- [8] A. Chilingarian et al., Particle bursts from thunderclouds: natural particle accelerators above our heads, *Phys. Rev. D* 83 (2011) 062001.
- [9] A. Chilingarian, B. Mailyan, L. Vanyan, Recovering of the energy spectra of electrons and gamma rays coming from the thunderclouds, *Atmos. Res.* 114–115 (2012) 1–16.
- [10] A. Chilingarian et al., Neutron bursts associated with thunderstorms, *Phys. Rev. D* 85 (2012) 085017.
- [11] A. Chilingarian et al., Remarks on recent results on neutron production during thunderstorms, *Phys. Rev. D* 86 (2012) 093017.
- [12] A. Chilingarian, H. Mkrtchyan, Role of the Lower Positive Charge Region (LPCR) in initiation of the Thunderstorm Ground Enhancements (TGEs), *Phys. Rev. D* 86 (2012) 072003.
- [13] L. Dorman I, I. Dorman V, Possible influence of cosmic rays on climate through thunderstorm clouds, *Adv. Space Res.* 35 (2005) 476–483.
- [14] J.R. Dwyer, A fundamental limit on electric fields in air, *J. Geophys. Res.* 30 (20) (2003) 2055, <http://dx.doi.org/10.1029/2003GL017781>.
- [15] J.R. Dwyer, D.M. Smith, S.A. Cummer, High-energy atmospheric physics: terrestrial gamma-ray flashes and related phenomena, *Space Sci. Rev.* (2012), <http://dx.doi.org/10.1007/s11214-012-9894-0>.
- [16] J.R. Dwyer, M.M. Schaal, E. Cramer, S. Arabshahi, N. Liu, H.K. Rassoul, J.D. Hill, D.M. Jordan, M.A. Uman, Observation of a gamma-ray flash at ground level in association with a cloud-to-ground lightning return stroke, *J. Geophys. Res.* 117 (2012) A10303, <http://dx.doi.org/10.1029/2012JA017810>.
- [17] A.V. Gurevich, G.M. Milikh, R.A. Roussel-Dupre, Runaway electron mechanism of air breakdown and preconditioning during a thunderstorm, *Phys. Lett. A* 165 (1992) 463.
- [18] N.S. Khaerdinov, A.S. Lidvansky, V.B. Petkov, Cosmic rays and electric field of thunderclouds: evidence for acceleration of particles (runaway electrons), *Atmos. Res.* 76 (2005) 346–354.
- [19] B. Mailyan, A. Chilingarian, Investigation of diurnal variations of cosmic ray fluxes measured with using ASEC and NMDB monitors, *Adv. Space Res.* 45 (2010) 1380.
- [20] Y. Muraki et al., Effects of atmospheric electric fields on cosmic rays, *Phys. Rev. D* 69 (2004) 123010.
- [21] T. Sato, A. Endo, M. Zanki, N. Petoussi-Henss, K. Niita, Fluence-to-dose conversion coefficients for neutrons and protons calculated using the PHITS code and ICRP/ICRU adult reference computational phantoms, *Phys. Med. Biol.* 54 (2009) 1997.
- [22] M. Tavani et al., Terrestrial gamma-ray flashes as powerful particle accelerators, *Phys. Rev. Lett.* 106 (2011) 018501.
- [23] H. Tsuchiya, T. Enoto, S. Yamada, et al., Detection of high-energy gamma rays from winter thunderclouds, *Phys. Rev. Lett.* 99 (2007) 165002.
- [24] H. Tsuchiya, K. Hibino, K. Kawata, et al., Observation of thundercloud-related gamma rays and neutrons in Tibet, *Phys. Rev. D* 85 (2012) 092006.
- [25] C.T.R. Wilson, The acceleration of b particles in strong electric fields such as those of thunderclouds, *Proc. Cambridge Philos. Soc.* 22 (1925) 534–538, <http://dx.doi.org/10.1017/S0305004100003236>.
- [26] <http://www.davisnet.com/>.
- [27] <http://www.ihep.su/>.

**Thunderstorm ground enhancements: Gamma ray differential energy spectra**

A. Chilingarian, G. Hovsepyan, and L. Kozliner

*Yerevan Physics Institute, Alikhanyan Brothers 2, Yerevan 0036, Armenia*

(Received 8 July 2013; published 1 October 2013)

The shape and evolution of the energy spectra of the thunderstorm ground enhancement (TGE) electrons and gamma rays shed light on the origin of TGEs, on the relationship of modification of the energy spectra (MOS) and relativistic runaway electron avalanche processes, on the nature of the seed particles, and on the strength and elongation of an atmospheric electric field. However, till now the measurements of energy spectra of TGE electrons and gamma rays have been rather scarce. For the first time, we present differential energy spectra of gamma rays in the wide energy range 4–100 MeV for five TGE events detected in 2012–2013 at Aragats. We use the special technique of electron/gamma ray fraction determination to select TGE events with very small contamination of electrons. The network of large NaI spectrometers located 3200 m above sea level measured energy spectra of gamma rays. The power law indices of “small” TGEs are rather close to the background cosmic gamma ray spectrum ( $\gamma \sim -2$ ); thus, we may deduce that these small events are due to MOS of cosmic ray electrons in the electric field of a thundercloud. Larger TGEs measured by the NaI network and the two largest TGE events earlier recovered from energy releases in a 60-cm-thick scintillator have much steeper energy spectra typical for the avalanche process in atmosphere. The classification of TGEs according to intensity and gamma ray spectral index pointed toward two main mechanisms of the TGE gamma ray origin: the runaway process and modification of electron energy spectra in the thunderstorm atmospheres.

DOI: 10.1103/PhysRevD.88.073001

PACS numbers: 92.60.Pw, 13.40.-f, 94.05.Dd, 96.50.sb

**I. INTRODUCTION**

The boost of the secondary cosmic ray (CR) flux observed during thunderstorms, so-called thunderstorm ground enhancements (TGEs) [1,2], is the manifestation of high-energy processes in the terrestrial atmosphere [3]. The origin of TGEs is the strong electrical field in the thundercloud, giving rise to rather complicated physical phenomena, including at least six physical processes:

- (1) Relativistic runaway electron avalanches (RREA) [4–8];
- (2) Modification of the secondary cosmic ray (electrons, muons, protons and charged mesons) energy spectra [9–12];
- (3) Photonuclear reactions of gamma rays [13–16];
- (4) Attenuation of the cosmic ray muon flux [1,17];
- (5) Roentgen and gamma radiation from the lightning [18];
- (6) Prolonged (2–3 hours and more) enhancement of the low-energy (1–3 MeV) cosmic ray flux [19].

Starting in 2008, experimental facilities of the Aragats Space Environmental Center (ASEC) [20,21] have routinely measured time series and energy spectra of secondary cosmic ray fluxes. During these years, several new particle detectors were designed and fabricated, having a lower energy threshold and the ability to distinguish charged and neutral fluxes [22,23]. The variety of ASEC particle detectors allows us for the first time to detect RREA process in the atmosphere [2], recover both the electron and gamma ray energy spectra of the largest TGEs, and develop the model of the TGE process [12].

The statistical analysis of more than 300 TGE events, including TGE seasonal and daytime distributions, TGE amplitude, and duration graphs, are presented in [24]; the time series of hundreds of particle-measuring channels can be assessed online using multivariate visualization code ADEI [25] following the link <http://crd.yerphi.am/ADEI>.

The shape and evolution of the energy spectra of the TGE electrons and gamma rays shed light on the origin of TGE, on the relationship of MOS and RREA processes, on the nature of the seed particles, and on the strength and elongation of atmospheric electric field. However, till now the precise measurements of energy spectra of TGE electrons and gamma rays are rather scarce. The available gamma ray energy spectra measured with detectors located on Earth’s surface [8,15,26–28] and in near space<sup>1</sup> [30,31] are based on rather small statistics and usually are averaged over many events. The variety and large sizes of ASEC detectors allow precise measurements of the gamma ray differential energy spectra of individual TGE events. Solving the inverse problem and “unfolding” the gamma ray spectra by multiple solutions of the direct problem, we estimate the electron integral spectra and gamma ray differential spectra of the two largest TGE events on September 19, 2009, and October 4, 2010 (see details in [12]). The energy deposit spectra measured by the 60-cm-thick plastic scintillators of the ASNT detector were used for recovering the gamma ray differential energy spectra

<sup>1</sup>Cumulative gamma ray energy spectra of so-called terrestrial gamma flashes (TGFs) [29].

A. CHILINGARIAN, G. HOVSEPYAN, AND L. KOZLINER

(see details in [1]). The energy deposits of gamma rays incident on the 60-cm-thick scintillators located in the lightproof housings overviewed by photomultipliers were digitized and spectra were stored each minute. Assuming the analytic form of the possible RREA gamma ray spectra (power, exponential, or power with exponential cutoff), we tune free parameters (number of gamma rays fallen on the roof and spectral indices) by minimizing the “quality” function describing the closeness of deposit spectra simulated with GEANT code to the experimentally measured ones. Gamma rays were traced through the material of the roof above the detector and trough of the detector itself.

However, the length of 1.5 radiation lengths only is not enough to unambiguously measure gamma ray energy. The network of “deep” NaI crystals (12.5 cm thickness,  $\sim 5.2$  radiation lengths) used for energy spectra measurement in a current study allows direct measurements of the gamma ray energy and estimation of the energy spectra without indirect methods of solving the inverse problem. For the first time, we present differential energy spectra of gamma rays in a wide energy range 4–100 MeV for five TGE events detected in 2012–2013 at Aragats. We use a special technique to select TGE events with very small contamination of electrons. Depending on the location of the thundercloud above the particle detectors, the relative fraction of the TGE electrons and gamma rays reaching the detector changes. Usually gamma rays are abundant due to much stronger attenuation of the electrons in the atmosphere; though we detect several “electron” TGEs [32], signaling that under some conditions, not yet fully understood, the electron flux can be prevailing. In the present paper, our goal is to investigate TGE gamma ray energy spectra for getting insight into their origin and for calibration of the ASEC particle detectors.

In the second section of the paper we present the technique of TGE event selection and detector output

PHYSICAL REVIEW D **88**, 073001 (2013)

simulation. In Secs. III and IV, we describe the method of the electron/gamma ray ratio estimation. In the fifth section, we present measured gamma ray spectra. In Sec. VI, we calibrate the ASEC particle detectors by the integral gamma ray energy spectrum and in the conclusion we discuss the origin of the TGE events.

## II. TGE DETECTION AND DETECTOR SIMULATION

On June 19, 2013, all particle detectors of the Aragats Space Environmental Center registered large thunderstorm ground enhancement. The Aragats multidirectional muon monitor (AMMM), the detector having a minimal relative error (RE) of 1-minute time series, consists of twenty-nine  $1\text{-m}^2$ , 5-cm-thick scintillators, placed in lightproof iron boxes. A light capture cone and photomultiplier tubes are located on the top of each scintillator. On June 19, only 20 of 29 scintillators were operational. The large area of the detector provides maximal sensitivity to low-energy gamma rays and electrons of TGE. The relative error of the AMMM detector is  $\sim 0.1\%$  for 1-minute time series.

The TGE was uncommonly lengthy ( $\sim 1$  hour, 7:00–8:00, with a maximum at 7:40); usually, TGE duration did not exceed 20 minutes (see [24]). As we see in Fig. 1, disturbance of the near-surface electric field starting at 7:00 originated a rise in particle flux. At 7:30, the electric field reached a value of  $-27$  kV/m and stayed in the high negative domain till 7:52 (the minimum of field,  $-31$  kV/m, was reached at 7:43). Simultaneously, the particle flux reached peak at 7:40 and consequently attenuated at 7:52 with the decay of the negative near-surface electric field. At the peak flux, there were 88,000 additional particles detected; the background value of cosmic ray flux was  $1,020,000 \pm 1048$  particles per minute. Flux enhancement of 8.6% corresponds to 86 standard deviations from mean value. Other ASEC detectors also detected the

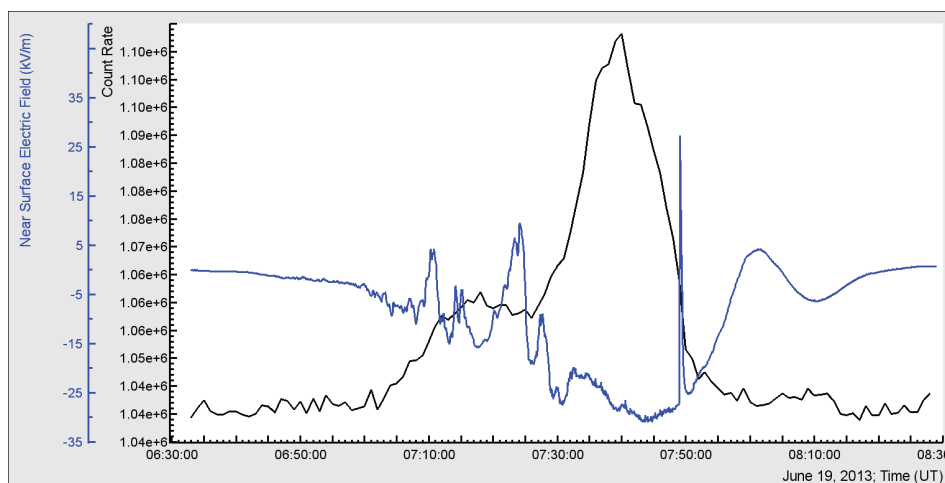


FIG. 1 (color online). TGE registered by the AMMM detector: 20 outdoor plastic scintillators; 1-minute time series of particle flux and near-surface electric field.

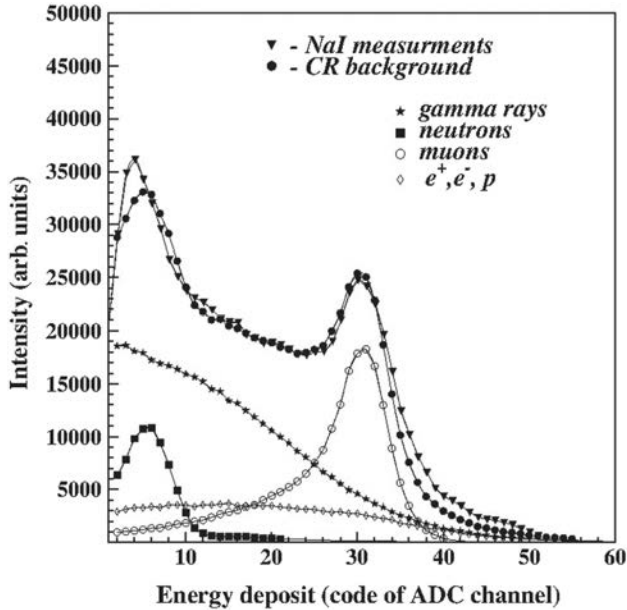


FIG. 2. Measured and simulated energy deposit spectra with the response to various species of secondary CRs.

same TGE with high significance. The large NaI crystals used for spectrometric measurements are sensitive to gamma rays and electrons from TGE as well as to different species of secondary CR. For the calibration of the spectrometer, we imitate the incident CR flux and simulate the response of the detector. The measured and simulated channel-to-channel spectra of the ADC codes are depicted in Fig. 2. We also demonstrate in the same figure the

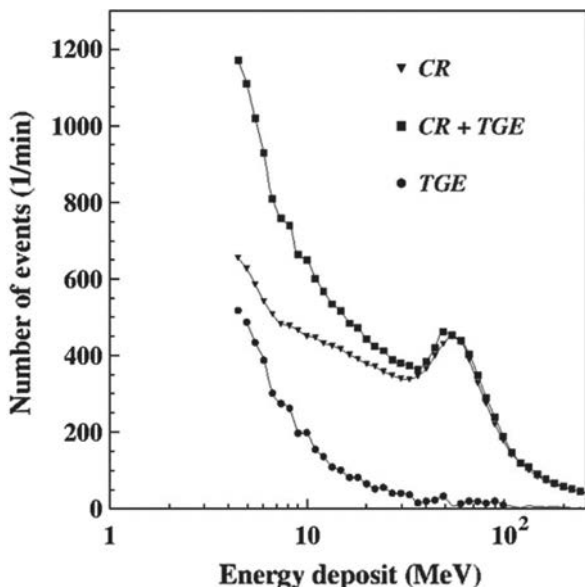


FIG. 3. Total energy deposit spectrum measured at 7:36 UT on June 19, 2013; background spectrum measured by the same NaI network 1 hour prior to TGE; and the residual TGE spectrum.

contribution of the main species of secondary cosmic rays: gamma rays, neutrons, and muons. The simulated and measured energy deposits coincide rather well; it gives us a possibility to determine the gamma ray energy as a function of the channel number. By the “muon” peak corresponding to the 30th channel of the energy deposit histogram ( $\sim 60$  MeV), we check the relation of the ADC codes to the energy deposits in MeVs.

Data acquisition electronics collects and stores 1-minute energy deposits from each of five NaI crystals. After examining the time series of particle fluxes and electric field disturbances, we determine the minute of maximum flux, and the corresponding energy deposit spectrum is compared with the background spectrum. The background spectrum was measured 1 hour prior to TGE and the mean of the 60 one-minute energy deposit spectra was used.

In Fig. 3 we can see the energy deposit spectrum (CR + TGE) measured at 7:36 UT on June 19, 2013 by five NaI crystals; the mean CR background spectrum; and the TGE spectrum obtained by the channel-to-channel subtraction of background.

### III. ESTIMATION OF THE GAMMA RAY-ELECTRON RELATIVE FRACTIONS IN TGE BY STAND STACKED DETECTOR

The “STAND1” detector comprises three layers of 1-cm-thick, 1-m<sup>2</sup> sensitive area molded plastic scintillators (Fig. 4; see details in [23]). Light from scintillator by optical spectrum-shifter fibers is reradiated to the long-wavelength region and passed to the photomultiplier FEU-115M (PM). The maximum of luminescence is emitted at a 420-nm wavelength and the luminescence time is about 2.3 ns [33]. The tuning of the STAND1 detector consists in selections of PM high voltage and discrimination thresholds. The threshold should be chosen to guarantee both high efficiency of signal detection and maximal suppression of PM noise. Proper tuning of the detector provides  $\sim 99\%$  efficiency of charged particle detection. The data acquisition system counts and stores all coincidences of the detector channels.

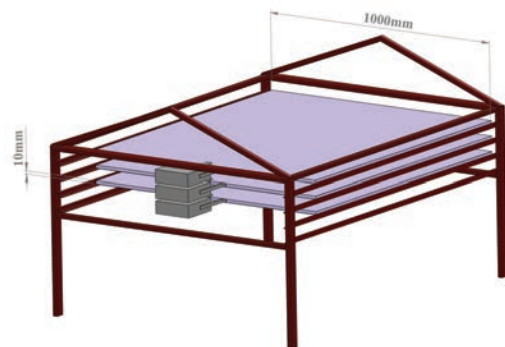


FIG. 4 (color online). STAND1 detector setup.

Coincidence “100” means that only the upper detector registers a particle. This combination registered low-energy electrons with an efficiency of  $\sim 99\%$  (we assume that the efficiency of electron registration in the second scintillator also is  $99\%$ ). We estimate the minimal energy of an electron stopping in the upper detector and giving a signal to be  $\sim 1.4$  MeV; it is the lowest energy threshold among all ASEC detectors. Gamma ray detecting efficiency of this combination is about  $2\%$ . For the coincidence 010, the gamma ray detection efficiency is increased to  $\sim 3\%$  due to creation of electron-positron pairs in the substance of the upper scintillator. Coincidence “111” means that all three layers register particles; the minimal energy of charged particles giving a signal in all three layers is  $\sim 12$  MeV.

The number of particles detected by the 100 coincidence at 7:36 on June 19, 2013, was  $N(100) = 32830$ , and the mean value measured by the time series of STAND1 just before the TGE was 22,220; thus, the difference of 10,630 can be attributed to TGE particle flux. The number of particles detected by the 010 combination at 7:36 on June 19, 2013, was  $N(010) = 25,590$ , and the mean value measured by the time series of STAND1 just before the TGE was 18,100; thus, the difference of 7,490 may be attributed to TGE particle flux. By these counts, we can estimate the flux (the number of particles per square meter per minute) of electrons  $N_e$  and gamma rays  $N_g$  above the detector:

$$\begin{aligned} N(100) &= N_e p(100/e) + N_g p(100/g) \\ N(010) &= N_e p(010/e) + N_g p(010/g). \end{aligned} \quad (1)$$

$p(100/e, g)$  and  $p(010/e, g)$  are the conditional probabilities to register electrons or gamma rays by 100 and 010 combinations. By calibration, confirmed with detector response simulations, we estimate these conditional probabilities as follows:

$$\begin{aligned} p(100/e) &= 0.99 & p(100/g) &= 0.02 \\ p(010/e) &= (1-p(100/e))p(100/e) = 0.0099 \\ p(010/g) &= (1-p(100/g))p(010/g) = 0.0294. \end{aligned} \quad (2)$$

Solving the system of equations (1) with coefficients (2), we readily get  $N_e = 5,629$ ,  $N_g = 252,866$  per minute per square meter. Thus, on June 19, 2013, the majority of TGE particles were gamma rays, and the fraction of electrons was  $N_e/N_g \sim 2.2\%$ . As we mention above, the evaluated fluxes and calculated electron–gamma ray ratio are associated with the lowest energy threshold of electron detection of  $\sim 1.5$  MeV.

#### IV. ESTIMATION OF THE GAMMA RAY-ELECTRON RELATIVE FRACTIONS IN TGE BY CUBE DETECTOR

The Cube assembly (Fig. 5) consists of two 20-cm-thick scintillators of  $0.25\text{-m}^2$  area each, enfolded by 1-cm-thick,

1-m<sup>2</sup> area scintillators. This design ensures that no particle may hit the inside 20 cm without hitting the surrounding “veto” scintillators.

The 20-cm-thick plastic scintillators are overviewed by the photomultiplier PM-49 with a large cathode operating in a low-noise regime. Surrounding detectors (six units) are 1-cm-thick molded plastic scintillators [33].

The efficiency of neutral component detection by 1-cm-thick scintillators is  $\sim 2\%$  and weakly depends on the energy of gamma rays. The energy losses of passing electrons and muons in 20-cm-thick plastic scintillator are  $\sim 40$  MeV. Taking into account the construction material of the detector (2-mm iron tilt and 1-cm plastic scintillator), and the roof of the building (1-mm iron tilt), the electron registration energy threshold for the upper 20-cm-thick scintillator is estimated to be about 8 MeV and the bottom one  $\sim 40$  MeV for the vertical flux. The obtained efficiency of gamma ray registration equals  $\sim 20\%$  and weakly depends on energy. By using measurements from Cube’s inner 20-cm-thick scintillators with and without veto signal included, we obtain the following system of linear equations:

$$\begin{aligned} N(20\text{ cm}) &= N_e p(20\text{ cm}/e) + N_g p(20\text{ cm}/g) \\ N^v(20\text{ cm}) &= N_e p^v(20\text{ cm}/e) + N_g p^v(20\text{ cm}/g), \end{aligned} \quad (3)$$

where  $p(20\text{ cm}/e)$  and  $p(20\text{ cm}/g)$  are the conditional probabilities to register electrons or gamma rays by a 20-cm scintillator. Accordingly,  $p^v(20\text{ cm}/e)$  and  $p^v(20\text{ cm}/g)$  are the conditional probabilities to register electrons or gamma rays by Cube’s 20-cm upper scintillator with veto switched on. By calibration, confirmed with detector response simulations, we estimate these conditional probabilities as follows:

$$\begin{aligned} p(20\text{ cm}/e) &= 0.99 & p(20\text{ cm}/g) &= 0.2 \\ p(1\text{ cm}/e) &= 0.98 & p(1\text{ cm}/g) &= 0.02 \\ p^v(20\text{ cm}/e) &= (1-p(1\text{ cm}/e))p(20\text{ cm}/e) \\ &= (1-0.98)0.99 = 0.0198 \\ p^v(20\text{ cm}/g) &= (1-p(1\text{ cm}/g))p(20\text{ cm}/g) \\ &= (1-0.02)0.2 = 0.196. \end{aligned} \quad (4)$$

The number of particles detected by the 20-cm-thick upper scintillator at 7:36 on June 19, 2013, was  $N_u = 12,920$ , and the mean value measured by the Cube time series just before the TGE was 10,900; thus, the difference of 2020 can be attributed to TGE particle flux. The number of particles detected by the same detector with veto signal involved at 7:36 on June 19, 2013, was  $N_u^v = 6245$ , and the mean value measured by the appropriate time series before the TGE was 4543; thus, the difference of 1702 can be attributed to TGE particle flux. By these counts, we may estimate the flux (the number of particles per square meter per minute) of electrons  $N_e$  and gamma rays  $N_g$  above

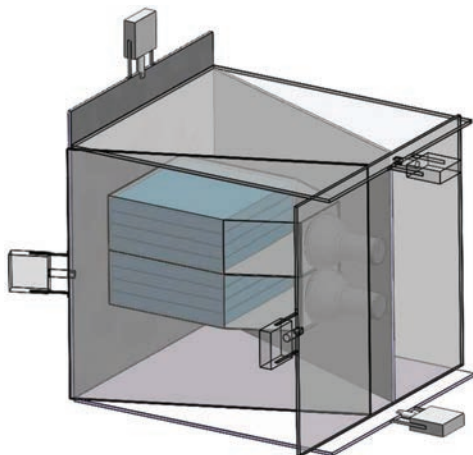


FIG. 5 (color online). Cube detector assembly design.

the detector. Solving the system of equations (3) with coefficients (4), we readily get  $N_e = 292$ ,  $N_g = 8654$  per minute per square meter. Thus, on June 19, 2013, most of TGE particles were gamma rays; the fraction of electrons  $N_e/N_g \sim 3.4\%$ .

The fraction of electrons obtained by the Cube detector is larger than that obtained by the STAND1 detector because the energy threshold of the Cube detector is higher. At low energies, gamma rays are much more abundant.

#### V. MEASUREMENT OF THE DIFFERENTIAL ENERGY SPECTRA BY NAI CRYSTALS NETWORK

Selecting the TGE events with small electron fractions (less than 3%–4%),<sup>2</sup> we may neglect the electron contamination of gamma ray spectra and directly obtain the differential energy spectra by the energy deposits measured by NaI crystals.

The NaI network is located in the same experimental hall as the Cube detector; it consists of five NaI crystal scintillators in the sealed aluminum (1-mm-thick) housing. The NaI crystal is surrounded by 0.5 cm of magnesium by all sides (because the crystal is hygroscopic) with a transparent window directed to the photo-cathode of the photo-multiplier tube PM-49; see Fig. 6. The large cathode of PM-49 (15-cm diameter) provides good light collection. The spectral sensitivity range of PM-49 is 300–850 nm, which covers the spectrum of NaI(Tl) emission light. The sensitive area of each NaI crystal is  $\sim 0.032$  m<sup>2</sup>; the total area of the five crystals is  $\sim 0.16$  m<sup>2</sup>; the efficiency to detect gamma rays is  $\sim 80\%$ . Therefore, from the peak count rate of 24,300 measured at the flux and mean background count rate of 16900 results, we calculate the TGE gamma ray flux of 57,812 per square meter per minute.

<sup>2</sup>The accuracy of the electron fraction determination by Cube and STAND1 detectors was estimated to be  $\sim 1.5\%$ .

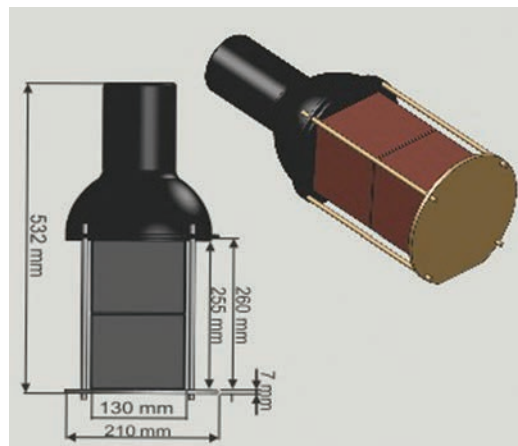


FIG. 6 (color online). NaI(Tl) crystal assembly.

After determining the fraction of electrons and gamma rays in TGE flux, we select several recent TGE events containing small proportions of electrons to investigate the differential gamma ray spectra measured by the network of NaI crystals. Gamma ray spectra presented in Figs. 7–11 were obtained by the summed intensity measured by five NaI crystals. The 1-minute background spectrum was obtained by averaging the 1-hour data (60 energy release histograms) measured before the enhancement of secondary cosmic ray flux. The TGE 1-minute spectrum was obtained by averaging 3–4 minute data around the flux maximum minute. On Figs. 7–11, the residual (gamma ray) spectra are placed.

For the channels of 3–4 MeV, NaI crystals underestimate the intensity due to lower efficiency of gamma ray detection near the electronic threshold. For the highest energies

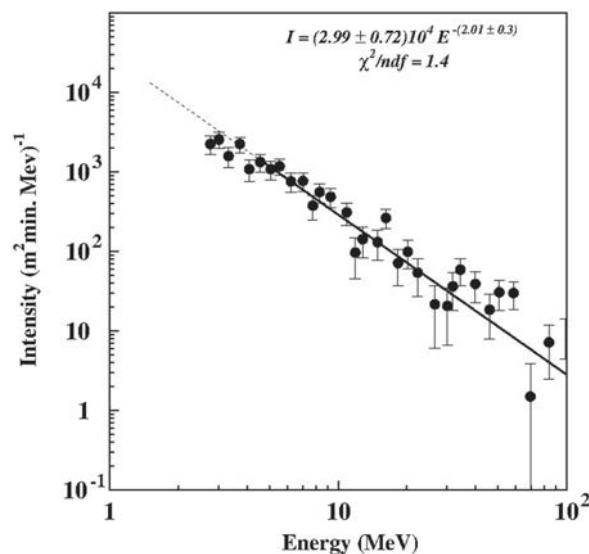


FIG. 7. Differential gamma ray energy spectrum; TGE of October 7, 2012; peak time at 14:09; exposition of 3 minutes.

A. CHILINGARIAN, G. HOVSEPYAN, AND L. KOZLINER

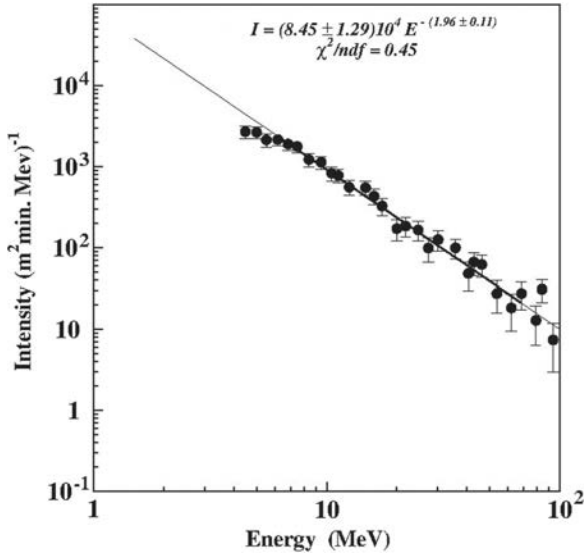


FIG. 8. Differential gamma ray energy spectrum; TGE of May 12, 2013; peak time at 06:36; exposition of 3 minutes.

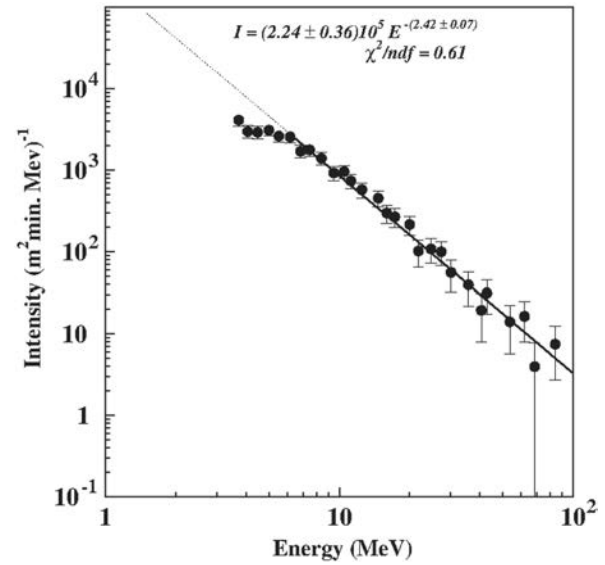
PHYSICAL REVIEW D **88**, 073001 (2013)

FIG. 10. Differential gamma ray energy spectrum; TGE of June 9, 2013; peak time at 21:47; exposition of 3 minutes.

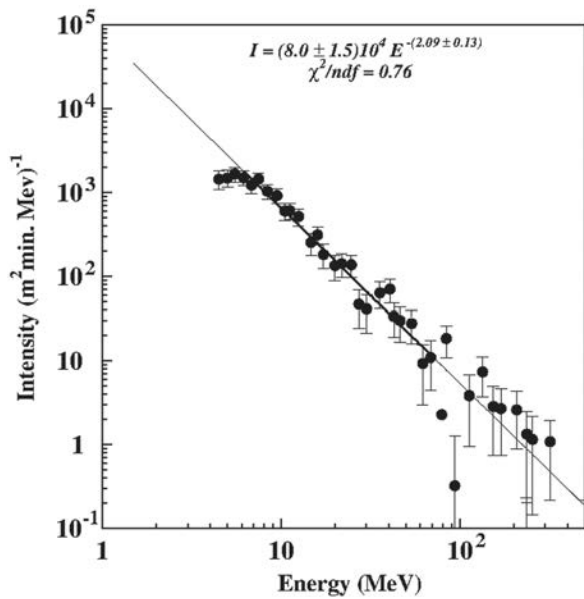


FIG. 9. Differential gamma ray energy spectrum; TGE of May 15, 2013; peak time at 12:30; exposition of 4 minutes.

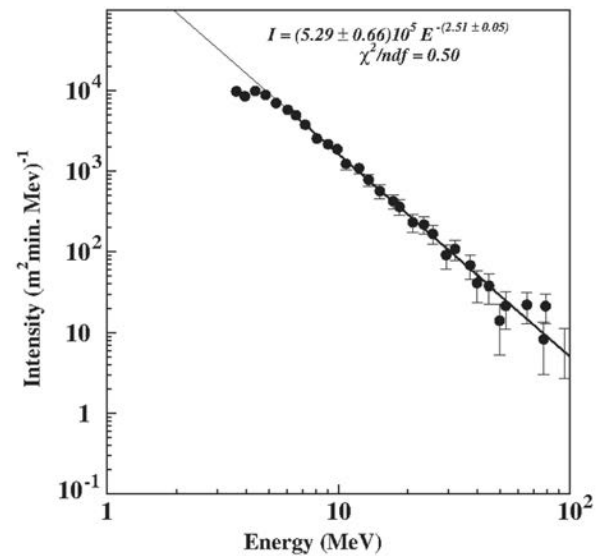


FIG. 11. Differential gamma ray energy spectrum; TGE of June 19, 2013; peak time at 07:36; exposition of 4 minutes.

(above 60 MeV), gamma rays may not deposit their whole energy in the crystal. The GEANT simulations were used to study these effects and appropriate corrections were introduced. Because of the high intensity of the June 19 TGE, it was possible to measure energy spectra separately by all five NaI crystals. As one can see in Fig. 12, spectra measured by all five NaI crystals are very close to one another. At energies above 30 MeV, low statistics lead to a larger variance of the spectra channels measured by the

individual crystals. However, as we can see in Fig. 11, the error bars of the overall spectra are rather small.

## VI. CHECKING THE THRESHOLD OF ARAGATS PARTICLE DETECTORS BY MEASURED GAMMA RAY INTEGRAL ENERGY SPECTRA

The ultimate check of the energy spectra measurements with NaI crystals will be an independent estimate of the particle flux by other ASEC detectors. The energy spectrum of gamma rays obtained by the NaI detector was compared with the detector response of the STAND1,

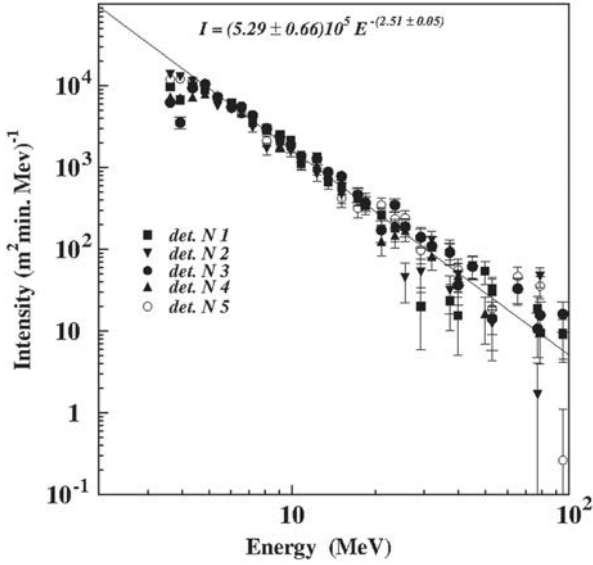


FIG. 12. Differential energy spectra of gamma rays measured by all five crystals of NaI detectors at 7:34–07:37 on June 19, 2013. The solid line represents the power law spectrum fitted by the sum of all five crystals.

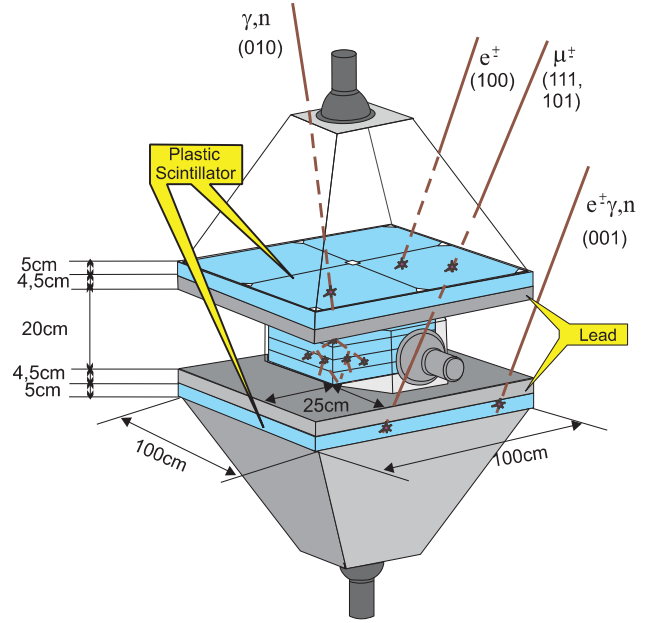


FIG. 13 (color online). SEVAN network basic measuring unit.

Cube, and SEVAN detectors. The integral spectrum of the NaI crystals on June 19, 2013, equals 57,812 per square meter per minute. The integral spectrum of gamma rays measured by the STAND1 detector was 252,870 per square meter per minute. The number of particles detected by the 20-cm-thick Cube bottom scintillator was  $N_b = 11,420$ , and the mean value measured by the Cube time series just before the TGE was 9642; thus, the difference of 1702 and flux of 31,424 gamma rays per square meter per minute can be attributed to TGE gamma ray flux.

The basic detecting unit of the SEVAN (Space Environmental Viewing and Analysis Network [34]) module (see Fig. 13) is located in the MAKET building 20 m apart from the outdoor STAND1 detector. The number of particles detected by the 20-cm-thick SEVAN middle scintillator at 7:36 on June 19, 2013, was  $N = 8269$ , and the mean value measured by the SEVAN time series just before the TGE was 7692; thus, the difference of 577 and flux of 11,540 gamma rays per square meter per minute<sup>3</sup> can be attributed to TGE gamma ray flux (electrons of MeV energies will be efficiently filtered in the detector material). Analogically, we estimate the integral energy spectrum measured by the upper scintillator of STAND1 detector, the bottom Cube detector, and the NaI detector itself. Thus, we have several integral energy spectrum measurements to be checked with the interpolated differential energy spectrum depicted in Fig. 11.

The spectrum shown in Fig. 14 by the solid line was obtained by integration of the differential spectrum measured by five NaI crystals, shown in Fig. 11. From the projection of the integral spectra of different detectors on the  $x$  axes, we readily obtain the thresholds of these detectors to register gamma rays. The integral spectrum measured by the STAND1 detector corresponds to a threshold energy of  $\sim 1.4$  MeV; the NaI threshold corresponds to

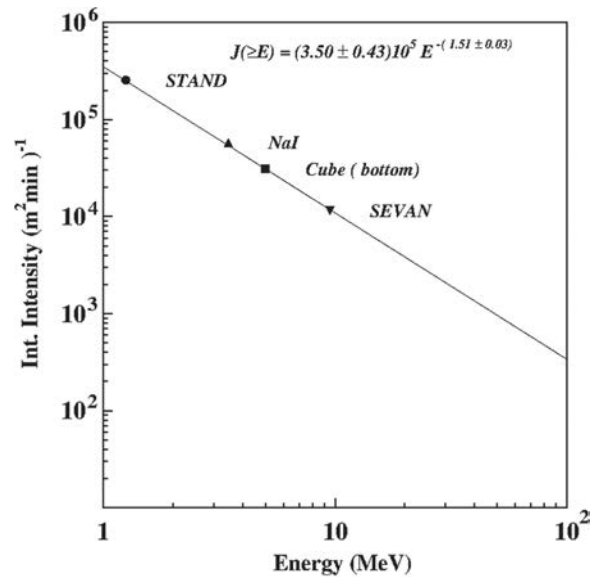


FIG. 14. Integral gamma ray energy spectrum; TGE of June 19, 2013; peak time at 07:36.

<sup>3</sup>The surface of SEVAN's middle scintillator is 0.25 m<sup>2</sup> and efficiency to detect gamma rays  $\sim 20\%$ .

TABLE I. Parameters of five differential energy spectra of gamma rays in TGEs with small electron contamination and parameters of the two largest TGE events.

| Event date             | Peak time | $A \text{ (m}^2 \text{ min MeV)}^{-1}$ | $-\gamma$       | Peak significance<br>( $N$ of $\sigma$ ) | TGE duration<br>(min) |
|------------------------|-----------|--|-----------------|--|-----------------------|
| 10/7/2012 <sup>a</sup> | 14:09     | $(2.99 \pm 0.72) \times 10^4$          | $2.01 \pm 0.3$  | 11                                       | 15                    |
| 5/12/2013 <sup>a</sup> | 06:36     | $(8.45 \pm 1.29) \times 10^4$          | $1.96 \pm 0.11$ | 23                                       | 14                    |
| 5/15/2013 <sup>a</sup> | 12:30     | $(8.0 \pm 1.5) \times 10^4$            | $2.09 \pm 0.33$ | 22                                       | 12                    |
| 6/9/2013 <sup>a</sup>  | 21:47     | $(2.24 \pm 0.36) \times 10^5$          | $2.42 \pm 0.07$ | 34                                       | 9                     |
| 6/19/2013 <sup>a</sup> | 07:36     | $(5.29 \pm 0.66) \times 10^5$          | $2.51 \pm 0.05$ | 36                                       | 74                    |
| 9/19/2009 <sup>b</sup> | 22:47     | $(5.2 \pm 2.4) \times 10^7$            | $3.4 \pm 0.25$  | 465                                      | 13                    |
| 10/4/2010 <sup>b</sup> | 18:23     | $(4.2 \pm 2.1) \times 10^7$            | $3.3 \pm 0.02$  | 164                                      | 12                    |

<sup>a</sup>Measured by the network of NaI crystals differential energy spectrum; peak significance and duration measured by the NaI network in the energy range 4–100 MeV.

<sup>b</sup>Differential energy spectrum recovered by the ASNT energy releases (60-cm-thick scintillators) in the energy range 10–100 MeV; peak significance and duration measured by 1-m<sup>2</sup>, 5-cm-thick plastic scintillator.

$\sim 3$  MeV, the Cube bottom scintillators to  $\sim 4$  MeV, and the SEVAN middle scintillator (below 4.5 cm of lead) to  $\sim 10$  MeV.

## VII. DISCUSSION AND CONCLUSIONS

The parameters of five gamma ray differential energy spectra measured by the NaI network, as well as parameters of the spectra of the two largest TGEs that occurred in 2009 and 2010, are depicted in Table I. We post in the table successively the TGE date, the intensity of 1-MeV gamma rays ( $A$ , the multiplier of power law energy spectra), the power law spectral index ( $-\gamma$ ), the significance of the peak at its maximal flux minute (in number of standard deviations from the mean value of count rate), and the duration of the TGE.

According to our model [35], the origin of TGE is a radiating region in the bottom of the cloud connected to the transient lower positive charged region that forms a lower dipole with the main negative charge region in the middle of the cloud. Intensive electrical field between these layers

accelerates electrons downward and gives birth to two processes:

The relativistic runaway electron avalanche process sustaining electron and gamma ray fluxes up to ten times or more above background cosmic ray intensity;

The modification of CR energy spectra process, prolonging the live time of electrons in thunderstorm atmosphere; those in turn radiate additional gamma rays.

TGEs usually occurred during negative near-surface electrical field varying from  $-10$  to  $-30$  kV/m (see Fig. 1); electric field in the thundercloud may be much more strong, reaching values of  $\sim 200$  kV/m. For releasing the RREA process at a 4000–5000 m height, a minimum 170 kV/m strength of electric field is required (the so-called threshold electric field [3]). Due to multiplication of electrons in the avalanche, the number of particles in the TGE may be very large, exceeding the cosmic ray background tens of times (see the last two rows of Table I and details in [1,2]). Simultaneously, the absolute value of the power law spectral index will be big, reflecting the fast attenuation of RREA electron spectra. Consequently, the

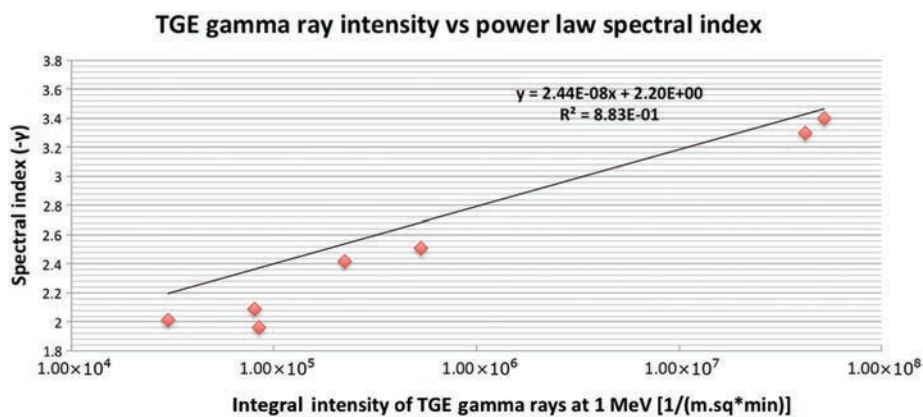


FIG. 15 (color online). Correlation of absolute value of power law spectral index and event intensity.

energy spectrum of RREA-TGE gamma rays also should be steep (see the last four rows of Table I; spectral indices equal  $-2.42$ ,  $-2.51$ ,  $-3.3$  and  $-3.4$ ).

If electric field is below the RREA threshold, only the MOS process will take place. The MOS process does not demand very large electric fields and enhances particle flux only by a few percent; however, it specifies a long tail of the gamma ray energy spectra extending up to 100 MeV [12]. A gamma ray spectrum extending up to 100 MeV also was obtained by facilities of the gamma ray observatory on board the AGILE satellite [36]. The MOS-TGE flux is weaker than the RREA-TGE flux and mainly consists of the additional gamma rays. The spectral indices of small TGEs posted in the first three rows of Table I are equal to  $-2.01$ ,  $-1.96$ ,  $-2.09$ , in good coincidence with spectra measured by the Japanese group [15,28].

The positive correlation of the absolute value of the power law spectral index and event intensity (see Fig. 15)

proves the existence of distinct RREA and MOS scenarios of TGE.<sup>4</sup>

Thus, we may conclude that the measured energy spectra of TGE gamma rays points toward two main mechanisms of the TGE origin: the runaway process and the modification of electron energy spectra in thunderstorm atmospheres.

## ACKNOWLEDGMENTS

This work was partly supported by Armenian government grants. The authors thank Karen Avagyan, Karen Arakelyan, and Arthur Reymers for assembling the NaI crystal network. The authors are grateful to Levon Vanyan for discussing different scenarios of TGE origination.

<sup>4</sup>The TGE origin may be only MOS process, if electric field in thundercloud is below the breakeven field value; if it is larger—both MOS and RREA processes may give rise to TGE.

- 
- [1] A. Chilingarian, A. Daryan, K. Arakelyan, A. Hovhannisyanyan, B. Mailyan, L. Melkumyan, G. Hovsepian, S. Chilingaryan, A. Reymers, and L. Vanyan, *Phys. Rev. D* **82**, 043009 (2010).
  - [2] A. Chilingarian, G. Hovsepian, and A. Hovhannisyanyan, *Phys. Rev. D* **83**, 062001 (2011).
  - [3] J. R. Dwyer, D. M. Smith, and S. A. Cummer, *Space Sci. Rev.* **173**, 133 (2012).
  - [4] C. T. R. Wilson, *Math. Proc. Cambridge Philos. Soc.* **22**, 534 (1925).
  - [5] A. V. Gurevich, G. M. Milikh, and R. A. Roussel-Dupre, *Phys. Lett. A* **165**, 463 (1992).
  - [6] L. P. Babich, E. N. Donskoi, I. M. Kutsyk, and A. Yu. Kudryavtsev, *Phys. Lett. A* **245**, 460 (1998).
  - [7] J. R. Dwyer, *Geophys. Res. Lett.* **30**, 2055 (2003).
  - [8] N. S. Khaerdinov, A. S. Lidvansky, and V. B. Petkov, *Atmos. Res.* **76**, 346 (2005).
  - [9] Y. Muraki *et al.*, *Phys. Rev. D* **69**, 123010 (2004).
  - [10] L. I. Dorman and I. V. Dorman, *Adv. Space Res.* **35**, 476 (2005).
  - [11] A. S. Lidvansky and N. S. Khaerdinov, *Izv. Ross. Akad. Nauk, Ser. Fiz.* **71**, 1052 (2009) [Bulletin of the Russian Academy of Sciences: Physics **71**, 1052 (2009)].
  - [12] A. Chilingarian, B. Mailyan, and L. Vanyan, *Atmos. Res.* **114–115**, 1 (2012).
  - [13] A. Chilingarian, N. Bostanjyan, and L. Vanyan, *Phys. Rev. D* **85**, 085017 (2012).
  - [14] A. Chilingarian, N. Bostanjyan, T. Karapetyan, and L. Vanyan, *Phys. Rev. D* **86**, 093017 (2012).
  - [15] H. Tsuchiya, K. Hibino, and K. Kawataetal, *Phys. Rev. D* **85**, 092006 (2012).
  - [16] L. P. Babich, E. I. Bochkov, A. N. Zalyalov, and I. M. Kutsyk, *Pis'ma Zh. Eksp. Teor. Fiz.* **97**, 333 (2013) [JETP Lett. **97**, 333 (2013)].
  - [17] A. S. Lidvansky and N. S. Khaerdinov, *Izv. Ross. Akad. Nauk, Ser. Fiz.* **73**, 415 (2009) [Bulletin of the Russian Academy of Sciences: Physics **73**, 415 (2009)].
  - [18] J. R. Dwyer, M. M. Schaal, E. Cramer, S. Arabshahi, N. Liu, H. K. Rassoul, J. D. Hill, D. M. Jordan, and M. A. Uman, *J. Geophys. Res.* **117**, A10303 (2012).
  - [19] A. V. Germanenko, Yu. V. Balabin, E. V. Vashenyuk, B. B. Gvozdevsky, and L. I. Schur, *Astrophys. Space Sci. Trans.* **7**, 471 (2011).
  - [20] A. Chilingarian *et al.*, *J. Phys. G* **29**, 939 (2003).
  - [21] A. Chilingarian *et al.*, *Nucl. Instrum. Methods Phys. Res., Sect. A* **543**, 483 (2005).
  - [22] K. Arakelyan, K. Avakyan, A. Chilingarian, A. Daryan, L. Melkumyan, D. Pokhsraryana, and D. Sargsyan, *J. Phys. Conf. Ser.* **409**, 012223 (2013).
  - [23] K. Avakyan, K. Arakelyan, A. Chilingarian, A. Daryan, L. Kozliner, B. Mailyan, G. Hovsepian, D. Pokhsraryana, and D. Sargsyan, *J. Phys. Conf. Ser.* **409**, 012218 (2013).
  - [24] A. Chilingarian, T. Karapetyan, and L. Melkumyan, *Adv. Space Res.* **52**, 1178 (2013).
  - [25] S. Chilingaryan, A. Beglarian, A. Kopmann, and S. Vöcking, *J. Phys. Conf. Ser.* **219**, 042034 (2010).
  - [26] A. S. Lidvansky and N. S. Khaerdinov, *Izv. Ross. Akad. Nauk, Ser. Fiz.* **73**, 418 (2009) [Bulletin of the Russian Academy of Sciences: Physics **73**, 418 (2009)].
  - [27] H. Tsuchiya *et al.*, *Phys. Rev. Lett.* **99**, 165002 (2007).
  - [28] H. Tsuchiya *et al.*, *J. Geophys. Res.* **116**, D09113 (2011).
  - [29] G. J. Fishman *et al.*, *Science* **264**, 1313 (1994).
  - [30] D. M. Smith, L. I. Lopez, R. P. Lin, and C. P. Barrington-Leigh, *Science* **307**, 1085 (2005).
  - [31] M. S. Brigs *et al.*, *J. Geophys. Res.* **115**, A07323 (2010).

A. CHILINGARIAN, G. HOVSEPYAN, AND L. KOZLINER

PHYSICAL REVIEW D **88**, 073001 (2013)

- [32] A. Chilingarian, B. Mailyan, and L. Vanyan, *Astropart. Phys.* **48**, 1 (2013).
- [33] G. Britvich, V.G. Vasil'chenko, V.N. Kirichenko, S.I. Kuptsov, V.G. Lapshin, A.P. Soldatov, A.S. Solov'ev, V.I. Rykalin, S.K. Chernichenko, and I.V. Shein, *Instrum. Exp. Tech.* **45**, 644 (2002); G. Britvich *et al.*, <http://www.ihep.su/>.
- [34] A. Chilingarian and A. Reymers, *Ann. Geophys.* **26**, 249 (2008).
- [35] A. Chilingarian and R. Mkrtychyan, *Phys. Rev. D* **86**, 072003 (2012).
- [36] M. Tavani *et al.*, *Phys. Rev. Lett.* **106**, 018501 (2011).

## Role of the Lower Positive Charge Region (LPCR) in initiation of the Thunderstorm Ground Enhancements (TGEs)

A. Chilingarian\* and H. Mkrtchyan

*Yerevan Physics Institute, Alikhanyan Brothers 2, Yerevan, Armenia*

(Received 24 May 2012; published 8 October 2012)

Despite the ubiquity of thunderstorms, lightning, and related electrical phenomena, many important electromagnetic processes in our atmosphere are poorly understood; the key questions about the thundercloud electrification and lightning initiation remain unanswered. The bulk information on particle fluxes correlated with thunderstorm can be used to better understand the electrical structure of thunderclouds. Only very specific electric configuration of the lower part of the cloud can support the sustainable acceleration of the electrons. Our analysis is based on the thunderstorm data from the Aragats Mountain in Armenia, 3200 m above sea level. Varieties of particle detectors located at Aragats Space Environmental Center are registering neutral and charged particle fluxes correlated with thunderstorms, so-called Thunderstorm Ground Enhancements (TGEs). Simultaneously the electrical mills and lightning detectors are monitoring the near-surface electric field and type of lightning occurrences; weather stations are measuring plenty of meteorological parameters. In the present paper we relate particle fluxes to the electrical structure of thunderclouds, namely, to the origination of the Lower Positive Charged Region (LPCR) below the main negative charged layer in the middle of the thundercloud, and to lightning occurrences. Only after creation of the lower dipole in the thundercloud can the electrons be accelerated and particle flux be directed downward. Maturity of the LPCR is correlated with increasing particle fluxes. Thus, the temporal evolution of TGE gives direct evidence of the maturity of LPCR, its initiation, and its decaying.

DOI: 10.1103/PhysRevD.86.072003

PACS numbers: 92.60.Pw, 52.38.Ph, 82.33.Xj, 93.30.Db

### I. INTRODUCTION

Thunderstorms, because of their potential to kill and cause extensive property damage, are an important issue not only for researchers but also for society. However, in spite of many experimental and theoretical studies, the origin of electrification in clouds is still poorly understood; the layered structure of the thundercloud is variable and unexplained; and the relationship between electrification, lightning activity, and particle fluxes have not been unambiguously established [1].

Although there are big varieties of measures in the thundercloud electric field profiles, the following basic structure of the electric field in thunderclouds is widely accepted: from the ground up to the cloud base there is usually a low magnitude field (either positive or negative); a relatively small positively charged “pocket” is lowermost just at the cloud base (comprising only  $\sim 20\%$  of a higher negative charge); a larger positive field prolongs up to the negative charge layer at 1–2 km above the cloud base; and about 1–4 km above the negative layer the main positive charge is located [2]. The Lower Positive Charge Region (LPCR) with a main negative layer in the middle of the cloud represents the so-called lower dipole, responsible for the downward electron acceleration and also playing a major role in the initiation of cloud-to-ground (CG –) and intracloud (IC –) lightning occurrences. LPCR is

localized to a fairly small volume; therefore it should alter (at least locally) the electrical field at the ground. Holden *et al.* [3] concluded that the effect of the field attributable to LPCR’s is usually only observable at distances less than 1 km.

The acceleration of electrons in the strong electric fields inside thunderclouds was postulated by Wilson [4] in 1924. In 1992 Gurevich *et al.* [5] developed the theory of the runaway breakdown, now mostly referred to as relativistic runaway electron avalanches (RREA) [6]. In [7] we consider the alternative mechanism of electron enhancement in thunderclouds, namely, the modification of energy spectra (MOS) of charged cosmic-ray particles [8]. Both scenarios lead to enhancements of the electrons and gamma rays in the thunderclouds, and if the height of clouds is not very large, particle detectors located on the Earth’s surface can register enhancement of count rates of electrons and gamma rays, so-called Thunderstorm Ground Enhancements (TGEs), lasting as long as the lower dipole sustains electron acceleration. Various particle detectors (see Table I) of the Aragats Space Environmental Center (ASEC) [9,10] measure  $\sim 300$  TGEs during springs and autumns of 2009–2012 in the fluxes of electrons, gamma rays, and neutrons.

It has been suggested that RREAs seeded by cosmic-ray extensive air showers (EASs) could result in enough ionization to initiate lightning [11,12]. However, Babich [13] and Dwyer and Babich [14] argue that lateral diffusion and the relativistic feedback threshold on the amount of

\*chili@aragats.am

TABLE I. Characteristics and parameters of ASEC particle detectors.

| Detectors   | Mean count rate per minute | 10 MeV Gamma ray detection efficiency [%] | Electron detection threshold (efficiency) | Standard deviation and (relative standard deviation) | Percent of enhancement/ Number of standard deviations at 3:04 UT, May 11, 2012. |
|---|----------------------------|---|---|--|---|
| MAKET 5 cm thick 1 m <sup>2</sup> scintillator              | 26400                      | 1%  | 9 MeV (50%) 50 MeV (> 95%)                | 182 (0, 69%)   | 19%/28 $\sigma$   |
| STAND 3 cm thick 1 m <sup>2</sup> scintillator              | 32800                      | 4%  | 4 MeV (50%)                               | 218 (0, 67%)   | 48%/72 $\sigma$   |
| STAND 100 combination                                       | 19500                      | 1%  | 2 MeV (50%)                               | 160 (0, 82%)   | 60%/70 $\sigma$   |
| STAND 3 cm 1000 combination                                 | 6971                       | 4%  | 4 MeV (50%)                               | 93 (1, 33%)  | 60%/45 $\sigma$   |
| STAND 3 cm 1100 combination                                 | 3427                       | 0.2%                                      | 15 MeV (50%)                              | 57 (1, 65%)  | 33%/20 $\sigma$   |
| STAND 3 cm 1110 combination                                 | 2980                       | 0.01%                                     | 25 MeV (50%)                              | 57 (1, 91%)  | 10%/5 $\sigma$  |
| AMMM, 27 outside 5 cm thick, 1 m <sup>2</sup> scintillator  | 958000                     | 1%  | 9 MeV (50%) 50 MeV (> 95%)                | 1358 (0, 14%)  | 15%/110 $\sigma$  |
| NaI crystal, 12 × 12 × 24 cm                                | 3678                       | 85%                                       | 3 MeV (50%) 17 MeV (> 95%)                | 61 (1,67%)   | 33%/20 $\sigma$   |
| SEVAN, 5 cm thick 1 m <sup>2</sup> scintillator             | 26600                      | 4%  | 18 MeV (50%) 50 MeV (> 95%)               | 170 (0, 64%)   | 12%   |
| SEVAN, 100 combination                                      | 17800                      | 4%  | 18 MeV (50%)                              | 135 (0, 76%)   | 17%   |
| SEVAN, middle, 20 cm thick 0.25 m <sup>2</sup> scintillator | 7669, 6                    | 0, 4%                                     | 100 MeV (50%) 350 MeV (> 95%)             | 88 (1, 15%)  | 5%  |
| SEVAN 010 combination                                       | 2244, 5                    | 0, 4%                                     | 100 MeV (50%)                             | 43 (1, 9%)   | 13%   |

avalanche multiplication prevent a joint action of EASs and RREAs to initiate lightning. Nevertheless, they do not rule out that RREA acting on the ambient cosmic-ray flux could discharge the large scale electrical field in such a way that local electric field enhancements occur, potentially providing a high enough field region to allow lightning to initiate [15,16].

Additionally, Dwyer [1] pointed to the possibility that the gamma ray glows (the gamma ray component of the TGE) may be a manifestation of the steady state configuration of the electric field in which the charging currents are balanced by the discharge RREA currents. Lasting tens of minutes TGEs may affect lightning initiation, and research of the correlations of lightning and TGE can provide long missing clues to understand the lightning physics.

In this paper the correlations between thundercloud electrification (near-surface electrical field and type of lightning discharge) and measured particle fluxes were studied, thus invoking in the atmospheric electricity research a new type of key evidence—temporal evolution of the TGEs, the flux of gamma rays and electrons coming from thunderclouds and detected on the earth's surface by particle detectors [17,18]. For the first time we present simultaneous measurements of the particle fluxes, disturbances in the near-surface electrical field, and lightning initiations of different types.

## II. THE LOWER POSITIVE CHARGE REGION (LPCR) AND ITS INFLUENCE ON THE NEGATIVE CLOUD-TO-GROUND (CG - ) AND INTRACLOUD (IC - ) LIGHTNING OCCURRENCES

During the past three years of TGE research on Aragats ~300 significant enhancements of particle detector count rates were detected. After locating the field meters and lightning detectors in 2010–2011, we found that all TGEs were accompanied by the disturbances of the near-surface electric field and most of them with lightning occurrences. We started with classification of TGEs according to patterns of near-surface electrical field disturbances. Then we examined each class to get evidence for how the particle flux increases and what happens with lightning occurrences as a flux is enlarged. Our model of TGE initiation [7,18] suggests that electron acceleration could start only after the creation of the LPCR below the main negative charged region in the center of the cloud. If the electric field between two differently charged regions is strong enough, the RREA process is unleashed and runaway electrons generate gamma rays; gamma rays in turn, if energetic enough, can generate neutrons via photonuclear reactions. If the electric field is below the RREA threshold, then only the MOS process can result in additional fluxes, although much weaker compared with RREA.

Simpson and Scrase [19] found that many thunderstorms contain a region of the positive charge located below the main negatively charged layer in the middle of a

thundercloud; they speculated that the positive charge resided on precipitation particles. Measurements by Holden *et al.* [3] show that LPCR's are not always found because they are localized to a fairly small volume and are transient phenomena as well. LPCR's are short-lived because, being composed of precipitation, they fall out of the cloud and carry their charge to the ground. As the LPCR approaches the ground, it should alter (at least locally) the field at the ground; thus LPCRs are responsible for the field reversals [20]. Many researchers outline the dominant role the lower positive charge region plays in initiating/triggering an intracloud and the cloud-to-ground lightning discharge [21–23]. The influence of the LPCR on lightning leader propagation can be considered in the following steps:

- (a) While the negative charge accumulates at midlevel, it may not be energetically favorable to transfer the negative charge to ground in CG– lightning. Starting to develop a lower positive charge results in the enhancement of the electric field strength within the cloud and allows for negative charge transfer to ground in –CG lightning occurrence [24].
- (b) When the size and magnitude of LPCR are becoming considerably large, the negative (“inverse”<sup>1</sup>) intracloud discharges IC– (attempted leader) are expected to occur. Because of screening the positive charge, the descending negative leader may change its direction of propagation to horizontal and end up as IC–.

Thus, the existence of the LPCR is a necessary condition for the TGE unleashing and, also, for the lightning initiation. At the initial stage of the LPCR developing or at the stage of LPCR decaying the cloud-ground CG– lightning occurrences should be often; in contrast, during the mature stage of LPCR CG– lightnings are blocked, and mostly intracloud IC– lightning should occur. An example of the above-described scenario gives lightning studies on the central Tibetan Plateau at an altitude of 4508 m. The IC– flashes registered on Tibet were usually polarity inverted and occurred in the lower dipole. The large LPCR did not cause positive CG+ flashes to occur during the whole storm lifetime, and only negative CG– flashes were observed in the late stage of the storm [25]. Also, the flash rate was quite low. It is worthwhile to note that recently the TGE detection on Tibet also was reported [26].

### III. CHARACTERISTICS OF THE PARTICLE DETECTORS

Detection of the TGE events was made with particle detectors composed of plastic scintillators (see the description of the detector construction in [17]) and NaI crystals. Huge measured enhancements of the detector count rates

<sup>1</sup>The “normal” IC+ intracloud lightning occurs between main negative and positive layers of the dipole; the electric field is negative and electrons are accelerated upward.

are because both neutral and charged particles can generate signals in plastic scintillators, although with different efficiencies; see Table I. Therefore, to estimate energy spectra, we need to disentangle the mixture of electrons and gamma rays. Special experimental facilities were designed and installed at Aragats for separating electron and gamma ray fluxes. Two 20 cm thick plastic scintillators located inside the cube detector are completely surrounded by 1 cm thick molded plastic scintillators. Thick scintillators detect charged flux with very high efficiency (99%) and also neutral flux with efficiency 20%–30%. Thin scintillators also detect charged flux with very high efficiency (98%–99%), though the efficiency of detecting neutral flux is highly suppressed and equals 1%–2%. Using the advanced coincidences technique, it is possible to purify the neutral flux detected by inside scintillators, rejecting the charged flux by signals from surrounding thin scintillators. The calibration of the cube detector proves that the veto system (preventing the counting signal in the thick scintillator if there is a signal in at least one of the six surrounding thin scintillators) can reject 98% of the charged flux (see details in [7]). ASEC particle detectors are placed at high altitude, some of them under snow, and it is very difficult to keep a stable detector operation (high voltage, electronics thresholds, and other). However, high altitude station staff maintained detector operation 24 h daily for 12 months yearly, and online visualization programs ADAS [27] and ADEI [28] provide possibilities for the remote monitoring and control of the key parameters of detectors. All meteorological parameters, including atmospheric pressure are monitored; the barometric coefficients for all detectors are calculated and used for the count rate correction [29]. In Fig. 1 we post the characteristics of one of the recent TGE events and explain how we enumerate it. The minutely mean count rate ( $m$ ), variance ( $\sigma$ ), and relative error shown in the histogram agenda are calculated by the 3 h of fair weather data before TGE. The significance of peak at 3:04 Universal Time (UT) is enumerated in the so-called “number of sigmas,” dividing the peak amplitude (48%) by relative error (0.66%).

In Table I we present the statistical characteristics of some of the ASEC detectors, demonstrating as well their measurement of the May 11 TGE. The count rate and variance depends on the size of the detector and the amount of matter above it. The highest enhancement demonstrated stacked 1 cm and 3 cm thick plastic scintillators, STAND and STAND 3 cm. STAND consists of 3 stacked 1 cm thick scintillators, and STAND 3 of 4 3 cm thick stacked scintillators of 1 m<sup>2</sup> area each. The 1000 abbreviation means that the signal comes only from the upper scintillator and the particle was stopped in it; 1100—signal measured from 2 upper scintillators, etc. The MAKET scintillators have a thickness of 5 cm, and they are located under metallic housing; therefore the threshold is higher and the enhancement is lower. The smallest relative error 0.14% (and

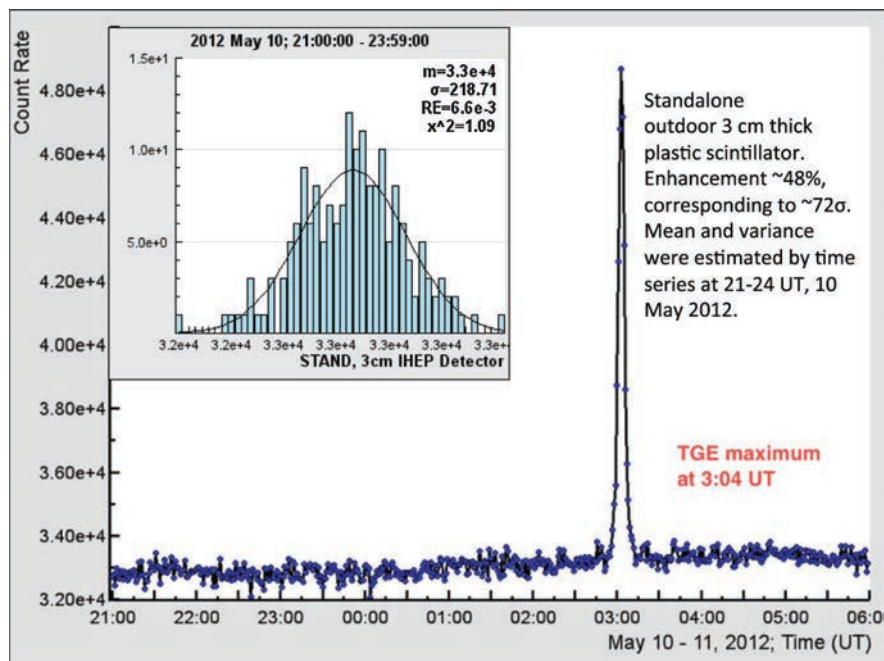


FIG. 1 (color online). Detection of the TGE occurred on May 11, 2012, by the outdoor 3-cm thick scintillator.

therefore largest significance  $110\sigma$ ) comprises from  $27\text{ m}^2$  area 5 cm thick scintillators; the largest relative error 2.06% from the NaI crystal of volume  $13.5 \times 13.5 \times 21$  cm.

In Table I we present the energy thresholds of electron detection at 50% and 95% efficiency and efficiencies of gamma ray detection; note the very high efficiency of NaI crystals owing to  $\sim 5$  radiation length thickness. The efficiency of particle detection by different combinations of stacked detectors allows the recovering of the energy spectra.

#### IV. CLASSIFICATION OF THE TGE EVENTS ACCORDING TO THE NEAR-SURFACE ELECTRICAL FIELD DISTURBANCES

Electric field meters<sup>2</sup> and lightning detectors (LD)<sup>3</sup> installed at Aragats as well as the multipurpose weather station<sup>4</sup> allow correlating TGEs with electric field

<sup>2</sup>Boltek firm electrical mill EFM100, measurement accuracy 5%, <http://www.boltek.com/efm100.html>; Boltek firm adopted the atmospheric electricity sign convention, and we adopted opposite, physics sign convention; therefore, the negative sign of the electrical field measured by the Boltek electrical mill corresponds to the positive charge above.

<sup>3</sup>Boltek's StormTracker Lightning Detection System, powered by the software from Astrogenic systems, define four types of lightning occurrences (CG<sup>-</sup>, CG<sup>+</sup> cloud-to ground negative and positive, IC<sup>-</sup>, IC<sup>+</sup> intracloud positive and negative, - in radii of 1, 3, and 5 km around the location of its antenna), <http://www.boltek.com/stormtracker>.

<sup>4</sup>Professional Davis Instruments Vantage Pro2, <http://www.davisnet.com/>.

disturbances, with occurrences of lightning of different types, and with other meteorological conditions (rain, atmospheric pressure, temperature, and humidity). LD's antenna consists of a crossed loop magnetic field sensor and electric field sensor. It records a signal when it detects an abrupt change in the electric field and can sense storms up to 350 miles away and can detect up to 3000 to 3500 strokes per second. For each lightning stroke, software analyzes a signal waveform in real time. To determine polarity (positive or negative) the software looks at the electric field at various points in the waveform. The discrimination between IC and CG is based on the shape and amplitude of the waveform, i.e., the rise and decline times, measured by the sensor through the change in electric field strength. These changes are strongest for CG discharges, where the decline time is the most important parameter; IC lightning generates much higher short-term energy at higher frequencies than CG strokes. When the electric field strength reaches a certain threshold value and rises further to a previously determined validation threshold, one can assume the electric field is attributable to a CG discharge. The direction is determined by looking at the magnetic field ratios for each stroke and crossed loop antenna direction finding principle. The initial distance is determined by looking at the signal strength. Software averages each stroke against a cluster of other strokes that are located toward the same direction, and from that derive a distance to the entire storm cell. Detection of the consequences of the IC<sup>-</sup> discharges without any CG discharge in the vicinity of the detector confirmed by the absence of lightning discharges from independent measurements of the EFM-100 electrical mill (the electrical mill detects only

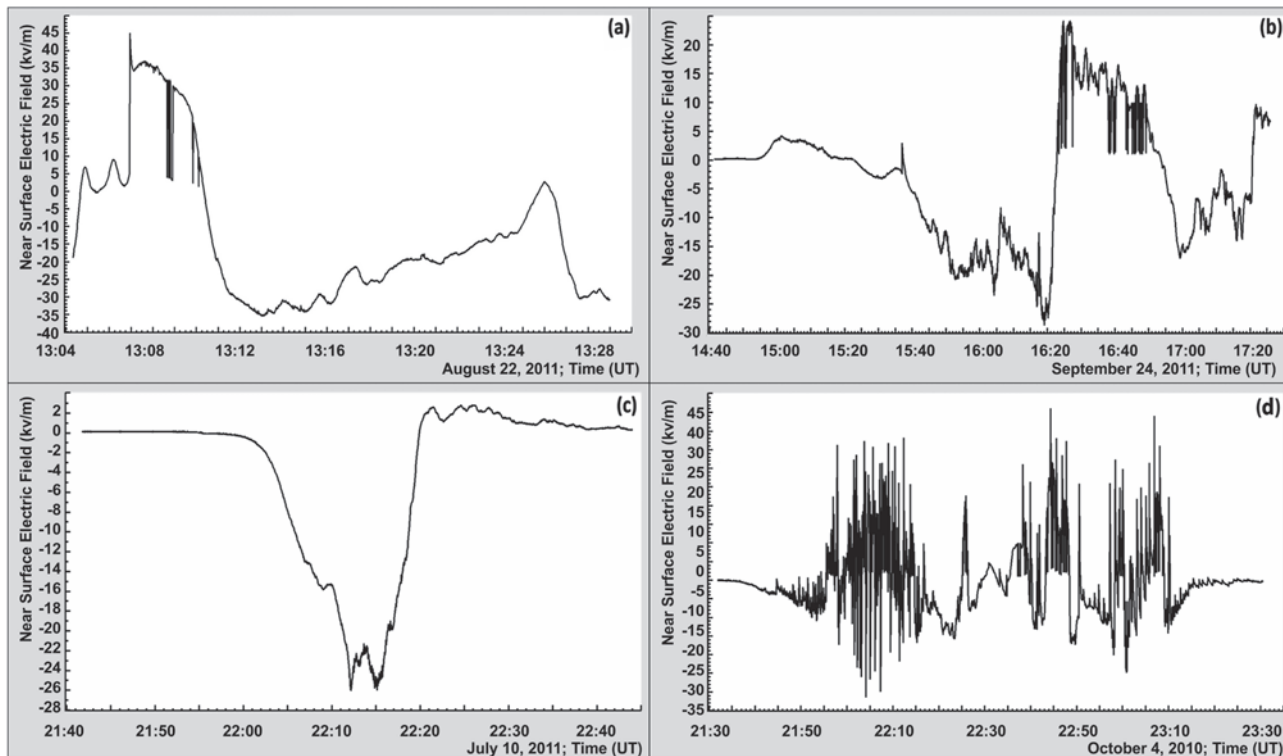


FIG. 2. Four patterns of the electric field disturbances during TGE events on Aragats.

cloud-to-ground discharges) can be accepted as highly reliable. Also comparisons of measurements made by the network of three identical EFM-100 electrical mills prove reliability and high accuracy (not worse than 10%) of near-surface electric field estimation.

The TGE amplitude (the percentage of enhancement of particle flux relative to the rather stable background of secondary cosmic rays) was measured by the outdoor 3 cm thick, 1 m<sup>2</sup> area plastic scintillators and checked by other particle detectors; see Table I. Time series of particle intensity, electric field measurements, lightning occurrences, and meteorological information are entered in the MySQL database and are visualized with ADEI multivariate visualization code.<sup>5</sup> The joint database of the TGE events accompanied by electrical field and lightning occurrence measurements consists of 98 events detected from October 2010 to May 2012. Examining disturbances of the near-surface electric field, we outline the following most typical patterns accompanied with TGE (see Fig. 2):

- (1) Electric field reversal from positive to negative [Fig. 2(a)]: field strength changes from a large (up to 50 kV/m) positive electric field to a low (down to -35 kV/m) negative value. We analyze six events

(depicted in Tables II and III) of this type from 31, and an example of the first type of events is presented in Fig. 3.

- (2) Electric field reversal from negative to positive [Fig. 2(b)]: changes from a low (down to -35 kV/m) negative electric field to a large positive electric field (~50 kV/m). We analyze four events (depicted in the Tables IV and V) of this type from 11; an example of the second type of events is presented in Fig. 4.
- (3) Electric field's abrupt decreases [Fig. 2(c)]: changes started from a fair weather value (few hundred volts) down to large negative values (-30 kV/m); we select five events of this type from 28 (see Tables VI and VII); an example of the third type of events is presented in Fig. 5. We also include in this category events started from the intermediate positive electrical field (~5 kV/m) and events having a large peak enhancement of electrical field in the middle of a negative electrical field period.
- (4) Multiple disturbances of a near-surface electrical field [Fig. 2(d)] accompanied by numerous lightnings. We classify 28 events of the fourth category; analyses of these events will be published elsewhere.

Usually all four types of TGE events were accompanied with precipitation and lightning occurrences; however, sometimes lightning and rain are missing.

<sup>5</sup>ADEI (Advances Data Extraction Infrastructure) is an AJAX based dynamic web interface facilitating browsing and extraction time series from various data sources, <http://adei.crd.yerphi.am/adei/>.

TABLE II. First types of TGE events according to changing pattern of the near-surface electric field.

| Date     | Duration of positive field | Maximal value of electric field | Duration of negative field | Minimal value of electric field | FDHM of TGE | Flux increase (max flux minute) | Rain duration |
|----------|----------------------------|---------------------------------|----------------------------|---------------------------------|-------------|---------------------------------|---------------|
| 04.10.10 | 18:14–18:20                | 28, 8 kV/m                      | 18:20–18:25                | –28, 8 kV/m                     | 18:22–18:23 | 76%                             | Missing data  |
| 24.05.11 | 13:17–13:26                | 22, 15 kV/m                     | 13:26–13:40                | –35, 2 kV/m                     | 13:29–13:38 | 3%                              | Missing data  |
| 27.05.11 | 13:05–13:10                | 45 kV/m                         | 13:10–13:25                | –35, 5 kV/m                     | 13:11–13:16 | 21%                             | Missing data  |
| 08.06.11 | 11:44–11:52                | 38, 68 kV/m                     | 11:54–12:18                | –30, 95 kV/m                    | 11:53–11:59 | 1, 7%                           | 11:53–12:47   |
| 15.07.11 | 21:05–21:24                | 14, 05 kV/m                     | 21:24–21:41                | –29, 3 kV/m                     | 21:26–21:35 | 2, 44%                          | No rain       |
| 22.08.11 | 22:06–22:14                | 17, 9 kV/m                      | 22:14–22:25                | –29, 95 kV/m                    | 22:14–22:20 | 8%                              | 22:16–23:09   |
| 20.09.11 | 10:09–10:20                | 21, 05 kV/m                     | 10:20–10:40                | –29, 45 kV/m                    | 10:22–10:28 | 2, 55%                          | 07:56–09:47   |

## V. TGE EVENTS OF THE FIRST TYPE

During the first type of events (see Fig. 3), the near-surface positive electric field reaching a strength of 40 kV/m after a series of lightning occurrences (usually very few occurrences were distributed among intracloud positive and negative lightning IC+ and IC– and cloud-to-ground lightnings CG–; see Table III) started to reverse, and simultaneously particle flux started to slowly rise at 13:10 UT. During the long period of negative near-surface electric field, we suppose that the larger in dimension and higher in charge magnitude LPCR developed at the base of the storm and electrons are accelerated downward by the lower dipole. Lasting ~10 min the negative near-surface electric field coincides in time with large particle flux; the developed LPCR creates a larger positive electric field in the cloud that increases the particle flux downward, peaking at ~13:13 UT when the negative field approaches the minimal strength of –35 kV/m. During several minutes of particle flux maximum IC+ and CG– lightning occurrences are highly suppressed and only IC– lightnings were observed.

Emerging large LPCR blocks the step leader propagation to the ground and turns it to intracloud IC– flash because the abundant lower positive charge made IC discharges energetically preferable. At 13:20 UT the LPCR contracted and particle flux decayed. Consequently diminished LPCR cannot block the lightning leader propagation to the ground any more, and several CG– lightnings occurred at 13:23 UT at the fully stopped particle flux.

The information on the first type of TGEs is posted in Table II. TGE duration comprises ~10 min; however, sometimes we detect long lasting tails of particle fluxes. To avoid possible ambiguity, we “normalize” the TGE duration by calculating the full duration of the TGE peak on the half-maximum (FDHM). In the first, second, and fourth columns we post the date of the TGE event and durations of the positive and negative fields; in the third and fifth columns we show the maximal and minimal values of the near-surface electrical field; the FDHM of the TGE peak and TGE amplitudes are presented in the sixth and seventh columns. In the last column we show information on rain; missing data denote the absence of the rain measurements. As we see in Table II, the range of the

TABLE III. Fractions of lightning occurrences of different types during positive and negative (FDHM) near-surface electric fields.

| Date   | Flash rate | Fraction of lightnings of different types within 1 km |     |     |     | Flash rate | Fraction of lightnings of different types within 3 km |      |     |     | Flash rate  | Fraction of lightnings of different types within 5 km |        |     |     |
|--|------------|---|-----|-----|-----|------------|---|------|-----|-----|-------------|---|--------|-----|-----|
|  |            | IC–   | IC+ | GC– | GC+ |            | IC–   | IC+  | GC– | GC+ |             | IC–   | IC+    | GC– | GC+ |
| 04.10.2010<br>Duration of positive field<br>(18:14–18:20 UT) | 0/ min     | 0%  | 0%  | 0%  | 0%  | 0, 17/ min | 0%  | 100% | 0%  | 0%  | 0, 5/ min   | 66, 7%  | 33, 3% | 0%  | 0%  |
| 04.10.2010<br>FDHM of TGE<br>(18:22–18:23 UT)                | 1/ min     | 100%  | 0%  | 0%  | 0%  | 2/ min     | 100%  | 0%   | 0%  | 0%  | 9/ min      | 100%  | 0%     | 0%  | 0%  |
| 27.05.2011<br>Duration of positive field<br>(13:05–13:10 UT) | 2, 2/ min  | 27%   | 55% | 18% | 0%  | 12, 6/ min | 36%   | 40%  | 24% | 0%  | 16, 2/ min  | 30%   | 39%    | 31% | 0%  |
| 27.05.2011<br>FDHM of TGE<br>(13:11–13:16 UT)                | 0, 4/ min  | 100%  | 0%  | 0%  | 0%  | 28, 2/ min | 97%   | 3%   | 0%  | 0%  | 106, 2/ min | 84%   | 15%    | 1%  | 0%  |
| 22.08.2011<br>Duration of positive field<br>(22:06–22:14 UT) | 0/ min     | 0%  | 0%  | 0%  | 0%  | 0/ min     | 0%  | 0%   | 0%  | 0%  | 0/ min      | 0%  | 0%     | 0%  | 0%  |
| 22.08.2011<br>FDHM of TGE<br>(22:06–22:20 UT)                | 15/ min    | 100%  | 0%  | 0%  | 0%  | 20/ min    | 100%  | 0%   | 0%  | 0%  | 22/ min     | 100%  | 0%     | 0%  | 0%  |

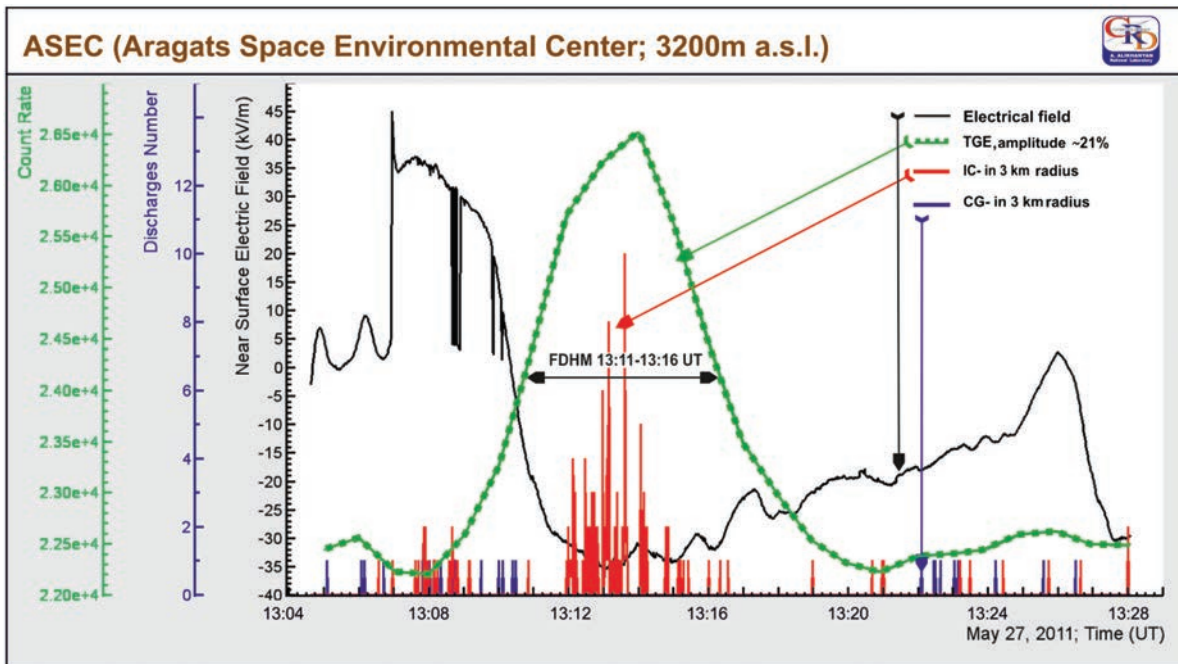


FIG. 3 (color online). TGE of the first type according to the pattern of the electric field disturbances; the black curve shows the changing electric field; the gray dotted curve shows the time series of the particle flux. Vertical gray lines denote IC– lightning and vertical darker lines CG– lightning occurrences within 3 km radius.

maximal values of the positive electric field varies 14–45 kV/m, duration 5–20 min. The maximal value of the negative field changes from –28 to –35 kV/m, duration 5–20 min. TGE amplitude changes from 2.5%

to 76%, and the FDHM is shorter than negative field duration and continues usually 4–9 min, although only once does it fall to 1 min for the super TGE on October 4, 2010.

TABLE IV. Second types of TGE events according to changing pattern of the near-surface electric field.

| Date     | Duration of negative field | Minimal value of electric field | Duration of positive field | Maximal value of electric field | FDHM of TGE | Flux increase (max flux minute) | Rain duration |
|----------|----------------------------|---------------------------------|----------------------------|---------------------------------|-------------|---------------------------------|---------------|
| 13.07.11 | 00:51–01:17                | –26, 55 kV/m                    | 01:17–01:36                | 24, 7 kV/m                      | 01:06–01:11 | 3, 92%                          | 00:59–01:47   |
| 24.09.11 | 15:37–16:22                | –28, 6 kV/m                     | 16:22–16:53                | 24 kV/m                         | 16:11–16:20 | 8, 05%                          | 15:17–16:26   |
| 25.09.11 | 11:31–11:53                | –32 kV/m                        | 11:53–12:09                | 12 kV/m                         | 11:38–11:47 | 3, 74%                          | 11:58–12:37   |
| 17.10.11 | 13:41–14:01                | –18 kV/m                        | 14:01–14:07                | 25 kV/m                         | 13:50–13:56 | 2, 82%                          | no rain       |

TABLE V. Fractions of lightning occurrences of different types during positive field and FDHM of TGE.

| Date   | Fraction of lightnings of different types within 1 km | Fraction of lightnings of different types within 3 km |     |     |     | Fraction of lightnings of different types within 5 km |            |        |        |       |             |            |     |     |     |     |
|--|---|---|-----|-----|-----|---|------------|--------|--------|-------|-------------|------------|-----|-----|-----|-----|
|  |   | Flash rate  | IC– | IC+ | GC– | GC+   | Flash rate | IC–    | IC+    | GC–   | GC+         | Flash rate | IC– | IC+ | GC– | GC+ |
| 13.07.2011 FDHM of TGE (01:06–01:11 UT)                | 0/ min  | 0%  | 0%  | 0%  | 0%  | 0, 2/ min   | 100%       | 0%     | 0%     | 0%    | 0, 8/ min   | 100%       | 0%  | 0%  | 0%  | 0%  |
| 13.07.2011 Duration of positive field (01:17–01:36 UT) | 0/ min  | 0%  | 0%  | 0%  | 0%  | 0/ min  | 0%         | 0%     | 0%     | 0%    | 0/ min      | 0%         | 0%  | 0%  | 0%  | 0%  |
| 24.09.2011 FDHM of TGE (16:11–16:20 UT)                | 69/ min   | 96%   | 1%  | 3%  | 0%  | 93, 78/ min   | 94%        | 2%     | 3%     | 1%    | 100, 5/ min | 92%        | 3%  | 4%  | 1%  |     |
| 24.09.2011 Duration of positive field (16:22–16:53 UT) | 3, 45/ min  | 40%   | 35% | 20% | 6%  | 15, 9/ min  | 52, 2%     | 23, 3% | 21, 1% | 3, 4% | 24/ min     | 47%        | 27% | 22% | 4%  |     |

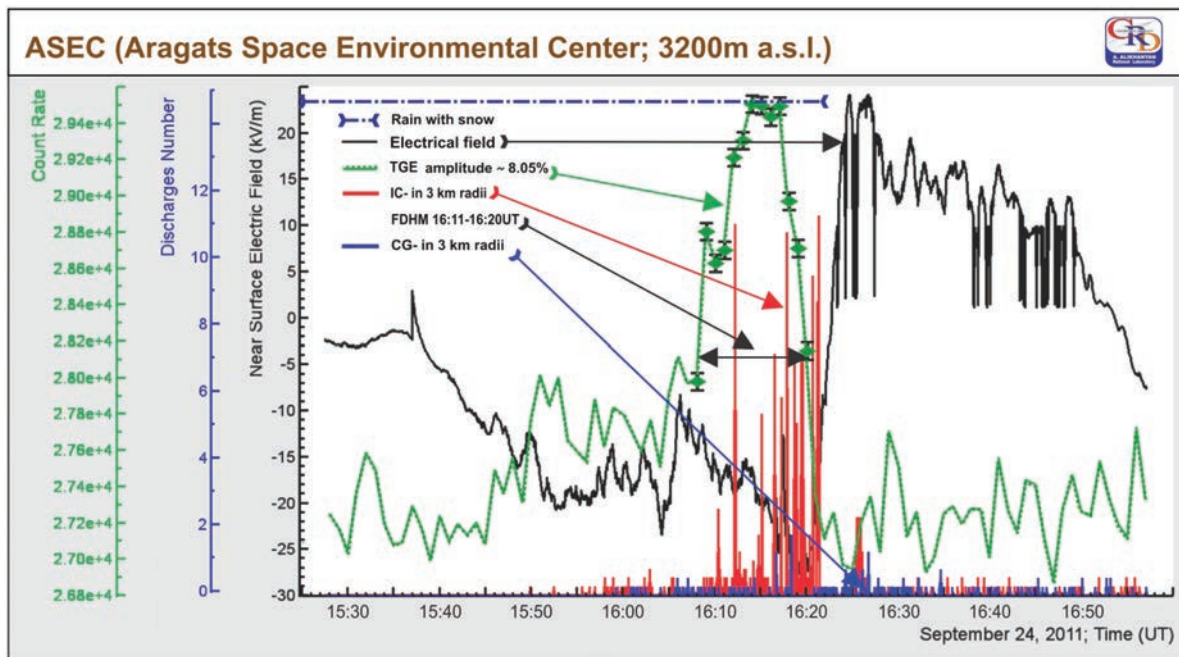


FIG. 4 (color online). TGE of the second type according to the pattern of the electric field disturbances; the black curve shows the changing electric field; the gray dotted curve shows the time series of the particle flux. Vertical gray lines denote IC– lightning and vertical darker lines CG– lightning occurrences within 3 km radius.

In the first column of Table III we post the date of the event and duration of the positive field and negative (FDHM) electrical field; in the second–fifth columns we show the flash rate (number of lightning occurrences per minute) and fractions of lightnings of different types during positive and negative fields (FDHM) in 1 km radius from detector location. The same information on frequency of lightnings for the radii 3 and 5 km is posted in the next columns. The pattern of frequencies is drastically different. If at the positive field the share of three types of lightning occurrences (intracloud positive and negative and cloud-to-ground negative) is approximately equal, at the negative field during FDHM we detect strong suppression of CG– and IC+ lightning occurrences (positive cloud-to-ground lightning IC+ is a rather rare occasion). In the vicinity of particle detectors in a 1 km radius we detect only IC– lightnings, and when enlarging the radius around

the detection site other types of lightnings occur; however, their fraction was negligible, only once reaching 20% (IC+ type at May 24, 2011, in 3 km radius). The mean flash rate during TGE FDHM is very moderate within a 1 km radius ranging from 0 to 1.5, confirming the results of the Tibet Plateau lightning occurrences study [23,25] in a 3 km radius, the rate is significantly larger: from 0.56 to 28.2. This finding supports recent results of the Japanese groups measuring the size of the radiation region within the thundercloud to be not more than 1 km [30,31].

## VI. TGE EVENTS OF THE SECOND TYPE

During the second type of the TGE events (see Fig. 4), the near-surface electric field gradually decreases from the near-zero value at 15:40 UT and remains in the negative domain near 40 min. At 16:10–16:22 UT particle flux

TABLE VI. Third types of TGE events according to changing pattern of the near-surface electric field.

| Date     | Duration of negative field | Minimal value of electric field | FDHM of TGE | Flux increase (max flux minute) | Rain duration |
|----------|----------------------------|---------------------------------|-------------|---------------------------------|---------------|
| 07.05.11 | 20:35–21:30                | –34, 5 kV/m                     | 21:11–21:15 | 4, 36%                          | Missing data  |
| 08.05.11 | 01:43–02:09                | –32 kV/m                        | 01:45–01:51 | 7, 5%                           | Missing data  |
| 12.06.11 | 09:11–10:15                | –26, 75 kV/m                    | 10:00–10:09 | 5, 17%                          | 10:38–11:11   |
| 10.07.11 | 21:56–22:20                | –26, 05 kV/m                    | 22:10–22:15 | 4, 36%                          | 22:15–22:35   |
| 13.10.11 | 11:24–11:50                | –29, 5 kV/m                     | 11:32–11:39 | 12%                             | No rain       |
| 16.10.11 | 23:59–00:14                | –17, 35 kV/m                    | 00:08–00:12 | 8, 83%                          | No rain       |
| 25.10.11 | 23:08–23:37                | –18, 55 kV/m                    | 23:24–23:33 | 2, 27%                          | No rain       |

TABLE VII. Fractions of lightning occurrences of different types at FDHM of TGE.

| Date                                  | Fraction of lightnings of different types within 1 km |        |         |        | Fraction of lightnings of different types within 3 km |            |      |     | Fraction of lightnings of different types within 5 km |     |             |        |       |     |     |
|---------------------------------------|---|--------|---------|--------|---|------------|------|-----|---|-----|-------------|--------|-------|-----|-----|
|                                       | Flash rate  | IC-    | IC+     | GC-    | GC+   | Flash rate | IC-  | IC+ | GC-   | GC+ | Flash rate  | IC-    | IC+   | GC- | GC+ |
| 07.05.11 FDHM of TGE (21:11–21:15 UT) | 58, 75/min  | 96, 2% | 21, 27% | 1, 07% | 0%  | 250, 5/min | 98%  | 1%  | 0%  | 0%  | 272, 25/min | 98, 2% | 1, 3% | 0%  | 0%  |
| 08.05.11 FDHM of TGE (01:45–01:51 UT) | 1/min   | 50%    | 0%      | 50%    | 0%  | 26, 17/min | 92%  | 1%  | 6%  | 1%  | 44, 3/min   | 93%    | 1%    | 5%  | 1%  |
| 12.06.11 FDHM of TGE (10:00–10:09 UT) | 4, 11/min   | 38%    | 43%     | 19%    | 0%  | 15, 9/min  | 67%  | 17% | 13%   | 3%  | 32, 11/min  | 73%    | 14%   | 11% | 2%  |
| 10.07.11 FDHM of TGE (22:10–22:15 UT) | 1, 6/min  | 100%   | 0%      | 0%     | 0%  | 10/min     | 74%  | 26% | 0%  | 0%  | 46, 8/min   | 62%    | 38%   | 0%  | 0%  |
| 13.10.11 FDHM of TGE (11:32–11:39 UT) | 14, 7/min   | 100%   | 0%      | 0%     | 0%  | 16/min     | 100% | 0%  | 0%  | 0%  | 16, 43/min  | 99%    | 0%    | 0%  | 0%  |

reaches a maximum of 8%, the electric field peaks  $-28$  kV/m at 16:19 UT, and simultaneously we observe highly enlarged lightning occurrences (see Fig. 4), mostly of the IC- type, and CG- lightning occurrences again were suppressed. At 16:24 UT an abrupt reversal of the field occurs, and the positive field peaked on 24.2 kV/m at 16:26 UT. The pattern of the lightning occurrences changed accordingly; see Tables IV and V.

We analyze four events of the second type (from 11) (see Table IV); the table information is the same as Table II. All three TGE started during the negative field; the field

strength is changing from  $-32$  to  $-18$  kV/m; and the duration range is 20–45 min. The range of the positive electric field is 12–25 kV/m, with a duration of 7–30 min. TGE amplitude changes from 2.8% to 8%, and FDHM changes from 7 to 9 min. The rain started during the negative field and ended with TGE fading.

Very large numbers of lightnings were registered on September 24, 2011; a considerable fraction was registered in the minute of the peak of the particle flux, but most of them were IC- . Depending on the distance, fractions of lightnings changed insignificantly. In the vicinity of

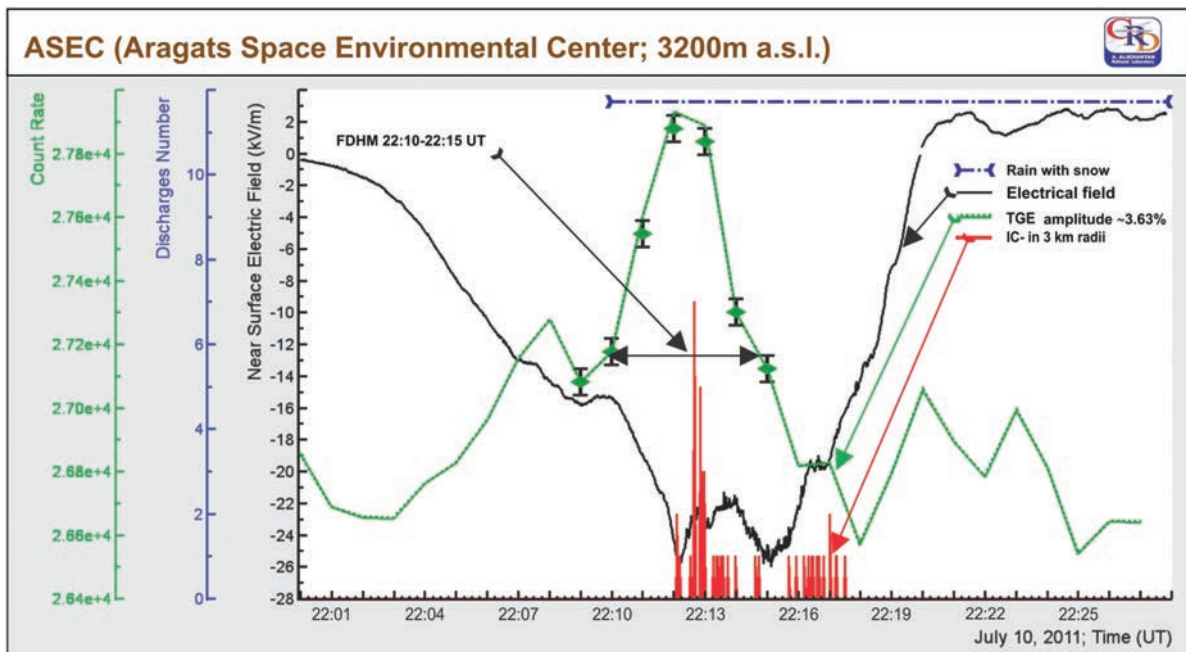


FIG. 5 (color online). TGE of the third type according to the pattern of the electric field disturbances; the black curve shows the changing electric field; the gray dotted curve shows the time series of the particle flux. Vertical gray lines denote IC- lightning occurrences within 3 km radius. Rain was detected during 22:15–22:35 UT.

particle detectors we detect plenty of the IC– lightnings; with enlarging of the radius other types of lightnings occur. On September 24, 2011, during the negative field we registered a large number of IC– lightnings; however, during the positive field we did not register any lightning. On this day the rain started during the positive field. Numbers of lightning occurrences of all types increased with the growth of the distance to the particle detectors.

### VII. TGE EVENTS OF THE THIRD TYPE

During the third type of events (see Fig. 5), the near-surface electric field gradually decreases from the near-zero value at 22:00 UT and remains in the negative domain near 20 min, peaking at  $-26$  kV/m on 22:12 and 22:15 UT; the particle flux starts to rise and peaks at 3.6% on 22:13 UT. After the start of the rain, the negative field returns very quickly to the near-zero value, and consequently the particle flux stopped.

IC– lightning occurrences started at the maximum of particle flux and continued till the flux faded. CG– lightning occurrences were not detected; IC+ lightnings occurred within 3 km radius around the particle detector location (see Table VII).

The third type of TGEs differs from the others as lightnings were registered only during the particle flux. We analyze five events of the third type from 28, and during some of them a large number of lightnings were registered (see Tables VI and VII).

As we see in Table VI, the value of the negative electric field varies from  $-34.5$  to  $-18$  kV/m, and the duration was 25–55 min. TGE amplitude changes from 2.27% to 12%, and FDHM of TGE varies from 4 to 9 min. In two events we detected 100% IC– lightnings in 1 and 3 km radius. During the other events, the fraction of IC– lightnings also predominate, and lightning occurrences of CG– and IC+ were suppressed.

Table VII presents frequencies of lightning occurrences around the minute of maximal flux of TGE. In 1 km radius we detected only IC–; with enlarging the radius around the detection, as we see, IC+ lightnings occur also.

### VIII. CONCLUSION

Incorporation of the information on the changing particle fluxes measured during thunderstorms proves the model of LPCR as it was formulated in points (a) and (b) of Sec. II. LPCR and the lower dipole are transient and local phenomena; LPCR is created during minutes, with consequent acceleration of electrons in the lower dipole resulting in enlarged particle flux (TGE). Particle flux is a measure of the LPCR maturity; it reaches maximum at the largest LPCR size and decays on LPCR contracting fully agreeing with findings made in Tibet [23,25]. The negative polarity of the electric field signals

that the LPCR is creating, and with developing LPCR the particle flux has consequently been rising; simultaneously mature LPCR prevents negative CG– flashes owing to an abundant lower positive charge making intracloud IC– flashes preferable (see also [22]). The negative CG– discharges occurred in the late stage of the storm on the degradation of the LPCR when the particle flux stopped. Therefore, scenarios (a) and (b) of Sec. II are enabled successively during one and the same thunderstorm. Aragats thunderstorm data also confirm the finding from Tibetan thunderstorms that emerged LPCR did not cause positive CG+ flashes. The characteristic time scale of maturing the LPCR is  $\sim 10$  min coinciding with estimates from thunderstorms at the Tibet Plateau.

The technique of measuring particle fluxes simultaneously with near-surface electric field and lightning occurrences of different types first developed and used on Aragats allows following up on the creation of the LPCR and its contraction. The maximal flux of gamma rays detected at the surface (and corresponding maximal flux of the electrons within the lower dipole) pointed at the maximal positive electric field in the cloud and, correspondingly, on the maximal dimension and charge of the LPCR. The distance between the main negatively charged layer in the middle of a cloud and LPCR should be significantly large to provide the large potential drop necessary for the electron acceleration. Fading of the gamma ray flux evidences the degradation of the LPCR. Measured particle flux along with registered lightning occurrences of the different types allows research of the fine structure of the thunderstorm, including the time evolution of the LPCR and ongoing processes of intracloud lightning initiation and electron avalanche propagation.

In several events the particle fluxes (TGEs) precede lightning occurrences, thus demonstrating that the downward moving streamer can use the conductive channel opened by the downward electron-gamma ray avalanche (see [32]); however, for some of the TGEs the frequency of lightning occurrences at maximal particle flux is very low, signaling that in some circumstances the particle acceleration and IC– lightning occurrences can compete.

### ACKNOWLEDGMENTS

The authors highly appreciate the discussions of the topics related to the presented paper at seminars of the Cosmic-Ray Division of Alikhanyan National Lab. Arakelyan Karen and Pokhsranyan David were instrumental in installing and preparing software for treating the time series of electric field and lightning measurements. Reymers Artur provides data transfer from the particle detectors to databases at CRD headquarters. Suren Chilingaryan tuned ADEI data visualization code for cosmic-ray monitoring. Narine Khachatryan designed figures. To all of them the authors express gratitude for fruitful collaboration.

## ROLE OF THE LOWER POSITIVE CHARGE REGION ...

- [1] J.R. Dwyer, D.M. Smith, and S.A. Cummer, *Space Sci. Rev.*, doi: 10.1007/s11214-012-9894-0 (2012).
- [2] M. Stolzenburg, T.C. Marshall, and W.D. Rust, *J. Geophys. Res.* **103**, 14079 (1998).
- [3] D.N. Holden, C.R. Holmes, C.B. Moore, W.P. Winn, J.W. Cobb, J.E. Griswold, and D.M. Lytle, *Local Charge Concentration in Thunderclouds, in Sixth International Conference on Atmospheric Electricity* (University of Manchester, Manchester, England, 1980).
- [4] C.T.R. Wilson, *Proc. Cambridge Philos. Soc.* **22**, 534 (1925).
- [5] A.V. Gurevich, G.M. Milikh, and R.A. Roussel-Dupré, *Phys. Lett.* **165A**, 463 (1992).
- [6] L.P. Babich, I.M. Kutsyk, E.N. Donskoy, and A.Y. Kudryavtsev, *Phys. Lett. A* **245**, 460 (1998).
- [7] A. Chilingarian, B. Mailyan, and L. Vanyan, *Atmos. Res.* **114-115**, 1 (2012).
- [8] L.I. Dorman and I.V. Dorman, *Adv. Space Res.* **35**, 476 (2005).
- [9] A. Chilingarian *et al.*, *Nucl. Instrum. Methods Phys. Res., Sect. A*, **543**, 483 (2005).
- [10] A. Chilingarian *et al.*, *J. Phys. G* **29**, 939 (2003).
- [11] A.V. Gurevich and G.M. Milikh, *Phys. Lett. A* **262**, 457 (1999).
- [12] A.V. Gurevich, L.M. Duncan, A.N. Karashtin, and K.P. Zybin, *Phys. Lett. A* **312**, 228 (2003).
- [13] L.P. Babich, E.I. Bochkov, and I.M. Kutsyk, *Geomagn. Aeron.* **49**, 232 (2009).
- [14] J.R. Dwyer and L. Babich, *J. Geophys. Res.* **116**, A09301 (2011).
- [15] J.R. Dwyer and D.M. Smith, *Geophys. Res. Lett.* **32**, L08811 (2005).
- [16] L.P. Babich, E.I. Bochkov, and I.M. Kutsyk, *J. Exp. Theor. Phys.* **112**, 902 (2011).
- [17] A. Chilingarian, A. Daryan, K. Arakelyan, A. Hovhannisyan, B. Mailyan, L. Melkumyan, G. Hovsepian, S. Chilingaryan,

PHYSICAL REVIEW D **86**, 072003 (2012)

- A. Reymers, and L. Vanyan, *Phys. Rev. D* **82**, 043009 (2010).
- [18] A. Chilingarian, G. Hovsepian, and A. Hovhannisyan, *Phys. Rev. D* **83**, 062001 (2011).
- [19] G. Simpson and F.J. Scrase, *Proc. R. Soc. A* **161**, 309 (1937).
- [20] C.B. Moore and B. Vonnegut, *The Thundercloud, in Lightning*, edited by R.H. Golde (Academic, New York, 1977).
- [21] S.D. Pawar and A.K. Kamra, *J. Geophys. Res.* **109**, D02205 (2004).
- [22] A. Nag and V.A. Rakov, *Geophys. Res. Lett.* **36**, L05815 (2009).
- [23] X. Qie, T. Zhang, C. Chen, G. Zhang, T. Zhang, and X. Kong, *Atmos. Res.* **91**, 244 (2009).
- [24] E.R. Williams, M.E. Weber, and R.E. Orville, *J. Geophys. Res.* **94**, 13213 (1989).
- [25] X. Qie, T. Zhang, G. Zhang, T. Zhang, and W. Wei, *Geophys. Res. Lett.* **32**, L05814 (2005).
- [26] P. Salvini, *Proceedings of the workshop, Aragats-2011, Nor Amberd, Armenia* (Cosmic Ray Division, Yerevan Physics Institute, Yerevan, Armenia, 2012).
- [27] S. Chilingaryan, A. Chilingarian, V. Danielyan, and W. Eppler, *J. Phys. Conf. Ser.* **119**, 082001 (2008).
- [28] S. Chilingaryan, A. Beglarian, A. Kopmann, and S. Voekling, *J. Phys. Conf. Ser.* **219**, 042034 (2010).
- [29] A. Chilingarian and T. Karapetyan, *Adv. Space Res.* **47**, 1140 (2011).
- [30] H. Tsuchiya, T. Enoto, S. Yamada, T. Yuasa, K. Nakazawa, T. Kitaguchi, M. Kawaharada, M. Kokubun, H. Kato, M. Okano, and K. Makishima, *J. Geophys. Res.* **116**, D09113 (2011).
- [31] T. Torii, T. Sugita, M. Kamogawa, Y. Watanabe, and K. Kusunoki, *Geophys. Res. Lett.* **38**, L24801 (2011).
- [32] D.M. Smith, B.J. Hazelton, B.W. Grefenstette, J.R. Dwyer, R.H. Holzworth, and E.H. Lay, *J. Geophys. Res.* **115**, A00E49 (2010).

**Remarks on recent results on neutron production during thunderstorms**

A. Chilingarian,\* N. Bostanjyan, T. Karapetyan, and L. Vanyan

*Yerevan Physics Institute, Alikhanyan Brothers 2, Yerevan 000036, Armenia*

(Received 24 June 2012; published 13 November 2012)

We analyze the neutron fluxes correlated with thunderstorm activity recently measured at mountain altitudes by the Tien-Shan, Tibet, and Aragats groups. We perform simulations of the photonuclear reactions of gamma rays born in the electron-gamma ray avalanches and calculate the expected count rates of the neutron detectors used by the three groups. We also present results of an independent experiment performed at the Nor Amberd high altitude research station in Armenia. Our analysis supports the Tibet and Aragats groups' conclusions on the photonuclear nature of thunderstorm-correlated neutrons (directly in the neutron monitor and in the atmosphere). The photonuclear reactions of the gamma rays born in the electron-photon avalanches in the thunderstorm atmospheres interacting with the air atoms and with lead producer of a neutron monitor can provide neutron yield compatible with additional count of neutron monitors registered during thunderstorm ground enhancements.

DOI: 10.1103/PhysRevD.86.093017

PACS numbers: 92.60.Pw, 13.40.-f, 94.05.Dd

**I. INTRODUCTION: NEUTRON PRODUCTION SIMULATIONS**

Recently, three papers were published [1–3] on measuring the sizable neutron fluxes that were registered during thunderstorms. All three measurements were done at high altitudes<sup>1</sup> with neutron monitors [4] and thermal neutron counters. The Aragats and Tibet groups measure coinciding in time with neutrons gamma ray fluxes, although the Tibet group with a very high threshold of 40 MeV. Plastic scintillators (60 and 40 cm thick) were used to detect gamma rays. The Aragats and Tien-Shan groups, in addition to NMs, also used counters that were sensitive to neutrons (energy range of 0.025–1 eV). In all three experiments, the near surface electric field was monitored; at Tien-Shan and Mt. Aragats, the atmospheric discharges were monitored as well.

However, the three groups drastically differ in their explanations of the origin of neutron flux. The Tien-Shan group reports large fluxes of thermal neutrons correlated with atmospheric discharges; the Aragats and Tibet groups do not relate the neutron flux to lightning occurrences, but rather to photonuclear reactions of the bremsstrahlung gamma rays born in the relativistic runaway electron avalanches (RREA) [5] (also referred to as runaway breakdown [6]) in the thunderstorm atmospheres. However, the Tibet group assumes that gamma rays directly initiate NM counts by photonuclear reactions with lead producer of NM [3]; the Aragats group accepts the photonuclear reaction of the RREA gamma rays with the atmosphere as a source of neutrons [1].

The Tien-Shan group's hypothesis on the origin of neutrons is based on the large thermal neutron flux detected by an outdoor neutron detector correlated in time with

atmospheric discharges. To prove their claims, the Tibet and Aragats groups, along with presenting the measured neutron fluxes, also perform the Geant4 simulations to calculate the detector response. To resolve apparent ambiguity and to clarify neutron production mechanisms, we analyze in depth the simulation schemes used for predicting the neutron yield.

In Ref. [7], the neutron production was simulated by placing the “parent” photon source at heights of 5, 7.5, 10, 15, and 20 km in the atmosphere. Gamma ray energies were drawn from the bremsstrahlung spectrum initiated by the electrons in the atmosphere regions where electrical field is above the RREA threshold. For these heights and the used gamma ray spectrum, the neutron yield relative to gamma ray flux above the photonuclear reaction threshold ( $\sim 10$  MeV) was estimated to be  $\sim 0.6\%$ .

Reference [8] simulated a homogeneous gamma ray source in the form of a disk located at the fixed altitude. The gamma ray energy was simulated according to universal spectrum of bremsstrahlung photons initiated by the RREA electrons. The neutron yield relative to 10 MeV photon flux was estimated to be  $\sim 0.43\%$ . The authors conclude that most likely the photonuclear reactions in the air account for the neutron flux increases observed at mountain altitudes.

The model used by the Aragats group for neutron yield estimation was the same as described above. The relative yield of neutrons was estimated to be 0.3–0.6%, depending on the simulation conditions [1].

The simulations performed in Ref. [3] confirmed the above-mentioned estimates of relative neutron yield. By combining neutron and photon fluxes with an efficiency of NM to register gamma rays with energies above 10 MeV and neutrons above 1 keV (Fig. 1 of Ref. [3]), the Tibet group found that bremsstrahlung gamma rays interacting with lead producer of NM explained the signal obtained by the Tibet NM, and neutrons born in photonuclear

\*chili@aragats.am

<sup>1</sup>Aragats, 3200 m; Tien-Shan, 3340 m; Tibet, 4300 m.

CHILINGARIAN *et al.*

reactions in the atmosphere give only a small fraction of the signal.

Additionally they conclude, “Consequently, not neutrons but gamma rays may possibly dominate enhancements detected by the Aragats neutron monitor (ANM).”

To check this statement and to decide on the nature of the detected peaks in the ANM, we perform a simulation of the RREA process in the strong electric field of the thunderstorm atmosphere. Instead of putting the gamma ray source on the fixed height, we directly simulate the RREA process using the seed electrons from the ambient cosmic ray population and follow the unleashed electron-gamma-ray avalanches till their attenuation. The electron and gamma ray content of RREA as well as neutrons born in the photonuclear reactions were traced till ground level. Also, we inject electrons not from one point but from an extended area. According to estimates done in Refs. [9,10] the gamma ray emitting area has dimensions of 600–700 m. The locality of the particle-emitting region is explained by the small sizes of the lower positive charge region (LPCR) [11] located on the base of the cloud. LPCR with a negatively charged region above it in the thundercloud constitutes the so-called lower dipole, which accelerates electrons downward. Therefore, the size of the particle-emitting region cannot be greater than the size of the LPCR.

From the survived particles’ rates we calculate the neutron and photon fluxes reaching the detector location on 3200 m asl. Due to much broader neutron angular distribution compared with the gamma ray one, the neutron relative yield will be a strictly increasing function of the distance from the projection of the center of radiation region in the thundercloud to the detector location (see Fig. 1). The bremsstrahlung gamma rays are producing

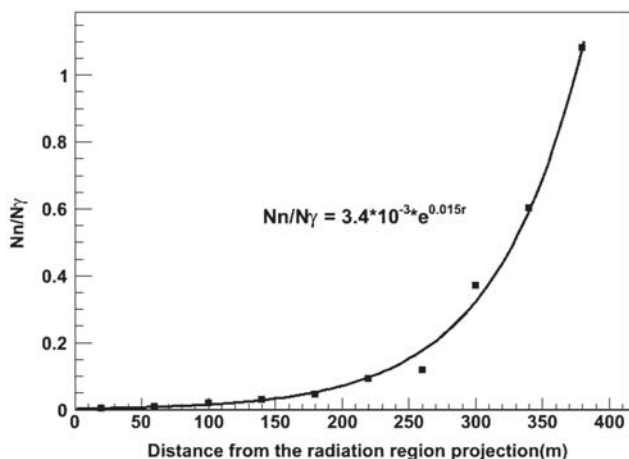


FIG. 1. Dependence of the neutron/gamma ray ratio on distance from the projection of the radiating region. Gamma rays are injected from an altitude of 4700 m according to energy spectrum measured during TGE on October 4, 2010. The detectors were located at 3200 m.

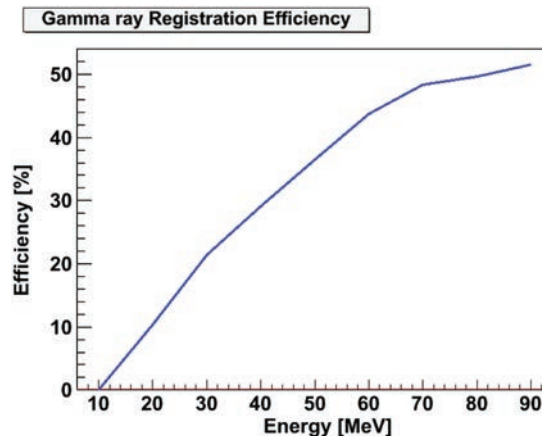


FIG. 2 (color online). The energy dependence of the photon detection efficiency by the 60-cm-thick scintillator.

in the narrow cones around vertically accelerated electrons; in contrast, neutrons emitted by the exciting nucleolus are distributed much broader.

## II. EXPLAINING NEUTRON MONITOR COUNTS: PHOTONUCLEAR REACTIONS IN THE AIR AND IN LEAD

To calculate the yield of neutrons from the photonuclear reactions of the gamma ray flux in lead, we need to recover the gamma ray flux fallen on the neutron monitor. The shape of the gamma ray flux will not differ significantly from the shape of the flux above the roof of the building, which we recovered and published in Ref. [12] for the two largest thunderstorm ground enhancements (TGEs) detected on September 19, 2009 and October 4, 2010 (see details in Refs. [13,14]). The energy dependence of the efficiency of gamma ray registration by the 60-cm-thick scintillator of the Aragats Solar Neutron Telescope is depicted in Fig. 2.

In Table I we demonstrate the bin-to-bin folding of the power law energy spectrum<sup>2</sup> with energy dependent efficiency acquired from Fig. 2. In the first column we depict the energy bin; in the second column we show the fraction of this particular bin relative to the energy range of 10–100 MeV; in the third column we show the efficiency of photon registration in this bin; in the last column we show the “folded” efficiency of the bin—the relative fraction multiplied to efficiency.

The aggregate folded efficiency of ASNT to register gamma ray flux fallen on the detector equals  $\sim 8\%$ ; we obtain this value by summing the “partial” efficiencies from the last column. Taking into account the registration efficiency and proceeding from the count rate enhancement of 10 280 per minute per  $\text{m}^2$  at the maximal flux minute as measured by ASNT on October 4, 2010, we come to

<sup>2</sup>For simplicity we assume the differential energy spectrum of gamma rays in the form of  $dN/dE \sim E^{-3}$ .

## REMARKS ON RECENT RESULTS ON NEUTRON ...

TABLE I. The efficiency of gamma ray registration by ASNT (gamma ray spectrum is adopted from Chilingarian *et al.*, 2012b,  $dN/dE \sim E^{-3}$ ).

| Bin size [MeV] | Bin fraction [%] | Efficiency of registration [%] | “Folded” efficiency |
|----------------|------------------|--------------------------------|---------------------|
| 10–20          | 75.00            | 4.83                           | 0.0362              |
| 20–30          | 13.89            | 15.66                          | 0.0217              |
| 30–40          | 4.86             | 25.58                          | 0.0124              |
| 40–50          | 2.25             | 33.21                          | 0.0074              |
| 50–60          | 1.22             | 40.11                          | 0.0049              |
| 60–70          | 0.74             | 45.23                          | 0.0033              |
| 70–80          | 0.48             | 48.76                          | 0.0023              |
| 80–90          | 0.33             | 51.07                          | 0.0016              |
| 90–100         | 0.23             | 51.94                          | 0.0012              |

gamma ray flux incident the neutron monitor of  $10\,280/0.08 \sim 130\,000$  per minute per  $m^2$ . To estimate how many counts in NM this flux will generate, we adopt from Fig. 1 of Ref. [3] the energy dependence of the NM efficiency to detect photons. Analogically with Table I, we obtain partial efficiencies to register gamma rays (via generated in the lead neutrons) by NM; the details are depicted in Table II.

The aggregate efficiency of the registration of gamma rays obtained by summing the partial efficiencies depicted in the last column equals  $\sim 0.095\%$ . The expected NM count rate we obtain by multiplying the incident gamma ray flux on the aggregate detection efficiency  $130\,000 * 0.00095 \sim 120$  counts per minute per  $m^2$ , in good agreement with the measurement by the Aragats NM on October 4 (ANM) (see Table 2 of Ref. [1]).

The estimate of expected NM counts from another “super TGE” on September 19, 2009 [13] also proves hypothesis of neutron producing by photons in lead absorber. The number of additional gamma rays detected by ASNT on September 19 was 7452 per minute per  $m^2$ ; the recovered gamma ray flux above NM was  $7452/0.08 \sim 93\,000$  per minute per  $m^2$ ; the number of

TABLE II. The efficiency of gamma ray registration by neutron monitor (gamma ray spectrum is adopted from Chilingarian *et al.*, 2012b,  $dN/dE \sim E^{-3}$ ).

| Bin size [MeV] | Bin fraction [%] | Efficiency of registration [%] | “Folded” efficiency |
|----------------|------------------|--------------------------------|---------------------|
| 10–20          | 75.00            | 0.10                           | 0.000750            |
| 20–30          | 13.89            | 0.09                           | 0.000130            |
| 30–40          | 4.86             | 0.04                           | 1.94E-05            |
| 40–50          | 2.25             | 0.08                           | 0.000018            |
| 50–60          | 1.22             | 0.09                           | 0.000011            |
| 60–70          | 0.74             | 0.10                           | 7.37E-06            |
| 70–80          | 0.48             | 0.10                           | 4.78E-06            |
| 80–90          | 0.33             | 0.10                           | 3.28E-06            |
| 90–100         | 0.23             | 0.10                           | 3.28E-06            |

PHYSICAL REVIEW D **86**, 093017 (2012)

expected ANM was  $93\,000 * 0.00095 \sim 88$  counts per minute per  $m^2$ , compatible with what was measured in the experiment.

However, from Table 2 of Ref. [1] we see that only for these two “super events,” the large intensity of gamma rays can generate in lead enough neutrons to explain the detected NM count rate. For rest 10 smaller by gamma ray content events the neutron yield will be too small to explain the additional NM counts by the direct gamma rays’ interactions with lead producer of NM. If we again look at Fig. 1, we can see that small neutron/gamma ray ratios and corresponding large gamma ray fluxes can occur infrequently when the radiating region is just above the detector. At any offset of the detector location related to the radiated region in the thundercloud, the gamma ray content will quickly diminish. In contrast, the neutron content due to a much broader angular distribution will remain more or less constant on much larger distances. Therefore, we can expect that the neutron content on large distances can reach several tens of percent of detected gamma ray flux, and if the radiation region is far from the detector location site we can detect only neutrons without gamma ray contribution. This category of neutron events (much more abundant compared with the “large gamma” events considered above) can be explained by the photonuclear reactions of gamma rays in the atmosphere. For the ten “small” events from Table 2 of Ref. [1], we can estimate that the neutron/gamma ray ratio is equal to  $\sim 5\text{--}15\%$ , which is rather probable from pure geometrical consideration. We do not recover gamma ray intensity for the small events due to the scarcity of the energy deposit histograms measured by the 60-cm-thick scintillator. However, we can roughly estimate this intensity by considering the count rates and recovered intensities of the two largest events. The numbers of counts and recovered intensities above the roof of a building for the September 19, 2009 and October 4, 2010 events are correspondingly, 7452–104 000 and 10 280 and 153 000 per minute per  $m^2$ . The ratio of recovered/detected is 14 and 14.9, and the mean is 14.5. By the analogy, we can estimate the intensity of the May 21, 2009 event’s registered gamma ray enhancement of 1920 as  $1920 * 14.5 = 27\,840$  gamma rays per minute per  $m^2$ . If we assume a neutron/gamma ray ratio of 10%, we will have 2784 neutrons above the roof of the building, and proceeding from the aggregate efficiency of detecting photonuclear neutron spectra estimated to be 2.4%, we come to expect neutron monitor counts of 67 per minute per  $m^2$ , which is in good agreement with the 83 counts per minute per  $m^2$  measured by ANM.

### III. CHECK OF HYPOTHESIS ON THERMAL NEUTRON FLUXES

Reference [2] reported the registration of intensive fluxes of low-energy neutrons generated during thunderstorms. The authors connect registered neutron fluxes with

atmospheric discharges. Unfortunately, the empirical data on neutron detector count rates were not supported by the detector response calculation and with a model of neutron generation. Only several episodes of the detected one-minute count rate enhancements that were possibly correlated in time with the lightning occurrences were presented. Reported observations were done with the Tien-Shan 18NM64 neutron monitor (TSNM) and thermal neutron counters (TSNC) located outdoors and indoors, respectively (see Fig. 2 in Ref. [15]). The counters were filled with  $\text{He}^3$  gas. Because of the absence of producing and moderating material, these counters can register effectively only neutrons having energies in the range of 0.01–1 eV Gurevich *et al.*, 2012. On August 20, 2010 at 12:54, 12:56, 12:58, 13:00, and on August 10, 2010 at 8:06 and 8:08 the external counters register the following enhancements [2]: 1558, 720, 758, 2055, 1673, and 1225 per minute. The same type of TSNM counters located indoors (internal) register the following enhancements: 641, 418, 323, 716, 927, and 922 per minute, i.e., 35–75% of the outdoor (external) counters.

Neutron fluxes fell on the roof of the building where the TSNM and indoor (internal) TSNC were located. The building roof matter was comprised of 2 mm iron tilt, 20 cm carbon [2], and 2.5 cm wood. The Geant4 simulations of the neutron transport through the roof material demonstrated that only 7% (compared with 35–75% calculated above) of the thermal neutron flux can penetrate the roof.

To compare the reported TSNM counts with those expected from the detector response calculation, we have to recover the intensity of thermal neutrons that fell on the roof. A product of the registration efficiency and the total area of six helium counters is  $0.45 \text{ m}^2$  [15]. Accordingly, we readily obtain the flux of thermal neutrons for six considered neutron events: 3462, 1600, 1684, 4567, 3717, and 2722 neutrons per  $\text{m}^2$  per minute. Assuming 0.5% efficiency [2] of TSNM to detect thermal neutrons, we cannot expect more than 40 counts of the TSNM for all six neutron events. However, the TSNM counts reported in Ref. [2] are 804, 1136, 913, 587, 2821, and 2112 per minute.

We can assume that along with thermal neutron flux there is also a flux of neutrons born in photonuclear reaction in the thunderstorm atmosphere not detected by the outdoor TSNC. To date, the maximal estimated neutron flux at Mt. Aragats is  $\sim 5000$  neutrons per  $\text{m}^2$  per minute. By considering the higher location of Tien-Shan we can double this number and assume that photonuclear neutron flux at Tien-Shan can reach 10000 neutrons per  $\text{m}^2$  per minute. Geant4 simulations demonstrate that only  $\sim 20\%$  of photonuclear neutrons can penetrate the roof material; additionally, the 20-cm-thick carbon layer effectively thermalized neutrons, and 97% of the initial neutrons incident on the indoor detectors will be thermalized.

Therefore, 2000 (20% of 10000) neutrons per minute per  $\text{m}^2$  falling on the indoor TSNM will generate approximately the same number of counts (40 per minute per  $\text{m}^2$ ) as the thermal neutron flux. Thus, the hypothesis of the photonuclear nature of neutron flux in Tien-Shan also cannot explain the reported count rate enhancements. Measured by the outdoor TSNC, thermal neutron flux should be five to ten times more intensive to explain the TSNC counts and 20–50 times more intensive to explain the TSNM counts.

#### IV. SIMULTANEOUS DETECTION OF CHARGED AND NEUTRAL FLUXES BY NOR AMBERD DETECTOR ASSEMBLY

New experimental evidence on neutron production correlated with thunderstorms originates from another experimental setup located on the slopes of Mt. Aragats at the Nor Amberd research station. The experimental facilities located at Nor Amberd operated as a part of the Aragats Space Environmental Center [16] and measure fluxes of gamma rays, thermal and high-energy neutrons, and high-energy muons; we consider the registration of multiple particle fluxes as an absolutely necessary condition for making physical inference on the neutron origin.

Detector assemblies measuring secondary cosmic ray fluxes that originated from protons and ions accelerated on the Sun and in the Galaxy are located on the slopes of Mt. Aragats at the Nor Amberd research station at 2000 m above sea level. The Nor Amberd detecting system consists of an 18NM64 neutron monitor (NANM) with three sections of six neutron counters in each, and a multidirectional muon monitor (NAMMM) with two layers of 5-cm-thick plastic scintillators overviewed by a photomultiplier above and below two sections of NANM. Also included are two proportional counters without a lead producer and a polyethylene moderator for detecting thermal neutrons (see Fig. 3). The energy threshold of the upper scintillators is determined by the roof matter and by data acquisition electronics and equals  $\sim 10$  MeV. The upper scintillator registered charged flux above the threshold with very high efficiency reaching 99%; however, the 5-cm plastic scintillator also registers neutral flux (gamma rays and neutrons) although with much smaller efficiency of  $\sim 5$ –10%. The bottom layer of scintillators is located under a significant amount of matter including 10 cm of lead and its energy threshold is  $\sim 350$  MeV; therefore, the bottom layer measures mostly high-energy muons.

Data acquisition electronics calculates all possible coincidences of the upper and bottom scintillators for both sections of the NAMMM. By counting the coincidences of upper and bottom scintillators it is possible to monitor muon fluxes for 12 incident directions. The NANM operates with three dead times ranging from 0.4 to 1250  $\mu\text{s}$ . The monitor counts with shortest dead time give possibility

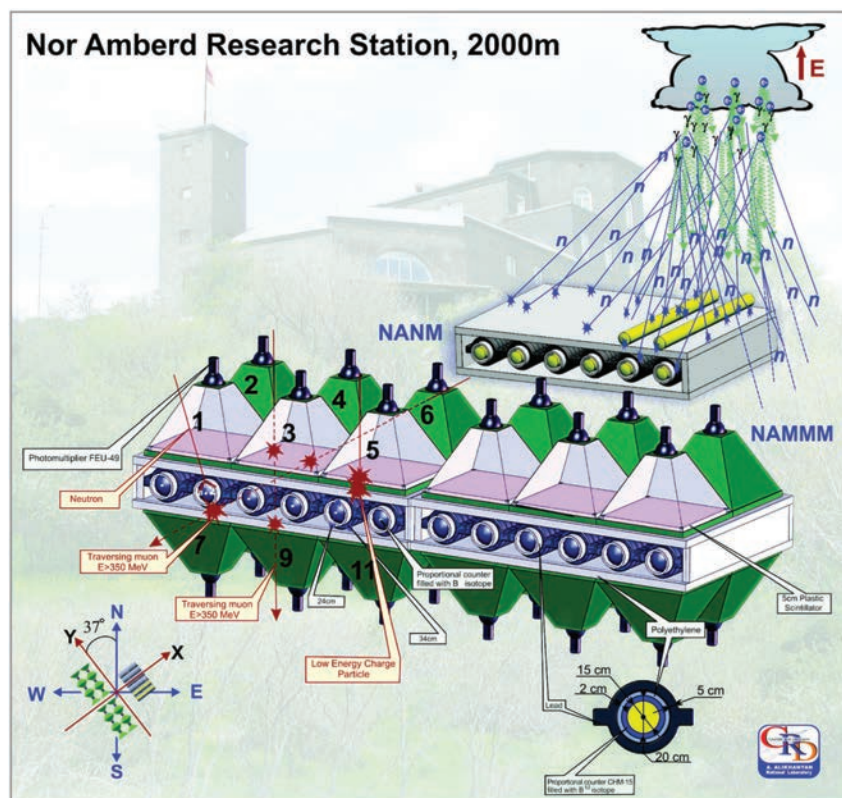


FIG. 3 (color online). Nor Amberd multidirectional muon monitor arranged above and below two sections of the Nor Amberd Neutron Monitor; “bare” proportional counters are located on the third section of NANM.

to count almost all thermal neutrons entering the sensitive volume of the proportional chamber; the long dead time provides a one-to-one relation between the counts and the high energy atmospheric hadrons incident on the detector. If neutron bursts are incident on detector the shortest dead time will provide a registration of almost all neutrons; the longer dead time will miss additional neutrons coming simultaneously within  $1250 \mu\text{s}$ .

In Fig. 4 we post the measured enhancements of time series taken on March 28, 2009 of one-minute count rates of NAMMM top (mostly gamma rays) and bottom layers (mostly muons) as well as NANM one-minute time series corresponding to shortest dead time.

The statistical accuracy of the measurements and significances of the detected peaks are posted in Table III. In Fig. 4 we see a large enhancement of the counts in the upper layer of NAMMM conditioned in the absence of a signal in the lower layer (combination 10—a signal in the upper layer and no signals in the bottom layer of the scintillators); a significant enhancement of the count rate of the neutron monitor and a depletion of counts of high-energy muons. The deficit of muons measured simultaneously with an enhancement of gamma rays is one of the characteristics of the so-called TGEs (see details in Ref. [12]).

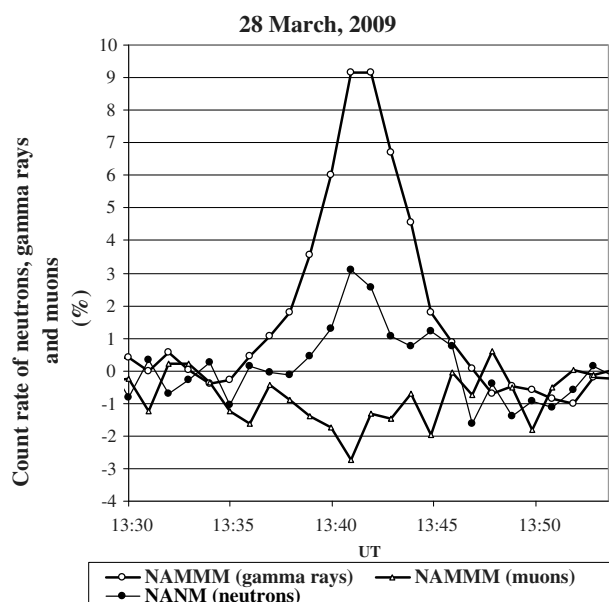


FIG. 4. The one-minute time series of count rates of upper and top layers of NANM and NAMMM.

TABLE III. Statistical characteristics of detectors and detected peaks and dips on March 28, 2009 at 13:43.

| Detector   | Mean count rate per minute | Standard deviation-SD ( $\sigma$ ) and relative standard deviation | Percent of enhancement | Number of SD ( $\sigma$ ) in peak | Number of additional particles (or deficit for muons) at minute of maximal excess ( $\text{min}^{-1} \text{m}^{-2}$ ) |
|--|----------------------------|--|------------------------|-----------------------------------|---|
| NANM neutrons  | 30000                      | 300 (1%)   | 3.2%                   | $3.2\sigma$                       | 53  |
| NAMMM upper (10)                                     | 121150                     | 348 (0.29%)  | 9.2%                   | $32\sigma$                        | 924   |
| NAMMM (muons > 350 MeV); vertical direction excluded | 24000                      | 155 (0.65%)  | -2, 2%                 | $3.5\sigma$                       | -45   |

## V. POSSIBLE SYSTEMATIC ERRORS

The assumed in the simulations charge structure of the thundercloud (strengths and elongations of the electric field, cloud height, and size of the radiating region); although they are in good agreement with rare *in situ* measurements they, can significantly deviate from the conditions of the Aragats thunderstorms, which give rise to detected TGE events. We do not measure the elongation and strength of the electrical field in the particular thundercloud. We also do not directly measure the size of the radiation region in the thundercloud. Therefore, the obtained estimates of the neutron-to-gamma-ray ratio give us overall understanding of the neutron generation process and dependence on the parameters that we cannot locate yet (distance to and geometry of the radiation region).

Estimating the neutron monitor efficiency for low-energy neutrons ( $> 1$  keV) and photons ( $> 10$  MeV) by simulations with Geant4 code is rather difficult due to very small values of efficiencies ( $\sim 0.1$ – $2\%$ ).

In our Geant4 simulations of the Tien-Shan detectors response we used known from publications detector setup. However, it possibly changed from the published one during the experiment. Additional calculations are needed (better by the Tien-Shan group) to finally understand the measurements presented in Ref. [2].

## VI. CONCLUSIONS

We analyzed the data on recently reported neutron fluxes correlated with thunderstorms. The Tibet group explained the detected count rate enhancement in the neutron monitor by the previously neglected direct registration of gamma ray photons by NM. According to their estimates, the photonuclear reactions of gamma rays in

lead producer of NM exceed the contribution of the neutrons born in the photonuclear reactions in the atmosphere. The Aragats group supported another hypothesis of the neutron production in the photonuclear reactions in the atmosphere.

A new realistic simulation of the RREA process in the thunderstorm atmosphere checked the situation. We found that the explanation of the Tibet group is supported by a new simulation if the radiation region is just above the neutron detector. At any offset of the radiation region relative to the detector location, the contribution to the NM counts of direct gamma ray interactions in a lead absorber quickly diminished and the “atmospheric” neutron contribution enlarged.

Therefore, both photonuclear processes in the air and in the lead absorber of NM should be considered to explain the neutron fluxes correlated with thunderstorms.

Also, we find that the simulations of neutron yield with gamma ray source located on the fixed altitude above the detector gives optimistically biased relative neutron yield. Proceeding from the thermal neutron count rates measured by the outdoor thermal neutron counter reported in Ref. [2], we calculate the expected counts of the indoor Tien-Shan neutron monitor and the indoor thermal neutron counter taking into account the detector response. The calculated fluxes of the indoor detectors are much lower than the reported ones. Thus, the reported data on indoor and outdoor detectors are not consistent.

The Aragats and Tibet measurements do not support the hypothesis of particle fluxes directly related to the atmospheric discharges, accepted by the Tien-Shan group. Accordingly, during the developed lower positive charge region in the thundercloud (necessary condition of the creation of lower dipole accelerated electrons downward), the flash rate is quite low [11,17].

[1] A. Chilingarian, N. Bostanjyan, and L. Vanyan, Phys. Rev. D **85**, 085017 (2012).

[2] A. V. Gurevich, V. P. Antonova, A. P. Chubenko, A. N. Karashtin, G. G. Mitko, M. O. Ptitsyn, V. A. Ryabov,

A. L. Shepetov, Y. V. Shlyugaev, L. I. Vildanova, and K. P. Zybin, Phys. Rev. Lett. **108**, 125001 (2012).

[3] H. Tsuchiya, K. Hibino, K. Kawata *et al.*, Phys. Rev. D **85**, 092006 (2012).

## REMARKS ON RECENT RESULTS ON NEUTRON ...

PHYSICAL REVIEW D **86**, 093017 (2012)

- [4] C. J. Hatton and H. Carmichel, *Can. J. Phys.* **42**, 2443 (1964).
- [5] L. P. Babich, I. M. Kutsyk, E. N. Donskoy, and A. Y. Kudryavtsev, *Phys. Lett. A* **245**, 460 (1998).
- [6] A. V. Gurevich, G. M. Milikh, and R. A. Roussel-Dupre, *Phys. Lett. A* **165**, 463 (1992).
- [7] B. E. Carlson, N. G. Lehtinen, and U. S. Inan, *J. Geophys. Res.* **115**, a00e19 (2010).
- [8] L. P. Babich, E. I. Bochkov, I. M. Kutsyk, and R. A. Roussel-Dupre, *J. Geophys. Res.* **115**, A00E28 (2010).
- [9] H. Tsuchiya *et al.*, *J. Geophys. Res.* **116**, D09113 (2011).
- [10] T. Torii, T. Sugita, M. Kamogawa, Y. Watanabe, and K. Kusunoki, *Geophys. Res. Lett.* **38**, L24801 (2011).
- [11] A. Chilingarian and R. Mkrtychyan, *Phys. Rev. D* **86**, 072003 (2012).
- [12] A. Chilingarian, B. Mailyan, and L. Vanyan, *Atmos. Res.* **114–115**, 1 (2012).
- [13] A. Chilingarian, A. Daryan, K. Arakelyan, A. Hovhannisyan, B. Mailyan, L. Melkumyan, G. Hovsepyan, S. Chilingaryan, A. Reymers, and L. Vanyan, *Phys. Rev. D* **82**, 043009 (2010).
- [14] A. Chilingarian, G. Hovsepyan, and A. Hovhannisyan, *Phys. Rev. D* **83**, 062001 (2011).
- [15] A. P. Chubenko, A. L. Shepetov, V. P. Antonova, P. A. Chubenko, and S. V. Kryukov, *J. Phys. G* **35**, 085202 (2008).
- [16] A. Chilingarian *et al.*, *Nucl. Instrum. Methods Phys. Res., Sect. A* **543**, 483 (2005).
- [17] X. Qie, T. Zhang, G. Zhang, T. Zhang, and X. Kong, *Atmos. Res.* **91**, 244 (2009).

## Preliminary analysis of the unusual TGE event detected by ASEC monitors at 19 October 2013

*A.Chilingarian, G.Hovsepyan, E.Mnatsakanyan, A.Reymers*

*Yerevan Physics Institute, Alikhanyan Brothers 2, Yerevan, Armenia*

---

**Abstract:** Research of the Thunderstorm ground enhancements (TGEs) on Mt. Aragats continued with new particle detectors and Data acquisition electronics allowing 10-fold lowering of the energy thresholds of particle detectors (from 1.5-2 MeV down to 100 KeV); and - detection of a second duration time series instead of previously measured minute time series. New experimental techniques disclose some unexpected features of the TGEs detected by Aragats particle detectors at 19 October 2013. We present a detailed description of this event, including meteorological conditions, near surface electric field disturbances and the time series of multiple detectors measuring particle fluxes on altitude 3200 m below thundercloud.

---

### 1. INTRODUCTION

The separation of positive and negative charges in thundercloud and existence of a stable ambient population of MeV electrons in atmosphere constitutes a natural electron accelerator directed additional fluxes of electrons to the Earth's surface (Thunderstorm ground enhancements, TGEs, Chilingarian et al., 2011) and to open space (Terrestrial gamma flashes, TGFs, Fishman et al., 1994). Recent measurements of the TGEs shed light on the size of the particle emitting region (Tsushya et al., 2011; Torii et al., 2011); 2 modes of electron acceleration (Chilingarian, Vanyan and Mailyan, 2012); energy spectra of electrons (Chilingarian, Mailyan, Vanyan et al., 2013) and gamma rays (Chilingarian, Hovsepyan, Kozliner, 2013); and on the nature of the lower dipole accelerating electrons downward (Chilingarian, 2014). Vast amount of TGE events registered on mountain Aragats on altitude 3200 m in 2009-2013 (see statistical analysis of TGE events in Chilingarian, Karapetyan and Melkymyan, 2013) allows to develop a comprehensive model of TGE initiation. The majority of events occurred during prolonged periods of negative near-surface electric field lasting from a few till tens of minutes. Energy of accelerated electrons can reach ~40-50 MeV; flux of electron and gamma rays with energies above few MeV can exceed cosmic ray background up to 10 times. High intensities are due to unleashing of the Relativistic Runaway electron Avalanches (RREA, Wilson, 1925, Gurevich et al., 1992, Babich et al., 1998); large energies of gamma rays due to MODifying of the electron energy Spectra (MOS process, Lidvansky and Khaerdinov, 2009; Chilingarian, Mailyan and Vanyan, 2012).

Further researches of the TGE phenomena on Mt. Aragats are connected with 10-fold lowering of the energy thresholds of particle detectors (from 1.5-2 MeV down to 100 KeV) and with detection of a second duration time series instead of previously measured minute time series. New experimental techniques disclose some unexpected features of the TGE detected by Aragats particle detectors at 19 October 2013. We present a detailed description of this event, including meteorological conditions, near surface electric field disturbances and the time series of multiple detectors measuring particle fluxes on altitude 3200 m just below thundercloud.

### 2. CONDITIONS ON ARAGATS AT AFTERNOON 19 OCTOBER 2013

At 19 October 2013 weather at Aragats station was smoggy; according to All Sky Cam<sup>1</sup> monitoring, see Fig. 1 the cloud was sitting just on the Earth's surface at 15:10 – 15:40.



*Figure 1. The entire sky field of view of Aragats station at October 19, 2013, 11:20 UT.*

The index of UV radiation<sup>2</sup> and strength of solar radiation at the moment of maximal particle flux (between 11:21-11:22) was minimal see Fig. 2. Consequently, the cloud cover fraction was maximal, don't allow solar and UV radiation to reach Earth's surface.

---

<sup>1</sup>The Moonglow Technologies All Sky Cam gives you a live video view of the entire sky, day or night, rain or shine, <http://www.moonglowtech.com/products/AllSkyCam/index.shtml>

<sup>2</sup> Measured by Vantage Pro2 weather station, [http://www.davisnet.com/weather/products/wx\\_product\\_do.cs.asp?pnum=06152](http://www.davisnet.com/weather/products/wx_product_do.cs.asp?pnum=06152)

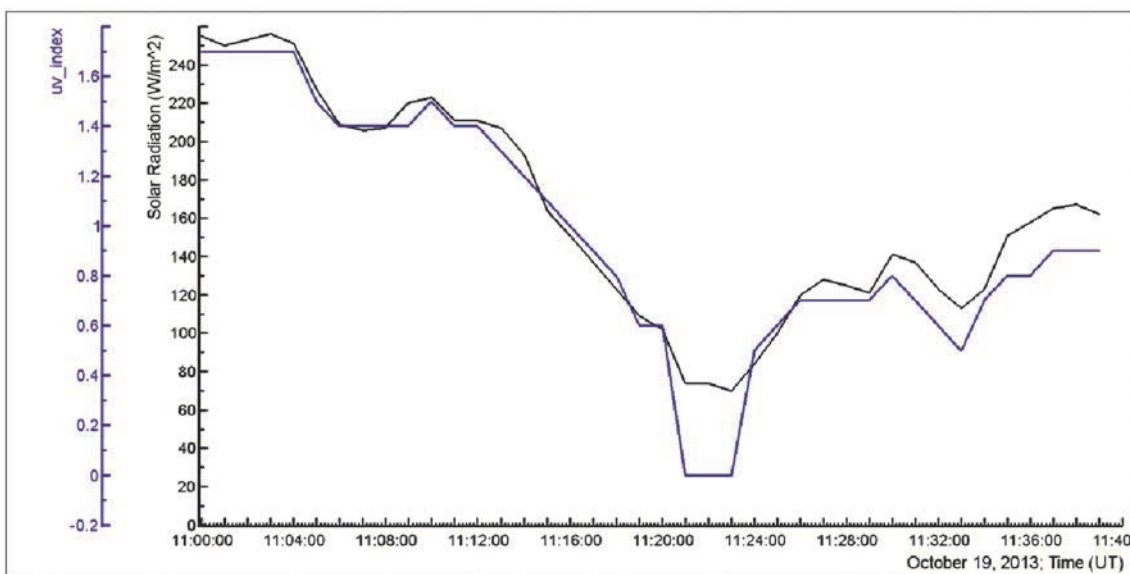


Figure 2. The index of UV radiation and strength of solar radiation

### 3. NEAR SURFACE ELECTRIC FIELD AND LIGHTNING OCCURRENCE

The near surface electric field is measured with two electric mills of EFM-100 type located on Aragats station 3200 m above sea level<sup>3</sup>. Both devices are located on the masts above the roofs of buildings; the distance between electric mills is ~300 m (see Fig. 4); the height difference is ~ 20 m. The readings of the electric mills are enumerated and stored 20 times per second; however, usually only the mean values of these 20 measurements appears in the data base as 1-second time series.

EFM-100 electric mills were calibrated during operation in one and the same place on the roof of MAKET building. After relocation of the second mill above the metallic housing of the Gamma array on the roof of the flat concrete calorimeter the reading of the second mill differs from readings of the same type device located on the roof of MAKET building. We can attribute this difference both to changing electric field and location site peculiarities; nevertheless, usually both devices demonstrate rather coherent measurements, see Fig. 4. On October 19 after 11:17 we can see in Fig. 5 very large differences in the device readings, becoming drastic after 11:19. The pattern of disturbances of electric field measured by devices located on distance of ~300 m becomes absolutely different. EFM located on Gamma from 10:19 till 10:21 measures continuous enlargement of the electric field from -23 kV/m to +22 kV/m.; corresponding enlargement of the field measured by EFM located on MAKET was smaller from -6 kV/m to 10 kV/m. After nearby lightning at 11:20:53 the electric mill near GAMMA detector fails and do not provide any data before restarting next day; many particle detectors as well failure for several seconds and some of them stopped..

Fast increase of the electric field was accompanied with unprecedented coherent enhancement of the particle flux to be discussed in the next section.



Figure 3. GOOGLE map of Aragats station with locations of 2 electric mills on the roof of MAKET building and on one of GAMMA detectors scintillators housing.

<sup>3</sup> Boltek firm electrical mill EFM100, <http://www.boltek.com/efm100.html>;

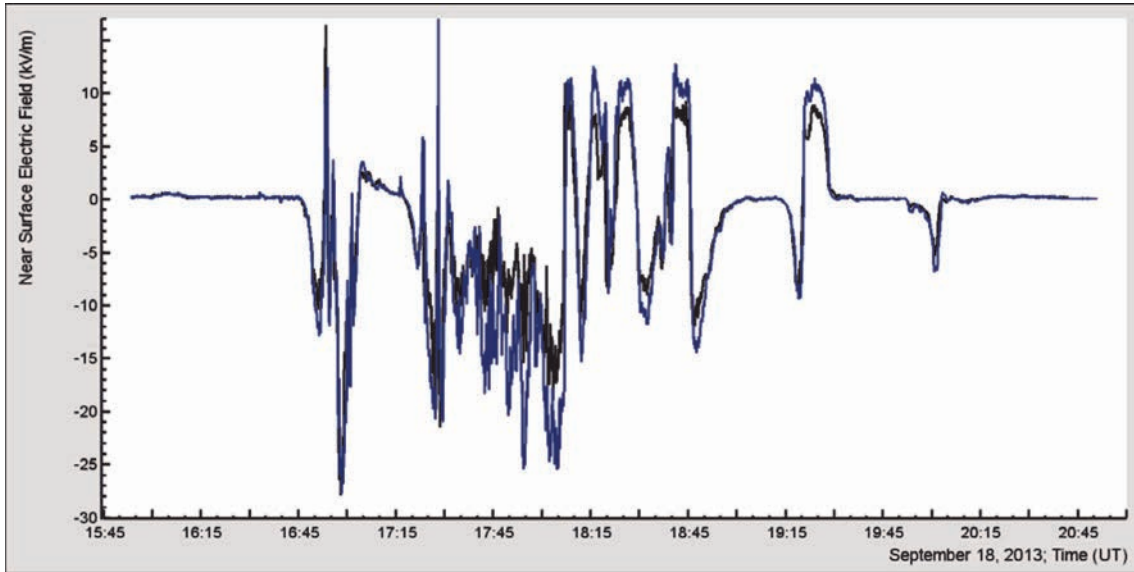


Figure 4. Comparison of the 2 electric mills readings; location of both is depicted in Fig.3

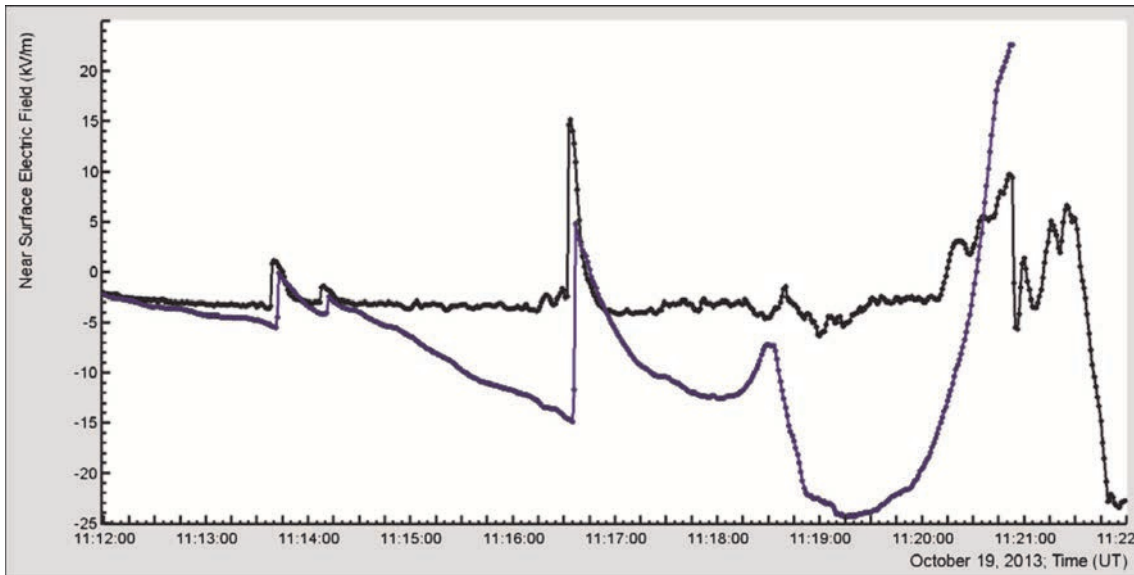


Figure 5. Disturbance of electric field measured by 2 electric mills of Boltek firm; in the insert in left top corner the 50 msec time series of MAKET electric mill are demonstrated.

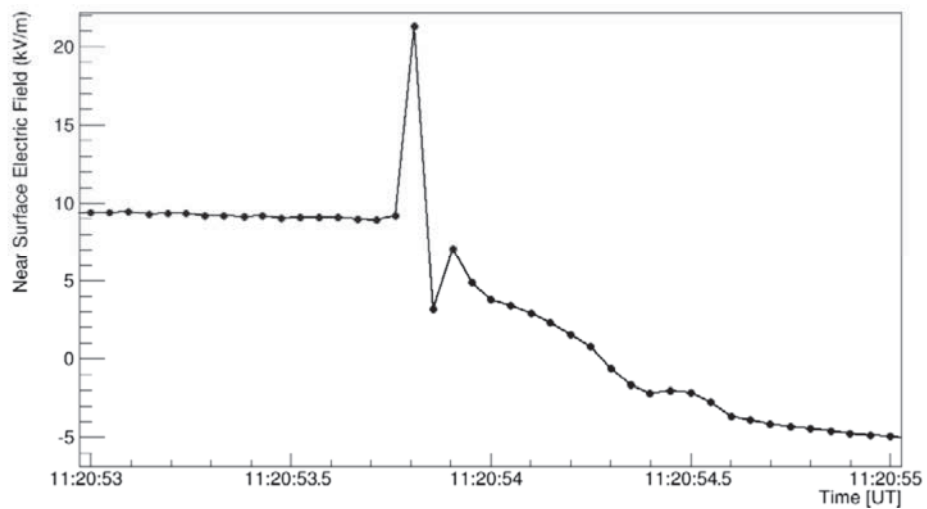


Figure 6. Sharp enhancement of near surface electric field measured by EFM-100 electric mill located on the roof of Maket building.

As we mention in the beginning of the section, electrical mills of EFM-100 type provide readings with frequency 20 Hz, and in Fig. 6 we can see 50 msec time series measured around 11:20:53 UT by electric mill located on the roof of MAKET building. Detected very sharp (duration less than 50 msec, see Fig.6) 20 kV/m peak do not significantly influence the second-averaged reading (at 11:20:53) which equals  $\sim 3$  kV/m. This electric field sharp enhancement and decay coincides with nearby -IC lightning flash, registered by another BOLTEK device – lightning detector of LD-250 type running NextStorm discharge identifying software. Station staff also reports very strong lightning occurred about 15:20 local time.

#### 4. SHORT TGE AT 19 OCTOBER 2013 MEASURED BY VARIOUS PARTICLE DETECTORS

Availability of the one-second time series gives possibility to reveal short TGEs with duration less than 1 minute<sup>4</sup>. In Fig. 8 we depict the significance of the TGE lasting less than 1 minute from 11:19:57 till 11:19:53. The same TGE in 1-minute time series gives only one spike (see Fig. 10, where STAND1 detector time series are depicted) usually treated previously as a core of Extensive Air Shower (EAS) occasionally hitting the detector. Precise detection of changing count rates not only reveals new TGE events, but also discovers new type relation of TGE with the near surface electric field. In the Fig. 7 we demonstrate 1-second time series of 3 cm thick outdoor plastic scintillator count rates along with time series of near surface electric field as measured by EFM-100 electric mill located on the Gamma calorimeter roof. It is worth to mention unprecedented high positive correlation of count rate and near surface electric field (correlation coefficient  $r=0.99$ )<sup>5</sup>. The 1 m<sup>2</sup> area plastic scintillator count rate of  $\sim 530$  per second well agrees with expected charged particle flux with energies above  $\sim 7$  MeV on altitude 3200 m. Rather small relative error for 1-second time series  $\sim 4.4\%$  provide huge reliability of the peak – 34 standard deviations ( $\sigma$ ) above the mean value.

Other particle detectors also demonstrate huge enhancements. Belonging to the ASNT one of four 60 cm thick indoor plastic scintillators (see detailed description of detector in Chilingarian et al., 2010) enhances count rate up to 10,054 from the mean 3079  $\pm$  55; which corresponds to  $\sim 230\%$  of enhancement and  $\sim 130 \sigma$  reliability, see Fig. 8. New low threshold CsI and NaI detectors as well as 3 cm

thick outdoor scintillator demonstrates the peak with significance of  $\sim 30 \sigma$ .

Although the thundercloud was rather low above Aragats station we thought that TGE mostly consists of gamma rays with small contamination of electrons.

Our arguments are based on the huge peak measured by the 60 cm thick plastic scintillator apparent in the Fig. 8. Indoors location of this detector under significant amounts of matter prevents detection of electron with energies below 25-30 MeV. Another proves of gamma ray prevailing is closeness of peaks of 100 and 010 coincidences measured by STAND1 detector see Fig. 9. Probability of electrons to be registered in lower scintillator without being detected in upper one is very small, see details in Chilingarian, Hovsepian and Kozliner, 2012. In Fig. 10 we post time series of the count rates of various particle detectors with different electronic thresholds. The low threshold CsI detector ( $\sim 100$  KeV, CR background  $\sim 70,000$  per m<sup>2</sup>, per sec.) measures 70,000 additional gamma rays, see Table 1.

In Table 1 we enumerate the TGE fluxes measured by various particle detectors those time series were posted in Figures 8 and 10. We recover the TGE fluxes under the assumption that majority of particle were gamma rays. Energy thresholds of these particles are different, as well as the gamma ray detection efficiencies.

*Table 1. Estimates of cosmic ray and TGE gamma ray flux by various detectors*

|                    | Mean<br>(CR)<br>count rate | TGE<br>peak | Detector<br>area (m <sup>2</sup> ) | Det.<br>eff. | CR flux*<br>(1/m <sup>2</sup> sec) | TGE<br>Flux**<br>(1/m <sup>2</sup> sec) |
|--------------------|----------------------------|-------------|------------------------------------|--------------|------------------------------------|---|
| ScI                | 689 $\pm$ 25               | 1450        | 0.0135                             | 0.8          | 50,000                             | 70,000                                  |
| 3cm<br>thick sc.   | 532 $\pm$ 23               | 1320        | 1                                  | 0.02         | 532                                | 40,000                                  |
| 60 cm<br>thick sc. | 3080 $\pm$<br>55           | 10054       | 1                                  | 0.20         | 3080                               | 35,000                                  |
| NaI                | 75 $\pm$ 10                | 370         | 0.032                              | 0.8          | 2340                               | 11,500                                  |

\*Flux of all particles normalized to 1 m<sup>2</sup> detector area, \*\*Flux of gamma ray TGE normalized to detector area and efficiency to detect gamma rays

The differential energy spectrum of TGE was measured by 10-sec histograms of energy releases in 60 cm thick scintillator depicted in Fig. 11. The underestimation of the intensity of lower energies can be explained by attenuation of the low energy gamma rays in the matter above the detector

<sup>4</sup> To detect 1-second time series we use data acquisition card developed for the network of cosmic ray detectors located on roofs of school buildings, Hansen et al., 2004.

<sup>5</sup> TGEs lasting minutes and more usually occur during periods of negative near-surface electric field, Chilingarian and Mkrtchyan, 2012)

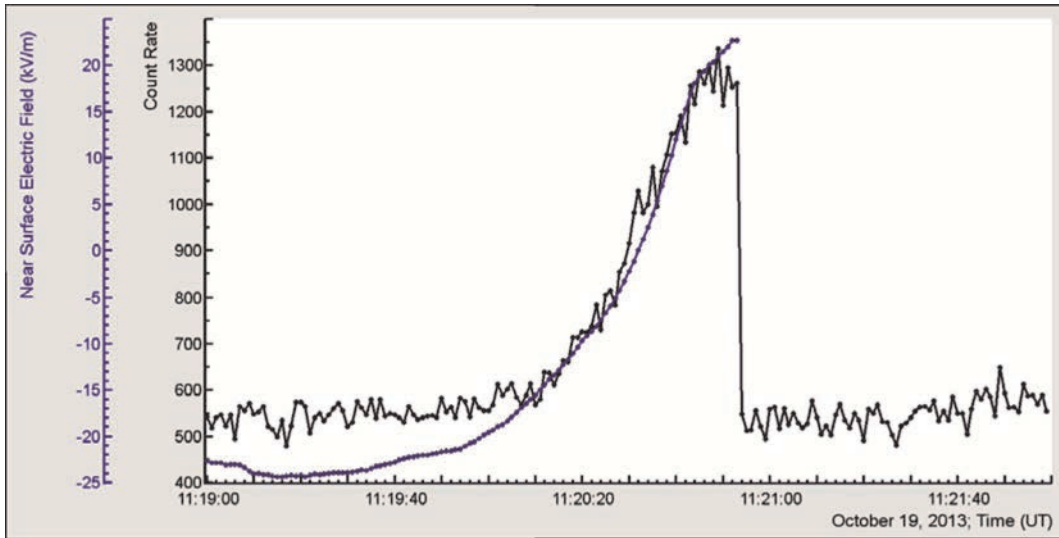


Figure 7. 1-second time series of electric field disturbances (EFM 100 on roof of Gamma calorimeter) and particle flux enhancement (3 cm thick outdoor plastic scintillator).

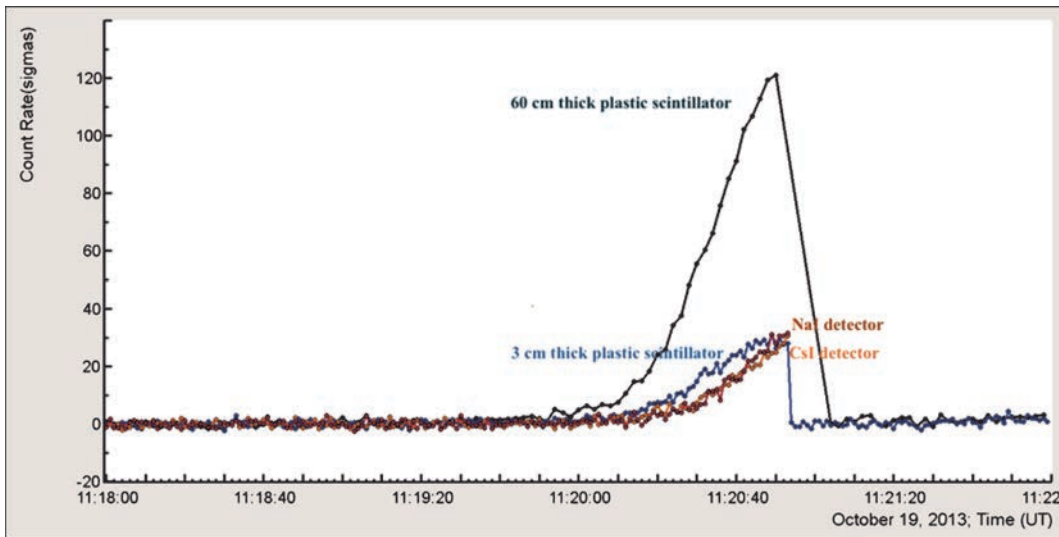


Figure 8. Significances of the peaks detected by different particle detectors at 19 October 2013, 11:19:20 – 11:19:21

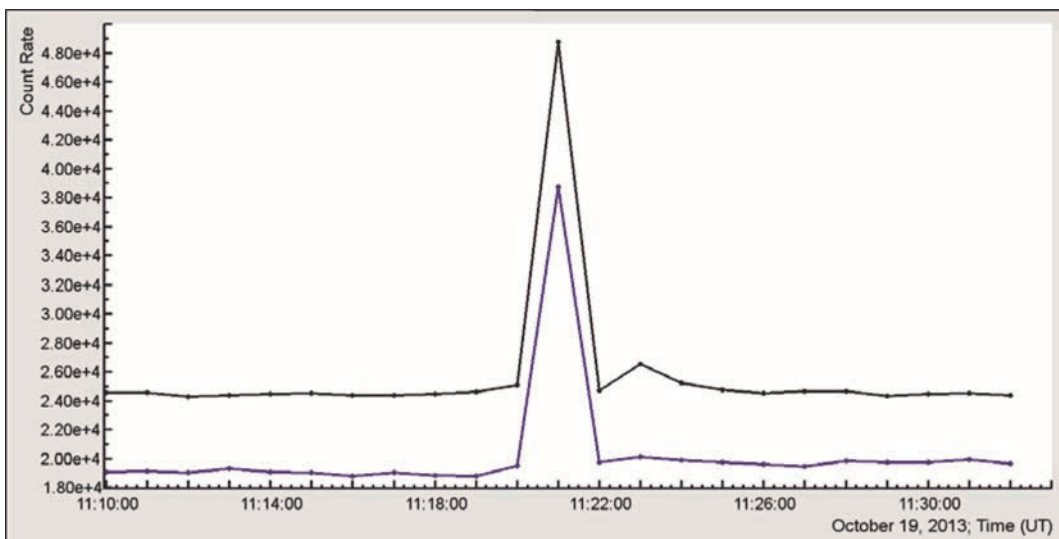


Figure 9. 1-minute time series of STAND1 detector; 100 coincidence (upper) and 010 coincidences

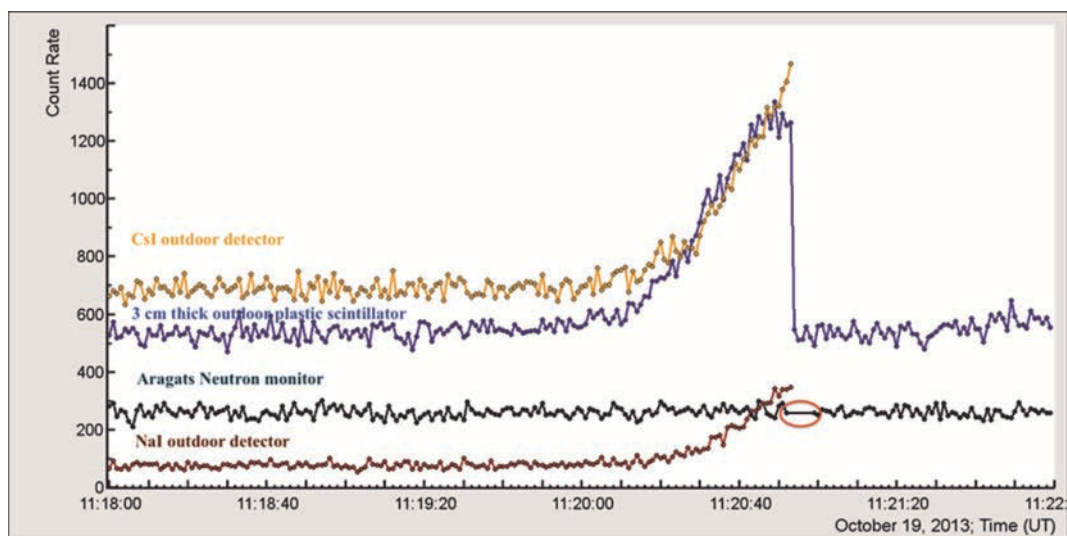


Figure 10. 1-second time series of different particle detectors

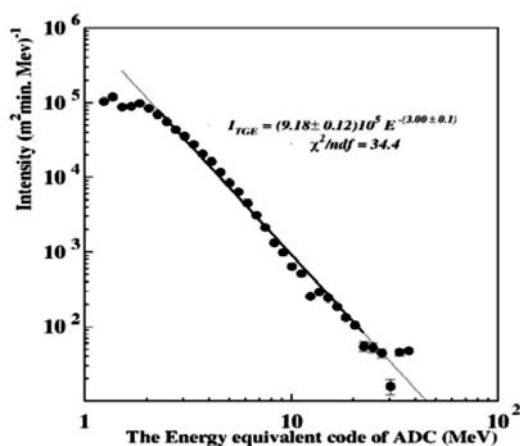


Figure 11. The differential energy spectrum of 19 October TGE measured by 60cm thick plastic scintillator.

### 5. ABRUPT DECAY OF TGE; LAST SECOND MEASUREMENTS

The TGE event abruptly decays at 11:20:53, probably due to atmospheric discharge detected by the lightning monitor and by abrupt (within 50 msec, see Fig. 6) reduction of the near surface electric field. Data acquisition electronics (DAQ) of several particle detectors fail the same second (NaI, CsI, see Fig. 10); DAQ electronics of other detectors lost connection with on-line computer due to saturation. In Fig. 8 we can see gap in 60 cm. thick scintillator readings lasting from 11:20:51 till 11:21:03. In Fig. 10 are depicted time series of Aragats neutron monitor (ArNM), demonstrating no enhancements; however the ArNM DAQ electronics also failed from 11:20:53 till 11:20:58. The DAQ electronics of Aragats monitors was designed and fabricated for the Space Weather research (Arakelyan et al., 2007). Solar modulation effects on the middle latitudes usually do not exceed a few tens of percent; therefore the maximal count rate of DAQ electronics was designed to be not more than 500% of CR background count rate. For Aragats detectors maximal of 10 KHz acceptable signal frequencies was established. TGE events detected so far fit this limit and no saturation was detected. However, at

11:20:53 seem this limit was surpassed. The very unusual behavior of particle detector pose questions on possible huge particle flux related to very strong lightning (Dwyer et al., 2012). Most dramatic enhancement demonstrates new “Muon”<sup>6</sup> detector, those scintillators are located under thick layers of lead and rubber, see Fig. 12.

Table 2 One-second time series of the «Muon» detector and outdoor 3 cm thick scintillator

| 9 October 2013 11: | 3 cm thick below 7.5 cm lead | 1 cm thick below 9 cm lead | 1 cm thick below 15 cm lead | 3 cm thick outdoor scint. |
|--------------------|------------------------------|----------------------------|-----------------------------|---------------------------|
| 10:20-11:19        | 270 +/- 17                   | 218 +/- 15                 | 138 +/- 12                  | 530 +/- 23                |
| 11:20:40           | 270                          | 222                        | 128                         | 1153                      |
| 11:20:41           | 273                          | 210                        | 151                         | 1190                      |
| 11:20:42           | 299                          | 238                        | 155                         | 1133                      |
| 11:20:43           | 293                          | 227                        | 134                         | 1256                      |
| 11:20:44           | 244                          | 207                        | 132                         | 1216                      |
| 11:20:45           | 247                          | 225                        | 138                         | 1285                      |
| 11:20:46           | 264                          | 240                        | 149                         | 1260                      |
| 11:20:47           | 275                          | 227                        | 133                         | 1293                      |
| 11:20:48           | 296                          | 223                        | 147                         | 1244                      |
| 11:20:49           | 312                          | 218                        | 145                         | 1336                      |
| 11:20:50           | 291                          | 215                        | 145                         | 1213                      |
| 11:20:51           | 293                          | 233                        | 143                         | 1294                      |
| 11:20:52           | 286                          | 240                        | 144                         | 1253                      |
| 11:20:53           | 389                          | 357                        | 184                         | 1262                      |
| 11:20:54           | 258                          | 216                        | 142                         | 548                       |
| 11:20:55           | 265                          | 223                        | 122                         | 512                       |
| 11:20:56           | 256                          | 200                        | 141                         | 513                       |
| 11:20:57           | 255                          | 222                        | 136                         | 556                       |
| 11:20:58           | 256                          | 201                        | 142                         | 520                       |
| 11:20:59           | 269                          | 226                        | 148                         | 493                       |
| 11:21:00           | 249                          | 204                        | 142                         | 559                       |

<sup>6</sup> Usually only high energy muons of secondary cosmic rays can penetrate thick lead absorber

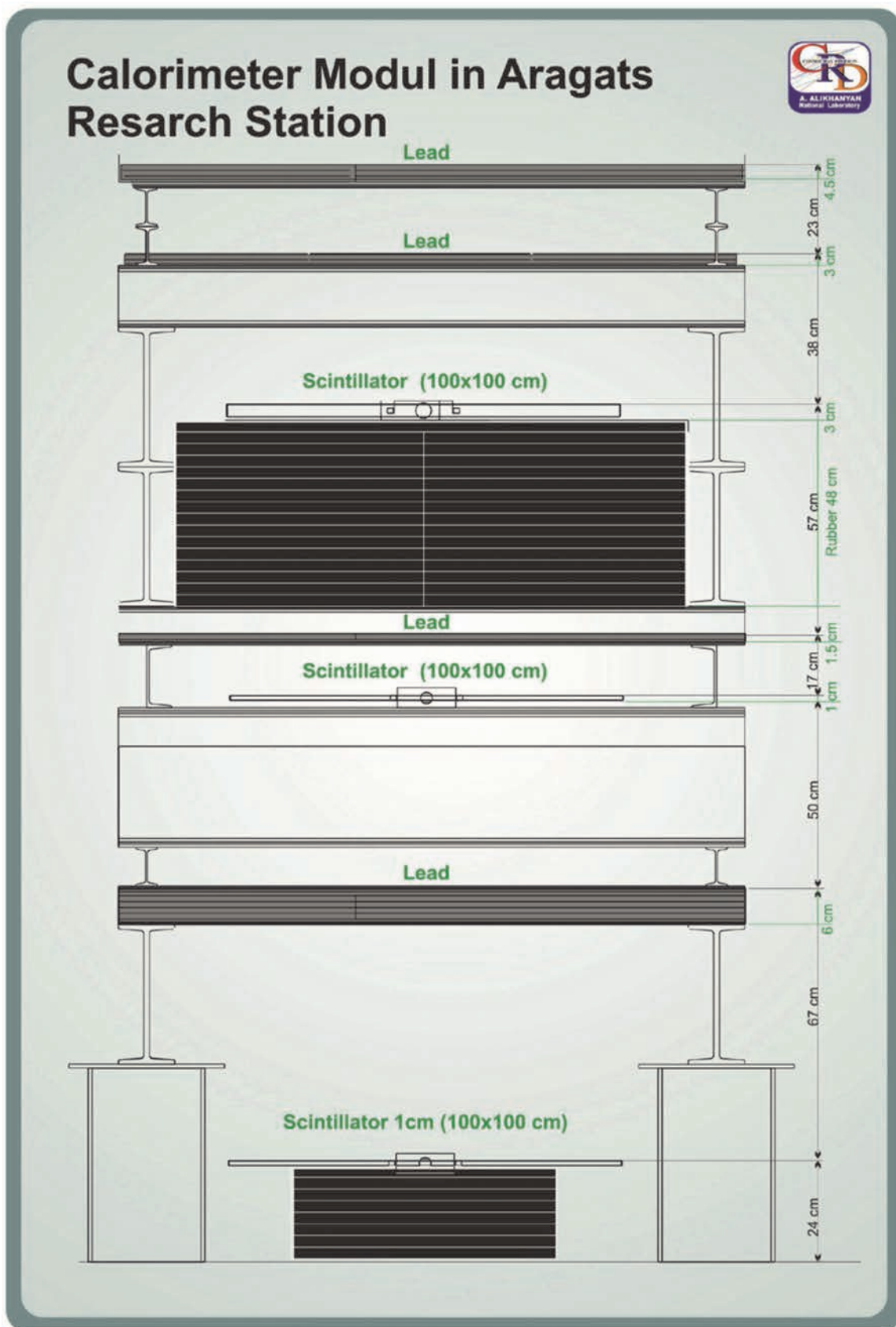


Figure 12. The “muon” detector consisted of 3 plastic scintillators under substantial amount of lead and carbon (rubber).

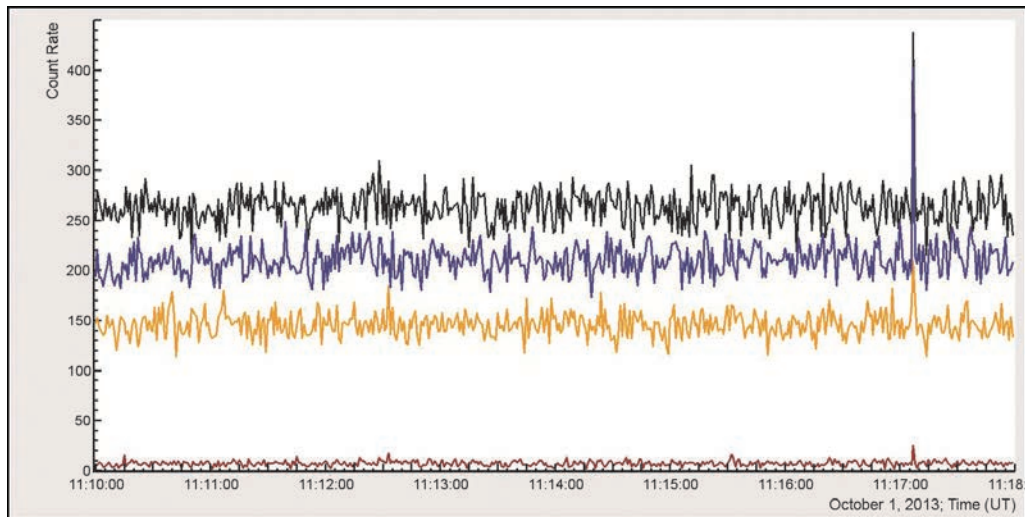


Figure 13. One-second time series of muon detectors scintillators as measured at October 1, 2013.

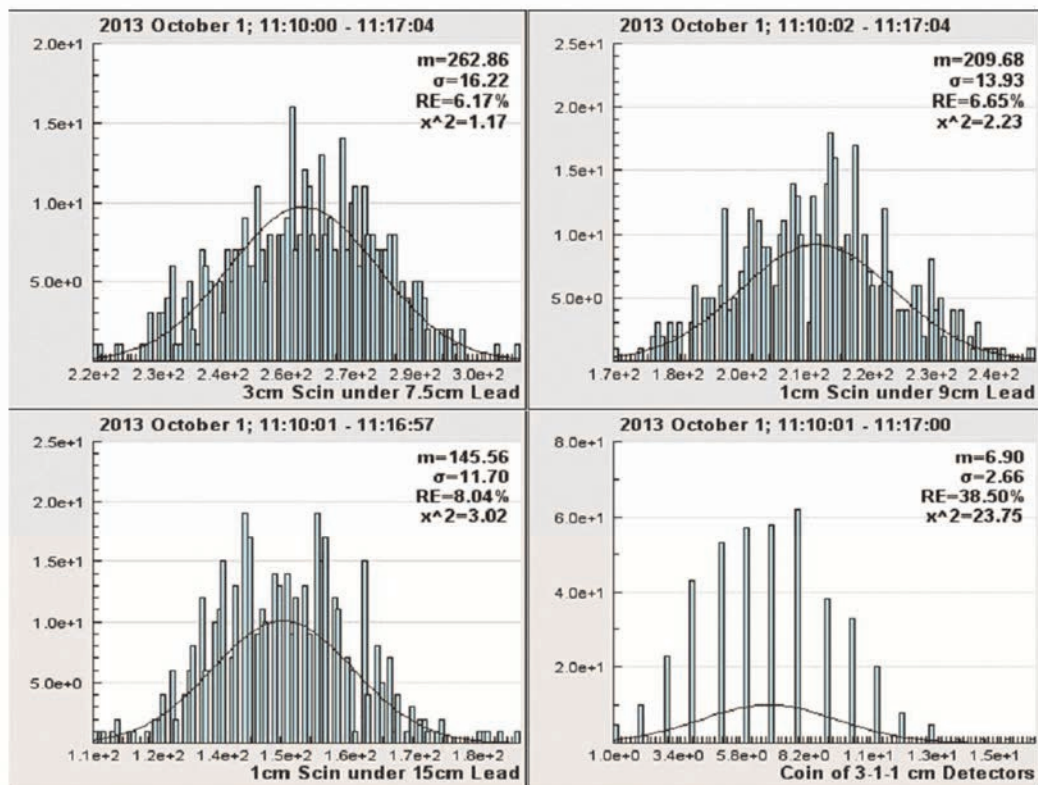


Figure 14. The mean count rates of muon detector scintillators measured before count rate enhancement at 11:17:07, October 1, 2013.

In Tab. 2 we depict the second-by-second count rates of the 3 scintillators of muon detector and – 3-cm thick outdoor scintillator. We can detect large enhancement at 11:20:53.

After exploring the event occurred on October 19 we examine time series of the muon detector and discover several analogical enhancements; however not accompanied by electronics failure. In Figs 13 we demonstrate one of these events and in Fig.14 - the histograms of the count rates as measured before the enhancement; used for estimating mean and variance of count rates for calculation of peak “height” and significance.

In Table 3 we depicted mean count rates (with variances) and enhancement values (difference between

peak and mean) of 6 enhancements measured by “Muon” detector during 5 months from October 2013 till March 2014. Very short enhancements detected as spikes in 1-second time series are due to hitting of the detector by the core of an Extensive air shower (EAS), containing high-energy particles. The probability of such events we can estimate as  $\sim 3 \cdot 10^{-7}$  (~once a month) and it is highly improbable that occasionally at 11:20:53 EAS hit the detector simultaneously with the decay of TGE and atmospheric discharge.

The selection of events was done according to presence of significant peaks in muon detector; only then the peaks were searched in neutron detector.

**Table 3. Mean values and variances of the muon and neutron detectors count rates; values and significances of the one-second peaks in time-series**

| Date/time                  | Sc 1         | Sc 2     | Sc 3    | Coins.  | ArNM     |
|----------------------------|--------------|----------|---------|---------|----------|
| 1/10/2013<br>mean          | 263±16       | 210±14   | 145±12  | 7±3     | 324±28   |
| 11:17:07<br>peak<br>(diff) | 173<br>(11σ) | 192(14σ) | 65(5σ)  | 18(6σ)  | 124(5σ)  |
| 19/10/201<br>3mean         | 270±17       | 217±15   | 138±12  | 7±3     |          |
| 11:20:53<br>peak<br>(diff) | 115(7σ)      | 138(9σ)  | 46(4σ)  | 31(10σ) | -        |
| 30/11/201<br>3mean         | 281±18       | 213±16   | 132±13  | 6±3     | 330±28   |
| 8:31:36<br>peak<br>(diff)  | 161(9σ)      | 124(8σ)  | 112(9σ) | 18(6σ)  | 236(9σ)  |
| 28/12/201<br>3mean         | 267±17       | 202±14   | 113±11  | 5±2     | 483±33   |
| 14:55:41<br>peak<br>(diff) | 91(5σ)       | 109(8σ)  | 35(3σ)  | 10(5σ)  | 525(19σ) |
| 21/2/2014<br>mean          | 260±14       | 191±15   | 136±13  | 6±3     | 341±25   |
| 21:43:53<br>peak<br>(diff) | 334(25σ)     | 199(13σ) | 90(6σ)  | 33(8σ)  | 201(8σ)  |
| 8/3/2014<br>mean           | 269±16       | 186±13   | 133±12  | 6±2     | 330±28   |
| 6:05:50<br>peak<br>(diff)  | 208(25σ)     | 116(8σ)  | 71(6σ)  | 11(5σ)  | 236(9σ)  |

The relation between “height” ( $z$  scores, numbers of standard deviations –  $N\sigma$ ) of peaks in muon and neutron detectors depends on relative position of EAS axes concern location of detectors. Centers of muon and neutron detectors are  $\sim 20$  m from each other and EASes initiated by primary protons with energy 50-100 TeV can originate signals simultaneously in both detectors. Only 8 (11 at 28.12.2013) proportional chambers of ArNM from 16 were operational; large count rate enhancement was detected when the dead time after each from many successive counts of the proportional chambers of neutron monitor was only 400 nsec. Small dead time allows registering almost all secondary particles (hadrons, muons, gamma rays) hitting the detector.

The mean count rays in layers of muon detector is inverse proportional to the amount of lead above each of them; however the height of peak in half of events is larger in the second layer than in the first one. It can be explained by initiation of additional particles in the thick rubber layers above the middle detector see Fig. 10

## 5. DISCUSSION

TGE detected at 19 October 2013 reveals some new physical characteristics of the high-energy phenomena in the atmosphere. The short duration and very strong positive correlation with near surface electric field differ significantly from previously investigated and classified TGE events (see the TGE classification scheme in Chilingarian and Mkrtchyan, 2012 and in Chilingarian, Karapetyan and Melkumyan, 2013). Registered meteorological conditions and near surface electric field disturbances point on very strong fast changing local atmospheric processes at Aragats.

The possible saturation of particle detectors and muon detector peaks coinciding with TGE decay and atmospheric discharge, possibly pointed on the very intense gamma ray (neutron?) fluxes related to lightning process. However, this conclusion needs detailed Monte Carlo simulation of the muon detector response, now underway.

## 6. REFERENCES

- [1] A. V. Agafonov, A. V. Bagulya, O. D. Dalkarov, et al., Observation of Neutron Bursts Produced by Laboratory High-Voltage Atmospheric Discharge, PRL 111, 115003 (2013).
- [2] Babich, L.P., Kutsyk, I.M., Donskoy, E.N., Kudryavtsev, A.Yu. (1998), New data on space and time scales of relativistic runaway electron avalanche for thunderstorm environment: Monte Carlo calculations, Physics Letters, Section A: General, Atomic and Solid State Physics, 245 (5), pp. 460-470.
- [3] Briggs, M. S., G. J. Fishman, V. Connaughton, (2010), First results on terrestrial gamma ray flashes from the Fermi Gamma-ray Burst Monitor J. Geophys. Res., 115.
- [4] Chilingarian, A., Arakelyan, K., Avakyan, K., et al., 2005. Correlated measurements of secondary cosmic ray fluxes by the Aragats Space-Environmental Center monitors. Nucl. Instrum. Methods Phys. Res., Sect. A 543 (2–3), 483–496.
- [5] Chilingarian, A., Daryan, A., Arakelyan, K., et al., (2010), Ground-based observations of thunderstorm-correlated fluxes of high-energy electrons, gamma rays, and neutrons. Phys. Rev. D 82, 043009.
- [6] Chilingarian, A., Hovsepyan, G., Hovhannisyan, A., (2011), Particle bursts from thunderclouds: natural particle accelerators above our heads. Phys. Rev. D 83, 062001.
- [7] Chilingarian A., Mailyan B., and Vanyan L., (2012), Recovering of the energy spectra of electrons and gamma rays coming from the thunderclouds, Atmospheric Research 114–115, 1–16.
- [8] Chilingarian, A., Mkrtchyan, H. (2012), Role of the lower positive charge region (LPCR) in initiation of the thunderstorm ground enhancements (TGEs). Phys. Rev. D 86, 072003.
- [9] A.Chilingarian, T. Karapetan, L.Melkumyan, Statistical analysis of the Thunderstorm Ground Enhancements (TGEs) detected on Mt. Aragats. J. Adv. Space Res. 52, 1178 (2013).
- [10] Chilingarian, G. Hovsepyan, and L. Kozliner, Thunderstorm ground enhancements: Gamma ray differential energy spectra, Physical Review D 88, 073001 (2013).
- [11] Dwyer, J.R., Smith, D.M., Cummer, S.A. (2012) High-energy atmospheric physics: terrestrial gamma-ray flashes and related phenomena, Space Sci. Rev.
- [12] J.R. Dwyer, M.A. Uman, The physics of lightning, Physics Reports (2013),  
<http://dx.doi.org/10.1016/j.physrep.2013.09.004>

- [13] Dwyer, J. R., M. M. Schaal, E. Cramer, S. Arabshahi, N. Liu, H. K. Rassoul, J. D. Hill, D. M. Jordan, and M. A. Uman (2012), Observation of a gamma-ray flash at ground level in association with a cloud-to-ground lightning return stroke, *J. Geophys. Res.*, 117, A10303, doi:10.1029/2012JA017810.
- [14] Fishman, G.J., Bhat, P.N., Mallozzi, et al., (1994) Discovery of intense 536 gamma ray flashes of atmospheric origin, *Science* 264 (5163), 1313– 537 1316.
- [15] Gurevich, A.V., Milikh, G.M., Roussel-Dupre, R. (1992), Runaway electron mechanism of air breakdown and preconditioning during a thunderstorm, *Physics Letters A*, 165 (5-6), pp. 463-468.
- [16] Gurevich, A.V., Karashtin A.N. (2013), Runaway Breakdown and Hydrometeors in Lightning Initiation, *PRL* 110, 185005.
- [17] Hansen S., et al., “Low Cost Data Acquisition Card for Network Cosmic Ray Detector”, *IEEE Trans. Nucl. Sci.*, 2004, v51, issue 3, p. 926-930
- [18] A. S. Lidvansky and N. S. Khaerdinov, *Izv. Ross. Akad. Nauk, Ser. Fiz.* 71, 1052 (2009) [Bulletin of the Russian Academy of Sciences: Physics 71, 1052 (2009)].
- [19] Torii, T., Sugita, T., Kamogawa, M., et al. Migrating source of energetic radiation generated by thunderstorm activity. *Geophys. Res. Lett.* 38, L24801, 2011.
- [20] Tsuchiya, H., Enoto, T., Yamada, S., et al. Long-duration gamma ray emissions from 2007 and 2008 winter thunderstorms. *J. Geophys. Res.* 116, D09113, 2011.
- [21] Wilson, C.T.R. (1925), The acceleration of  $\beta$ -particles in strong electric fields such as those of thunderclouds, *Proc. Cambridge Philos. Soc.*, 22, pp. 534-538. Cited 62 times.

# On the origin of the particle fluxes from the thunderclouds: Energy spectra analysis

*A.Chilingarian, G.Hovsepyan, L.Vanyan*

*Yerevan Physics Institute, Alikhanyan Brothers 2, Yerevan, Armenia*

---

**Abstract:** Simultaneous measurements of the gamma ray differential energy spectra, electric field disturbances, and lightning occurrences provided by experimental facilities located at Mt. Aragats in Armenia allows establishing of the model of particle acceleration and propagation in thunderstorm atmosphere and furthermore to estimate the intracloud electric field, one of the most important parameters in meteorology which is very difficult to measure by direct or indirect methods. For the first time we presented the dynamics of energy spectra changes on minute-to-minute bases. The observed relations of power law energy spectra index and flux intensity allow outlining the particular process of electron acceleration in the thundercloud. We present comparisons of measured and modeled thunderstorm ground enhancements (TGEs) observed in May-June 2013 at Mt. Aragats at altitude 3200 m. We prove that the origin of small TGEs is the MOS process – modification of energy spectra of cosmic ray electrons in the electric fields of thunderclouds. The gamma ray differential energy spectra are well described with power law function with power indexes  $-1.7 - -2.2$  for electric field strengths  $0.8 - 1.6$  kV/cm. When the intracloud field rise and reaches the threshold to unleash the relativistic runaway electron avalanches the intensity of TGE exponentially rose and at energies up to 20 MeV the exponential function describes gamma ray differential spectra. At the higher energies power law describes the spectra rather well with an enlarged absolute value of spectral index. These modeled features also well coincide with experimental observations of largest TGE events at Aragats when direct evidence of avalanche propagation from thunderclouds was obtained. The good agreement of characteristics of experimental and simulated TGEs allows estimation of intracloud electric field by the observed TGE parameters.

---

## 1. INTRODUCTION

Recent reports on intense fluxes of high-energy electrons, gamma rays and neutrons associated with thunderstorms illustrate that new interesting physics is still being discovered in our atmosphere (Dwyer, Smith and Cummer, 2012, Dwyer and Cummer, 2013). Measuring as much as possible parameters of particle fluxes, electric field disturbances and meteorological environments allows for the first time simultaneously detect and describe electron, gamma ray and neutron fluxes from the thundercloud (Chilingarian et al., 2010), observe relativistic runaway electron avalanches (Chilingarian et al., 2011) and finally develop comprehensive model of the Thunderstorm ground enhancement (TGE, Chilingarian, 2014, the name introduced in Chilingarian et al., 2011<sup>7</sup>).

Due to difficulties of observation of the key parameter - spatial distribution of the intracloud electric field research of high-energy phenomena in atmosphere heavily used computer simulation with inherent simplifications. Thus, the problem of proving adequateness of modeling in new discipline has also a major importance. Here we report experimental observations of intense gamma ray fluxes by surface particle detectors located at mountain altitudes supported by modeling of particle propagation in the thunderstorm atmosphere. The parameters estimated both

from simulations and observations allow direct comparisons and unambiguous physical inference on the nature of the TGEs. TGE originated from the lower dipole between the main negatively charged layer in the middle of the thundercloud and the transient Lower positive charge region (LPCR, Chilingarian and Mkrtchyan, 2012) in the bottom of the thundercloud. The lower dipole accelerates electrons from the ambient population of secondary cosmic rays (CR) downward. The electric field effectively transfers energy to the electrons MODifying their energy Spectra (MOS process, Lidvansky et al., 2007, Chilingarian, Mailyan and Vanyan, 2012), extending their lifetime and consequently their probability to radiate gamma rays. As thunderclouds at mountain altitudes usually are very close to the Earth's surface, the electron and gamma ray fluxes escaping from thunderclouds do not completely attenuate in the atmosphere and reach earth's surface enhancing rather stable CR "background" flux in the energy range up to 100 MeV.

If the electric field strength exceeds the critical value, the Relativistic Runaway Avalanches (RREA, Wilson, 1925, Gurevich et al., 1992, Babich et al., 1998) may be unleashed, enlarging the electron and gamma ray fluxes several times. RREA avalanches, called Extensive Cloud Showers (ECS, Chilingarian et al., 2011), are systematically different from the Extensive Air Showers (EASs) originating from the galaxy or from high-energy solar cosmic rays incident on the Earth's atmosphere. The near-surface location of thunderclouds at Aragats allows the direct observation of the RREA avalanches and the "switching on" of the rather rare RREA mechanism.

---

<sup>7</sup> Another name has been given to "thunderstorm" particles ("gamma-ray glows", see discussion in Dwyer and Cummer, 2013). However, we will continue to refer to this emission as Thunderstorm Ground Enhancements (TGEs), since it directly reflects the observed physical phenomenon and is directly linked to the analogical phenomena as Terrestrial gamma flashes (TGFs) and GLE – Ground level enhancement.

The simulation of the TGEs was performed with the GEANT4 code with the suitable electric field and thundercloud location (strength  $\sim 1.8$  kV/cm at 5000 m, elongation  $\sim 1$  km, height above earth's surface 50-200 m); and with seed electrons from an ambient population of CRs. Used model successfully reproduces the observed largest Aragats TGE events, detected by particle detectors of Aragats Space Environmental Center (ASEC, Chilingarian et al., 2005) including electron, gamma ray and neutron fluxes. However, only a few from hundreds of detected TGEs exhibit huge particle multiplication inherent for avalanche processes. Most of the enhancements embedded in the time series of the particle count rates are rather small - only few percent above the cosmic ray background (see statistical analysis of TGE events in Chilingarian, Karapetyan and Melkumyan, 2013). The simulations of secondary cosmic ray electron propagation in weak electric fields (with the strengths smaller than the threshold value  $E_{th}$ , necessary for starting RREA process<sup>8</sup>) were performed. The strength of the electric fields does not exceed the threshold value to unleash runaway electron avalanches. Nonetheless, these fields provide additional energy to CR electrons by modifying their spectra; consequently Cosmic Ray (CR) electron live time increases, and additional path lengths in the atmosphere enlarge the probability of radiation processes. As a result, we obtain additional gamma rays at the observation level. Terrestrial gamma flashes (TGFs) and Thunderstorm ground enhancements (TGEs) are usually explained by invoking a runaway process, requiring very strong electric fields emerging in clouds. For instance, in reference (Dwyer et al., 2012) was stated: "Any intense burst of gamma-rays in our atmosphere with energies exceeding 7 MeV, almost certainly is produced by runaway electrons experiencing RREA multiplication". However, we will demonstrate dominating contribution of MOS process in TGEs initiation and its exclusive responsibility in generation of particles above 50 MeV. The MOS process only can provide sufficient number of gamma rays with energies larger comparing with the ones provided by the RREA process, although with much smaller intensity. We investigate the dependence of the MOS process on the strength of electric field in a thundercloud and for the first time use the information on the dynamic of TGE development. Minute-to-minute differential energy spectra of gamma rays measured by the NaI spectrometers located at altitude 3200 m. (see details in Chilingarian, Hovsepyan and Kozliner, 2013) was used to compare the power law indexes and intensities of the dynamically changing spectra with GEANT4 simulations to relate characteristics of measured TGEs to electric field strength in thunderclouds.

## 2. SIMULATION OF MOS PROCESS

The GEANT4 code was used for simulation of the electron propagation and acceleration in the thunderstorm

<sup>8</sup> Monte Carlo simulations have shown that the minimum electric field required for electrons to run away and propagate long distances is  $E_{th} = 2.8 \times 10^5$  V/m  $\times$  n (Dwyer, 2003; Babich et al., 2004), where n is the density of air relative to that at sea level at standard conditions.

atmosphere. The secondary cosmic ray electrons at altitudes 4000 – 5000 m were used as seed particles; the particle detectors were located at 3200 m; the uniform electric field with the fixed strength in the range of 0,8 – 1.6 kV/cm was switched on, which is smaller than the threshold strength  $E_{th} = 1.63$  kV/cm for 4000 m height – electric field requested for the initiation of runaway electron avalanche. For comparisons of RREA and MOS processes electric field strength of 1.7 and 1,8 was used in simulations as well.

We use as seeds CR electrons with energies up to 300 MeV. All electrons and gamma rays born in the atmosphere were followed and stored. The obtained "thunderstorm" gamma ray spectrum is compared with the ambient CR spectrum in Figs 1-2; spectrum of surplus gamma rays prolonged up to 100 MeV. MOS/CR ratio is  $\sim 10\%$  up to energies of  $\sim 20$  MeV. Then the ratio is quickly decreased, demonstrating that MOS process provides minor enhancement of gamma rays above energies of  $\sim 50$  MeV; nonetheless large area of ASEC particle detectors can reliably register these small enhancements. As we can see from Fig. 1, the TGE gamma ray spectrum is well fitted by a power law function as well as its "parent" electron energy spectrum, which confirms TGE generation by MOS. To consider the influence of high-energy electrons on TGE gamma ray energy spectrum, the gamma rays originated from electrons with energies from 1 to 100 MeV are compared in Fig. 2 with energy spectrum obtained from electrons with energies up to 300 MeV. As we can see in Fig. 2 if electric field strength is low (0.8 kV/cm) the number of gamma rays originated from electrons with energies 1-100 MeV is much smaller, than the number of gamma rays originated from electrons with energies 100-300 MeV, although the number of seed electrons with energies 1- 100MeV is 10 times more than the number of electrons with energies 100-300 MeV. This relation well coincides with energy dependence of the bremsstrahlung probability in atmosphere. However, with the raising of thundercloud electric field the contribution of low energy electrons become prevailing

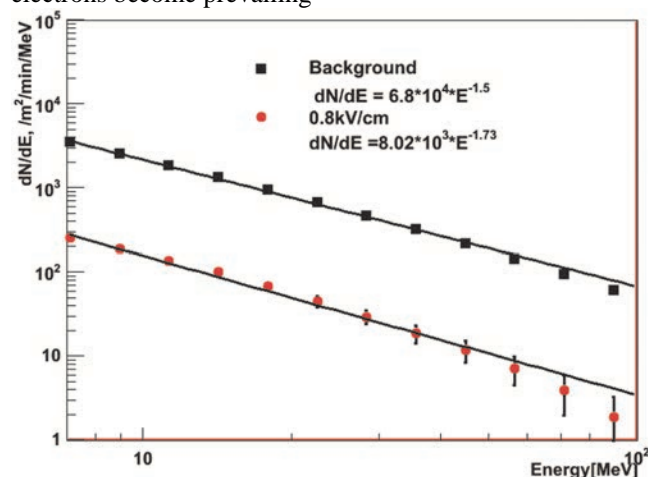


Figure 1. Comparison of the ambient secondary CR gamma ray spectrum with the MOS gamma ray spectrum at 3200 m altitude; electric field strength 0,8 kV/cm

<sup>9</sup> The energy spectra of secondary cosmic rays born in interactions of primary protons and stripped nuclei with atmosphere well described by power law similar to spectrum of primary particles.

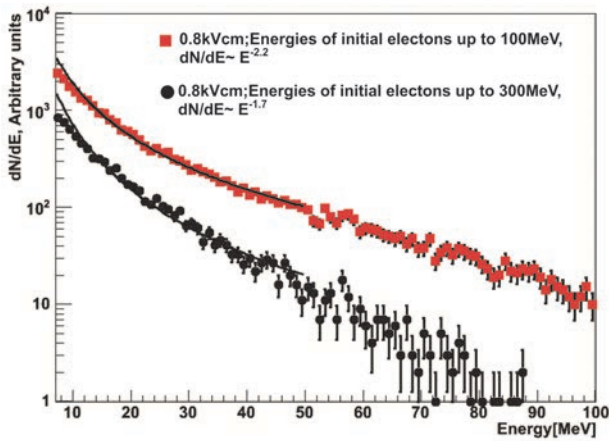


Figure 2. Comparison of gamma ray spectra originated from electrons with energies from intervals 100-300 and 1-100 MeV; electric field strength - 0,8 kV/cm

In Fig. 3 the dependence of MOS gamma ray spectra on electric field strength is shown. We can see that not only the number of gamma rays increases with the electric field strength, but also the absolute value of the spectral indexes increases by more than 1 unit. For the field with strength 0.8 kV/cm the energy spectra is described by power law  $dN/dE \sim E^{-1.73}$ , for electric field with 1.7 kV/cm strength the gamma ray spectrum is -  $dN/dE \sim E^{-2.9}$ .

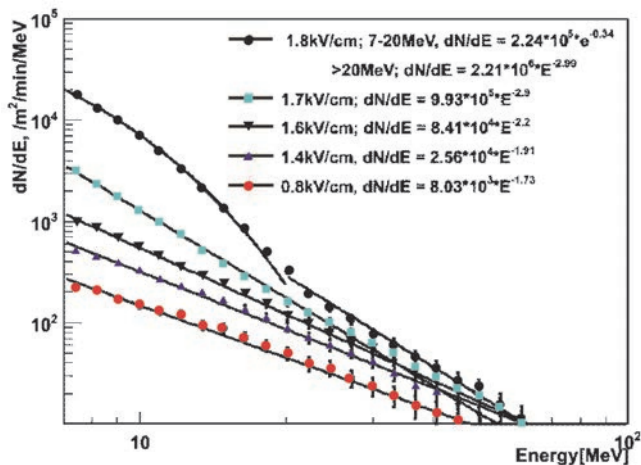


Figure 3. Differential energy spectra of gamma rays generated by secondary cosmic ray electrons in atmospheric by electric fields of different strength; observation level - 3200m. Energy range 7-100 MeV

At electric fields 1.7 kV/cm and more the RREA process already play a role and at 1.8 kV/cm we can see the exponential shape of gamma ray energy spectrum in energy range 7-20 MeV. Thus we can see the obvious distinction of TGE origin depending on the atmospheric electric field. For the thundercloud location above  $\sim 3400$  m and relatively weak electric fields the pure MOS process is responsible for initiation of TGEs. Gamma ray fluxes are limited and absolute value of the energy spectra index not exceeds 2.2. With enlarging the electric field strength above 1.7 kV/cm the avalanche process greatly enlarge the gamma ray flux and power index reaches values of  $\sim 3$ .

### 3. TGE FLUX TEMPORAL EVOLUTION AND ITS CONNECTION WITH CHANGING INTRACLOUD ELECTRIC FIELD

Network of NaI spectrometers located on altitude 3200 m allows measuring dynamic change of the differential energy spectra of gamma rays on the one-minute scale (Chilingarian, Hovsepyan and Kozliner, 2013). The gamma ray differential energy spectra of TGEs detected in May-June 2013 were fitted by a power law in the energy range of 7-100 MeV. In Fig. 4 we post characteristics of 42 gamma ray energy spectra measured at May 12, May 15 and June 19, 2013. As a measure of TGE intensity we use the intensity of the extrapolated to 1 MeV differential energy spectrum. 5 large NaI crystals provide enough statistics for the reliable approximation of energy spectra. For instance, the minute-to-minute surplus of count rate registered on 19 June 7:28 - 7:45 changes from 3000 to 7000; total number of registered gamma quanta were  $\sim 80,000$ .

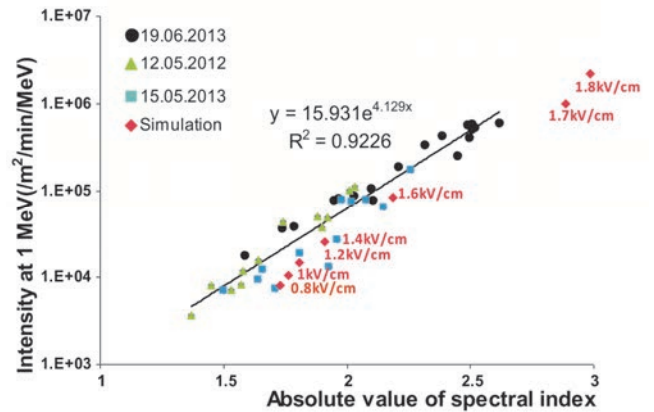


Figure 4. Correlation between intensity and power index of the gamma ray flux of TGE; the electric field strength is written near symbols representing simulations of the TGE process.

In the scatter plot (Fig. 4, TGE intensity – absolute value of spectral index) we add the simulation results from Fig. 3. As we can see from Fig. 4 there is overall agreement of experimentally observed and modeled TGEs. The left part of scatter plot (below the electric field of 1.7 kV/cm) corresponds to the MOS process. Starting from 1.7 kV/cm “switching on” RREA process exponentially increases the intensity. Correspondingly, the absolute value of the power index of the extrapolate energy spectra fit rise up to  $\sim 3$ .

### 4. DISCUSSION AND CONCLUSIONS

We demonstrate that modest electric fields not reaching RREA threshold initiate TGEs in the thunderstorm atmosphere. The power law shape of the gamma ray differential energy spectra coincides with “parent” spectra of CR secondary electrons and tends to harden with enlarging of the electric field. When intracloud electric field reaches RREA initiation threshold TGE intensity exponentially grows. The power law function cannot describe the intensity rise any more and an exponential fit as we see in Figure 3 was suitable for the spectra interpolation at energies 7-20 MeV. At higher energies the power law fit describes spectrum rather well, proving the responsibility of MOS process for higher gamma ray energies. The absolute value of spectral index  $\sim 3$  obtained from simulation well coincides with experimentally

measured values measured for the largest TGEs with direct observation of individual runaway avalanches (Chilingarian et al., 2010, 2011).

The scatter plot of experimentally measured gamma ray energy spectra (TGE intensity at 1 MeV vs. absolute value of spectral index) demonstrates an apparent trend of the intensity exponential growth. The same trend exhibits the simulated events. It not only proves adequateness of simulation, but also gives the possibility to estimate electric field in thundercloud by the characteristics of the measured TGE energy spectra. The modeled TGE events provide graduation data for the observed spectra and further observed spectra can be used for estimation of the electric field strength within thundercloud.

Terrestrial Gamma flashes (TGFs, Fishman et al., 1994, Briggs et al., 2010) are believed to originate from electrons accelerated in the upper dipole between the main negative and main positive layer in the upper part of the thundercloud. Gamma rays emitted by accelerated upward electrons propagate in space (generating electron-positron pairs) and reach gamma ray spectrometers in orbit several hundred kilometers above the Earth's surface. The space-based gamma ray observatories are intended primarily to detect gamma bursts and other energetic processes in the Universe. Modified triggers of gamma ray events allow copious detection of the TGFs mostly from equatorial thunderstorms. However, the distant locations for the fast moving particle detectors lead to several difficulties in the development of the TGF model:

- The required number of seed electrons greatly exceeds the available electrons in secondary CRs; the proposed mechanism of “cold runaway” – acceleration of electrons by the strong electric fields in front of lightning leaders—is still not observed;
- Due to scarcity of detected particles, only cumulative energy spectra from all detected events are available for analysis and comparison with simulations; too few detected photons from each event are not enough for energy spectra recovering; in contrast millions of gamma ray photons detected from several TGEs allows detailed analysis of energy spectra evolution with time for individual events.

High-energy processes in the magnetosphere and atmosphere like TGEs, TGFs, TLEs (transient luminous events) and recently discovered relativistic electron acceleration in the Earth's outer radiation belt (Mozer et al., 2013) trigger various dynamic processes in the Earth's environments and have broad astrophysical relevance. Investigation of the «accelerated» structures in the Geospace plasmas can shed light on particle acceleration to much higher energy by the similar structures of space plasmas in the most distant objects in the Universe. As it was mentioned in (Zimbaro, 2013) the Earth's broad environment is a real laboratory for high-energy astrophysics.

Direct measurements of the intense particle fluxes at the Earth's surface may be used as well for tuning the parameters of TGF models. The spatial and energetic characteristic of the ECSs, and measured energy spectra of the TGE gamma rays and electrons, may be used for checking characteristics of the particle fluxes obtained in the TGF simulations. For instance reported by Italian group

prolongation of the cumulative gamma ray energy spectra up to 100 MeV (Tavani et al., 2012) can be checked by the intensity - power index relation depicted in Fig. 4.

## 5. REFERENCES

- [1] Babich, L.P., Kutsyk, I.M., Donskoy, E.N., Kudryavtsev, A.Yu. (1998), New data on space and time scales of relativistic runaway electron avalanche for thunderstorm environment: Monte Carlo calculations, *Physics Letters, Section A: General, Atomic and Solid State Physics*, 245 (5), pp. 460-470.
- [2] Briggs, M. S., G. J. Fishman, V. Connaughton, (2010), First results on terrestrial gamma ray flashes from the Fermi Gamma-ray Burst Monitor *J. Geophys. Res.*, 115.
- [3] Chilingarian, A., Arakelyan, K., Avakyan, K., et al., 2005. Correlated measurements of secondary cosmic ray fluxes by the Aragats Space-Environmental Center monitors. *Nucl. Instrum. Methods Phys. Res., Sect. A* 543 (2-3), 483-496.
- [4] Chilingarian, A., Daryan, A., Arakelyan, K., et al., (2010), Ground-based observations of thunderstorm-correlated fluxes of high-energy electrons, gamma rays, and neutrons. *Phys. Rev. D* 82, 043009.
- [5] Chilingarian, A., Hovsepyan, G., Hovhannisyan, A., (2011), Particle bursts from thunderclouds: natural particle accelerators above our heads. *Phys. Rev. D* 83, 062001.
- [6] Chilingarian A., Mailyan B., and Vanyan L., (2012), Recovering of the energy spectra of electrons and gamma rays coming from the thunderclouds, *Atmospheric Research* 114-115, 1-16.
- [7] Chilingarian, A., Mkrtchyan, H. (2012), Role of the lower positive charge region (LPCR) in initiation of the thunderstorm ground enhancements (TGEs). *Phys. Rev. D* 86, 072003.
- [8] A.Chilingarian, T. Karapetan, L.Melkumyan, Statistical analysis of the Thunderstorm Ground Enhancements (TGEs) detected on Mt. Aragats. *J. Adv. Space Res.* 52, 1178 (2013).
- [9] A. Chilingarian, G. Hovsepyan, and L. Kozliner, Thunderstorm ground enhancements: Gamma ray differential energy spectra, *Physical Review D* 88, 073001 (2013).
- [10] Dwyer, J. R., M. M. Schaal, E. Cramer, S. Arabshahi, N. Liu, H. K. Rassoul, J. D. Hill, D. M. Jordan, and M. A. Uman (2012), Observation of a gamma-ray flash at ground level in association with a cloud-to-ground lightning return stroke, *J. Geophys. Res.*, 117, A10303
- [11] Dwyer, J.R., Smith, D.M., Cummer, S.A. (2012) High-energy atmospheric physics: terrestrial gamma-ray flashes and related phenomena, *Space Sci. Rev.*
- [12] J.R. Dwyer, M.A. Uman, *The physics of lightning*, *Physics Reports* (2013), <http://dx.doi.org/10.1016/j.physrep.2013.09.004>
- [13] Fishman, G.J., Bhat, P.N., Mallozzi, et al., (1994) Discovery of intense 536 gamma ray flashes of atmospheric origin, *Science* 264 (5163), 1313- 537 1316.
- [14] Gurevich, A.V., Milikh, G.M., Roussel-Dupre, R. (1992), Runaway electron mechanism of air breakdown and

preconditioning during a thunderstorm, *Physics Letters A*, 165 (5-6), pp. 463-468.

- [15] Gurevich, A.V., Karashtin A.N. (2013), Runaway Breakdown and Hydrometeors in Lightning Initiation, PRL 110, 185005.
- [16] A.S. Lidvansky, N.S. Khaerdinov, (2007), published in *Izvestiya Rossiiskoi Akademii Nauk. Seriya Fizicheskaya*, 2007, Vol. 71, No. 7, pp. 1052–1055 (in Russian).

# Meteorological conditions during TGEs and estimation of the size of emitting region in the thundercloud

*A. Chilingarian*

*Yerevan Physics Institute, Alikhanyan Brothers 2, Yerevan, Armenia*

---

**Abstract:** We analyze thunderstorm ground enhancements detected on 3200 m altitude by facilities of Aragats research station in Armenia with simultaneously performed meteorological measurements. Measurements of solar radiation, wind speed and direction along with measurements of the duration of particle fluxes from a thundercloud allows to estimate the size of radiation emitting region to be ~ 600 m, which is compatible with our previous estimates and estimates of other groups..

---

## 1. INTRODUCTION

Thunderstorm Ground enhancement (TGE) comprises of fluxes of electrons, gamma rays and neutrons from the thunderclouds (Chilingarian et al., 2010, Chilingarian, Hovsepyan and Hovhannisyanyan, 2011). The TGE originated from an ambient population of Cosmic ray (CR) electrons accelerated in the strong electric fields emerging between main negatively charged layer in the middle of the thundercloud and transient Lower positively charged region (LPCR, Chilingarian and Mkrtchyan, 2012). Usually LPCR is sited on the rain droplets in the bottom of the cloud. We assume that the size of the radiation-emitting region in the thundercloud is determined by the LPCR size.

The meteorological conditions are crucial for TGE origination. The cloud should be low enough relative to earth's surface to prevent complete attenuation of particles in the air before reaching particle detectors; moving cloud should be positioned near-vertically at least few minutes above particle detectors, this condition pose limitations on emitting region size and wind speed. As well the current values of humidity and temperature in the cloud should allow creation of rain droplets.

We are aware of 3 attempts to estimate the emitting region size. Two Japanese groups use a spatially distributed network of particle detectors and measure a time delay of the registered TGEs. Armenian group use the muon directional anisotropy to derive estimate of emitting region location and size. Japan Tsuruga Power Station of the Japan Atomic Power Company monitors radiation situation (in the range 0.2–30 MeV) by cylindrical NaI detectors at each of three remote observation points in Tsuruga Peninsula facing the Sea of Japan. In 2010 they identify a migrating source of high-energy radiation; energetic radiation was emitted continuously from a downward hemispherical surface of 700 m radius the bottom of which was about 300 m above sea level (Rikee et al., 2011). Another Japanese group performs the Gamma-Ray Observation of Winter Thunderclouds (GROWTH) experiment at the Kashiwazaki-Kariwa nuclear power plant in the coastal area of the Sea of Japan where winter lightning is common. Simultaneous and delayed detections of TGEs by the two remote subsystems of particle detectors allows to conclude that emission from thunderclouds is likely to have illuminated a rather limited area, spreading over ~600 m on the ground (Tsuchiya et al., 2011). On 2000 m altitude at Nor Amberd research station of Yerevan Physics institute at 28 March 2011 a sizable anisotropy was detected in

different muon arrival directions simultaneously with large flux of gamma rays from the thundercloud. The largest deficit was detected from the (W-E) and (S-N) directions, 7 and 6% correspondingly. Using the map of the deficits in muon flux coming from different directions we estimate the most probable emitting region size to be not greater than ~700 m (Chilingarian, Bostanjyan and Karapetyan, 2013).

Variety of meteorological parameters measured at Aragats by the automated weather station<sup>10</sup> included the measurements of solar radiation, which allows estimation of time span when cloud is above detectors (of course only if TGE occurred at day-time) usually coincided with TGE duration. Measurements of wind speed and direction give possibility to estimate the size of emitting region in the bottom of thundercloud responsible for TGE<sup>11</sup>. In present paper we will describe the estimation of the emitting region size by facilities of Aragats research station located at 3200 m a.s.l. using meteorological information registered by automate weather station during large TGE of 19 June 2013.

## 2. TGE REGISTERED ON 19 JUNE, 2013

On 19 June 2013 ASEC particle detector registered long duration TGE, see Fig.1. Particle flux enhancement started at 7:02 reaching first maximum at 7:18. Then, after 8 minutes slight decay, flux started rise at 7:26 reaching TGE maximum of 7:39; thereafter abrupt attenuation culminated in returning to "background" CR flux value on 7:55. First maximum of TGE measured by 3-cm thick outdoor plastic scintillator have significance of ~ 10  $\sigma$ , second maximum ~ 39  $\sigma$ . Aragats multidirectional muon monitor (AMMM), the detector having a minimal relative error of 1-minute time series demonstrates much larger reliability - 86  $\sigma$ , see Fig. 1 of Chilingarian, Hovsepyan and Kozliner, 2013. The "standardized" duration of TGE is measured by calculating of the full duration of the TGE main peak on the half-maximum (FDHM). FDHM of the

---

<sup>10</sup> Professional Davis Instruments Vantage Pro2, <http://www.davisnet.com/>.

<sup>11</sup> For large TGEs the height of the cloud above earth's surface not exceed 50-100 m; electric field accelerates electrons vertically; therefore we assume that the size of emitting region in the thundercloud is not differ too much from the size of region on earth's surface eliminated by its radiation.

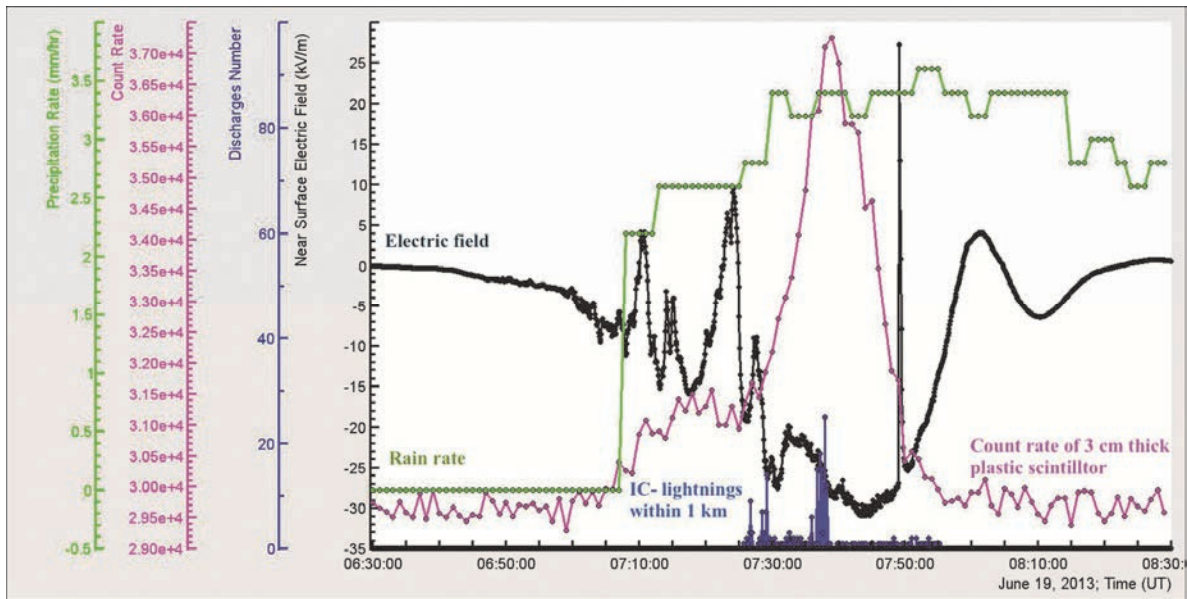


Figure 1. One-minute time series of TGE measured by 3 cm thick plastic scintillator; disturbances of near-surface electric field; IC- lightning occurrences within 1 km from lightning detector; and rain rate.

second peak of 19 June TGE equals 13 minutes (from 7:33 till 7:46 and is approximately symmetric relative to a maximum of 7:39).

According to a classification scheme based on the pattern of electric field disturbances (Chilingarian and Mkrtchyan, 2012) the TGE is related to the 3 types – up to tens of minute-long large negative near-surface electric field.

There was raining during whole period of TGE; i.e. rain droplets were present in the bottom of the cloud when additional particle fluxes were detected and lightning discharges and disturbances of electric field were observed. According to the TGE model (Chilingarian, 2014) presence of rain droplets is the necessary condition of lower dipole developing, which accelerated electrons downward in the direction to Earth's surface. With the rising phase of TGE lightning detector registers radio-emission from numerous of intracloud discharges (IC-) or/and Extensive cloud showers (ECSes, Chilingarian and Hovsepyan, 2013). During the 1.5 minutes on a rising stage of TGE (7:36:47 – 7:36:17) near 200 radio pulses, classified by Next Storm software as intracloud IC- lightnings were detected. On the

Thundercloud contains rain droplets on which Lower positive charge region (LPCR) was sited and electric field was lowered during FDHM with a mean value of  $\sim -27 \pm 3$  KV/m. Electrons were accelerated in the cloud just above particle detectors culminating in maximal flux at 7:39.

We suppose that changing particle flux is connected with moving of the thundercloud above the detector. The detector was exposed to radiation emitting “window” in a

decaying stage of TGE during 4.5 minutes (7:38:32 – 7:43) only 15 radio pulses were detected.

### 3. ATMOSPHERIC CONDITIONS ON 19 JUNE, 2013 DURING TGE

TGE occurs at suddenly changed meteorological conditions at observation site, see Fig. 2. At 6:52 solar radiation abruptly decreased as well as the outside temperature. We relate it to cloud appearance and shadowing of the sun. During the whole TGE duration (7:03 - 7:55) mean solar energy reaching the earth's surface was  $\sim 39 \pm 9$  W/m<sup>2</sup>; mean temperature  $\sim 2.7 \pm 0.7$  C°. During FDHM (7:33 - 7:46) mean solar energy reaching the earth's surface was even less  $\sim 30 \pm 1.5$  W/m<sup>2</sup>; mean temperature  $\sim 1.8 \pm 0.1$  C°. Both averaged radiation and temperature (and especially FDHM averaged) are significantly lower compared with pre-TGE values. Mean value of UV doze measured in minimal erythemal doses (MED) units' declines to zero value approximately in the whole TGE period. Therefore, we conclude that during FDHM thundercloud was directly above particle detectors.

thundercloud during passing of it above detectors. And knowing wind speed and duration of large flux, we can estimate the emitting region size. The pattern of wind directions during TGE, see Fig.3, also demonstrate strict changes after TGE decay. During FDHM (7:33 - 7:46) mean wind speed was  $\sim 0.74 \pm 0.44$  m/sec; the mean wind direction was to North  $\sim 288 \pm 24$ N; it abruptly changes to 28N after TGE attenuation.

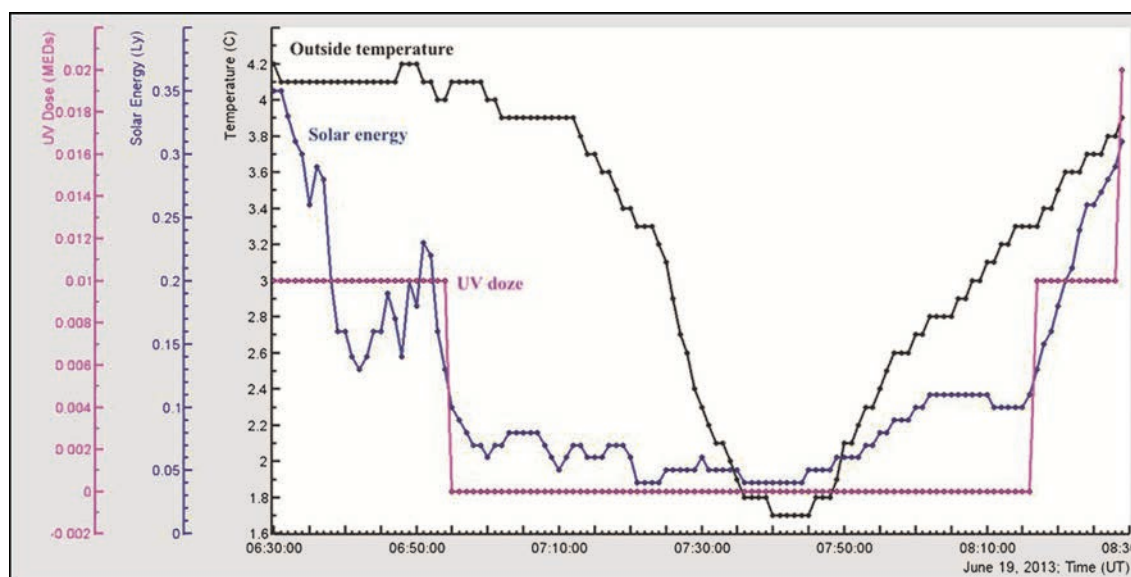


Figure 2. Temperature, Solar and UV radiation below the thundercloud.

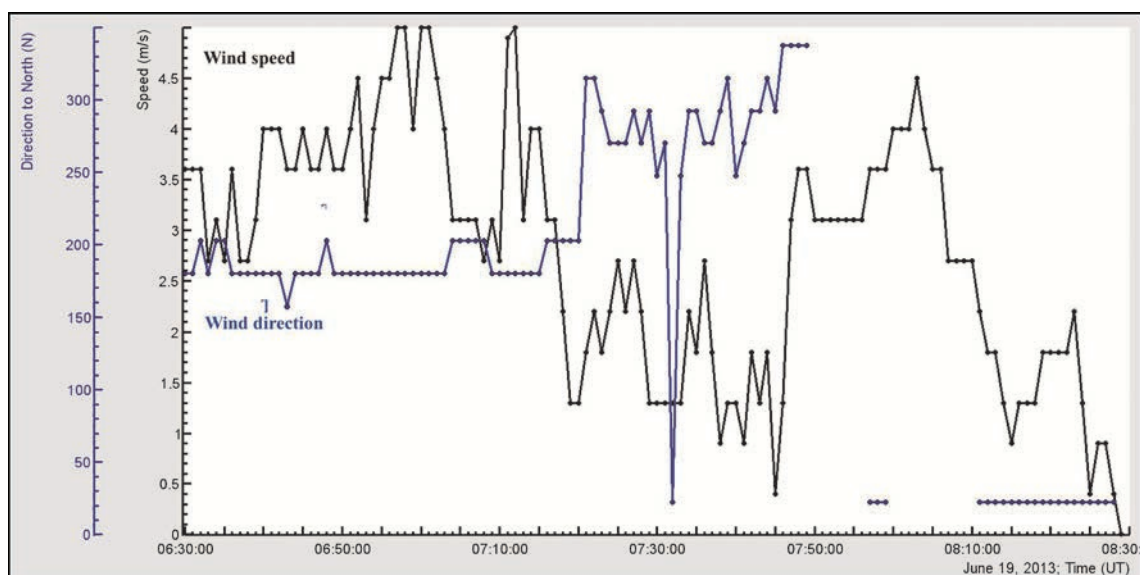


Figure 3. Speed and direction of wind during TGE

#### 4. POSSIBILITY TO RECOVER CLOUD SIZE

From the Google map of Aragats station in Fig. 4 we can see that the cloud will first illuminate 3 cm thick 1 m<sup>2</sup> area outdoor scintillator located nearby MAKET building and only then reach the concrete calorimeter of GAMMA array on roof of which 5 cm thick 1 m<sup>2</sup> area scintillators are located. Indeed 1-minute time series of 5 cm thick scintillators peaked at 7:40, one minute later than 3 cm thick scintillator see Fig. 5. The peak of 3 cm thick scintillator is very smooth as we can see on 1-sec time series of the same scintillator on the right insert to Fig. 5. From 1-second time series, we can estimate the peak location between 7:38:30 and 7:39. Unfortunately second time series are not available for Gamma scintillators. On

the left insert we put the pattern of delayed correlations between 2 scintillators. The largest correlation occurred on 0 delay. Unfortunately 1-minute accuracy do not allow estimating the exact pattern of moving clouds, nonetheless we can make a rough estimate of cloud size based on wind speed and time of illumination. We will assume that only during FDMH the “core” of electrified cloud was above detector (the lower values of flux can be explained by scattered gamma rays). Direction of wind was approximately constant we can estimate the distance cloud crosses during 13 minutes of FDMH to be ~ 600 m. Well coinciding with our previous estimates and Japanese group data.

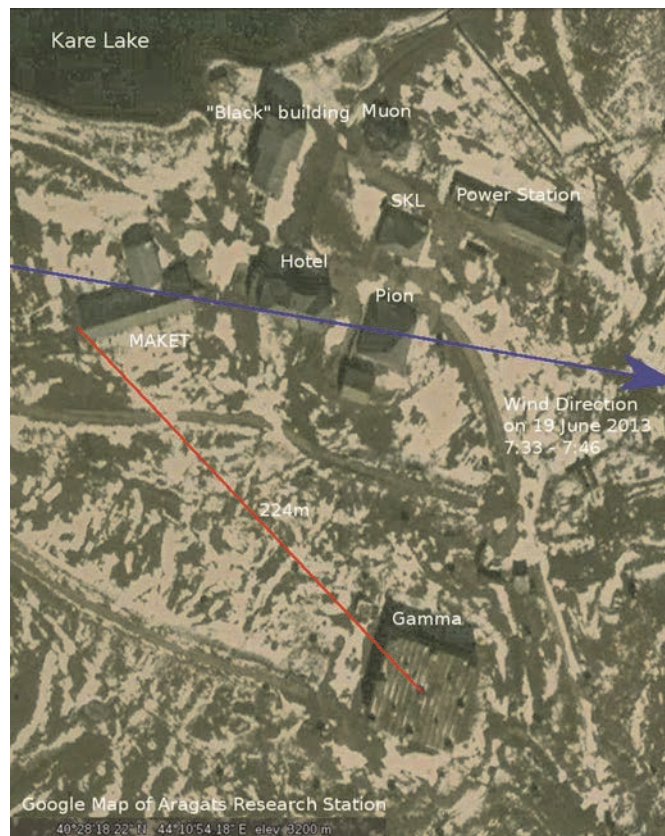


Figure 4. Particle detectors location at Aragats research station and mean wind direction during large particle flux on 19 June 2013

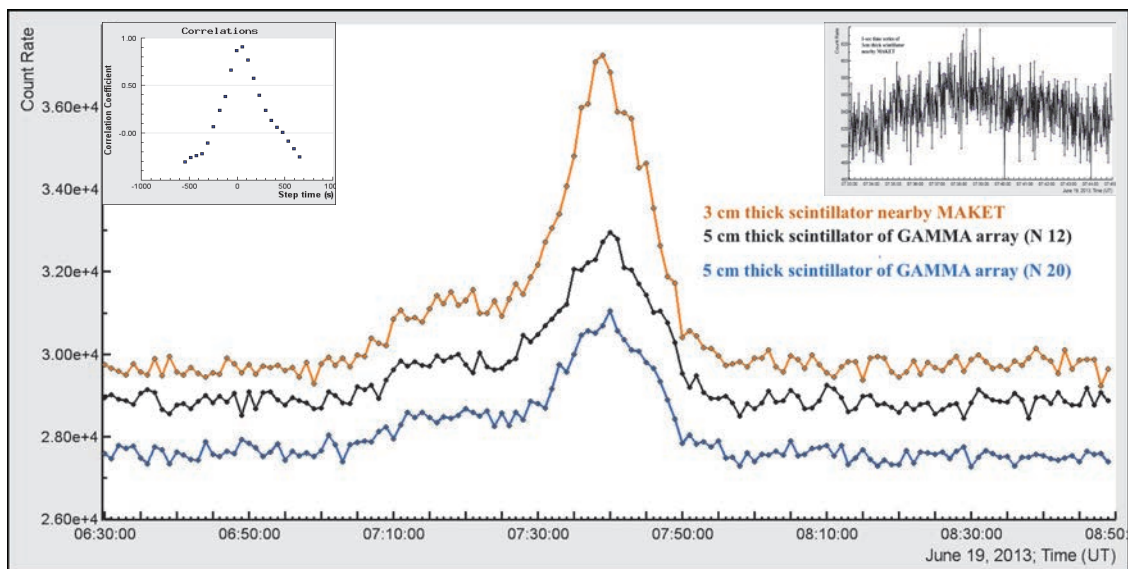


Figure 5. One-minute time series of remote particle detectors. In the left insert the “delayed” correlation of 3 cm thick scintillator located nearby MAKET building and 5 cm thick scintillator located ~300 m apart on the roof of GAMMA colorimeter; in the right insert – one-second time series of 3 cm thick scintillator.

5. CONCLUSIONS

The model of TGE initiation (Chilingarian, 2014) anticipates the development of the lower positive charge region (LCPR) as a necessary condition of electron acceleration in thunderclouds. LPCR is localized to a fairly small volume; Holden et al., 1980 concluded that the effect of the field attributable to LPCR’s is usually only observable at distances less than 1 km. Therefore, it should alter locally the electrical field configuration in the thundercloud and the lower dipole formed by LPCR and

much larger main negative charged layer in the middle of thundercloud also should be local.

Our estimate of the radiation emitting region in the thundercloud which illuminates earth’s surface just below thundercloud ~800 m well coincide with estimates from other experiments performed at sea level and mountain altitudes and with Holden’s et al., estimate. Therefore, we conclude that usually radiation emitting region in the thundercloud do not exceed 0.5 - 1.5 km size and for the

TGE registered at 19 June 2013 TGE by Aragats research station facilities at altitude 3200 m was ~ 600 m.

## 6. REFERENCES

- [1] Chilingarian, A., Daryan, A., Arakelyan, K., et al., (2010), Ground-based observations of thunderstorm-correlated fluxes of high-energy electrons, gamma rays, and neutrons. *Phys. Rev. D* 82, 043009.
- [2] Chilingarian, A., Hovsepyan, G., Hovhannisyan, A., (2011), Particle bursts from thunderclouds: natural particle accelerators above our heads. *Phys. Rev. D* 83, 062001.
- [3] Chilingarian, A., Mkrtychyan, H. (2012), Role of the lower positive charge region (LPCR) in initiation of the thunderstorm ground enhancements (TGEs). *Phys. Rev. D* 86, 072003. the possibility of location of radiation-emitting region in thundercloud, *Journal of Physics: Conference Series* 409 (2013) 012217.
- [4] Chilingarian A., Bostanjyan N., Karapetyan T., On the possibility of location of radiation-emitting region in thundercloud, *Journal of Physics: Conference Series* 409 (2013) 012217.
- [5] Chilingarian A., Hovsepyan G., Extensive Cloud Showers (ECS) – New High-Energy Phenomena Resulting from the Thunderstorm Atmospheres, *Journal of Physics: Conference Series* 409 (2013) 012221
- [6] Chilingarian A., Thunderstorm Ground Enhancements - model and relation to lightning flashes, *Journal of Atmospheric and Solar-Terrestrial Physics* 107 (2014) 68–76
- [7] Holden D. N., Holmes C. R., Winn W. P., Cobb J. W., Griswold J. E., and Lytle D.M., Local Charge Concentration in Thunderclouds, in *Sixth International Conference on Atmospheric Electricity* (University of Manchester, Manchester, England, 1980).
- [8] Torii, T., Sugita, T., Kamogawa, M., et al. Migrating source of energetic radiation generated by thunderstorm activity. *Geophys. Res. Lett.* 38, L24801, 2011.
- [9] Tsuchiya, H., Enoto, T., Yamada, S., et al. Long-duration gamma ray emissions from 2007 and 2008 winter thunderstorms. *J. Geophys. Res.* 116, D09113, 2011.

## RELEC Mission: TLE and Relativistic Electron Precipitations

*M. Panasyuk, S. Svertilov, V. Bogomolov, G. Garipov, N. Veden'kin*

*Skobel'tsyn Institute of Nuclear Physics, Moscow State University*

---

**Abstract:** The main goal of RELEC mission is studying of magnetosphere relativistic electron precipitation and its acting on the upper Atmosphere as well as transient luminous events (TLE) observation in wide range of electromagnetic spectrum. The RELEC set of instruments includes two identical detectors of X- and gamma-rays of high temporal resolution and sensitivity (DRGE-1 & DRGE-2), three axe directed detectors of energetic electrons and protons DRGE-3, UV TLE imager MTEL, UV detector DUV, low-frequency analyser NchA, radio-frequency analyser RchA, dosimeter module DOSTEL, module of electronics intended for commands and data collection BE. During the RELEC mission following experiments will be provided:

- simultaneous observations of energetic electron & proton flux (energy range  $\sim 0.1$ -10.0 MeV and low-frequency ( $\sim 0.1$ -10 kHz) electromagnetic wave field intensity variations with high temporal resolution ( $\sim 1$  ms);
  - fine time structure ( $\sim 1$  mcs) measurements of transient atmospheric events in UV, X- and gamma rays with a possibility of optical imaging with resolution of  $\sim$ km in wide FOV;
  - measurements of electron flux pitch-angle distribution in dynamical range from  $\sim 0.1$  up to 105 part/cm<sup>2</sup>s;
  - monitoring of charge and neutral background particles in different areas of near-Earth space.
- 

### 1. INTRODUCTION

New geophysical phenomena connected with electrical discharges in the upper atmosphere, such as "Sprites", "Elves" and "Blue jets", accompanying "ordinary" lightning were discovered recently, and now are studied with growing intensity. Those phenomena in visible and UV light are defined as transient luminous events (TLE) and interpreted as light produced by electrical discharge between clouds and ionosphere. But some experimental data, first of all the anomalous X-ray and gamma-ray flashes (bursts) are out of the frame of standard theory of electric strike and indicate a possible important role of high-energy electrons. From this point, the new mechanism of a strike, so-called "the strike on a run-away electrons" is of great interest [1]. This new physical phenomenon was predicted before [2], and to the present has been studied theoretically in details, sees the paper [3] at this workshop and references listed there.

Observations on-board the Compton Gamma-Ray Observatory (CGRO) and RHESSI of intensive gamma-ray bursts [4, 5] are of fundamental interest. Those bursts were observed from the regions of intensive thunderstorm formation. The duration of gamma-ray bursts is of about few milliseconds and the energy spectrum is like a run-away electron bremsstrahlung with typical energies at several hundreds KeV. The intensity of photons in such a burst detected at near-Earth orbit (400-500 km) is rather high, about 100 photon/cm<sup>2</sup>s.

In theory of strike on run-away electrons the visible and UV light should accompany the gamma-ray burst. This theory suggests the primary "seed" electrons as provocateurs of strike. The interesting problem is origin of such electrons. Are they precipitated from the Earth's

radiation belts or they are produced in cosmic ray interactions in the atmosphere?

We know from balloon [6] and space [7,8,9,10] experiments that energetic electrons are precipitating from the Earth's radiation belt at high latitudes (the phenomenon was called PRE). The precipitating electrons may produce the UV glow of the atmosphere as was observed in [11]. It was shown that the PRE fluxes substantially increase during geomagnetic disturbances. The precipitation causes catastrophic losses of the electrons and even ruins the outer Earth radiation belt (ERB) [12,13,14]. The relativistic electron precipitation could be either gradual with typical time of hours or very fast, much shorter than second. In the latter case those electrons may be "seed" ones needed for initiating the strike on run-away electrons and be responsible for TLE, for example, UV flashes observed in [11]. However, the problem of TLE association with PRE is not solved yet, because of lack of experimental data.

Other possible origin of seed electrons is electrons produced by cosmic rays in the atmosphere. For example, intensive flux of electrons is produced in extensive air showers (EAS), generated by very high energy primary cosmic ray particles. In order to distinguish between the ERB- and EAS-initiated TLE we should develop sophisticated methods of measuring gamma-ray flashes, TLE and the seed electrons simultaneously.

In principle, high energy electrons generated in the atmospheric discharge could be an additional source of filling up ERB's. In equatorial region ( $L \sim 1-2$ ) where most of atmospheric electrical discharges occurred those electrons are the only source responsible for generating sporadic, short in time ERB's. The low intensity atmosphere glow symmetrical to the magnetic equator

observed in [11, 15] is interesting evidence in favor of this hypothesis.

In view of above considerations the development of space observation of atmosphere transient phenomena in various wavelength ranges simultaneously with measurements of electrons at the orbit is very important. Space observations have the advantage of covering large area of the atmosphere needed for search and measuring the rare events of high-energy electron and gamma-ray flashes. For understanding the nature of atmospheric electric discharges it is necessary to realize remote observations in radio, optical, ultraviolet, hard X-ray and gamma-ray bands with extremely high ( $\sim 1 \mu\text{s}$ ) time resolution.

## 2. RELEC MISSION

RELEC satellite should be launched in approximately 2010 to the solar synchronous orbit with height about 650 km. The aims of RELEC mission are following:

- simultaneous observations of energetic electron & proton flux (energy range  $\sim 0.1$ -10.0 MeV and low-frequency ( $\sim 0.1$ -10 kHz) electromagnetic wave field intensity variations with high temporal resolution ( $\sim 1$  ms);
- fine time structure ( $\sim 1$  mcs) measurements of transient atmospheric events in UV, X- and gamma rays with a possibility of optical imaging with resolution of  $\sim$ km in wide FOV;
- measurements of electron flux pitch-angle distribution in dynamical range from  $\sim 0.1$  up to  $10^5$  part/cm<sup>2</sup>s;
- monitoring of charge and neutral background particles in different areas of near-Earth space.

The RELEC set of instruments includes two identical detectors of X- and gamma-rays of high temporal resolution and sensitivity (DRGE-1 & DRGE-2), three axe directed detectors of energetic electrons and protons DRGE-3, UV TLE imager MTEL, UV detector DUV, module of charge and neutral particle detectors BChK, low-frequency analyzer NchA, radio-frequency analyser RchA, dosimeter module DOSTEL, module of commands and data collection BSKU.

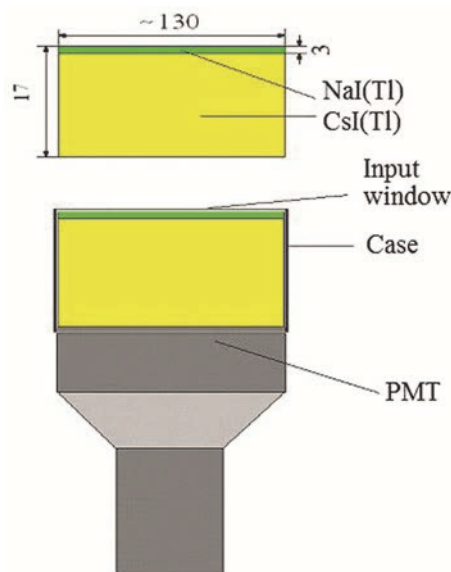


Figure 1. Phoswich detector drge 1(2).

DRGE-1 (DRGE-2) instrument is based on two identical NaI(Tl)/CsI(Tl)/plastic scintillation phoswich detectors (Fig. 1), both directed toward the Earth. Their physical parameters are presented in Table 1.

Table 1.

|   |   |
|---|---|
| Energy range                                    | 0.01-2.0 MeV                            |
| Effective area (total $\sim 800 \text{ cm}^2$ ) | $\sim 200 \text{ cm}^2$                 |
| Temporal resolution                             | 0.1 mcs                                 |
| Sensitivity                                     | $\sim 5 \cdot 10^{-9} \text{ erg/cm}^2$ |

DRGE-3 instrument consists from three identical NaI(Tl)/CsI(Tl)/plastic scintillation phoswich detectors, directed along three axe mutually normal (as Cartesian coordinate system), see Fig. 2. Its physical parameters are presented in Table 2.

Table 2.

|                     | electrons                           | protons                             |
|---------------------|-------------------------------------|-------------------------------------|
| Energy range        | 0.1-10.0 MeV                        | 1.0-100.0 MeV                       |
| Geom. factor        | $\sim 2 \text{ cm}^2\text{sr}$      | $\sim 2 \text{ cm}^2\text{sr}$      |
| Temporal resolution | 1.0 ms                              | 1.0 ms                              |
| Sensitivity         | $\sim 10 \text{ part/cm}^2\text{s}$ | $\sim 10 \text{ part/cm}^2\text{s}$ |

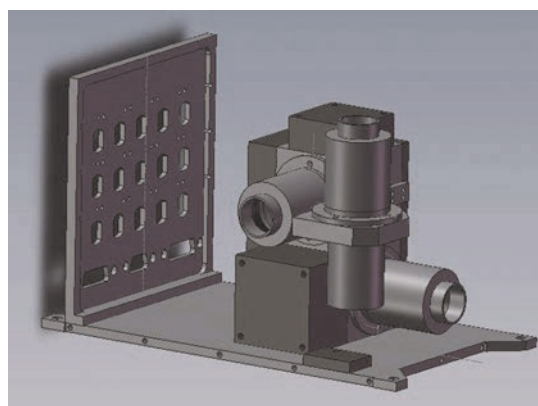


Figure 2. Three axis DRGE instrument.

The MTEL imager and DUV are the same instruments as in Tatiana-2 project.

BChK instrument consists from the number of detectors of different kind of space radiation, i.e. silicon, CsI(Tl), BGO, LBO, Geiger counters, which provided monitor measuring of  $>300$  KeV electron fluxes and  $>50$  MeV proton fluxes as well as detection of 0.05 – 1 MeV gamma-quanta and 0.1 – 30 MeV neutrons.

Low-frequency analyser NChA consists of two electric field meters, Ferro-probe magnetometer with separate electronic unit and spectrum-analyser unit. It provides measurements of two electric field components and one (or two) magnetic field component in frequency band 20 Hz - 20 kHz with number of spectral components 1024, frequency step 20 Hz and time resolution 2 s. A possible meter configuration is shown in Fig. 3.

The RChA instrument is an electronic module devoted to measure electrical and magnetic components of radio frequency emissions in the frequency range from 100 kHz up to 15.0 MHz. The instrument contains the following major parts.

Main electronic box 1 item

Loop H-field antenna 3 item  
 H antenna boom 1 item  
 Dipole E-field antenna 3 items  
 E antenna boom 1 item

The RChA instrument main characteristics are presented in Table 3.

**Table 3**

|                     |                                    |
|---------------------|------------------------------------|
| Frequency range     | 100.0 [kHz] to 15.0 [MHz]          |
| Spectrum resolution | 10.0 [kHz] (from 0.1 to 1.0 MHz)   |
| and                 | 100.0 [kHz] (from 1.0 to 15.0 MHz) |
| Dynamic range [dB]  | 70.0 (TBC)                         |



**Figure 3. RChA detector.**

DOSTEL instrument is dosimeter unit intended for a background radiation measurements.

The ground-based support of RELEC mission with optic and VLF/ELF measurements of thunderstorm and lightning activity is also supposed.

### 3. REFERENCES

- [1] A.V. Gurevich and K.P. Zybin. Breakdown on runaway electrons and electric discharges during thunderstorms. *Uspekhy Physicheskikh Nauk*, v. 171. pp. 1177 – 1199, 2001.
- [2] A.V. Gurevich. On theory of the runaway electron effect. *JETP*, v. 39, pp. 1296-1301, 1960.
- [3] L.P. Babich et al , this workshop.
- [4] G.J. Fishman, Bhat P.N., Mallozzi R., Horack J.M., Koshut T., Kouveliotou C., Pendleton G.N., Meegan C.A., Wilson R.B., Paciesas W.S., Goodman S.J., Christian H.J. Discovery of Intense Gamma – Ray Flashes of Atmospheric Origin., *Science*, 264, 1313-1316, 1994.
- [5] Smith D.M., Lopez L.I., Lin R. P., RHESSI Terrestrial Gamma-ray Flashes: Current Status, [http://sprg.ssl.berkeley.edu/atmos/tgf/dsmith\\_annot.pdf](http://sprg.ssl.berkeley.edu/atmos/tgf/dsmith_annot.pdf) 2005.
- [6] Makhmutov et al., Results of the analysis of electron precipitation events observed in the polar atmosphere, Proc. XXVI Annual Seminar “Physics of Auroral Phenomena”, Apatity, 70-73, 2003.
- [7] Friedel, R.H.W., G.D. Reeves, T. Obara, Relativistic electron dynamics in the inner magnetosphere - a review, *J. Atmos. Sol. Terr. Phys.*, 64, 265– 282, 2002.
- [8] Dmitriev A.V., and J.-K. Chao, Dependence of geosynchronous relativistic electron enhancements on geomagnetic parameters, *J. Geophys. Res.*, 108(A11), 1388, doi:10.1029/2002JA009664, 2003.
- [9] Bucik, R., K. Kudela, A.V. Dmitriev, S.N. Kuznetsov, I.N. Myagkova, S.P. Ryumin, Review of electron fluxes within the local drift loss cone: Measurements on CORONAS-I, *J. Adv. Space Res.*, 36(10), 1979-1983, 2005.
- [10] Dmitriev A., N. Crosby, J.-K. Chao, Interplanetary sources of space weather disturbances in 1997 to 2000, *Space Weather*, 3(3), S03001, 10.1029/2004SW000104, 2005.
- [11] Garipov G.K., Khrenov B.A., Panasyuk M.I., Tulupov V.I., Shirokov A.V., Yashin I.V. and Salazar H., UV radiation from the atmosphere: Results of the MSU “Tatiana” satellite measurements, *Astroparticle Physics*, 24, 400-408, 2005.
- [12] Lorentzen, K.R., Looper, M.D., and Blake, J.B., Relativistic electron microbursts during the GEM storms, *Geophys. Res. Lett.*, 28:2573-2576, 2001.
- [13] Dmitriev, A.V., Bakhareva M.F., Suvorova A.V., Relationship between dynamics of the relativistic electrons in the outer radiation belt and solar wind parameters, *Solar Terrestrial Physics*, 2(115), Irkutsk, 182-184, 2002 (in Russian)
- [14] Green, J. C., T. G. Onsager, T. P. O'Brien, D. N. Baker, Testing loss mechanisms capable of rapidly depleting relativistic electron flux in the Earth's outer radiation belt, *J. Geophys. Res.*, 109(12), A12211, 10.1029/2004JA010579, 2004.
- [15] Christensen, A. B., L. J. Paxton, S. Avery, J. Craven, G. Crowley, D. C. Humm, H. Kil, R. R. Meier, C.-I. Meng, D. Morrison, B. S. Ogorzalek, P. Straus, D. J. Strickland, R. M. Swenson, R. L. Walterscheid, B. Wolven, and Y. Zhang, Initial observations with the Global Ultraviolet Imager (GUVI) in the NASA TIMED satellite mission, *J. Geophys. Res.*, 108 (A12), 1451, 2003.
- [16] I.H. Park this workshop.
- [17] Garipov G.K., Khrenov B.A. and Panasyuk M.I., Correlation of atmospheric UV transient events with lunar phase. *Geophys. Research Lett.*, 35, L10807;doi: 10.1029/2007 GL032679, 2008.

## Observation of the compact intercloud discharges onboard of microsatellite Chibis-M

*M. S. Dolgonosov<sup>1,2</sup>, V. M. Gotlib<sup>1,2</sup>, L.M. Zelenyi<sup>1</sup>, D.I. Vavilov<sup>1</sup>, V. Rakov<sup>2,3</sup>*

<sup>1</sup>*Space Research Institute of the RAS, 84/32 Profsoyuznaya str., Moscow 117997, Russia.*

<sup>2</sup>*Institute of Applied Physics of the RAS, 46 Ulyanov str., Nizhny Novgorod 603950, Russia*

<sup>3</sup>*Department of Electrical and Computer Engineering, University of Florida, Gainesville, Florida USA,*

---

**Abstract:** Microsatellite "Chibis-M" was launched at the orbit in 25 January 2012. The main goal of the mission is to study lightning activity at the upper atmosphere in different parts of the spectrum. Microsatellite carries radio frequency analyzer, UV and IR detectors, fast optical camera and plasma spectrum analyzer. In this paper pay special attention to the data set of Compact Intracloud Discharges (CIDs) registered onboard of the spacecraft for the first 17 months operation on orbit. This data set includes 280 events. We also introduce new features of VHF emission from terrestrial atmosphere, namely, wide band patterns in spectrogram duration around 150  $\mu$ s. This pattern might be considered as made up of overlapping set of different VHF radio emissions from CIDs. The origin of these patterns could be associated with consequences of gamma ray and positron feedback during developing of avalanches of relativistic particles discussed by Dwyer [2003] that leads to the multiplicity of radio bursts. On the basis of comparison with lightning distribution TRRM mission we draw conclusion that CIDs are related to the normal lightning process. Peaks of CIDs detection over West coast of Africa, Malay Archipelago and area near the Central America allocate these regions as main sources of CID's generation in terrestrial atmosphere.

---

### 1. INTRODUCTION

For many years it was paid attention to the exploring of Very High Frequency radio emission from physical processes originated in the upper terrestrial atmosphere by means of ground facilities (e.g. Le Vine [1980]; Serhan et al. [1980]; Weidman et al. [1981]; Willett et al. [1990]; Mäkelä et al. [2007]; Thomas et al. [2001]; Lan et al. [2011]) as well radio receivers onboard satellites (e.g. Holden et al. [1995]; Massey and Holden [1995]; Jacobson et al. [1999, 2000, 2011]; Jacobson and Light [2012]). Recently interest in this phenomena has been rekindled by discovering Compact Intracloud Discharges (CIDs), firstly reported by Le Vine [1980] and received its moniker due to the inferred relatively small spatial size [Smith et al., 1999]. On the basis of experimental data it was found that shortest radiating channel length of CIDs less than 1000 m [Smith et al., 1999; Nag and Rakov, 2010; Nag et al., 2010]. It is assumed that the current wave had a smooth rise with zero-to-peak rise-time of order some of  $\mu$ s and total duration of 10-30  $\mu$ s with VHF radio emission stronger than those emitted by first return strokes of CG flashes [Le Vine, 1980; Willett et al., 1989; Smith et al., 1999]. It was also shown that CIDs are different from other phenomena producing bipolar electric field waveform. Sometimes CIDs are referred as Narrow Bipolar Pulses (NBPs) or Narrow Bipolar Events (NBEs) (e.g. Willett et al. [1990]). In the current work we will use term "CID" because this term more fully and in extensor represents nature of the phenomena under consideration.

Observation of CIDs radio emission from space provided unique opportunity to discover them all over the world and to collect statistics of its global distribution [Holden et al., 1995; Jacobson et al., 1999]. These new possibilities revealed some new features of CIDs: radio receivers onboard of the satellite registered pair of the

signals separated by tens of microseconds [Holden et al., 1995]. These two pairs were interpreted as being due to reflection from the direct path to radio receiver above the ionosphere and the second signal originated from the ground reflection of the first one [Massey and Holden, 1995]. These pair got moniker "transion-spheric pulse pair" (TIPP). Detailed observations on CID alias NBP and their associated VHF TIPP were presented in publications based on FORTE ([Jacobson, 2003a, b]).

In this paper we introduce capabilities of the radio receiver onboard of microsatellite "Chibis-M" and results of CIDs observation by this instrument. The obtained data allow us to estimate statistics gathered during first 17 months of "Chibis-M" flight of CIDs global occurrence vs. local time, latitude and longitude and compare it with earlier results (ALEXIS and FORTE), e.g. [Holden et al., 1995; Jacobson et al., 1999].

### 2. RADIO FREQUENCY ANALYZER ONBOARD OF THE MICROSATELLITE "CHIBIS-M"

Microsatellite "Chibis-M" was developed on the platform originally designed at the Special Engineering Department of Space Science Institute of Russian Academy of Science in 2011. Mission was launched at the orbit in 25 January 2012 under the auspices of the Russian Academy of Sciences and S.P. Korolev Rocket and Space Corporation "ENERGIA". The main goal of the "Chibis-M" project is to study lightning phenomena at the upper atmosphere of the Earth. The principle idea underling the scientific payload of the "Chibis-M" creation was the joint observations of the lightning emission at different parts of the spectrum. To realize this idea the following set of instruments was installed onboard: Radio Frequency Analyzer (RFA), UV and IR detectors (DUF), Roentgen and Gamma detector (RGD), Plasma Spectrum Analyzer

(PSA) and Fast Optical Camera (FOC). Here we give only a brief sketch of the microsatellite, the more detailed description of the launching scheme and spacecraft by itself will be given in a separate engineering paper. In following papers we will introduce the capabilities and performance of the UV and IR payloads and the numerous scientific findings of each payload in concert each other. Meanwhile, it is worth to mention some important spacecraft parameters. The microsatellite orbit is circular with inclination  $51^\circ$ . Starting elevation above sea level was 545 km and at the writing time of this paper was  $\sim 500$  km. The total mass of the satellite is 40 kg. Scientific payload consists 10.8 kg that is about 27% of the total spacecraft's weight.

The data presented are obtained from the radio receiver (RFA) carried by "Chibis-M". This instrument contains one pass-band in the range 26-48 MHz, with a nominal digitized at 96 megasamples/s. The radio channel is connected to a simple passive dipole-like antenna with total length 4 m with a null along the spacecraft. The antenna is mounted on the bottom of the platform. The RFA implemented advances of similar triggering scheme used by radio receivers aboard FORTE. Receiver's pass-band has embedded within it five independent triggering sub-bands having 2.4-MHz of bandwidth. In the work presented here, the trigger was derived from coincidence of first three sub-band triggers (starting with the lowest frequency). This triggering scheme immune RFA from saturation because of the presence of the man-made narrow band communication signals broadcasting over populated areas. The software onboard "Chibis-M" allows changing as number and order of sub-bands as an instrument that formed the trigger by ground command. Especially, in some cases formation of the trigger was passed to DUF instrument similar to optical instrument onboard "Universitetsky-Tatiana-2" [Garipov et al., 2011].

The Scientific Data Accumulation System (SDAS) contains enough memory (256 Mb) for up to 2.56 s (cumulative) of 8-bit data from RFA. Each record is triggered (see above) and has adjustable pre-trigger/post-trigger records with a trigger at the center of the record. Initially operation of RFA has started with 1 and 3 ms records with trigger at the center of the frame. Now recorded frame length is 50 ms. The SDAS is capable of retriggering a new record within microseconds of the end of the previous one. To manage data downlink and mission control tracking headquarters was organized on the basis of the Space Research Institute of RAS. The scientific data downlink occurs at different stations up to several downloads per day.

Data acquisition commenced at the end of April 2012 and has continued without serious interruption through the writing of this paper.

### 3. EXPERIMENTAL DATA

The database of presented events were collected onboard microsatellite "Chibis-M" since the end of April 2012 up to the begging of September 2013. Since the April 2012 the elevation of the satellite orbit decreased from 545 km to 480 km (Ask Anton!!!). Initial footprint of the antenna was about 2725 km along longitude and latitude, or

$\sim 35^\circ$  at the equator, so the footprint diminished on  $\sim 10\%$  for this period. The spectrogram of events detected on 6 of April, 2013 at UT 23:52:10.723 is shown in the Fig.1. The spectrogram's Fourier's moving time window is 512 samples (or  $\sim 5.33 \mu\text{s}$  time width) and overlaps with previous 256 samples. For these parameters the spectral resolution is  $\sim 0.19$  MHz. No other filtering techniques were applied. The length of the recorded frame was 50 ms, but for the sake of readability and discrimination of all structures of the signal spectrum we presents only 1 ms part of the frame. The full record and some other examples of VHF emission detected onboard "Chibis-M" are available as an auxiliary material of the current paper. Sub-satellite local time at that moment was  $\sim 00:07$  (late night). The event occurred over Atlantic Ocean and near West coast of Africa ( $4^\circ\text{N}$ ,  $4^\circ\text{E}$ ). Because the direct path to the continent was less then one thousand kilometer, there is a probability of generation of this particular event over land.

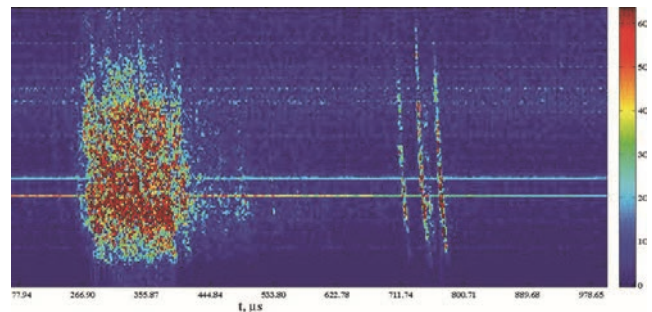


Figure 1. Spectrograms of one exemplary Compact Intercloud Discharge (CID) detection occurred 6 of April, 2013 at UT 23:52:10.723 over Africa (see text for description).

In this figure triplet of sharp CIDs succeeded some VHF "noise" with  $150 \mu\text{s}$  duration. This "noise" might be considered as a "fabric" made up of CIDs patches. In the paper of Dwyer [2003] author accomplished Monte Carlo simulation of the runaway breakdown of air and took into account all the important interactions involving runaway electrons, energy losses through ionization and atomic excitation and Møller scattering. Moreover, unlike earlier work, this simulation includes bremsstrahlung production of x-rays and gamma-rays and the subsequent propagation of the photons, including photoelectric absorption, Compton scattering and pair production. It was shown that due to the gamma ray and positron feedback mechanisms new CIDs (or avalanches, in term of the Dwyer's paper) could be generated. Latter Dwyer and Cummer [2013] calculated radio emission from terrestrial gamma-ray flashes (TGF). It was shown that shorter TGF generates more intensive radio emission (ibid Fig.5). Combining these two ideas it might be set up hypothesis that VHF patterns succeeding triplet of single CIDs as presented in Fig.1 are continuous number of CIDs (or avalanches) by itself originated in the same process as predicted in paper [Dwyer, 2003]. We intend to provide detailed analysis of this hypothesis on the basis of RFA data in our further papers.

Triplet of "separate" CIDs in Fig.1 revealed distinctive ionospheric dispersion widely studied on previous detection of VHF emission onboard satellites, e.g. [Holden et al., 1995; Massey and Holden, 1995; Jacobson et al., 1999,

2000; Jacobson, 2003b; Moses and Jacobson, 2004]. Approximately the group delay  $\tau$  of the wave packet could be described as following:

$$\tau \sim 1.34 \times [N/(10^{17} \text{ m}^{-2})] \times [f/(100 \text{ MHz})]^{-2} \quad (1)$$

where  $N$  is slant total electron content,  $f$  is radio frequency in MHz. For this particular event TEC is  $-0.8 \cdot 10^{17} \text{ m}^{-2}$ . Estimated slant TEC for most of "Chibis-M" data is less comparing to the FORTE or Blackbeard due to the lower elevation of the satellite. Continuous wave carrier mapped into straight two intensive lines around 30 MHz and multiple faint along the whole range of the instrument.

To analyze statistical properties of registered CIDs we choose only records with "separated" CIDs and its arbitrary position in a frame. Due to the relatively long recording time (up to 50  $\mu\text{s}$ ) it was imprinted up to tens of CIDs in some frames. Nevertheless, frames with or not numerous "bursts" were counted as equivalent. Total number of selected in such way frames is 280. The compiled statistics of CIDs global distribution presented in Fig.2-Fig.4. Figures 2 and 3 represent probability of CIDs detection calculated by dividing number of events in each bin over the total number of bins (bin size 10 in each figure). According to Fig.2 the data set has slight bias toward northern hemisphere. This fact accounts for the prevailing two "northern" summers in data set. In between  $\pm 10$  contains - 55% of all events. Though detections of VHF "bursts" dominates close to equator the time spent by the satellite in range between  $\pm 10$  is equal to 46%. This fact seems to us very unusual and we are going to collect more data within rest of satellite lifetime to check it again. ? provided distribution of CIDs (or TIPP) with latitude based on FORTE data set. Though authors did not provided any information (ask A. Ledkov about possibility to count it!!) about satellite trajectory, distribution of VHF records onboard FORTE satellite revealed the similar to our bell-shaped distribution (see Fig.2 and explanation in the text).

Fig.3 presents percentage of CIDs detection in longitudes. Peaks at  $0^\circ$  and  $350^\circ$  of East longitudes correspond to the West (Atlantic) coast of Africa, peak at  $100^\circ$  corresponds to Malay Archipelago. Increase of probability between  $250^\circ$  and  $300^\circ$  corresponds to area near the Central America. In general, this figure match the essential part of the distribution present by Holden et al. [1995] (see Fig.5).

Fig.4 represents distribution of recorded events onboard of "Chibis-M" over local time at sub-satellite point. This figure also represents main features of the distribution presented by [Holden et al., 1995] (Fig.4): "The two peaks at afternoon and just after midnight are consistent with peaks in the frequency of thunderstorm occurrence". To illustrate this idea it worth to compare Fig.4 with satellite observation of lightning presented, for example, by Tropical Rainfall Measurement Mission (TRMM) Peterson and Liu [2011]. Please, note that in the latter paper authors calculated occurrence of lightning over land and ocean separately, thus to compare their results with Fig.4 one have to sum up percentages on Fig.4a and Fig.4b in the paper of Peterson and Liu [2011]. Moreover our data set caught quite period of impulses generation before the noon. The other gap in CIDs generation was revealed just before the 3 PM.

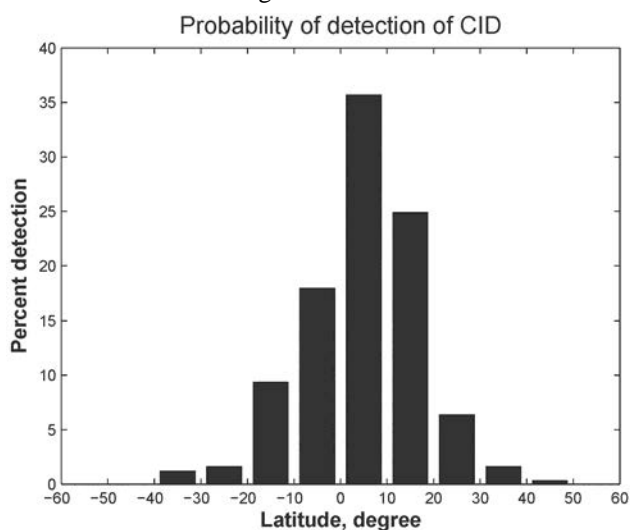


Figure 2. Distribution of detected events (CID) as a function of local latitude at the sub-satellite position.

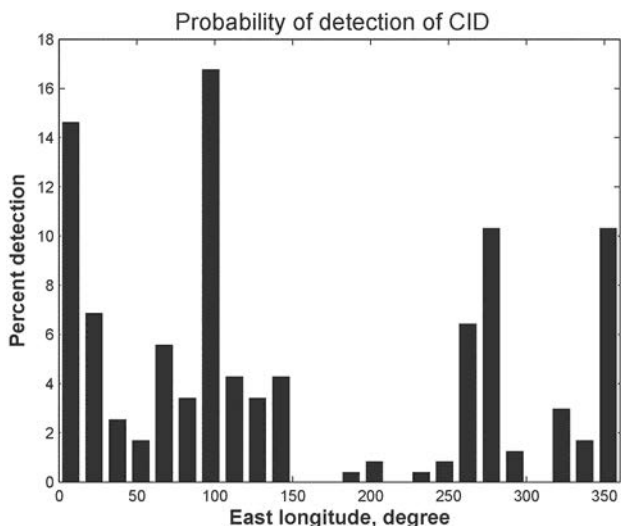


Figure 3. Distribution of detected events (CID) as a function of local longitude at the sub-satellite position.

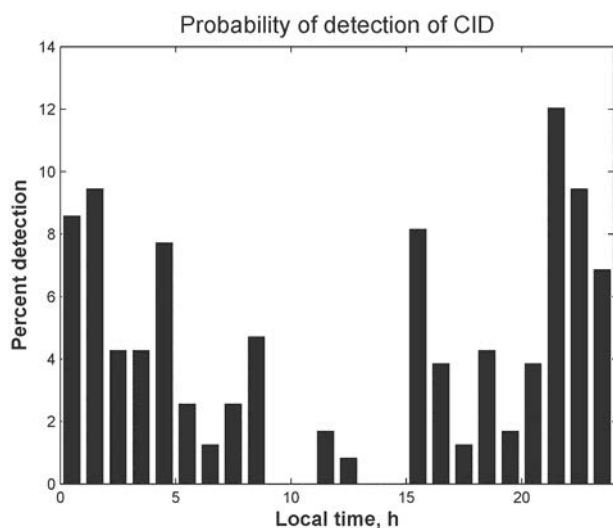


Figure 4. Distribution of detected events (CID) as a function of local time at the sub-satellite position.

## 4. ACKNOWLEDGMENTS

We would like to thank A. V. Gurevich for useful suggestions. The research leading to these results was financially supported by the Russian Government (contract No. 14.B25.31.0023) and partially by the RFBR (research project No. 13-0512102 and No. 12-02-92614).

## 5. SUMMARY

In this paper we have presented statistics of the global distribution of Compact Inter- cloud Discharges (CIDs) obtained by Radio Frequency Analyzer (RFA) onboard of the microsatellite "Chibis-M" for the first 17 months of operation. New features of VHF emission were discussed, namely, wide band patterns in spectrogram duration around 150 $\mu$ s (see Fig.1, from 266  $\mu$ s). This "noise" might be considered as a "fabric" made up of overlapping set of different VHF radio emissions from CIDs. The origin of this patterns could be associated with consequences of gamma-ray and positron feedback during developing of avalanches of relativistic particles discussed in following papers [Dwyer , 2003; Dwyer and Cummer , 2013] that leads to the multiplicity of radio bursts. In following papers we are going to study this hypothesis more carefully. Detected properties of radio emission from "separate" CIDs completely coincide with previously studied records of Blackbeard and FORTE satellites (e.g. Holden et al. [1995]; Jacobson et al. [1999]).

The compiled distribution of recorded events Fig.2- Fig.3 give a good fit to the previously reported observation (Fig.4-5 in Holden et al. [1995] and Fig.2 in Jacobson et al. [1999]). On the basis of comparison with lightning distribution over the land and ocean [Peterson and Liu, 2011] one could draw conclusion that CIDs are related to the normal lightning process. Peaks of CIDs detection the West (Atlantic) coast of Africa, Malay Archipelago and area near the Central America allocate these regions as main sources of CID's generation in terrestrial atmosphere.

## 6. REFERENCES

- [1] electric fields in air, *Geophysical Research Letters*, 30(20), 2055, doi:10.1029/2003GL017781.
- [2] Dwyer, J. R., and S. A. Cummer (2013), Radio emissions from terrestrial gamma-ray flashes, *Journal of Geophysical Research: Space Physics*, 118(6), 3769-3790, doi: 10.1002/jgra.50188
- [3] Garipov, G. K., B. A. Khrenov, P. A. Klimov, V. V. Klimenko, E. A. Mareev, O. Martines, V. S. Morozenko, M. I. Panasyuk, I. H. Park, E. Ponce, H. Salazar, V. I. Tulupov, N. N. Vedenkin, and I. V. Yashin (2011), Global Transients in ultraviolet and red-infrared ranges from data of the "Universitetsky-Tatiana-2" satellite, eprint arXiv:1112.0894, p. 19.
- [4] Holden, D. N., C. P. Munson, and J. C. Devenport (1995), Dwyer, J. R. (2003), A fundamental limit on Satellite observations of transionospheric pulse pairs, *Geophysical Research Letters*, 22(8), 889-892, doi: 10.1029/95GL00432.
- [5] Jacobson, A. R. (2003a), How do the strongest radio pulses from thunderstorms relate to lightning flashes?, *Journal of Geophysical Research*, 108(D24), 4778, doi: 10.1029/2003JD003936.
- [6] Jacobson, A. R. (2003b), Bimodal radio frequency pulse distribution of intracloud-lightning signals recorded by the FORTE satellite, *Journal of Geophysical Research*, 108(D9), 4266, doi:10.1029/2002JD002613.
- [7] Jacobson, A. R., and T. E. L. Light (2012), Revisiting "Narrow Bipolar Event" intracloud lightning using the FORTE satellite, *Annales Geophysicae*, 30(2), 389-404, doi:10.5194/angeo-30-389-2012.
- [8] Jacobson, A. R., S. O. Knox, R. Franz, and D. C. Enemark (1999), FORTE observations of lightning radio-frequency signatures: Capabilities and basic results, *Radio Science*, 34 (2), 337, doi:10.1029/1998RS900043.
- [9] Jacobson, A. R., K. L. Cummins, M. Carter, P. Klingner, D. Roussel-Dupre, and S. O. Knox (2000), FORTE radio-frequency observations of lightning strokes detected by the National Lightning Detection Network, *Journal of Geophysical Research*, 105(D12), 15,653, doi:10.1029/2000JD900103.
- [10] Jacobson, A. R., R. H. Holzworth, and X.-M. Shao (2011), Observations of multi-microsecond VHF pulsetrains in energetic intracloud lightning discharges, *Annales Geophysicae*, 29(9), 1587-1604, doi:10.5194/angeo-29-15872011.
- [11] Lan, Y., Y.-j. Zhang, W.-s. Dong, W.-t. Lu, H.-y. Liu, and D. Zheng (2011), Broadband analysis of chaotic pulse trains generated by negative cloud-to-ground lightning discharge, *Journal of Geophysical Research*, 116(D17), D17,109, doi: 10.1029/2010JD015159.
- [12] Le Vine, D. M. (1980), Sources of the strongest RF radiation from lightning, *Journal of Geophysical Research*, 85(C7), 4091, doi:10.1029/JC085iC07p04091.
- [13] Makela, J., M. Edirisinghe, M. Fernando, R. Montano, and V. Cooray (2007), HF radiation emitted by chaotic leader processes, *Journal of Atmospheric and Solar-Terrestrial Physics*, 69(6), 707-720, doi:10.1016/j.jastp.2007.01.003.
- [14] Massey, R. S., and D. N. Holden (1995), Phenomenology of transionospheric pulse pairs, *Radio Science*, 30(5), 1645-1659, doi:10.1029/95RS01563.
- [15] Moses, R. W., and A. R. Jacobson (2004), Ionospheric profiling through radio- frequency signals recorded by the FORTE satellite, with comparison to the International Reference Ionosphere, *Advances in Space Research*, 34 (9), 2096-2103, doi: 10.1016/j.asr.2004.02.018.
- [16] Nag, A., and V. A. Rakov (2010), Compact intracloud lightning discharges: 1. Mechanism of electromagnetic radiation and modeling, *Journal of Geophysical Research*, 115(D20), D20,102, doi:10.1029/2010JD014235.
- [17] Nag, A., V. A. Rakov, D. Tsalikis, and J. A. Cramer (2010), On phenomenology of compact intracloud lightning discharges, *Journal of Geophysical Research*, 115(D14), D14,115, doi:10.1029/2009JD012957.

- [18] Peterson, M., and C. Liu (2011), Global statistics of lightning in anvil and stratiform regions over the tropics and subtropics observed by the Tropical Rainfall Measuring Mission, *Journal of Geophysical Research*, 116(D23), D23,201, doi: 10.1029/2011JD015908.
- [19] Serhan, G. I., M. A. Uman, D. G. Childers, and Y. T. Lin (1980), The RF spectra of first and subsequent lightning return strokes in the 1- to 200-km range, *Radio Science*, 15(6), 1089, doi:10.1029/RS015i006p01089.
- [20] Smith, D. A., X. M. Shao, D. N. Holden, C. T. Rhodes, M. Brook, P. R. Krehbiel, M. Stanley, W. Rison, and R. J. Thomas (1999), A distinct class of isolated intracloud lightning discharges and their associated radio emissions, *Journal of Geophysical Research*, 104 (D4), 4189, doi:10.1029/1998JD200045.
- [22] Thomas, R. J., P. R. Krehbiel, W. Rison, T. Hamlin, J. Harlin, and D. Shown (2001), Observations of VHF source powers radiated by lightning, *Geophysical Research Letters*, 28(1), 143-146, doi:10.1029/2000GL011464.
- [23] Weidman, C. D., E. P. Krider, and M. A. Uman (1981), Lightning amplitude spectra in the interval from 100 kHz to 20 MHz, *Geophysical Research Letters*, 8(8), 931, doi:10.1029/GL008i008p00931.
- [24] Willett, J. C., J. C. Bailey, and E. P. Krider (1989), A class of unusual lightning electric field waveforms with very strong high-frequency radiation, *Journal of Geophysical Research*, 94 (D13), 16,255, doi:10.1029/JD094iD13p16255.
- [25] Willett, J. C., J. C. Bailey, C. Leteinturier, and E. P. Krider (1990), Lightning electromagnetic radiation field spectra in the interval from 0.2 to 20 MHz, *Journal of Geophysical Research*, 95(D12), 20,367, doi:10.1029/JD095iD12p20367.

## Observing terrestrial gamma flashes at ground level and balloon altitudes

*M. L. Cherry<sup>1</sup>, R. A. Ringuette<sup>1</sup>, G.L. Case<sup>2</sup>, D. J. Granger<sup>1</sup>,  
T. G. Guzik<sup>1</sup>, M. F. Stewart<sup>1</sup>, J. P. Wefel<sup>1</sup>*

<sup>1</sup>*Dept. of Physics and Astronomy, Louisiana State University, Baton Rouge, LA 70803 USA*

<sup>2</sup>*Department of Physics, La Sierra University, Riverside, CA 92515 USA*

---

**Abstract:** Twenty-four Terrestrial Gamma ray Flashes (TGFs) -- short, intense bursts of electrons, positrons, and energetic photons originating from terrestrial thunderstorms -- have been detected at ground level with an array of NaI(Tl) scintillators. During 2.6 years of observation, the TETRA (TGF and Energetic Thunderstorm Rooftop Array) experiment at Louisiana State University has detected a sample of bursts of gamma rays with durations 0.02 - 4.2 msec and deposited energy 50 keV to over 2 MeV associated with nearby lightning. Of the 24 events, three are coincident events observed by detectors separated by ~1000 m. Nine of the events occurred within 6 msec and 3 miles of negative polarity cloud-to-ground lightning strokes with measured currents in excess of 20 kA. The events reported here constitute the first catalog of TGFs observed at ground level in close proximity to the acceleration site. A high altitude balloon payload has also been developed and tested to look for TGFs from above thunderstorms; the balloon observation program is also described.

---

### 1. INTRODUCTION

Intense millisecond-scale bursts of gamma rays produced by upward-moving electrons accelerated to energies of tens of MeV or more have been detected with satellite instruments. These Terrestrial Gamma Flashes (TGFs) have been shown to be associated mainly with positive polarity intracloud lightning, with the particle acceleration occurring at altitudes of 10 - 15 km. We show here that negative polarity cloud-to-ground lightning accelerates particles downward and produces gamma rays with energies of at least 2 MeV. We present a sample of 24 TGFs detected at ground level associated with nearby (< 3 miles) lightning observed over approximately 2.6 years mainly during spring and summer thunderstorms in Louisiana.

TGFs have been observed from space by multiple instruments<sup>1-12</sup>, typically detected close to the sub-satellite point<sup>4</sup> and correlated both with regions of high thunderstorm activity<sup>6,13,14</sup> and with individual positive polarity intracloud (+IC) and possibly positive cloud-to-ground (+CG) lightning discharges to within 1 - 2 msec<sup>15-17</sup>. (Positive polarity is needed to produce the upward beam of electrons and secondary photons necessary for detection of TGFs from space<sup>8,18</sup>.) Lightning flashes are known to emit a large fraction of their electromagnetic energy into low frequency (0.3 - 30 kHz) atmospheric radio signals (sferics), which can be located accurately by arrival time measurements in a worldwide radio receiver network<sup>19</sup>. TGFs are well correlated both with sferics<sup>15,20</sup> and with high resolution lightning data<sup>14,17,21</sup>.

TGF observations from satellite platforms are limited to events apparently beamed upward with a ~30° half-angle cone and large enough to be detected even in the presence of attenuation and Compton scattering by the atmosphere<sup>17,22-24</sup>. Although these events observed from space are extremely intense (gamma ray rates in excess of 300 kHz measured with BATSE), the bulk of the events are presumably smaller events which can only be observed

much closer to the lightning -- i.e., at aircraft or balloon altitude or at ground level<sup>2,10,25,26</sup>. Dwyer<sup>27</sup> has suggested a possible downward-directed positron and gamma ray signature from TGFs. Observations at ground level are necessary to observe the downward component, to better understand the TGF intensity distribution and emission pattern, to understand whether the observed 30° beaming is intrinsic to the emission process or is the result of atmospheric attenuation, and to measure the spectrum vs altitude relationship. As a practical consideration, it has been suggested that lightning-induced gamma rays might produce a significant radiation exposure for airplane passengers flying close to a lightning stroke<sup>28</sup>.

The majority of ground-level observation projects currently focus on correlating satellite-observed TGFs with lightning and measuring possible associated magnetic signatures<sup>29,30</sup>. The ICLRT project, however, has observed two gamma ray bursts, one in association with triggered lightning of negative polarity<sup>31</sup> and another in association with nearby negative polarity cloud-to-ground (-CG) lightning<sup>32</sup>. TGFs associated with negative polarity lightning strikes, as with the ICLRT events, produce downward beams of photons which can be detected from the ground. ICLRT operates in a triggered mode, requiring either a triggered lightning current above 6 kA or the simultaneous trigger of two optical sensors. The array of particle detectors at Aragats Space Environment Center has detected thunderstorm-associated ground enhancements above 7 MeV with timescales of microseconds and tens of minutes<sup>33,34</sup>. These have been detected approximately once per year and seem to be correlated with -IC lightning. In addition, a mountain-top detector has observed three millisecond bursts of X-rays associated with CG lightning<sup>35</sup>. Longer duration (40 seconds to minutes or longer) X-ray and gamma ray events have been reported previously from the ground<sup>36,37</sup>, but the only other case in which a TGF-like event with millisecond emission of MeV gammas has been observed from within the atmosphere is

the observation by the ADELE instrument<sup>25</sup> aboard an aircraft at an altitude of 14 km.

Here we present observations from July 2010 through February 2013 of twenty-four TGF-like events in which 50 keV - 2 MeV gamma rays are observed at ground level in shorter than 5 msec bursts associated with nearby negative polarity lightning. We then also describe a program to detect TGFs from balloon altitudes.

## 2. GROUND-BASED DETECTOR ARRAY (TETRA)

**1. Detector Description:** The TGF and Energetic Thunderstorm Rooftop Array (TETRA, described in more detail in ref. 38) consists of an array of twelve 19 cm × 19 cm × 5 mm NaI(Tl) scintillators designed to detect the gamma ray emissions from nearby lightning flashes over the range 50 keV - 2 MeV. The scintillators are mounted in four detector boxes, each containing three NaI detectors viewed by individual photomultiplier tubes (PMTs). The boxes are spaced at the corners of a ~700 × 1300 m<sup>2</sup> area on four high rooftops at the Baton Rouge campus of Louisiana State University (LSU) at latitude 30.41° and longitude -91.18°. Unlike ICLRT, TETRA operates in a self-triggered mode, allowing for events to be recorded without requiring the direct detection of lightning.

Each TETRA detector box contains three NaI scintillator plates hermetically sealed between a 6.4 mm thick glass optical window on one flat face and a 0.75 mm thick Aluminum entrance window on the other face. An ultraviolet transmitting Lucite light-guide is coupled to the glass window, and an Electron Tubes 9390KB 130 mm photomultiplier tube with a standard bialkali photocathode views the light. The scintillator-PMT assemblies are housed in ~1" thick plastic foam insulation to prevent rapid temperature changes. Electronics boards in each detector box supply high voltage, amplify and shape the PMT outputs, provide an internal trigger for the data acquisition software, digitize the data, assign timestamps, and record ADC values for each event. The readout is capable of detecting events at a sustained rate of 30 kHz and a burst rate of up to 70 kHz. The data are then transferred over a wireless link to a central station for analysis. The initial version of the data acquisition software, used from October 2010 to January 2013, utilized a network time protocol to keep timestamps accurate to within approximately 2 msec and to monitor the absolute timing uncertainty. The current version of the software, implemented in January 2013, uses a GPS-disciplined clock to produce timestamps accurate to within 200 ns.

The ADC-to-energy conversion is calibrated with radioactive sources (<sup>22</sup>Na, <sup>137</sup>Cs, <sup>60</sup>Co). Individual detector energy resolution ranges from 9 to 13.5% FWHM at 662 keV and from 5.5 to 10.8% at 1.3 MeV. The total interaction probability in the NaI scintillators is 95% at 100 keV, 82% at 500 keV, and 10% at 1 MeV (with photoelectric interaction probabilities 93%, 26%, and 0.63% respectively). In addition to the three NaI scintillators, one detector box contains a one inch diameter by one inch thick cerium-doped lanthanum bromide (LaBr<sub>3</sub>:Ce) scintillator that provides high energy resolution measurements (3.5% FWHM at 662 keV) of intense events.

Beginning in October 2012, all boxes contain a bare PMT to check for electronic noise.

Data are accumulated for a day at a time for each of the four detector boxes individually. The daily analysis software selects events with signals corresponding to at least 50 keV deposited energy within 1 msec. The data are then binned into 2 msec bins and assigned a timestamp. TETRA triggers are selected with counts/2 msec at least 20 standard deviations above the mean for the day. Once days with excessive electronic noise or other instrumental problems are removed, there are 835.09 days of live time and 1303 TETRA triggers.

**2. Results:** In Fig. 1, the heavy black line shows a time history of > 50 keV count rates for the three NaI photomultiplier tubes in a single detector box for one day. The total count rate, plotted in counts per minute, is reasonably constant for the first seventeen hours, and then increases by a factor of approximately 2 beginning at about 1800 CST. The small peak in the count rate seen at about 1200 CST is due to noise in the system seen only in a single PMT on a 60-second timescale. The thin black histogram near the bottom shows the local radar reflectivity in decibels acquired from www.wunderground.com, indicating rain, thunderstorms, hail, or strong winds. The increase in the NaI detector rate is clearly correlated with rainstorms. The gamma ray spectrum, measured during a rain event with the high resolution LaBr<sub>3</sub>:Ce detector mounted together with the NaI detectors in one of the detector boxes, shows the presence of 295, 352, 609, 1120, and 1764 keV Bi<sup>214</sup> and Pb<sup>214</sup> lines characteristic of radon decay<sup>38</sup>.

60-second intervals in which the NaI detector count rate is 3 standard deviations higher than the average rate for the day; these are correlated with the peak of the extended rise at the time of the rainstorms. TETRA triggers are defined as intervals during which the rate in a 2 msec window exceeds the day's average by 20  $\sigma$ . The TETRA trigger observed is indicated near the top of the plot as an open square. (For a typical average counting rate of 8900 min<sup>-1</sup> in a detector box above 50 keV, a 20  $\sigma$  excess corresponds to 10 counts in the three PMTs in a detector box within a 2 msec

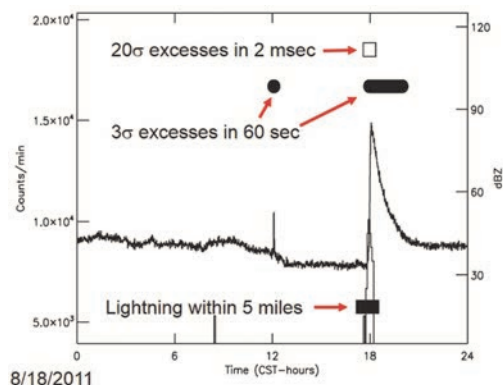


Figure 1. Summed NaI counting rate per minute in Box 3 on 8/18/2011 (heavy black line, left hand scale). Thin black histogram near the bottom (right hand scale) shows radar reflectivity. The filled rectangle at the bottom marks times of lightning strikes within 5 miles. The row of filled circles near the top marks intervals in which the count rate in 60 sec bins exceeds the day's average by 3  $\sigma$ ; the open square marks the TETRA trigger, i.e., the interval when the rate in a 2 msec bin exceeds the day's average by 20  $\sigma$ .

Fig. 2 shows an expanded view of the data on the same day, illustrating the correlation of the triggers in individual boxes with lightning and cloud density overhead. Panel A shows the times of the triggers in each detector box. Panel B shows the rate per second of lightning strikes within 5 miles of the detectors, and Panel C shows the distance of all lightning strikes recorded by the USPLN network within 100 miles. Panel D shows the overhead cloud density.

producing at least one lightning flash within 5 miles of the detectors. Such events are classified as Event Candidates (ECs) and are listed in Table 1. Each event trigger time is listed, along with the number of lightning flashes detected within  $\pm 2.5$  minutes and 5 miles and the cloud density above TETRA. Also listed is the time difference to the lightning stroke closest in time to the event trigger, the distance to that lightning stroke, the current, the number of gamma rays detected in the EC, and the  $T_{90}$  duration of the event (i.e., the time over which a burst emits from 5% to 95% of its total measured counts in a single detector box).

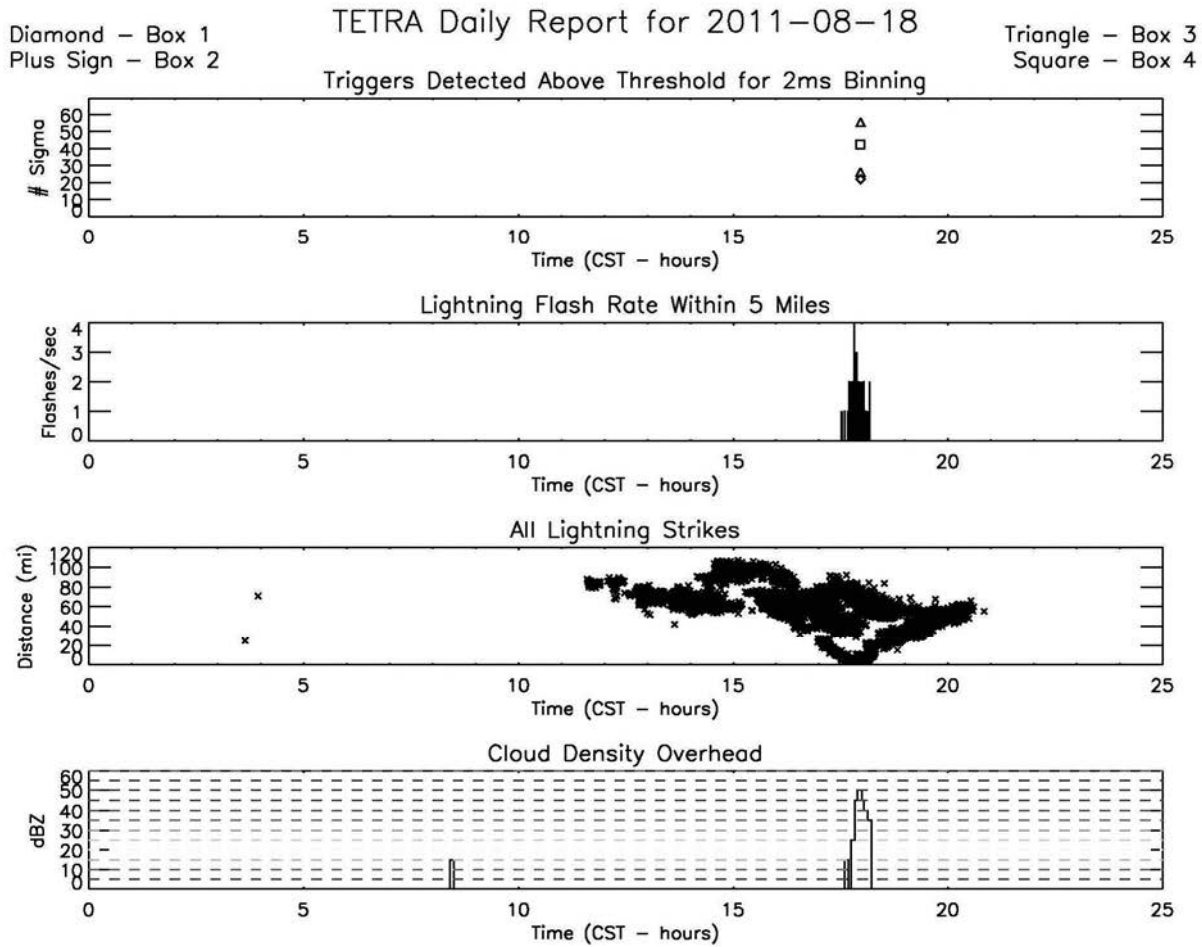


Figure 2. TETRA Report for 8/18/2011 events. Panel A (top): Triggers detected on 8/18/2011 (NaI signals above 50 keV in a single detector box with count rate per 2 msec in excess of 20  $\sigma$  above the 8/18/2011 daily mean counting rate). Box 1 triggers are indicated by plus signs, Box 3 by triangles and Box 4 by squares. Panel B: Rate per second of USPLN lightning strikes within 5 miles. Panel C: Distance to each recorded lightning strike within 100 miles. Panel D: Overhead cloud density.

The number of sigma above the mean is listed in the second to last column for each event. (For the first three events in the table, observed simultaneously in multiple detector boxes, the smallest number of sigma above the mean is listed. These coincident events, labeled Coincident Event Candidates – CECs – are discussed in more detail below.)

TETRA’s events, with an average of  $20 \pm 2$  photons detected, are significantly smaller than the typical events observed in space. For TETRA’s events, the  $T_{90}$  duration was calculated by considering all events detected within a  $\pm 3$  msec window around the trigger time, discarding the

first and last 5% of timestamps for each event, and recording the time difference between the first and last events remaining. The uncertainty in the  $T_{90}$  determination is approximately  $\pm 200$  msec based on Monte Carlo simulations of the data.

In each of the 24 events, 7 to 45  $\gamma$ -rays were detected within a time window of less than 5 msec, with the total energy deposited per event ranging from 2 to 32 MeV. The distances to the nearest lightning flashes were 0.4 - 2.9 miles. For 14 events, absolute timing was available with  $\sim 2$  msec accuracy.

| Date      | Trigger Time (CST) (hh-mm-ss) | Max Lightning Rate/sec within 5 mi. | Cloud Density (dBZ) | # Flashes within 5mi. and 5min. | Trigger-Lightning Difference (ms) | Lightning Distance (mi.) | Lightning Current (kA) | T90 Duration (us) | Total $\gamma$ rays Detected | Total Energy (MeV) | $\sigma$ Above Mean | Prob. of CEC |
|-----------|-------------------------------|-------------------------------------|---------------------|---------------------------------|-----------------------------------|--------------------------|------------------------|-------------------|------------------------------|--------------------|---------------------|--------------|
| 7/31/2011 | 16-21-44.976                  | 2                                   | 45                  | 12                              | -6                                | 1.4                      | -43.6                  | 702               | 22                           | 14.7               | 25.2                | 1.7E-06      |
| 7/31/2011 | 16-21-45.300                  | 2                                   | 45                  | 12                              | -4                                | 1.8                      | -29.1                  | 1326              | 24                           | 11.7               | 25.2                | 1.7E-06      |
| 8/18/2011 | 17-57-38.984                  | 4                                   | 50                  | 40                              | 6743                              | 1.3                      | -23.4                  | 1318              | 40                           | 20.3               | 22.5                | 1.2E-13      |
| 2/24/2011 | 23-11-15.787                  | 3                                   | 45                  | 1                               | -6                                | 2.9                      | -20.9                  | 953               | 20                           | 1.7                | 24.6                | -            |
| 7/29/2011 | 10-38-58.932                  | 6                                   | 45                  | 42                              | 5                                 | 0.4                      | -57.7                  | 153               | 8                            | 4.8                | 23.0                | -            |
| 8/18/2011 | 17-57-39.202                  | 4                                   | 50                  | 40                              | 6525                              | 1.3                      | -23.4                  | 24                | 7                            | 3.6                | 26.1                | -            |
| 3/12/2012 | 11-30-16.500                  | 6                                   | 45                  | 4                               | 5                                 | 1.6                      | -81.3                  | 1997              | 7                            | 3.2                | 21.8                | -            |
| 4/2/2012  | 12-29-30.554                  | 3                                   | 50                  | 8                               | 6                                 | 0.6                      | -29.9                  | 464               | 30                           | 31.6               | 104.3               | -            |
| 4/4/2012  | 02-49-21.900                  | 5                                   | 55                  | 21                              | -3                                | 1.9                      | -158.4                 | 515               | 24                           | 21.3               | 88.6                | -            |
| 8/5/2012  | 14-43-35.661                  | 7                                   | 40                  | 16                              | -849                              | 0.6                      | -56.5                  | 392               | 18                           | 12.4               | 40.6                | -            |
| 8/6/2012  | 19-17-33.359                  | 5                                   | 50                  | 1                               | 1017                              | 0.8                      | -23.1                  | 465               | 13                           | 4.5                | 21.9                | -            |
| 8/9/2012  | 15-27-29.804                  | 4                                   | 50                  | 21                              | 2                                 | 0.4                      | -27.8                  | 2412              | 12                           | 2.9                | 29.0                | -            |
| 8/9/2012  | 15-28-36.070                  | 4                                   | 50                  | 27                              | 80                                | 0.9                      | -36.7                  | 4217              | 24                           | 7.4                | 41.3                | -            |
| 8/9/2012  | 15-28-36.560                  | 4                                   | 50                  | 27                              | 2                                 | 0.8                      | -19.2                  | 146               | 12                           | 8.0                | 33.9                | -            |
| 6/6/2012  | 15-44-18                      | 6                                   | 55                  | 16                              | -                                 | -                        | -                      | 609               | 14                           | 8.5                | 45.7                | -            |
| 6/6/2012  | 15-37-31                      | 6                                   | 55                  | 40                              | -                                 | -                        | -                      | 865               | 45                           | 27.2               | 86.1                | -            |
| 6/6/2012  | 19-23-27                      | 6                                   | 55                  | 40                              | -                                 | -                        | -                      | 2979              | 18                           | 6.7                | 45.7                | -            |
| 6/6/2012  | 19-29-43                      | 6                                   | 55                  | 33                              | -                                 | -                        | -                      | 2376              | 24                           | 9.7                | 55.3                | -            |
| 6/6/2012  | 19-31-21                      | 6                                   | 55                  | 19                              | -                                 | -                        | -                      | 919               | 40                           | 29.8               | 48.3                | -            |
| 6/6/2012  | 19-32-41                      | 6                                   | 55                  | 19                              | -                                 | -                        | -                      | 827               | 9                            | 5.4                | 21.0                | -            |
| 6/6/2012  | 19-36-40                      | 6                                   | 55                  | 18                              | -                                 | -                        | -                      | 2035              | 8                            | 5.2                | 20.1                | -            |
| 6/6/2012  | 19-36-41                      | 6                                   | 55                  | 18                              | -                                 | -                        | -                      | 631               | 32                           | 31.4               | 63.1                | -            |
| 6/9/2012  | 13-40-16                      | 6                                   | 50                  | 1                               | -                                 | -                        | -                      | 1930              | 15                           | 8.6                | 55.1                | -            |
| 7/7/2012  | 17-38-45                      | 5                                   | 45                  | 1                               | -                                 | -                        | -                      | 510               | 14                           | 8.0                | 33.9                | -            |

**Table 1: Properties of the 24 Event Candidates. CECs are listed in the top section; ECs for which the absolute timing uncertainty is known are listed in the middle section; and ECs for which the absolute timing uncertainty is unknown are listed in the bottom section of the table. The date and time of each EC trigger are listed, along with the properties of the storm associated with each event. The properties of the associated lightning, event duration, number of gamma rays detected, total energy and event significance are also listed for each event. The probability of each CEC occurring is listed in the last column for the CECs.**

For each of these 14 events, lightning was observed within 7 seconds of the trigger time. Nine of these events were associated with -CG lightning detected within 6 msec of the trigger. Another 10 ECs were detected during June - July 2012 during a period when accurate trigger-lightning time differences were not recorded due to network timing difficulties. Eight of the ECs during that period were correlated with two intense thunderstorms that passed directly over TETRA on 6/6/2012.

Fig. 3 shows the individual detector hit rate and measured energies for a  $\pm 50$  msec window around the Event Candidate on 4/4/2012. The asterisk marks a lightning flash at a distance of 1.9 miles preceding the trigger by 3 msec. Measured energies ranged from 50 keV to 1.4 MeV with a burst duration ( $T_{90}$ ) of 515  $\mu$ sec.

The accidental rate of triggers coincident within 7 sec of a lightning flash that is less than 5 miles distant (i.e.,

events masquerading as ECs) is calculated based on the rate of TETRA triggers (due mainly to cosmic ray showers), the live time, and the duration of storm activity. The storm activity time is taken to be the sum of all time windows where there was lightning within 5 miles and 7 seconds and there was no electronic noise or other instrumental problems. For a total storm time of 12.65 hrs, we calculate the expected number of ECs due to accidental triggers to be 0.82. This assumes 100% lightning detection efficiency. The efficiency of the USPLN in our area has not been tested, however if we assume a similar sensitivity to that measured by Jacques et al.<sup>39</sup> for cloud-to-ground lightning with peak current in excess of 20 kA of approximately 25% to account for undetected lightning flashes, then we would expect 3.3 accidental ECs compared to the 14 observed.

Box 4 Events/us for 100ms Window Centered on 2012-04-04-02-49-21-901 (31 Events Found).  
Closest lightning strike was -4 ms and 1.9086 miles away with peak current of -158.4 kA.

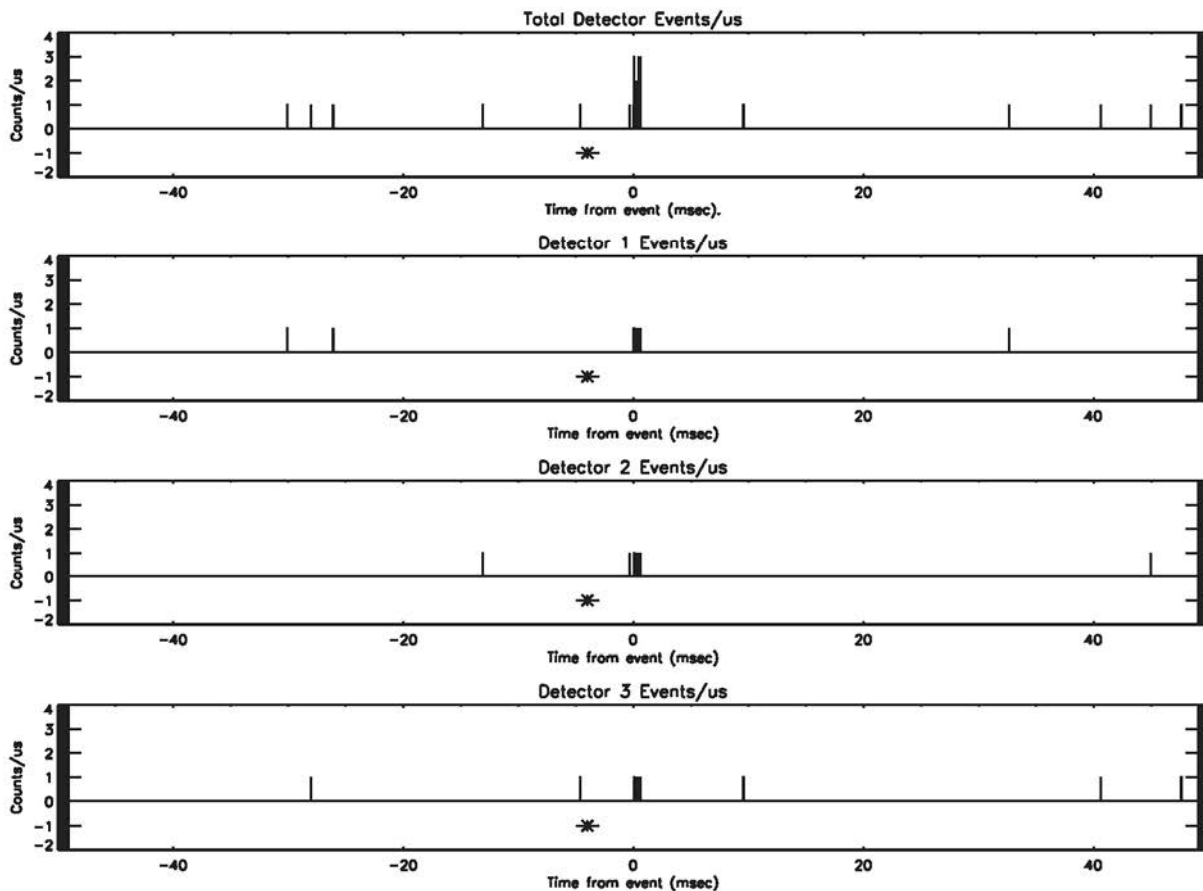


Figure 3a. Events/μsec measured over a 100 msec window centred on the Event Candidate on 4/4/2012. Top panel shows the count rate for the entire box, followed by the count rates for the individual NaI detectors.

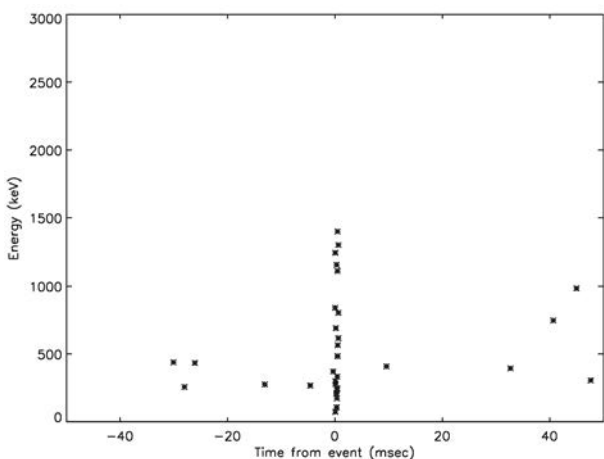


Figure 3b. Distribution of measured energies for the sum of the three detectors.

In three of the 24 ECs, triggers were recorded in two or more boxes separated by ~1000 m within less than ±2 msec. This is approximately the relative timing accuracy between separate boxes. All three of these Coincident Event Candidates (CECs) occurred in July and August of 2011, when storms in southern Louisiana tend to be associated with disturbances in the Gulf of Mexico rather than frontal lines. No CECs were detected when there was no lightning activity within 5 miles. If all discharges produce TGFs<sup>26</sup>,

then the rate of detection and the CEC distances point to either a range of intensities extending below the sensitivity limit of TETRA, strongly non-isotropic emission, or the possibility that the gamma ray emission is only indirectly associated with the lightning<sup>20</sup>. This can also occur if some gamma ray events are produced by intracloud (IC) strikes, since the USPLN data record primarily cloud-to-ground strikes.

The expected number of CECs due to random triggers is small: Given an initial EC with counting rate in one box in excess of 20 σ above the daily average, the likelihood that a second or third trigger occurred at random in another box within the timing uncertainty of 2 msec on the same day is estimated as  $(4 \text{ msec} \times N/86400 \text{ sec})^{b-1}$ , where N is the total number of random 20 σ triggers detected per day through February 2013 and b is the number of boxes triggered in the event. (For simplicity, we neglect here the increase in trigger rate during a thunderstorm shown in Fig. 1.) Multiplying by the number of ECs then gives the expected number of spurious CECs involving two boxes occurring by chance as  $1.7 \times 10^{-6}$ , as listed in Table 1.

### 3. BALLOON-BORNE DETECTOR (LAGO)

**1. Detector Description:** LAGO (Lightning-Associated Gamma ray Observer) consists of a balloon-

borne array of four 2.5 cm x 2.5 cm x 10 cm bismuth germanate (BGO) crystal scintillators designed to detect 300 keV – 20 MeV gamma rays due to nearby lightning at balloon altitudes (30-35 km). The BGO scintillators, originally used in the calorimeter for the ATIC cosmic ray experiment<sup>40</sup>, are arranged in a 2 x 2 array with one 3" (76 mm) diameter Lucite light-guide coupled to each end of the array. The light at each end is viewed by a 10-stage Electron Tubes 9305KFLA 78 mm photomultiplier tube (PMT) with a standard bi-alkali photocathode. The detector assembly is wrapped in white PVC and ~ 1" thick plastic foam insulation to prevent rapid temperature changes. The anode signal is used for the range 300 keV – 3 MeV and the 8th dynode for signals up to 20 MeV. LAGO uses the same electronics and readout as TETRA, except that a solid state hard drive is used for data recording during flight. Power to the payload and balloon-craft is supplied by two 30V battery packs mounted on the outside of the payload frame above the detector viewing angle. Temperatures of the BGO, PMTs, and electronics boards are monitored during flight and the payload's internal clock is synchronized during preflight procedures. The ADC-to-energy conversion is calibrated with radioactive sources (<sup>22</sup>Na, <sup>137</sup>Cs, <sup>60</sup>Co, <sup>232</sup>Th). Individual detector energy resolutions at 662 keV are 26.4% and 32.3% FWHM. Electronics boards are attached to the payload frame above the detector and the detector is mounted below the payload frame with an unobstructed view of gamma rays coming up from storms below the payload. In order that the payload can be launched within only a few hours of the approach of a promising storm, a strict limit is placed on the payload weight: LAGO is restricted to an instrument weight of 50 lbs. (23 kg).

**2. Results:** Payload integration and testing for the first LAGO campaign occurred in February 2012 at NASA's Columbia Scientific Balloon Facility in Palestine, TX. The standard CSBF equipment was integrated with the LAGO payload; the integrated payload was thermal vacuum tested; and the electrical and mechanical checkouts were completed. Once the payload was attached to the parachute, the weight of the full package was 80 lbs (36 kg).

An initial test flight of LAGO was conducted in September 2012 aboard the High Altitude Student Payload (HASP)<sup>41</sup>. The HASP/LAGO balloon payload was launched from Fort Sumner, NM and accumulated more than 8 hours above 110,000 ft (30 km). Measured count rates are plotted vs. the payload altitude in Fig. 4. The vertical line on the left and the initial dip in the low energy background rate indicates launch. The rate then increases on both high and low energy channels as the balloon payload passes the Pfozter maximum (~60,000 ft, 18 km) and decreases as the payload approaches float altitude above 110,000 ft (30 km).

Data were accumulated for the entire flight and transmitted via the internet to LSU for post-flight analysis. The analysis software selected events with signals corresponding to at least 200 keV deposited energy per channel within 1  $\mu$ sec. Anode signals above this energy seen on only one PMT are discarded as noise. The data were then binned into 2 msec bins and assigned a timestamp in the center of the bin. The significance of each

2 msec bin is calculated as the number of standard deviations above the average rate at float.

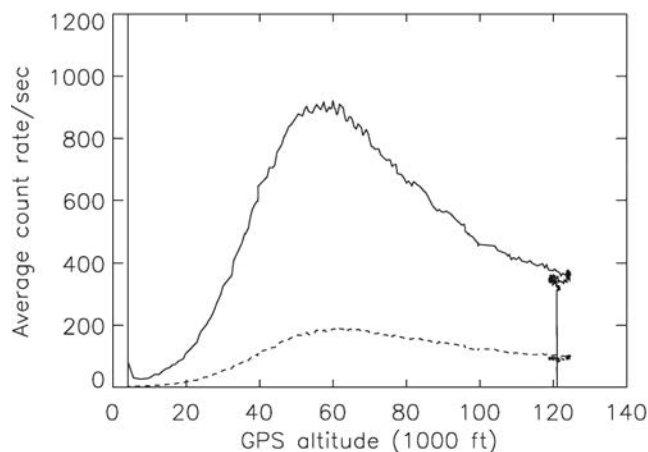


*Figure 4. Average count rate during 2012 flight. The solid line indicates the low energy count rate. The dashed line indicates the high energy count rate. The launch time is indicated by the vertical line on the left hand side of the plot.*

During the flight, the US Precision Lightning Network (USPLN) Unidata Program recorded 128 lightning strikes within a 50 mile radius of the payload. Of these lightning strikes, there was one IC strike of undetermined polarity 45 miles away from the payload. All the remaining strikes recorded within a 50 mile radius of the payload path were negative polarity CG lightning discharges. No 2 msec bins were detected at flight altitude at a level significantly higher than the background.

A second flight was attempted as part of the Fall 2013 CSBF Ft. Sumner campaign, this time with LAGO as an independent payload. The goal was to wait for a strong thunderstorm to approach closely to the launch site, and then to launch shortly before the arrival of the storm. No satisfactory storms appeared, and LAGO was not launched. The instrument has been returned to CSBF at Palestine, TX and is currently ready to be launched in the event of a promising flight opportunity.

#### 4. CONCLUSIONS

The gamma ray events observed at ground level by TETRA have durations ranging from 24  $\mu$ sec to 4.2 msec. The similarity of these event durations observed by TETRA to those reported by previous experiments suggests that the TETRA events are also generated by the RREA mechanism. Dwyer et al<sup>32</sup> compared the spectrum of x-rays from lightning to gamma rays from TGFs, showing a marked difference above 2 MeV, but the restricted energy range of TETRA and the low statistics make it impossible to draw strong conclusions from the observed TETRA spectra.

In contrast to the satellite observations, the two TGFs previously reported from the ground by ICLRT are associated with -CG lightning<sup>31,32</sup>. The 2009 ICLRT event produced  $\sim 10^{11}$  runaway electrons and was observed at a distance of  $\sim 2$  km. If the TETRA events are characterized by typical energy 500 keV and distance 1 mile, then atmospheric absorption attenuates the flux by a factor of  $\sim 4 \times 10^{-8}$  at sea level. Assuming isotropic emission at a

distance of 1 mile, a typical total of 20 photons observed in an event by TETRA then requires in excess of  $\sim 10^{18}$  photons at the source. Either the ground level TETRA events are beamed, or they are distinctly different from the ICLRT events.

We have presented data for a series of gamma ray events observed with a self-triggered ground array, suitable for observing weak events from nearby distances without a bias caused by a lightning trigger, and find that events with durations  $< 5$  msec and detected individual photon energies up to at least 2 MeV appear to be produced in conjunction with nearby -CG lightning. In two CECs, these are most closely associated with -CG events 1.4 and 1.8 miles away. In the other CEC event, the nearest detected lightning strike in time is more than 6 seconds after the gamma ray event. Either this gamma ray event is not correlated with nearby lightning, the associated CG lightning strike was missed by the lightning network, or the event was due to IC lightning that was not detected by the lightning network.

We have also described the LAGO payload designed to observe TGFs from nearby thunderstorms at balloon altitude. A successful engineering flight was conducted in September of 2012. The closest possibly positive polarity lightning was an IC flash at a distance of 45 miles. No significant gamma ray events were detected in the BGO above background. We note that, if TGFs are produced at a typical altitude of 15 km and a balloon flies at 30 km, then in order to be within an expected beaming angle of  $30^\circ$ , the instrument must be within approximately 5 miles of the thunderstorm. A light-weight, easily launched payload will be required for such a flight. LAGO is designed to satisfy this requirement, and is currently waiting for a suitable launch opportunity.

## 5. ACKNOWLEDGEMENTS

The lightning data were provided by the US Precision Lightning Network (USPLN) Unidata Program. Radar data were downloaded from <http://www.wunderground.com>. The authors would like to thank J. Isbert, B. Ellison, D. Smith and N. Cannady for their assistance with the project, and especially J. Fishman for valuable discussions. This project has been supported in part by NASA/Louisiana Board of Regents Cooperative Agreement NNX07AT62A and the Curry Foundation. R. Ringuette appreciates graduate fellowship support from the Louisiana Board of Regents.

## 6. REFERENCES

- [1] Fishman GJ, Bhat PN, Mallozzi R, Horack JM, et al. *Science*, 1994; 264: 5163, pp. 1313-1316.
- [2] Gjesteland T, Ostgaard N, Collier AB, Carlson BE, et al. *Geophys. Res. Lett.*, 2012; 39: L05102.
- [3] Smith DM, Lopez LI, Lin RP, Barrington-Leigh CP. *Science*, 2005; 307: 10.1126/science.1107466.
- [4] Grefenstette BW, Smith DM, Hazelton BJ, Lopez LI. *J. Geophys. Res.*, 2009; 114: A02314.
- [5] Marisaldi M, Argan A, Trois A, Guiliani A, et al. *Phys. Rev. Lett.*, 2010; 105: 128501.
- [6] Marisaldi M, Fuschino F, Labanti C, Bulgarelli A, et al. *Nuovo Cimento*, 2011; C034N3: 279-284.
- [7] Tavani M, Marisaldi M, Labanti C, Fuschino F, et al. *Phys. Rev. Lett.*, 2011; 106: 018501.
- [8] Cohen MB, Inan US, Said RK, Briggs MS, et al. *Geophys. Res. Lett.*, 2010; 37: L18806.
- [9] Fishman GJ, Briggs MS, Connaughton V, Bhat PN, et al. *J. Geophys. Res.*, 2011; 116: A07304.
- [10] Briggs MS, Xiong S, Connaughton V, Tierney D, et al. *J. Geophys. Res. Space Physics*, 2013; 118: doi: 10.1002/jgra.50205.
- [11] Grove JE, Checktman A, Briggs M, Connaughton V, et al. *The 2012 Fermi Symposium, Fermi Gamma-Ray Telescope, Monterey, CA, 2012*; (<http://fermi.gsfc.nasa.gov/science/mtgs/symposia/2012/program/c2/EGrove.pdf>).
- [12] A. Chilingarian et al., *J. Advanced Scientific Research*, 2014, to be published (Proc. TEPA 2013).
- [13] Cohen MB, Inan US, Fishman G. *J. Geophys. Res.*, 2006; 111: D24109.
- [14] Fuschino F, Marisaldi M, Labanti C, Barbiellini G, et al. *Geophys. Res. Lett.*, 2011; 38: L14806.
- [15] Inan US, Cohen MB, Said RK, Said DM, Lopez LI. *Geophys. Res. Lett.*, 2006; 33: L18802.
- [16] Stanley MA, Shao X-M, Smith DM, Lopez LI, et al. *Geophys. Res. Lett.*, 2006; 33: L06803.
- [17] Hazelton BJ, Grefenstette BW, Smith DM, Dwyer JR, et al. *Geophys. Res. Lett.*, 2009; 36: L01108.
- [18] Dwyer JR. *Geophys. Res. Lett.*, 2003; 30: 20, 2055.
- [19] Rodger CJ, Brundell JB, Holzworth RH, Lay EH. *Am. Inst. Phys. Conf. Proc.*, Coupling of thunderstorms and lightning discharges to near-Earth space: Proceedings of the Workshop, 2009; 1118: 15-20.
- [20] Connaughton V, Briggs MS, Xiong S, Dwyer JR, et al. *J. Geophys. Res.*, 2013; 118, 2313-2320.
- [21] Smith DM, Hazelton BJ, Grefenstette BW, Dwyer JR, et al. *J. Geophys. Res.*, 2010; 115: A00E49, [10.1029/2009JA014853](https://doi.org/10.1029/2009JA014853).
- [22] Grefenstette BW, Smith DM, Dwyer JR, Fishman GJ. *Geophys. Res. Lett.*, 2008; 35: L06802.
- [23] Østgaard N, Gjesteland T, Stadsnes J, Connell PH, et al. *J. Geophys. Res.*, 2008; 113, A02307.
- [24] Gjesteland T, Ostgaard N, Collier AB, Carlson BE, et al. *J. Geophys. Res.*, 2011; 116: A11313.
- [25] Smith DM, Dwyer JR, Hazelton BJ, Grefenstette BW, et al. *J. Geophys. Res.*, 2011; 116: D20124.
- [26] Østgaard NT, Gjesteland T, Hansen RS, Collier AB, et al. *J. Geophys. Res.*, 2012; 117: A03327, doi:10.1029/2011JA017365.
- [27] Dwyer JR. *J. Geophys. Res.*, 2012; 117: A02308.
- [28] Dwyer JR, Smith DM, Uman MA, Saleh Z, et al. *J. Geophys. Res.*, 2010; 115: D09206.
- [29] Cummer SA, Lu G, Briggs MS, Connaughton V, et al. *Geophys. Res. Lett.*, 2011; 38: L14810.
- [30] Lu G, Cummer SA, Li J, Han F, et al. *J. Geophys. Res.*, 2011; 116: A03316.

- [31] Dwyer JR, Rassoul HK, Al-Dayeh M, Caraway L, et al. *Geophys. Res. Lett.*, 2004; 31: L05119.
- [32] Dwyer JR, Schaal MM, Cramer E, Arabshahi S, et al. *J. Geophys. Res.*, 2012; 117: A10303.
- [33] Chilingarian A, Daryan A, Arakelyan K, Hovhannisyanyan A, et al. *Phys Rev D*, 2010; 82: 043009.
- [34] Chilingarian A, Hovsepyan G, Hovhannisyanyan A. *Phys Rev D*, 2011; 83: 062001.
- [35] Moore CB, Eack KB, Aulich GD, Rison W. *Geophys. Res. Lett.*, 2001; 28: 11, 2141.
- [36] Tsuchiya H, Enoto T, Yamada S, Yuasa T, et al. *J. Geophys. Res.*, 2011; 116: D09113.
- [37] Tsuchiya H, Enoto T, Iwata K, Yamada S, et al. *Phys. Rev. Lett.*, 2013; 111: 015001.
- [38] Ringuette R, Case GL, Cherry ML, Granger G, et al. *J. Geophys. Res.*, 2013; 118: doi:10.1002/2013JA019112.
- [39] Jacques AA, Koerner JP, Boucher TR. Proc. 91st American Meteorological Society Annual Meeting, 2011; <https://ams.confex.com/ams/91Annual/webprogram/Paper185527.html>.
- [40] Guzik, T.G. et al. *Adv. Space Res.*, 2004; 33: 1763.
- [41] Guzik TG, Besse S, Calongne A, Dominique A, et al. *Adv. Space Res.*, 2008; DOI: 10.1016/j.asr.2007.04.068

## Low energy threshold (0.1-2MeV) detector for registration of the Thunderstorm ground enhancements

A.Chilingarian, E. Mnatsakanyan, K. Avakyan, A. Reymers, L. Vanyan, T. Karapetyan

Yerevan Physics Institute

**Abstract.** For registration of  $\gamma$ -photons related to high-energy atmospheric phenomena in the low energy range (0,1 - 2 MeV) we have developed a new detector on the base of CsJ(Tl) crystals. Detectors have been installed on Nor – Amberd -2000m a.s.l. and Aragats -3200m a.s.l. research stations of Yerevan Physics Institute. Each detector consists of one CsJ(Tl) crystal (9 x 9 x 15 cm<sup>3</sup> size) covered with magnesium oxide on four sides. Exposed to atmospheric radiation upper side of detector is covered by 150 $\mu$ m beryllium window and 30  $\mu$ m aluminum foil. Detailed description and main properties of the detector, as well as first measurements of the long lasting Thunderstorm ground enhancement are presented in this report.

### 1. CSI(TL) DETECTOR DESIGN

The network of detectors located at Aragats Space Environment center (ASEC, Chilingarian et al., 2003) in Armenia is based on the assemblies of plastic and NaI(Tl) (thallium-doped sodium iodide) scintillators overviewed by photomultipliers (PMT). The front-end and Data acquisition (DAQ) electronics provides registration of  $\gamma$ -photons with energies greater than 1.5 MeV.

For the detailed investigation of Thunderstorm ground enhancement (TGE) phenomena it is very important to lower the energy range of detected  $\gamma$ -photons down to tens of keV. For this purpose we choose the single crystal of CsI(Tl) (thallium-doped cesium iodide), which has a high efficiency of  $\gamma$  ray detection and is less hygroscopic than NaI(Tl). Therefore, it is easily assembled into in laboratory conditions. Comparisons of CsI(Tl) and NaI(Tl) are given in Table 1..

Table 1. Properties of CsI(Tl) and NaI(Tl) crystals

|                             | CsI(Tl) | NaI(Tl) |
|-----------------------------|---------|---------|
| Photons/meV                 | 60,000  | 40,000  |
| Density(g/cm <sup>3</sup> ) | 4.53    | 3.67    |
| Decay Time(ns)              | 1050    | 230     |
| Peak emission (nm)          | 550     | 415     |
| Hygroscopic property        | modest  | strong  |

For registration of low-energy gamma-photons, the window's material of detector should be as thin as possible. On the other hand it must withstand the severe environment conditions on mountain altitudes, as the detector works outdoors.

The construction of the detector is presented in Fig.1. The detector consists of following parts

1. Platform;
2. Crystal housing box;
3. PMTs and electronics housing box.

Both boxes are removable and are attached with the platform by waterproof and light-tight gaskets. Two PMT (FEU-110 type) are directly attached to the bottom surfaces of the CsI(Tl) crystal. Dimensions of the crystal are 9x9x15cm<sup>3</sup>. As we can see in Fig.1 the upper side of crystal is covered with Beryllium plate of 150  $\mu$ m thickness and aluminum foil-10  $\mu$ m thickness (the window size - 9x15cm<sup>2</sup>).

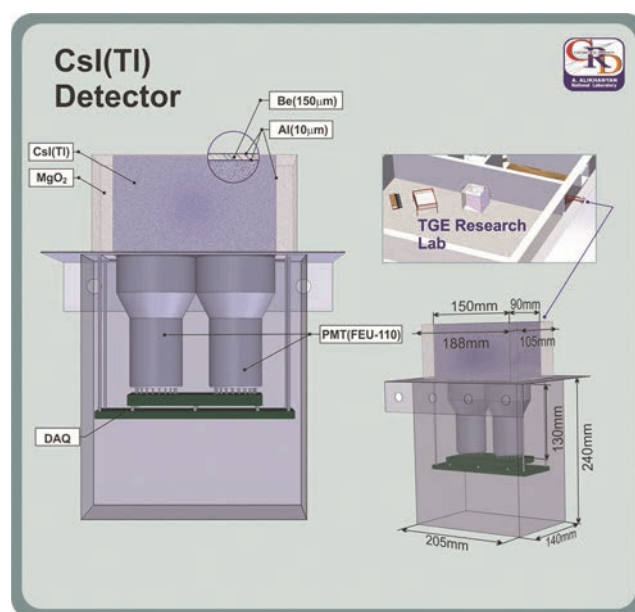


Figure 1. The construction of CsI(Tl) detector.

The total amount of window thickness is 36mg/cm<sup>2</sup>, that provides ~98% transparency for gamma-photons with energy greater than 50 keV. In order to shield the detector from natural low-energy environmental radiation lead slabs surround four sides of crystal box with 14 mm thickness. Signals from PMTs are sent to the DAQ system consisting of two channel amplifiers, discriminators, shapers and block of coincidence. Coincidence signal from 2 PMTs opens the gate, which transmits PMT signals to the logarithmic amplitude analyzer (LADC).

Table 2. The Physical Properties of the Detector

|                        |                           |
|------------------------|---------------------------|
| Effective Area         | 9x14,5=130cm <sup>2</sup> |
| Geometrical Acceptance | 400 cm <sup>2</sup> *sr   |
| Energy threshold       | 0,03 MeV                  |

Low threshold detector has two outputs for detection of 1-minute and 1 sec time series. 1-sec time series allows registration of very short TGEs with duration less than 1 minute, which escape from analyses if only 1-minute time-series are observed.

Energy calibration of detector was carried out using gamma-ray line of radionuclide source  $^{137}\text{Cs}$  (662 keV). The efficiency of detection gamma ray from radioactive source was estimated to be  $\sim 80\%$ .

For estimation of electron contamination in the TGE is used proportional counter (PC) (5 x 6 x 35 cm<sup>3</sup> size filled with 90% Ar+10% C<sub>4</sub>H<sub>4</sub>) with beryllium window (150 $\mu\text{m}$  thickness). The PC has low detection efficiency  $\sim 2\%$  for gamma ray detection, while for detection of electrons efficiency is more than 90%. 2 detectors were installed in Nor Amberd and Aragats in September 2013 and already register very interesting events.

## 2. PROLONGED THUNDERSTORM GROUND ENHANCEMENTS

The enhancements of the Secondary cosmic ray (SCR) flux observed during thunderstorms, so-called Thunderstorm ground enhancements (TGEs) are one of several types of modulation phenomenon along with solar modulation and atmospheric pressure and temperature modulations. The origin of SCR is large and small particle showers originated by interactions of protons and fully striped nuclei of the primary cosmic rays accelerated in our galaxy. Atmospheric meteorological conditions (pressure, temperature) can significantly change (modulate) MeV SCR intensity. Solar flares via sending abundant energy protons with energies up to 30 GeV (Chilingarian, 2009) also modulate SCR flux. Strong electrical fields in thundercloud represent a powerful modulation agent enhancing SCR flux on earth's surface 10 and more times, see details and references to original works in (Chilingarian, Hovsepyan and Kozliner, 2013). Electrification of the thundercloud give rise to a number of complicated physical processes including: Relativistic runaway electron avalanches (RREA), Modification of the secondary cosmic ray (electrons, muons, protons and charged mesons) energy spectra (MOS); Photonuclear reactions of gamma rays; Attenuation of the cosmic ray muon flux; Roentgen and gamma radiation from the lightning; Prolonged (2–3 hours and more) enhancement of the low-energy (0.1–2 MeV) SCR flux To study the last phenomenon the low energy particle detectors described in the previous section were designed and installed on research stations located on slopes of Mt. Aragats in Armenia.

We are aware of only very few reports on long-lasting enhancement of SCR related to thunderstorms/precipitations. Scintillation detectors (NaI(Tl) crystal the size of  $\varnothing 63$  20 mm with two outputs channels:  $> 20$  keV and  $> 100$  keV) located on high latitude CR research stations in Apatity and Barentsburg registered numerous gamma ray intensity enhancements of 5 - 50 % amplitude with duration from 2-3 hours to a day or more. The vast majority of these events are accompanied by solid or liquid precipitation. Authors of (Germanenko et al., 2011) climate that increases are not connected with the presence of radioactivity in precipitation, or an additional release of radon from the soil. It is also interesting to note that they report delayed correlation (particle flux maximum delayed 20-30 minutes relative to precipitation rate maximum). Thus, this group also confirms necessity of development of

the Lower positive charged region (LPCR, Chilingarian, 2014) for operation of lower dipole accelerating electrons in direction of earth.

The TGF and Energetic Thunderstorm Rooftop Array (TETRA) in Louisiana consists of an array of twelve 19 cm x 19 cm x 5 mm NaI(Tl) scintillators designed to detect the gamma ray in the energy range 50 keV - 2 MeV (Ringuette et al., 2013). Observed increases of the detector count rate are clearly correlated with rainstorms. The gamma ray spectrum, measured during a rain event with the high resolution LaBr<sub>3</sub>:Ce detector mounted together with the NaI detectors in one of the detector boxes, shows a clear indication of 295, 352, 609, 1120, and 1764 keV Bi<sub>214</sub> and Pb<sub>214</sub> lines characteristic of radon decay.

## 3. LONG-TERM TGE REGISTERED ON ARAGATS AT 19 OCTOBER 2013

Early morning 19 October (2:00 UT, corresponding to 6:00 local time) the clouds above Aragats station on altitude 3200 m start to fell and at 2:30 sit on the earth's surface till 6:00. During whole time of TGE visibility was strictly diminished down to 20-30 meters. Simultaneously rose count rate of particle detectors with low threshold (below 1.5 MeV), see Figure 2. During TGE lasting 4 hours from 2:00 till 6:00 2 distinct peaks were detected at 2:53 and 3:48. Maximal enhancement was detected by CsI spectrometer (13%), STAND1 plastic stacked scintillators (upper and middle layers) detect 9 and 8% enhancement and Geiger counter -  $\sim 6\%$  enhancement (corresponding reliability measured in numbers of standard deviations (number of  $\sigma$ , z-score) are (16, 23, 22 and 14  $\sigma$ ). The mean values and variances of 1-minute count rates were calculated by time series registered at 20:00 – 24:00 at previous day 18 October, see Fig. 3. Count rates of both NaI(Tl) and 3 cm thick plastic scintillator do not demonstrate any enhancement; therefore, we can conclude that energy of particles (electrons and gamma rays) comprising the TGE was below 4 MeV (the threshold energy of mentioned above detectors).

All 3 particle detectors measuring sizable long-term TGE, i.e. CsI spectrometer, Geiger counter, 1-cm thick scintillator provide electronic signals to 3 different data acquisition (DAQ) systems controlled by 3 separate on-line computers. Furthermore, particle detectors using the same DAQ as 3 detectors which have measured TGE (CsI, Geiger, first and second layers of STAND1), namely NaI, SEVAN and 3-cm thick scintillator do not demonstrate any signs of TGE. Therefore, we conclude that maximal energy of TGE was below 4 MeV, which is strictly different from "middle-term" TGEs ( $\sim 10$  minute elongation), which energy spectra prolongs up to 100 MeV (see energy spectra measured by NaI spectrometers in Chilingarian, Hovsepyan and Kozliner, 2013). The scatter plot of 2 detectors located on the distance of  $\sim 100$  m (see Fig. 4) demonstrates rather large correlation of the counts during 4 hours of TGE.

Further analysis of meteorological conditions during TGE proves that the model described in (Chilingarian, 2014) is applicable also for the long duration TGEs.

In Fig. 5 we can see that relative humidity rose from 70% at 1:00 till 86% at 2:00 when TGE started and reach 96% at TGE maximum. With humidity reaching 90% the near surface electric field disturbed and changed between -10 kV/m and 5 kV/m mostly in negative domain, see Fig. 5. High levels of humidity support creation of hydrometeors and their electrification.

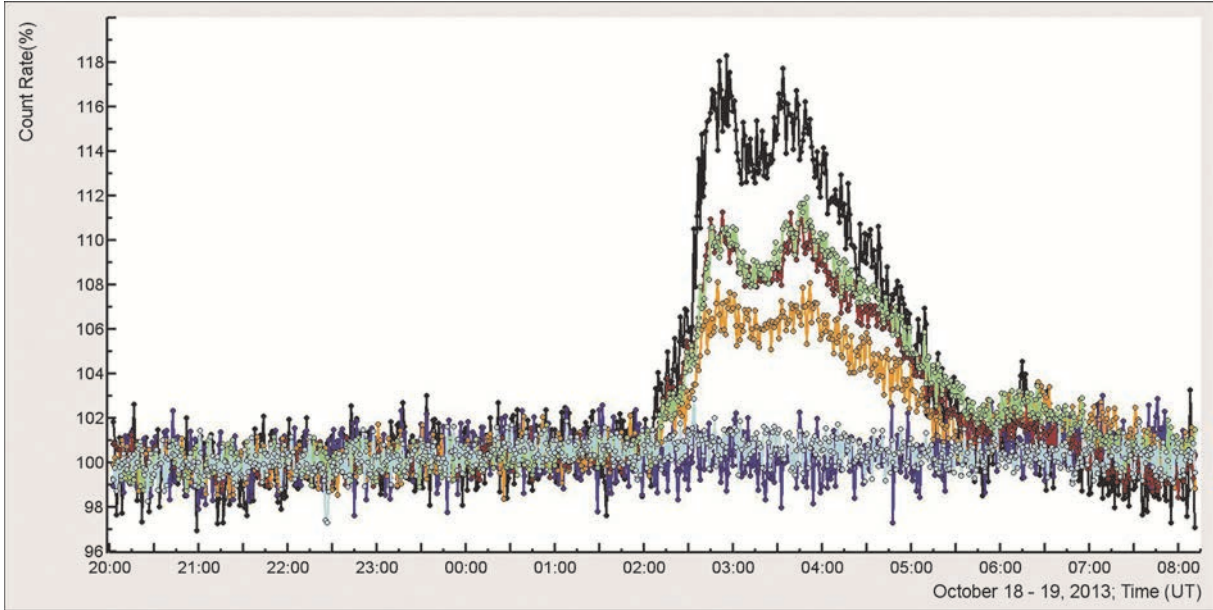


Figure 2. Relative enhancements of the count rates of particle detectors. From top to down: CsI spectrometer, 1cm thick top and middle scintillators of STAND, Geiger, 3 sm thick scintillator and sum of 4 NaI spectrometers.

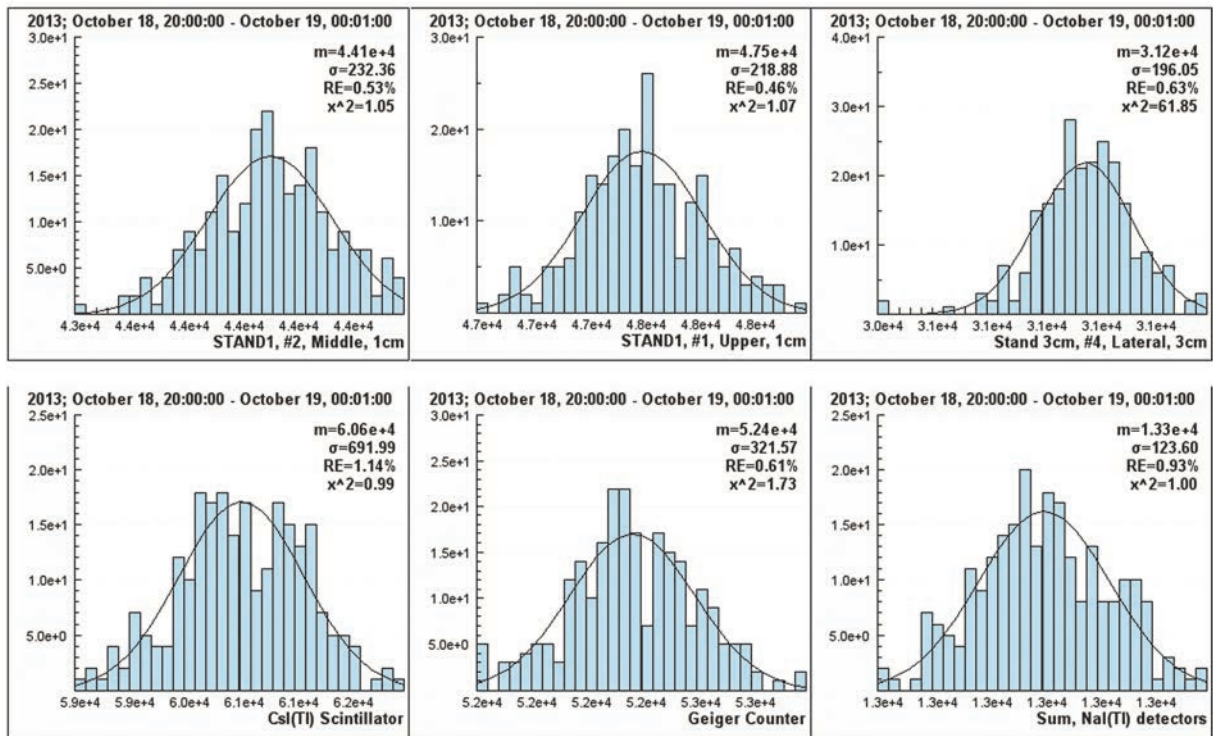


Figure 3. Mean values, variances, relative errors and goodness of Gaussian fit of histograms of time series measured at 20:00 - 24:00 18 October 2013.

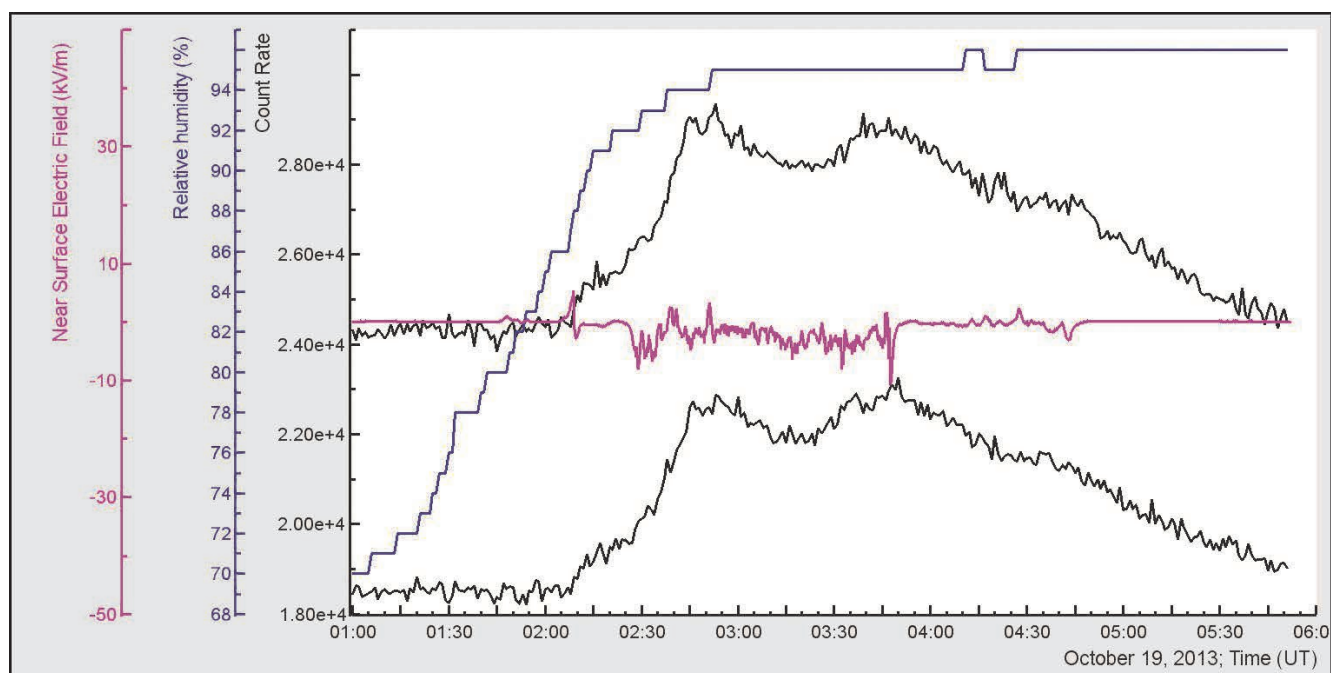
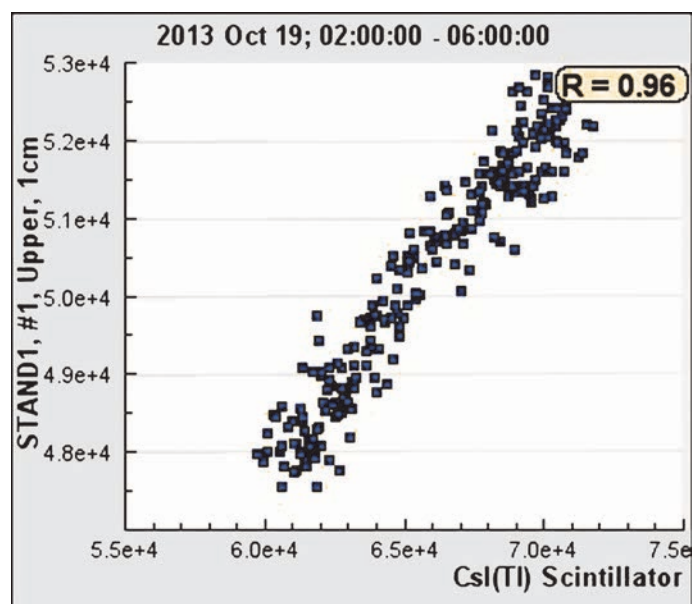


Figure 5. From top to down: relative humidity, count rate of 100 combination of STAND1 detector, disturbances of electric field, count rate of 010 combination of STAND1 detector measured during long-term TGE 02:00 – 06:00 19 October 2013

Table 3. Recovered intensity of electron and gamma ray flux above STAND1 detector

| Time<br>19.10.2013 | Peak 100/010    | Mean 100/010    | Diff/Signal   | electron<br>flux/m <sup>2</sup> min | γ flux/m <sup>2</sup> min |
|--------------------|-----------------|-----------------|---------------|-------------------------------------|---------------------------|
| 2:53               | 29175/<br>22388 | 24300/<br>18400 | 4900/<br>4000 | 2270                                | 132576                    |
| 3:48               | 28828/<br>23032 | 24300/<br>18400 | 4500/<br>4600 | 1457                                | 152847                    |

Emerged Lower positive charged region (LPCR) with located above main negative layer formed a lower dipole accelerated electrons downward. Electrons with additional energy acquired from electric field radiate additional gamma rays, which enhance SCR flux and consequently particle detector count rate. We depict in Fig. 5 time series of combinations 100 and 010 of STAND1 detector. The

count rates of these 2 combinations allow estimating fraction of electrons and gamma rays in TGE. (Chilingarian, Hovsepyan and Kozliner, 2013, equations 1 and 2) Recover gamma ray and electron fluxes incident on detector, are depicted in Tab. 3. In the second column of Tab. 3 we put the peak values of count rate as measured by 100/010 coincidences of STAND1 detector (signals only in

upper scintillator; signal only in middle scintillator). In the third column we depict mean (background) 1-minute count rates of the same coincidences measured on large statistics before the TGE. In the fourth column we put the estimate of the “signal” - difference between the peak count rates and background values. And in the 5 and 6 columns we depict the recovered fluxes of electrons and gamma rays.

As we can see from Tab. 3 the vast majority of the particles at 2:53 and 3:48 were gamma rays (electron fraction was 1.7 and 0.9% correspondingly). These estimates are related to near threshold energy of STAND1 detector  $\sim 1.5$  MeV. After calculating electron and gamma ray fluxes with STAND1 detector and proving that majority of particles in TGE are gamma rays we can estimate gamma ray flux also by other detectors including CsI spectrometer having the lowest energy threshold, see Tab. 4.

**Table 2. TGE gamma ray flux intensity as measured at 3:48 by 3 detectors with low energy threshold**

| Detector | Signal | Area [m <sup>2</sup> ] | Efficiency[%] | $\gamma$ flux/m <sup>2</sup> min |
|----------|--------|------------------------|---------------|----------------------------------|
| STAND1*  | -      | 1                      | -             | 152847                           |
| Geiger   | 4410   | 0.4                    | 3             | 367500                           |
| CsI      | 9400   | 0.013                  | 60            | 1205128                          |

\*Intensity measured by STAND1 detector was recovered by solving system of linear equations described above.

In Fig. 6 we depict the background gamma ray spectra as measured by new low-threshold spectrometers on altitudes 2000 and 3200 m a.s.l. Space-born observations of the low-energy gamma rays provide a unique window on nuclear de-excitation produced by nucleosynthesis in supernovae, radiation from black hole accretion disks, etc...; several missions are under preparation for a future all-sky survey with a high sensitivity (Tanaka et al., 2011). However, observation of this low-energy gamma rays is difficult because of a large backgrounds of photons produced in the hadronic process of galactic cosmic rays in the atmosphere and satellite itself. Therefore, upward gamma ray flux from atmospheric processes should be carefully estimated and measured. Gamma ray spectra measured on mountain altitudes can be used for the calibration of models of gamma ray fluxes produced in atmosphere and directed into the open space.

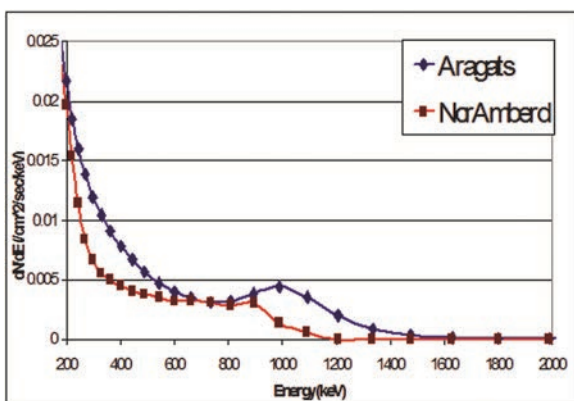


**Figure 6. Gamma ray differential energy spectra as measured by CsI spectrometer in Nor-Amberd (2000 m) and Aragats 3200 m**

The energy spectra of SCR gamma rays fast attenuated after 2 MeV. Gamma ray spectrum measured on Aragats have pronounced enhancement around 1 MeV. In Nor Amberd this enhancement is much weaker and is shifted to the left at 0.9 MeV.

The TGE differential energy spectra measured at 2 maximal flux minutes (see Fig. 7) comparing with background spectra have much more pronounced features between 0.5 and 1.5 MeV. Further analysis needed to clarify origin of these peaks.

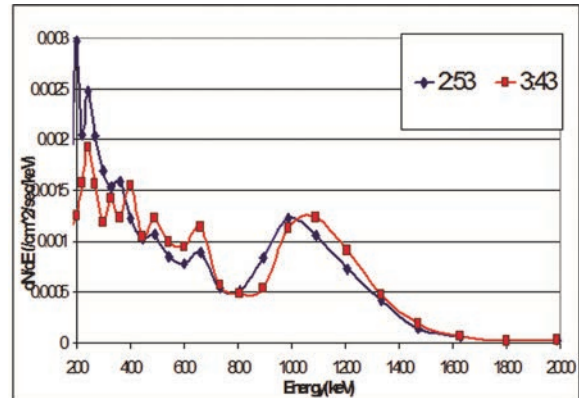


**Figure 7. The gamma ray differential energy spectra of long duration TGE event: 2 minutes of maximal flux. the spectra are obtained by subtracting of 1-minute spectra at maximal flux at 2:53 and 3:43 by the mean “background” gamma ray spectrum measured during 5 hours before the TGE event (see Fig. 6).**

#### 4. CONCLUSION AND FURTHER EFFORTS

The new detector on the base of CsI(Tl) crystals is excellent addition to the ASEC network of detectors, which allows to expand energy range of the registration of the gamma-photons to low energies (down to 0.1 meV).

First results of new spectrometer operation confirm the existence of long lasting TGEs comprising of low energy gamma rays confirming results of Apatity and TETRA groups. However, we yet cannot confirm the origin of gamma ray emission. Is it only due to gamma emission of the electrons accelerated in the lower dipole in the thundercloud or it is due to radiation of Radon “daughters” brought by thundercloud. Additional analysis of the fine structure of TGE energy spectra (Fig. 7) is required for confirming and identification of peaks seen in Fig. 7.

In future two low threshold spectrometers planned to be installed in Yerevan CRD headquarters and in new geophysics parameters monitoring site on Sevan lake.

#### 5. ACKNOWLEDGMENTS

We are grateful to A.Hovhannisyanyan, S. Parsamyan, Y. Khanikyanyan and

Aragats and Nor Amberd research stations staff for helping in installation of CsI spectrometers.

## 6. REFERENCES

- [1] A.Chilingaryan, K.Avakyan, V.Babayan et al., Aragats space-environmental centre: status and SEP forecasting possibilities, *J. P Hys. G: Nucl. Part. Phys.* 29 (2003) 939–951.
- [2] Chilingarian A., G. Hovsepyan, and L. Kozliner, Thunderstorm ground enhancements: Gamma ray differential energy spectra, *Physical Review D* 88, 073001 (2013).
- [3] A.Chilingarian, Thunderstorm Ground Enhancements - model and relation to lightning flashes, *Journal of Atmospheric and Solar-Terrestrial Physics* 107 (2014) 68–76.
- [4] A. Chilingarian, Statistical study of the detection of solar protons of highest energies at 20 January 2005, *Advances in Space Research* 43, (702-707), 2009.
- [5] A. V. Germanenko, Yu. V. Balabin, E. V. Vashenyuk, B. B. Gvozdevsky, and L. I. Schur, Features of the flux of gamma-radiation in the lower atmosphere during precipitation *Astrophys. Space Sci. Trans.* 7, 471 (2011).
- [6] A.Takada, H.Kubo, H.Nishimura, Observation of Diffuse Cosmic and Atmospheric Gamma Rays at Balloon Altitudes with an Electron-tracking Compton Camera, *Astrophys.J.* 733, 13(2011).
- [7] R.Ringuette, G.L. Case, M. L. Cherry et al., TETRA Observation of Gamma Rays at Ground Level Associated with Nearby Thunderstorms, *J. Geophysical Res: Space Phys.* 118, 1 (2013).

# Development of a Transportable LIDAR System for the Measuring Electric Field inside the clouds

A. Ghalumyan<sup>1</sup>, R. Hakhumyan<sup>1</sup>, H. Hakhumyan<sup>2</sup>

<sup>1</sup>Yerevan Physics Institute, Yerevan, Armenia.

<sup>2</sup>Institute For Physical Research, NAS RA, Ashtarak, Armenia.

**Annotation.** Intensive studies in fields of high-energy phenomena in the atmosphere revealed electron acceleration and the bremsstrahlung photons generation caused by the electric field emerging in the thunderclouds. Large quasi-electrostatic fields inside the clouds have a tripole structure with main negative layer in the middle of cloud, main positive on the top and smaller positive “pocket” sitting just on the bottom of cloud. The upper dipole is accelerated electrons upward and crossing ~500 km gamma rays from the electron-gamma ray avalanches are routinely detected by the facilities of orbiting gamma ray observatories (Terrestrial gamma flashes, TGFs). Lower dipole accelerates electrons downward and the networks of particle detectors located on the Earth’s surface observed hundreds of particle fluxes (so called, Extensive cloud showers, ECSes). Further studies demand knowledge of electrical field distribution inside clouds. We are suggesting a method of the remote measurement based on transportable LIDAR system using precise polarization technique.

## 1. BACKGROUND

Laser radar, also called LIDAR, is proving to be a powerful detection technique. It can provide information on topography and other characteristics of the structures in the Earth’s atmosphere. Using LIDAR systems it is possible to visualize the structure of atmosphere and to address a wide variety of important scientific questions from air pollution to climate change issues [1-3]. Knowledge of the dynamic changes is important for understanding ongoing patterns embedded in the atmosphere and predicting related effects of those changes.

A special interest is pointed to the study of the electron, gamma ray and neutron fluxes correlated with thunderstorm activities [5] (space based gamma ray observatories, sensors on aircraft and balloons surface particle detectors detect fluxes of gamma rays and electrons, which are correlated with thunderstorms), long-lasting particle multiplication and acceleration mechanisms in the thunderstorm atmosphere as well. These very important and yet poorly understood phenomena are now intensively researched both from space and from mountain altitude research stations. These recently discovered findings attract not only astrophysicist’s, but also meteorologist and atmospheric physicist’s attention.

It was suggested that streamer heads can produce fields up to several tens of millions volts per meter [4]. The electrical fields in the thunderstorm atmosphere gave the cosmic ray shower and/or electrons from the lightning leaders a boost by increasing the number of energetic particles through a multiplication process [6, 7] initially called runaway breakdown (RB), and now referred to as relativistic runaway electron avalanche (RREA).

The RREA mechanism can create large amounts of high-energy electrons and subsequently the gamma rays, as well as X rays and neutrons.

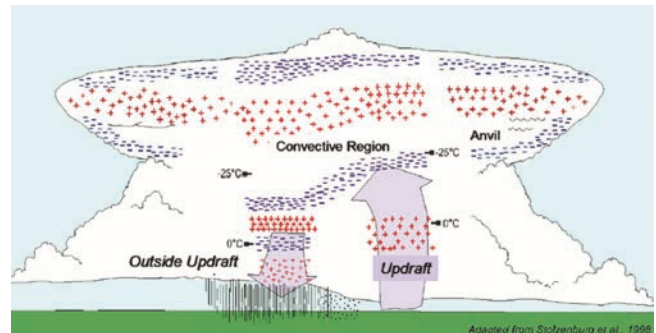


Figure 1. Illustration of particles fluxes inside the cloud.

Moreover, during last years Armenian physicists reported thunderstorm correlated new phenomena manifested by detection of 6 physical effects:

- Large fluxes of the electrons and gamma rays;
- Neutron fluxes;
- Microsecond bursts of the electrons;
- Depletion of the high energy muon flux;
- Large negative near-surface electrical field;
- Depletion of the cloud-ground lightning occurrences and enhancement of the intracloud lightning occurrences.

However, at present time there is no adequate experimental technique developed, which allows one to perform remote measurements of the strength of the electric field inside the clouds.

We are suggesting a measurement technique of the electrical field inside the clouds. This technique is based on measurement of the backscattered laser radiation polarization changes in the clouds.

As it is known there is strong electrical field inside the clouds. In the process of water evaporation from the ground, it transports electrical charges from the ground. Further, charged water vapours, which are forming the clouds, lead to the electrical charge accumulation inside the clouds. Due to the low temperatures on the high altitudes, water vapours cool down and form water droplets and small ice crystals.

The presence of the electrical field inside the clouds induces a strong polarization of these water droplets and ice crystals. Thus, polarization of water droplets and ice crystals induces artificial birefringence inside these droplets and crystals. Birefringence results in depolarization of the backscattered laser radiation from the clouds. It is obvious, that depolarization rate is a function of the birefringent centers density. Density of birefringent centers is directly connected to density of polarized water droplets and ice crystals. The density of such polarized particles in principle directly depends on the charge i.e. electric field inside the cloud.

So, measuring the depolarization rate of the initially linearly polarized scattered from the cloud laser radiation makes it possible to assess the strength of the electrostatic field inside clouds.

## 2. THE LIDAR SYSTEM

The LIDAR System contains three functional units:

– Laser Emitter of the polarized laser radiation, is a solid state, Q-switched oscillator- amplifier YAG:Nd<sup>3+</sup> laser with Second harmonic generator (SHG). It generates linearly polarized 8 ns pulses with 1.064  $\mu\text{m}$  and/or 0.532 nm wavelengths and repetition rate of 20 Hz (Fig.2.a+b).

– Receiving System of backscattered radiation, which contains Receiving telescope (RT), polarization beam splitter, separating orthogonal to each other polarized components of the backscattered radiation (Fig.2.c).

– Signal Detection and Processing System registers the orthogonal to each other polarized components of the backscattered radiation by means of high sensitivity photomultipliers (PM) and/or avalanche photodiodes (APD). It allows reducing the optical background noise by means of dichroic mirrors and narrow band interference filters to separate the signal according to wavelength as well as changing the field of view of the receiving telescope.

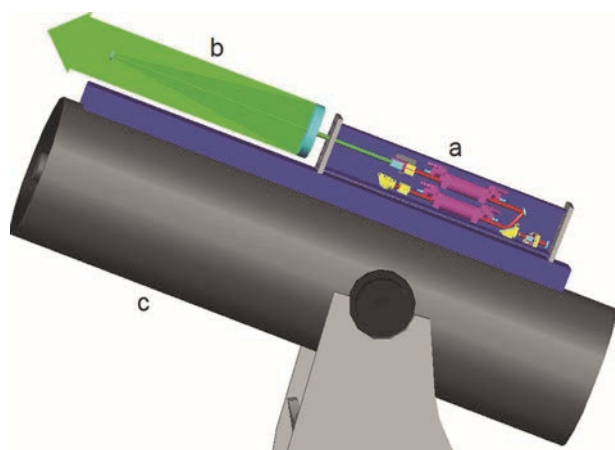


Figure 2. The LIDAR preliminary layout. Laser Emitter with the (a) laser and (b) Beam Expander, Receiving Telescope (c).

The signals from PM by different channels are passed to the signal registration system, which allows amplifying and processing of weak electrical signals. The first step of reducing the noise in the registration system is the separation of power electronics and laser Q-switching high voltage electronics (including ground) from the electronics.

Electronics triggering is organized by means of optical communication with outgoing laser pulse. System timing is performed with the use of a precision signal generator the gate input pulse of which is organized from laser pulse detector. The next step of reducing the noise is the triggering of photo detectors by means of triggering the bias voltage of the PM dynode or APD. The photo detectors detect the optical signals in the time window driven by the generator. The time window determines the spatial resolution of LIDAR system while the delay of the time window from the outgoing laser pulse determine the distance of backscattered signal from the LIDAR. Signal detection will be achieved using signal preamplifiers, amplifiers, signal amplitude discriminators and fast pulse-counting computer electronics.

Table 1. LIDAR system specifications

| <b>Transmitter</b>    |  |
|-----------------------|--|
| Laser                 | Nd:YAG   |
| Wavelengths           | 1.064 $\mu\text{m}$ and/or 532 nm                                  |
| Pulse energy          | 0.8 J (1.064 $\mu\text{m}$ ),<br>0.35 J (532 nm)                   |
| Rep rate              | 20 Hz  |
| Pulse duration (FWHM) | 8 ns   |
| Output beam diameter  | 100 mm   |
| Divergence            | 0.1 mrad   |
| <b>Receiver</b>       |  |
| Telescope             | Newtonian  |
| Diameter              | 250 mm   |
| Field of view         | 2 mrad   |
| Channels              | Parallel polarized, elastic<br>Perpendicular polarized,<br>elastic |
| Detectors             | Photomultipliers and/or<br>Avalanche Photodiodes                   |

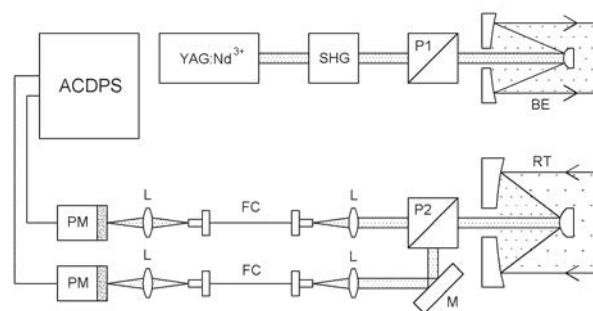


Figure 3. YAG:Nd<sup>3+</sup> – laser; SHG – second harmonic generator; P1, P2 – Glan Prisms; BE – beam expander; RT – receiving telescope; M – mirror; L – lenses; FC – fiber couplers; PM – photomultipliers; ACDPS – automated control, detection and processing system.

The LIDAR system will be able to measure the location of the electric field in the cloud, its extent, and structure as a function of time. By the measured ratio of the parallel and perpendicular polarized components of the elastic backscattered signal it will be possible to estimate the depolarization rate and strength of electric field within the cloud.

### 3. REFERENCES

- [1] A. Ansmann, M. Riebesell, C. Weitkamp, *Optics Letters* 15, p. 746 (1990).
- [2] D.N. Whiteman, S.H. Melfi, and R.A. Ferrare, *Appl. Optics* 31, p. 3068 (1992).
- [3] T.J. Duck, J.A. Whiteway, A.I. Carswell, *J. Geophys. Res.* 105, p. 22909 (2000).
- [4] K. Sassen, *Bull. Am. Meteorol. Soc.* 12, p. 1848 (1991).
- [5] A. Chilingarian, A. Daryan, K. Arakelyan, et al, *Phys. Rev. D* 82, 043009 (2010).
- [6] A.V. Gurevich, K.P. Zybin, *Physics Today* Vol. 58 (5), p. 37 (2005).
- [7] T.F. Bell, V.P. Pasko, U.S. Inan, *Geo. Res. Lett.* Vol. 22, p. 2127 (1995).

# Multi-purpose Pulse Analyzer for Cosmic Ray Research

*K. Arakelyan, A. Avetisyan, V. Danielyan, A. Daryan, D. Pokhsraryana*

*Cosmic Ray Division, Alikhanyan Physics Institute,  
Alikhanyan Brothers 2, Yerevan 375036, Armenia,*

---

Abstract: Multi-purpose pulse analyzer is intended for the pulse area measurements in scintillation detectors used in cosmic ray research. Area of Photomultiplier pulse (charge) is proportional to scintillation light. Therefore, measured charge is proportional to energy deposit of the particle in the scintillator. After proper calibration from histogram of energy releases it is possible to recover energy spectra of incident cosmic ray flux.

Pulse analyzers can be combined in devices with up to 32 channels. Devices measures count rates and pulse area values and can be programmed to provide information on coincidences of different channels. Analyzers are equipped with HV power sources and booster amplifiers thus implementing complete data acquisition solution for the large systems of particle detectors. Many types of such detectors are under operation in Aragats Space Environmental Center (ASEC). Due to remote control and remote tuning by the software, realized design meets rather severe requirements of multiyear stability and sophisticated operation in multi-channel multi-detector environment.

---

## 1. INTRODUCTION

System of the particle detectors operating at Aragats Space Environmental Center (ASEC) [1] is intended for investigation of the several phenomena manifested them by changing secondary cosmic ray (SCR) fluxes as measured on the earth's surface. Advanced features of such research provide several detector assemblies [2]-[7] equipped with flexible frontend and data acquisition electronics. It makes possible measuring different parameters of changing particle fluxes [2]. At the same time, electronic continuously monitors parameters of Data Acquisition System (DAQ) to keep them stable during multiyear operation.

The multi-purpose pulse analyzer is principal facility in ASEC electronics. It measures count rates and area of Photomultiplier (PM) pulses for all detectors and can be programmed to provide information about coincidences. Area of PM pulse is proportional to energy deposit of incident particle. Therefore, amplitude measurements are helpful for obtaining information on particle type and energy.

The simplest version provides 8 input channels i.e. can be used for consistent readout of 8 scintillators. The readout implies recording the pulse area of all detectors. The readout is triggered by pulse of any detector and all pulses coming during the "gate" interval are recorded. The "gate" value is chosen about 1 $\mu$ s, which ensures all particles recorded to belong to one "event". Nevertheless the gate can be reprogrammed to other value depending on the particular problem to be solved. At the same time, analyzer provides "event mask" which shows numbers of detectors hit by particle in this event. In addition, the analyzer can be programmed to record channel coincidences of interest and areas of all pulses in coincided detectors. Electronics have been developed for combining up to 4 Printed Circuit Boards (PCB) of 8-channel analyzer to obtain up to 32-channel device providing functionality described above [8].

Information is collected during one minute i.e. counters give numbers of pulses registered in each detector, numbers

of each type of coincidences, and the Analog-to-Digital Converters (ADC) give areas of all registered pulses. Thus, the output of analyzer is a set of 1-minute time series and histograms implemented in ADC codes.

Electronics combined with assembled detectors, including multilayered detectors interleaved by the lead filters, enables wide options for particle flux analysis. It becomes possible:

- to identify charged and neutral particles hitting detector [5];
- to measure histograms of energy releases [3];
- to estimate angles of incidence of particles hitting detector;
- to implement sophisticated "software" triggers selecting different physical conditions;
- to perform different event selection by implementing coincidence techniques [7].

Information on the number of particles hitting array of plastic scintillators is used also for the energy estimation of the incident particle showers initiated by a high-energy particle of Galactic Cosmic Rays (GCR). Mentioned tasks assigned to DAQ electronics are realized using integrated systems of Complex Programmable Logic Devices (CPLDs), microcontrollers and Field Programmable Gate Arrays (FPGA). Incorporation of the "intellectual" elements allows fulfilling rather complicated tasks mentioned above, also performing remote control and tuning of most crucial parameters of the detector. Analyzers equipped with autonomy HV power supplies and booster amplifiers represent full electronics set for assembled multichannel detectors.

## 2. LOGARITHMIC AMPLITUDE-TO-DIGITAL CONVERTER

The basic device in the pulse analyzer is the analog-to-digital converter (ADC). It transforms the area of PM output pulse into digital code. The ADC used in pulse

analyzer is a Logarithmic ADC (LADC) i.e. the output code  $N$  is linear function of logarithm of input charge  $q_N$ :

$$N = \text{int } D[\ln q_N - \ln q_{th}] \quad (1)$$

Here (threshold) is the minimum charge giving the code "1" to LADC output. The  $D$  factor (Decrement) defines the quantization step. Since the scale is logarithmic, the quantization step  $s$  denotes the ratio of amplitudes with adjacent codes  $s = U_k / U_{k-1}$ . Quantization step for developed LADC is chosen equal to 1.1052 i.e. next code accords to ~10% augment of amplitude. This quantization step accords to  $D=10$ .

The principle of developed logarithmic ADC operation is based on the measurement of decay time of oscillation in the parallel RC tank. The oscillations are caused by PM current pulses in the parallel RLC tank with a well-known Q-factor [9].

We are aware of several realizations of this principle [10]-[14]. In all these cases the PM of the scintillation detector, which can be considered as an almost perfect current source, was used as the generator of current pulses. The same principle and design has been used in development of gamma spectrometer [14].

LADCs are integrated into the pulse analyzer device placed in the control room. The PM pulse is sent from the particle detector to the control room through the impedance matched 50 Ohm coaxial transmission line for further processing. The buffer preamplifier with a +1 voltage gain amplifies the voltage pulse from the PM. The amplifier with the output resistance of 50 Ohm sends to LADC the pulse signal, completely repeating the shape of PM anode current pulse, see Fig 1.

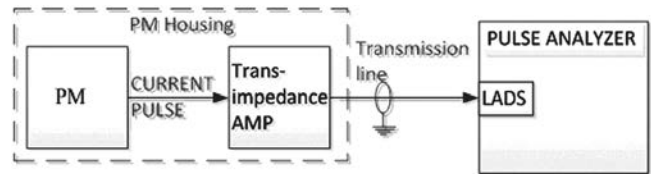


Figure 1. The scheme of signal transfer from PM to LADC.

The schematic diagram of LADC front-end is presented in Fig. 2. LADC input circuit (Fig.2) converts voltage pulse into current pulse.

The PM assembly is presented in Fig.3. In addition to signal electronics, it contains High Voltage (HV) power supply. RS-485 half-duplex port is used for remote programming and monitoring the HV value. Programming allows control HV in two hardware selectable ranges  $\pm 900V$  to  $2100V$  and  $\pm 1500$  to  $3000V$  in 2V steps. The schematic diagram of electronics located in the PM housing is presented in Fig. 4.

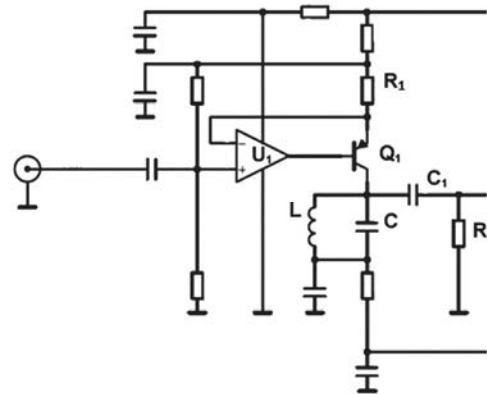


Figure 2. LADC input circuit transforming voltage impulse to current impulse

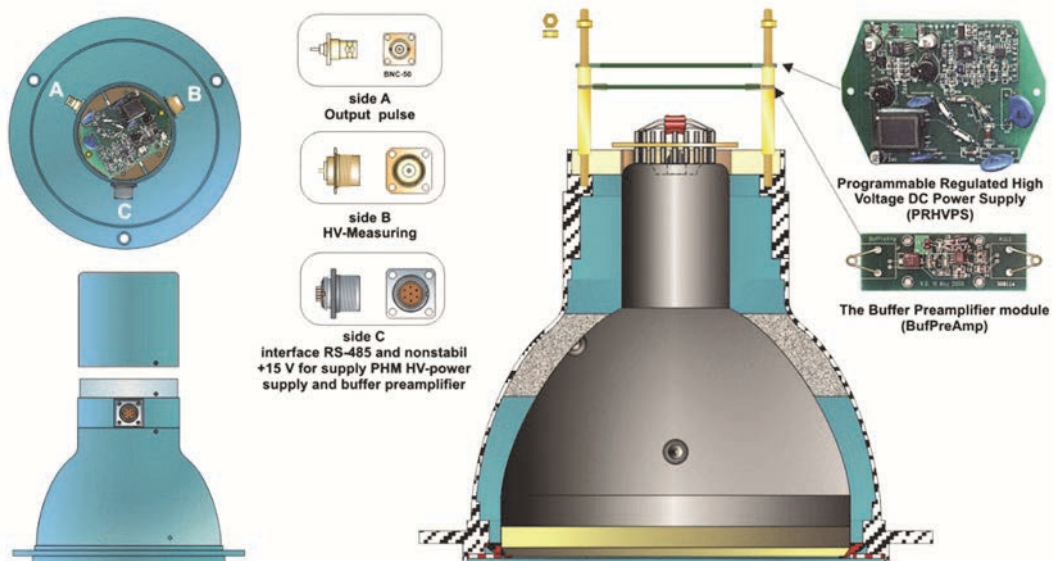


Figure 3. PM installation guide with housing, connectors and electronics

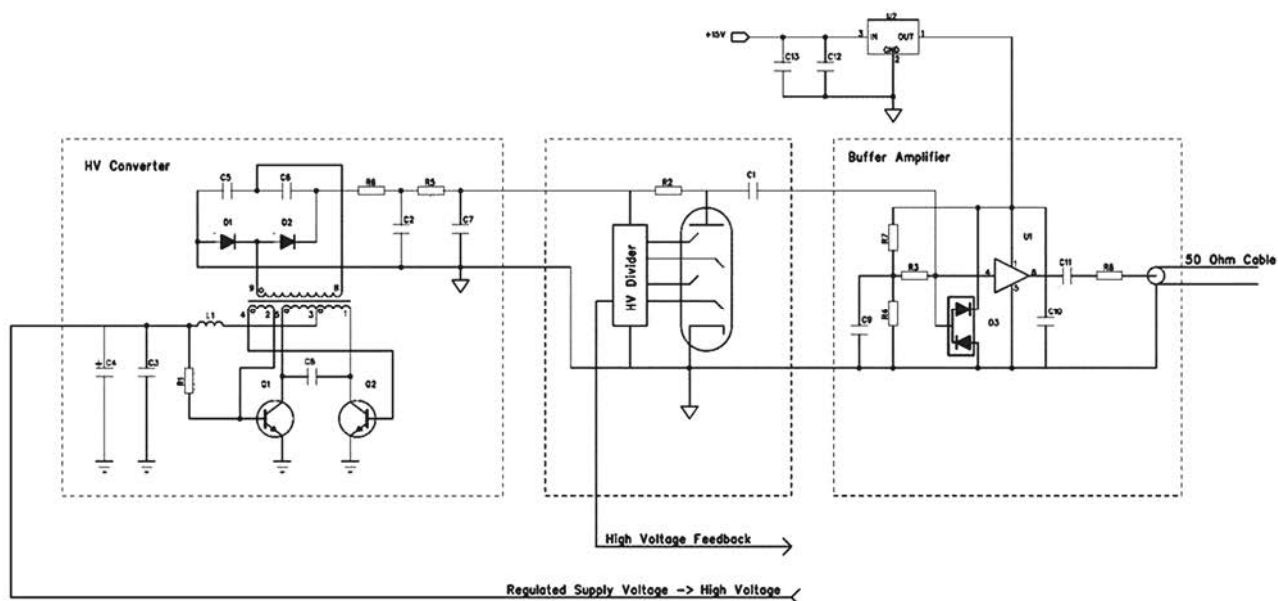


Figure 4. The electronics of PM case.

The voltage-to-current converter is assembled on the elements U1, Q1, R1. Its conversion gain is

$$Gain_{vi} = \frac{1}{R_1} = 2 \frac{mA}{V}$$

This value is selected so that the peak voltage on the oscillating LRC tank would be equal to the area of the input pulse. To guarantee the proportionality of the peak voltage on the oscillating LRC tank number of output pulses to the logarithm of input signal, the period of tank oscillation has to exceed the duration of input PM pulses no less than ~10 times [10].

The current pulse from the collector of Q1 transistor (see Fig.2) causes damping oscillations in the LCR tank (Figure 5).

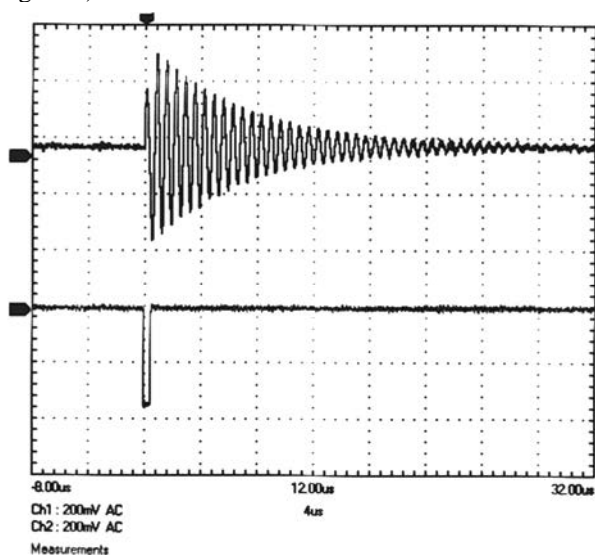


Figure 5. The input pulse, which causes the damping oscillations.

After the excitation of oscillations, their amplitude falls according to the law:

$$V = V_0 e^{-\frac{\omega t}{2Q}}, \quad (2)$$

where  $V_0$  is the the first half-wave voltage,  $\omega$  - the resonance frequency,  $Q$  - the quality factor of the tank.

If pulse duration does not exceed one tenth of the tank resonance period, the magnitude of first half-wave of oscillation on the RLC tank is proportional to the area of the current pulse shape [11]

$$V_0 = \frac{1}{C} \int I_{pulse} dt$$

Expression (2) allows for obtaining the time in which the oscillations reach the threshold value:

$$t = \frac{Q}{\pi} \ln \frac{V_0}{V_{TH}}$$

The number of periods in this time represents the output code and equals to

$$N = \text{int} \left[ \frac{Q}{\pi} \ln \frac{V_0}{V_{th}} \right], \quad (3)$$

where  $V_{th}$  is the threshold voltage of comparator and the  $Q/\pi$  value is the D-factor defined in expression (1).

Damping oscillations are amplified by the two-stage amplifier-limiter. The amplifier-limiter (Fig. 6) consists of two identical non-inverting stages on OA U2 and U3. The gain of each stage at 1 - 2 MHz operating frequency is equal to:

Here RFB is the feedback resistor, i.e.R1 in the first stage and R2 in the second one (Fig.6). The total gain of two-stage amplifier equals to

$$Gain_{STAGE} = 1 + \frac{R_{FB}}{R_0} = 6.1$$

The output signal from the amplifier enters the non-inverting input of comparator U4 (Figure 6). The threshold of the comparator is determined by the voltage entering

from the output of the Digital-to-Analog Converter (DAC). The threshold value digit is set by microcontroller which gets this code from DAQ PC controlled via Ethernet.

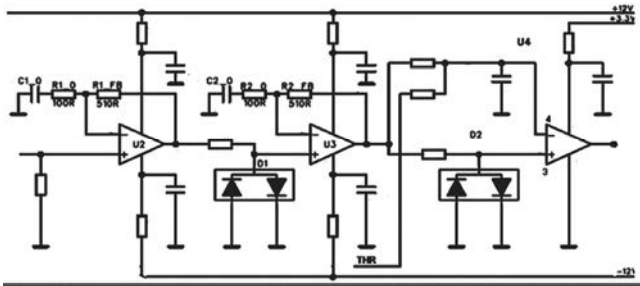


Figure 6. Amplifier-limiter and comparator circuit

At large signal, operational amplifiers go saturated, limiting the magnitude of damping oscillations. A larger level of limitation is provided by the diode limiters D1, D2. When the amplitude of oscillation decreases to the value close to the threshold, the amplifier returns to the linear work, because the threshold of the comparator is significantly lower than the limitation level. In view of a certain asymmetry of levels of limitation, the DC connection is used between the stages of the amplifier and the comparator to avoid the displacement of operating point after large input signals. At the same time, to decrease the influence of the possible temperature drift of input current of the U2 and the bias voltages of U2 and U3, the DC gain of the amplifier is limited to the value of 1 by means of capacitors C1\_0 and C2\_0. Since even in this case the zero drift at the U3 output can reach 20 mV, the threshold of U4 comparator is set with respect to the DC output voltage of the amplifier U3.

Since the rise time of PM pulse is about 70ns, then  $\sim 1.5$  MHz is sufficient choice for tank resonance frequency. So, the output signal is a sequence of standard pulses with  $\sim 1.5$  MHz frequency and the number of the pulses is proportional to the logarithm of the charge of the measured current pulse.

The equation (3) shows that for providing the conversion in accordance with D-factor, it is necessary to continuously monitor Q-factor for providing its stability. A highly reliable industrial inductor with high Q-factor is used as L. The desired resulting Q-factor is hard set by shunting LC tank with a stable and precise resistor R.

The maximum allowed amplitude at input of Operational Amplifier (OA) – U2 equals to 7V. The greater voltage values cause an anomalous damping of tank oscillations due to the sharp increase of the U2 input current.

### 3. ASSEMBLY OF MULTI-PURPOSE PULSE ANALYZER

The basic assembly of LADC-s providing flexible multifunctional abilities is the 8-channel LADC module. It is low-cost module designed for usage in multichannel detectors operating in ASEC.

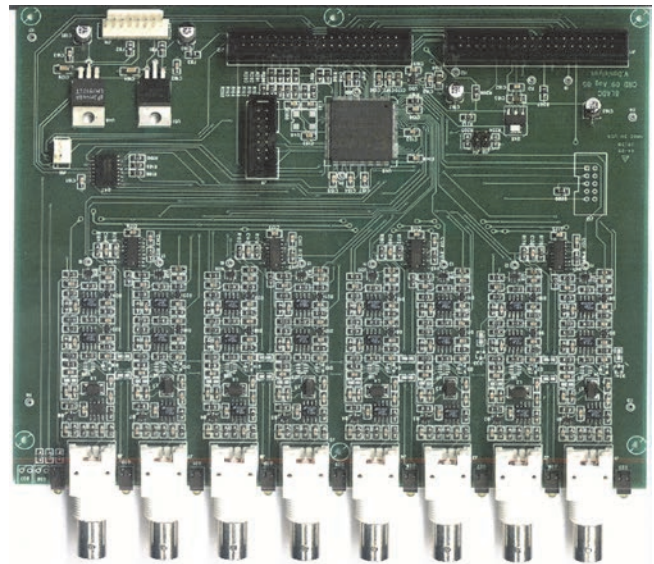


Figure 7. Printed-circuit board of 8LADC

All 8 LADC are located on one printed-circuit board (Fig.7). To simplify the installation and decrease the cost, external screens do not separate the channels from each other; the problem of the channel interaction is solved as follows. First, the inductors of the oscillatory tanks of adjacent channels are installed in a mutually perpendicular fashion, which sharply decreases the magnetic coupling. Secondly, by alternating the capacitances of contour capacitors, the resonance frequencies of adjacent channels are relatively shifted according to each other approximately by 10%.

In case of maximum amplitude values of input pulses, low oscillations can be observed in the adjacent channels. However, because of the sufficiently high values of the Q-factor, the oscillations increase gradually and up to the moment of the end of time gates (see below) they do not reach the lowest threshold level. The comparator threshold is set by the output signal of programmable DAC. One eight-channel DAC IC is used for threshold setting of all eight channels of the 8LADC board.

The output pulses of the comparator are taken to the IC of Complex Programmable Logic Device (CPLD) of the XILINX Cool Runner-II type that is used for identifying the event, counting the pulses of LADC outputs and sending the counters data to the microcontroller module.

All signals from the detectors received during the gate are considered as belonging to the same event. The gate value is set by CPLD and is indicated as a logical GATE signal. The identification of the event and the corresponding trigger of the gate are initiated by the pulse, received in any of the 8 channels. The information about detectors, which pulses were received during the gate interval, is read out and stored in the CPLD as a bite mask, named EVENT, in which one bit corresponds to the one input channel. The 1 sign of the bit means that the pulse from the detector entered this channel during the gate period. The gate duration is fixed with the binary code (Ngate) hard soldered on the input pins GWIDTH0-GWIDTH3 of CPLD and is equal to

$$T_{Gate} = \frac{N_{Gate} + 1}{12} \mu S$$

In our case  $N_{GATE}$ , is selected equal to 7, which corresponds to the gate duration of 0.666  $\mu s$ . This value ensures time sufficiently large to register all pulses caused by one physical event taking into account the spread of detector parameters, the lengths of coupling cables and so on. On the other hand, it reduces the probability of registering two different events as one to the negligibly low value.

With the beginning of the time gate, the inputs of all eight counters in CPLD opens and counters start counting the pulses of the packets entering from the LADC outputs. The signal DURATION, reporting to the microcontroller that the process of event registering goes on is generated when the event starts. This signal is removed approximately in 1 microsecond after the longest pulse packet ends. When the signal ends the inputs of all counters are closed and the microcontroller begins reading out the information accumulated in CPLD: EVENT byte and one byte for each of eight channels.

After registering channel information, the microcontroller issues the RESET pulse on CPLD, indicating the end of event. Receiving this pulse, CPLD resets all counters and EVENT byte into the initial (zero) state. Thus, the system is ready to register the next event.

The total dead time of system consists of the count time of the pulse packet plus the information processing time of the microcontroller

$$T_{DEAD} = T_{PACKET} + T_{PROCESSING} ,$$

$$\text{where } T_{PROCESSING} = 20 \mu S \pm 10\% .$$

Maximum dead time accounts to about 75 $\mu s$  for the longest case of the maximal input pulse amplitude. Direct testing by means of pulse generator showed that analyzer allows for maximal frequency of 15 kHz per channel.

The 8LADC module is designed in such a way that up to four 8LADC boards can be assembled into one 16 or 32-channel module. 16-channel version of analyzer is presented in picture



Figure 8. The 16-channel analyzer

The C32USB microcontroller module has been developed to interconnect 8LADS modules into 32-channel DAQ system. Figure 9 demonstrates such connection carried out with flat cables with 5 connectors on each. To simplify the construction, all connectors are fixed to the cable directly, without any over-twisting for the selection of the device number (practice standard for PC). Instead, each of four boards is identified by the address set collected on the board with jumpers.

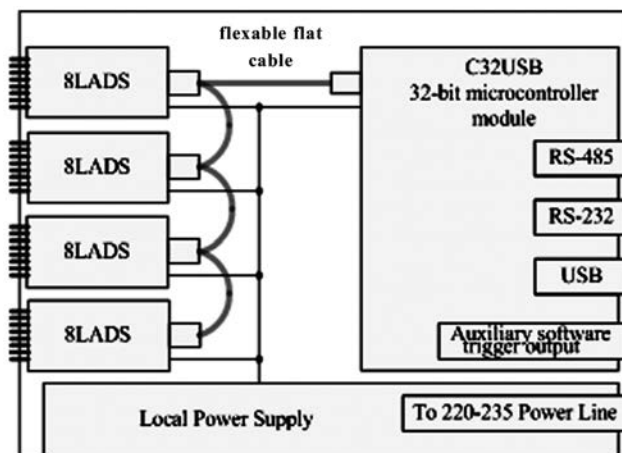


Figure 9. Four 8LADCs and microcontroller modules assembling in one 32LADC unit

When cascading it is important to satisfy the following condition: the impulse arrival on the entrance of any of the LADC boards is considered as an event, whereas completion of longest of the pulse packets of all boards is viewed as the end of an event. Therefore, the CPLD outputs for the signals GATE and DURATION are programmed as outputs with the open collector and the logical inputs connected to it. This allows combining these signals as a wired OR.

The information readout from CPLD of the 8LADC boards into the microcontroller module C32USB is provided by the parallel code on the 8-bit bus. Eight 8-bit pulse counts of LADC and one 8-bit EVENT register are addresses inside CPLD. To address them, it is necessary to have the 4-bit address, presented by the microcontroller at the lines SEL0-SEL3. The addresses from 0 to 7 are used to select each of 8 counters, while any address in range 8-15 selects one and the same register - the register of event mask (EVENT).

The C32USB module is based on the NXP company LPC2138 microcontroller of the ARM. It is designed as a multifunctional embedded data processing device for the initial on-line processing of data of arbitrary nature. The flexibility of the module application is provided by the possibility to work with any interface included in the system. The following interfaces are realized:

- RS-232 for the connection to PC COM port. The rate of exchange is up to 115200 Baud. This port can be used for the microcontroller IC firmware reprogramming.
- USB 1- for connection to PC with virtual COM port driver. The exchange is provided through the UART micro-controller interface. The rate of exchange is up to 115200 Baud. This port can be used also for the microcontroller IC firmware reprogramming.
- USB 2- for the high-speed exchange of information between PC and the microcontroller. Uses the parallel exchange of information between the USB interface IC and the microcontroller. The program access from the PC is provided with the driver of virtual COM port with the speed of exchange up to 115200 Baud and with DLL driver, which, in theory, can ensure the rate of exchange approaching the maximum speed, full USB2 - 10 MBaud.

- RS-485 is used for connecting the microcontroller to the local detector control system DCS network.

As the electronic devices, assembled on the basis of C32USB module can be used for the detector setups placed in distant places with difficult maintenance, it is very important to have WEB interface not only for the installation of the detector parameters (thresholds, the voltage of PM supply), but also for the reprogramming of microcontroller itself. This possibility is necessary for the software modernization at changing conditions of physical experiments, i.e. for changing of so called “software triggers”, selecting data for different physical problems. Software triggers are altered by replacement of the consequences of coincidence and anti-coincidence, replacement of the conditions of the program-generated triggers and so on. Two of the realized interfaces make it possible to remote reprogramming the microcontroller by WEB interface.

The microcontroller software consists of system and problem-oriented parts. The system part includes initialization of I/O ports, watchdog and interval timers, interruption handlers and main input-output, local network managing, and other similar functions.

The problem-oriented part of micro-controller software, called Aragats Data Acquisition System (ADAS) [15] includes pre-processing, storage and sending to the host PC data, collected from the detectors. In particular, the amplitude spectrum for each of the detectors is accumulated, coincidences and anti-coincidence are processed, the particle arrival directions statistics is accumulated, the program triggers are generated and so on. The software is written in the C language, using the free distributed GNUARM software. Some fragments of the code are written on the assembler to achieve the peak output.

#### 4. CALIBRATION MEASUREMENTS

The operational characteristics of LADS are crucial for correct operation of the pulse analyzer. Values of the following parameters are of utmost importance:

- Quantization step (or decrement)
- Dynamic range

Precise knowledge of these parameters is necessary for correct code conversion of the PM output into charge and then to energy release. The oscillogram of PM pulse is depicted in Fig.10. Total width of the pulse is ~100 ns.

The calibration measurements were carried out by means of Tektronix TDS2024 oscilloscope and TGP110 pulse generator; the pulse range was 20 - 200 ns with amplitudes from 37 mV to 9.5 V.

Measurements proved that code value depends on  $\tau \times A$  product, where  $A$  is the pulse amplitude and  $\tau$  is its duration. This measurement proves that output code depends on the area of input pulse. This conclusion is correct for pulses of arbitrary shape if the duration do not exceed ~100 ns.

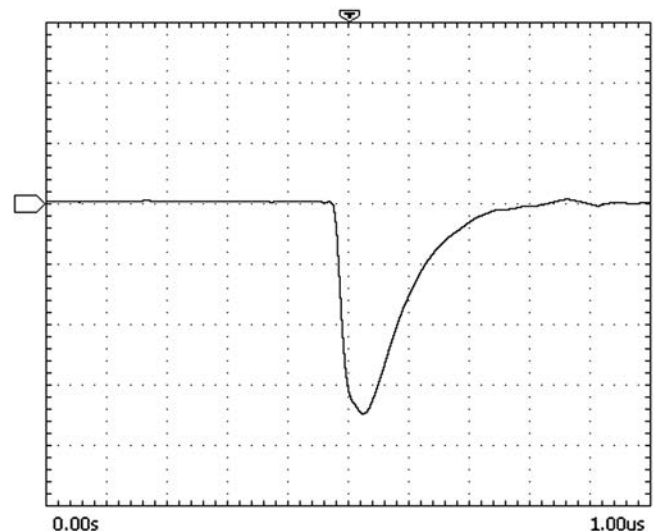


Figure 10. Example of PM pulse oscillogram.

The second measurement was carried out to determine the maximum allowed input pulse amplitude. This value depends on U1 OA saturation (see Fig.2). The measured value of saturation level is equal to 6.6 V. The third measurement was carried out to determine the dynamic range of LADS. The dynamic range depends on comparator threshold, since maximum value is restricted to 6.6V. Microcontroller sets this threshold value, which it gets from DAQ PC controlled via Ethernet. The threshold value of 130 corresponds to 56 mV threshold; in this case, the dynamic range equals to 120. The threshold value 70 corresponds to 7.5mV threshold; in that case, the dynamic range equals to 900.

The fourth measurement concerns the possible electromagnetic interference (EMI) between the channels of pulse analyzer. These tests were carried out by feeding the pulse with magnitude 6V to the inputs of adjacent channels. No changes of code in the neighboring channels were observed.

Quantization step was estimated by determining the D-factor (decrement) defined by expression (1). Rectangular pulses with constant width of 100ns were applied in all measurements. The change of pulse area was performed by changing the pulse magnitude  $U$ . Therefore we rewrite the (1) in the form:

$$N(U) = \text{int } D[\ln U_N - \ln U_{th}] \quad (4)$$

The aim of these measurements is to check the logarithmic functional form of code  $N(U)$  and to determine D-factor. In Fig.11 an example of LADC conversion characteristic is depicted in arbitrary units. The step curve  $N(U)$  is the conversion characteristic and the dashed curve  $A(U)$  is its envelope.

The most precise method for decrement determination is fitting the experimental curve by logarithmic law. The parameters of the fit give the values of decrement. Measured conversion characteristics are given in Fig.12, 13.

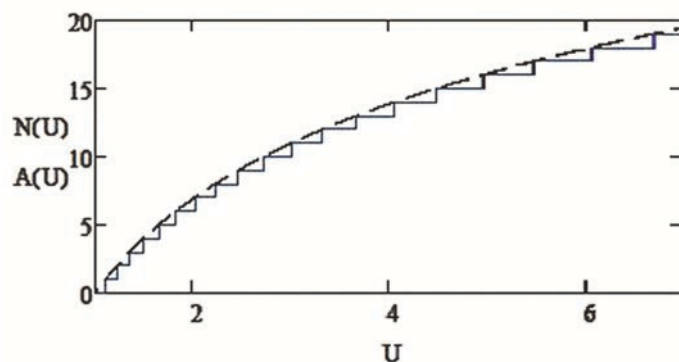


Figure 11. LADC conversion characteristic

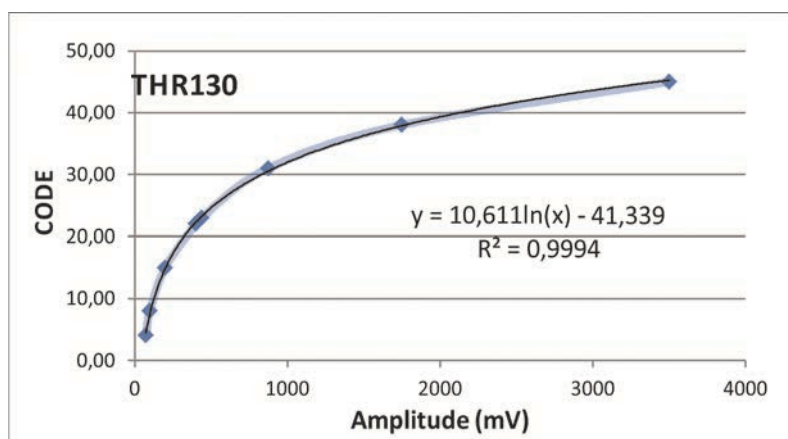


Figure 12. Measured conversion characteristic with threshold 56mV and its logarithmic fit

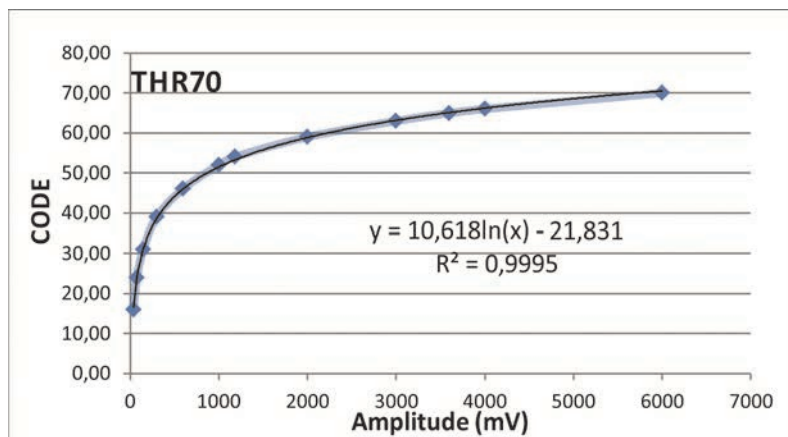


Figure 13. Measured conversion characteristic with threshold 7.5mV and its logarithmic fit

The values of decrement obtained from equation of fit chart are 10.611 for threshold 56mV and 10,618 for threshold 7.5mV. Small Chi-square ( $R^2$ ) values prove good agreement of obtained curves with logarithmic law. The thresholds obtained from equation of fit chart are 49.2mV for threshold code 130 and 7.8mV for threshold code 70. The measured value of decrement corresponds to quantization step of 10%. Decrement varies for different channels in the range  $\pm 2.5\%$  and thresholds  $\pm 5\%$ , see Tab. 1 where values of decrements and thresholds for all 8 channels are given.

Table 1. The decrements and thresholds of 8-channel analyzer.

| Channel          | Decrement | Threshold (mV) |
|------------------|-----------|----------------|
| 1                | 10.52     | 50.81          |
| 2                | 10.76     | 53.39          |
| 3                | 10.77     | 53.39          |
| 4                | 10.92     | 51.30          |
| 5                | 10.97     | 52.62          |
| 6                | 10.82     | 48.68          |
| 7                | 10.25     | 46.72          |
| 8                | 10.41     | 54.31          |
| average          | 10.68     | 51.37          |
| st. dev.         | 0.25      | 2.61           |
| st. dev/ average | 2.4%      | 5.07%          |

The exact value of decrement of LADC in each channel is used for code conversion. Other method of decrement estimation is given in [16].

## 5. CONCLUSION

Described DAQ electronics was implemented for majority of particle detectors operated in particle detector networks located on slopes of Mt. Aragats and in Yerevan headquarters of Cosmic Ray Division. Particle detectors ASNT, STAND-3cm, NaI(Tl), CUBE, NAMMM, CUBE-3cm. demonstrate stable operation during 24 hours 12 month monitoring of the changing secondary cosmic ray flux. Many papers were published based on the new physical results enabled by flexible and powerful DAQ system. System is still under extensive operation since 2008.

## 6. REFERENCES

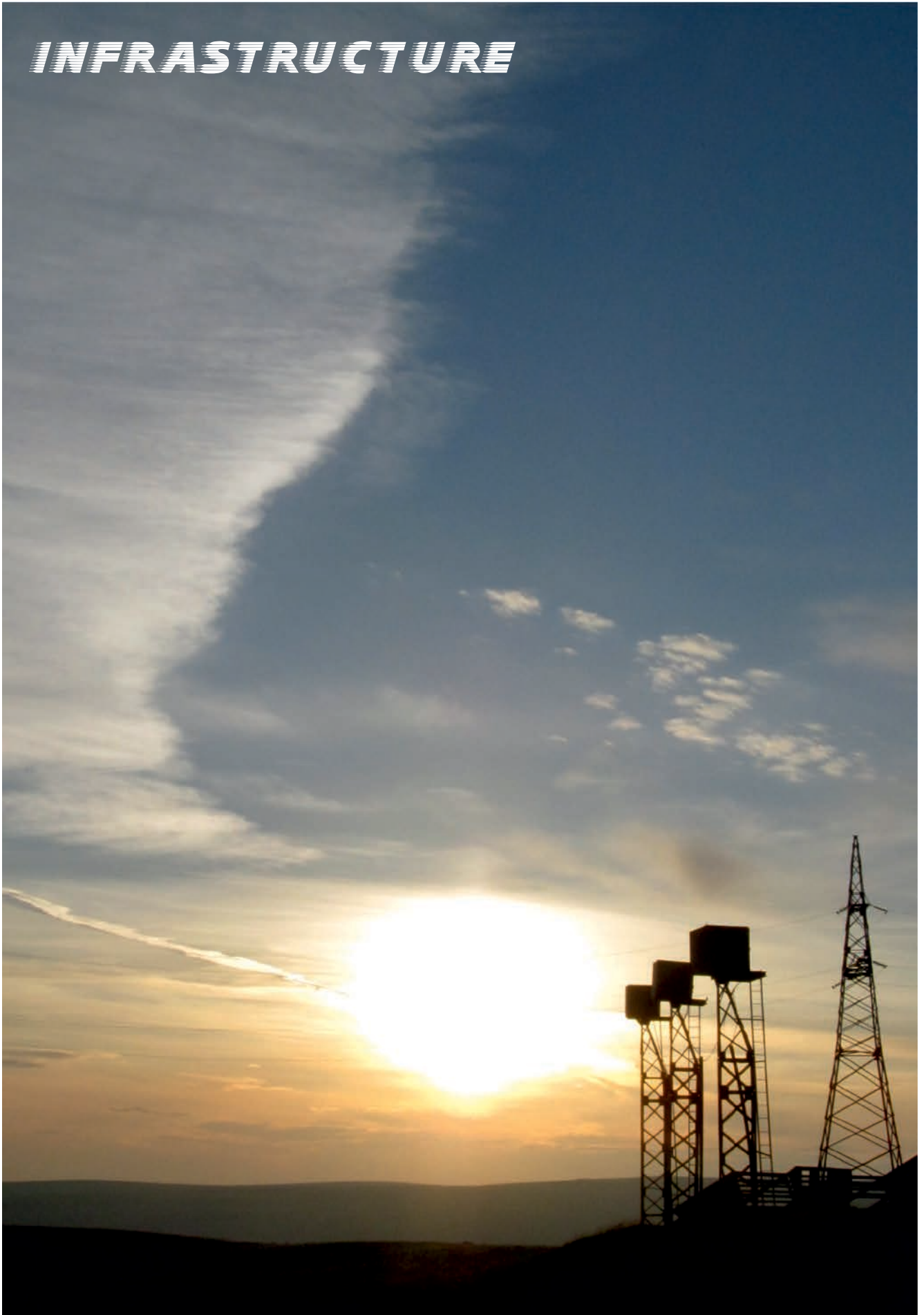
- [1] Chilingarian A.A., Avagyan K., Babayan V. et al. Aragats Space-Environmental Center: status and SEP forecasting possibilities. *J.Phys. G:Nucl.Part.Phys.* 29, pp. 939-952, 2003.
- [2] Chilingarian A.A., Arakelyan K., Avagyan K., et al. Correlated measurements of secondary cosmic ray fluxes by the Aragats Space Environmental Centre monitors. *NIM, A543*, pp. 483-496, 2005.
- [3] Chilingarian A., Melkumyan L., Hovsepyan G., Reymers A. The response function of the Aragats Solar Neutron Telescope, *NIM. A 574*, pp 255-263, 2007.
- [4] Chilingarian A.A. and Reymers A. Investigations of the response of hybrid particle detectors for the Space Environmental Viewing and Analysis Network (SEVAN), *Ann. Geophys.*, 26, pp. 249-257, 2008.
- [5] A. Chilingarian, G. Hovsepyan, K. Arakelyan, et al; Space Environmental Viewing and Analysis Network (SEVAN), *Earth, Moon and Planets: Volume 104, Issue 1 (2009)*, page 195
- [6] D. Roša, Ch. Angelov, K. Arakelyan, et al. SEVAN CRO Particle Detector for Solar Physics and Space Weather Research; *Cent. Eur.Astrophys.Bull.* 34 (2010) 1, 115–122
- [7] A. Chilingarian, A. Daryan, K. Arakelyan, A. Hovhannisyanyan, B. Mailyan, L. Melkumyan, G. Hovsepyan; Ground-based observations of thunderstorm-correlated fluxes of high-energy electrons, gamma rays, and neutrons; DOI: 10.1103/PhysRevD.82.043009
- [8] Arakelyan K., Chilingarian A., et al.: New electronics for the Aragats Space-Environmental Center (ASEC) particle detectors, *Proceedings of International Symposium FORGES, Nor-Amberd, Ar-menia*, pp. 105-116, 2008.
- [9] Gadalog A.N., Kaganov I.I., Silaev A.A. , Pribori I *Technika Eksperimenta N1*, pp.39, 1973.
- [10] [A. N. Gadalog, Yu.V. Mineev, I.D. Rapoport, Pribori I *Technika Eksperimenta N5 (1966)* 144 (in Russian).
- [11] [Daryan A.V, Dolganov S.A., Khachatryan A.R., Preprint *YerPhI 1485(2)*, 1997.
- [12] Silaev A.A., Silant'ev O.A., *Facilities and Techniques of Experiment N1*, pp.100, 1981.
- [13] Stepanov V.I., V.I. Stepanov, *Pribori I Technika Eksperimenta N3 (1969)* pp.115(in Russian) *Facilities and Techniques of Experiment N3*, pp.115, 1969.
- [14] L.T. Tsankov, A.G. Mitev, CH.B. Lenev. *NIM, A533*, pp. 509-515, 2004.
- [15] S. Chilingaryan, A. Chilingarian, V. Danielyan, W. Eppler. *Journal Of Physics: Conference Series 119 (2008)* 082001
- [16] L. Melkumyan, A. Daryan. *Proc. Of International Symposium "Thunderstorms and Elementary Particles Acceleration"*, TEPA - 2010



# PHOTOGALLERY



# ***INFRASTRUCTURE***





Cosmic Ray research at the high altitude station on Mt. Aragats started in 1943 by the Artem and Abraham Alikhanyans. The Aragats station is 3200m above the sea level and the Nor-Amberd station is 2000 m above sea level. The Aragats cosmic ray research stations include all the necessary conditions for stable year-round operation: electric network, computer network, facilities for detectors, conference rooms, heated dormitories and restaurants for the staff spending one-month shifts to maintain the stations. The upper station is located above the tree line on the shore of lake Kar. Both stations lie on solid rock of volcanic origin.



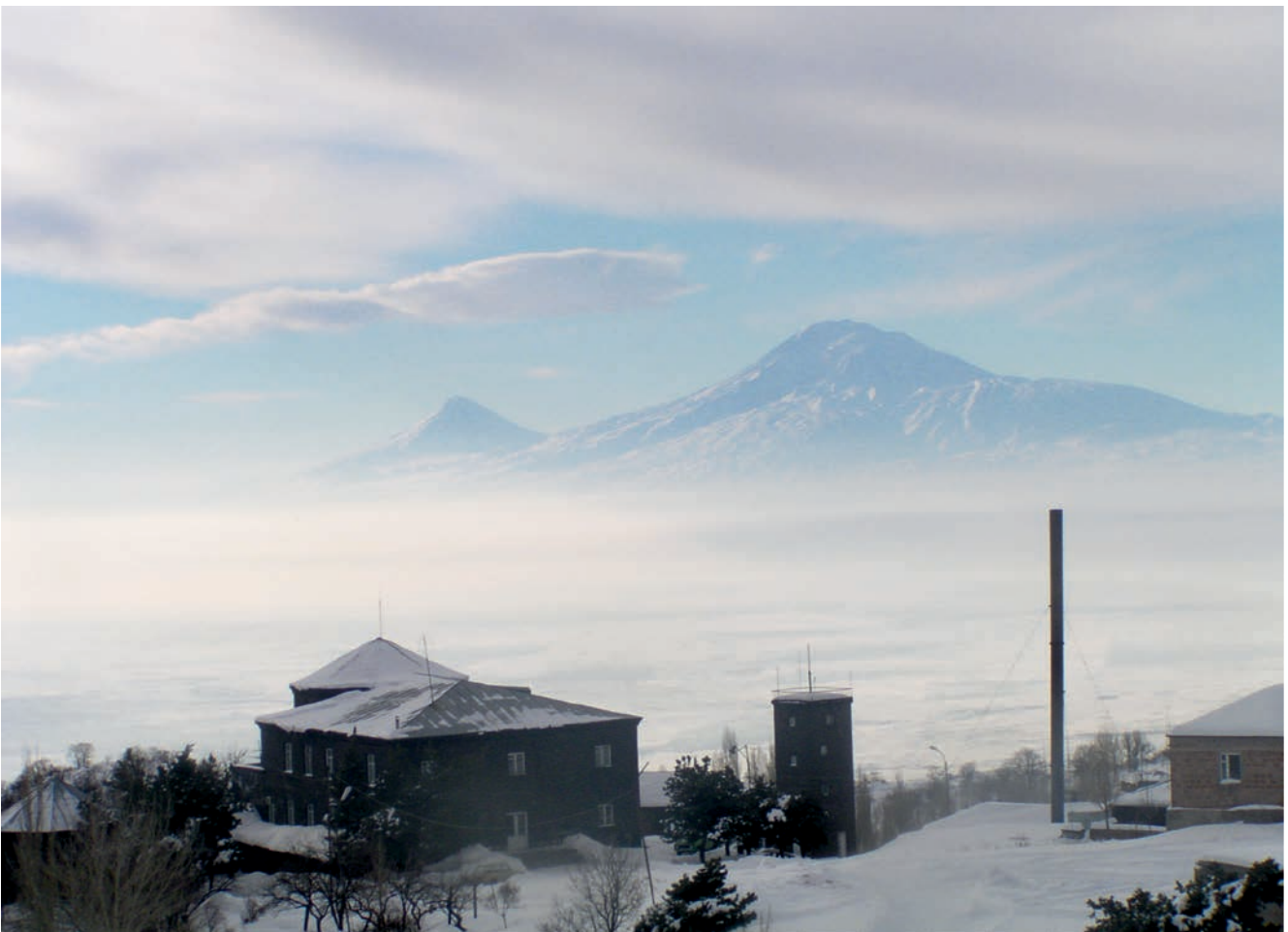




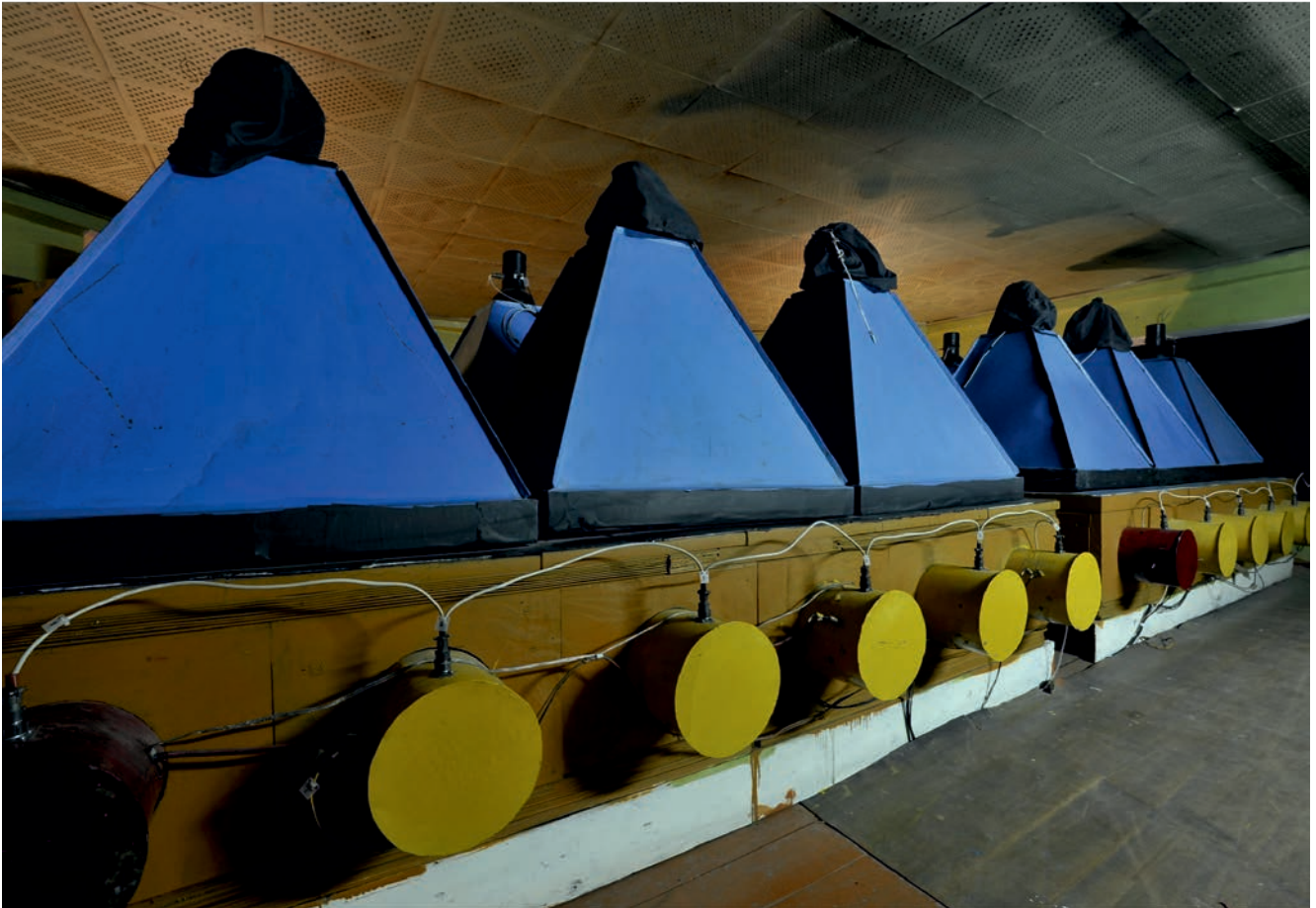


Nor-Amberd station ensures flawless operation of the installations used for cosmic ray variations study. The station is also used as an intervening point on the way to Aragats station in winter. The station is a comfortable site for organizing conferences and workshops.





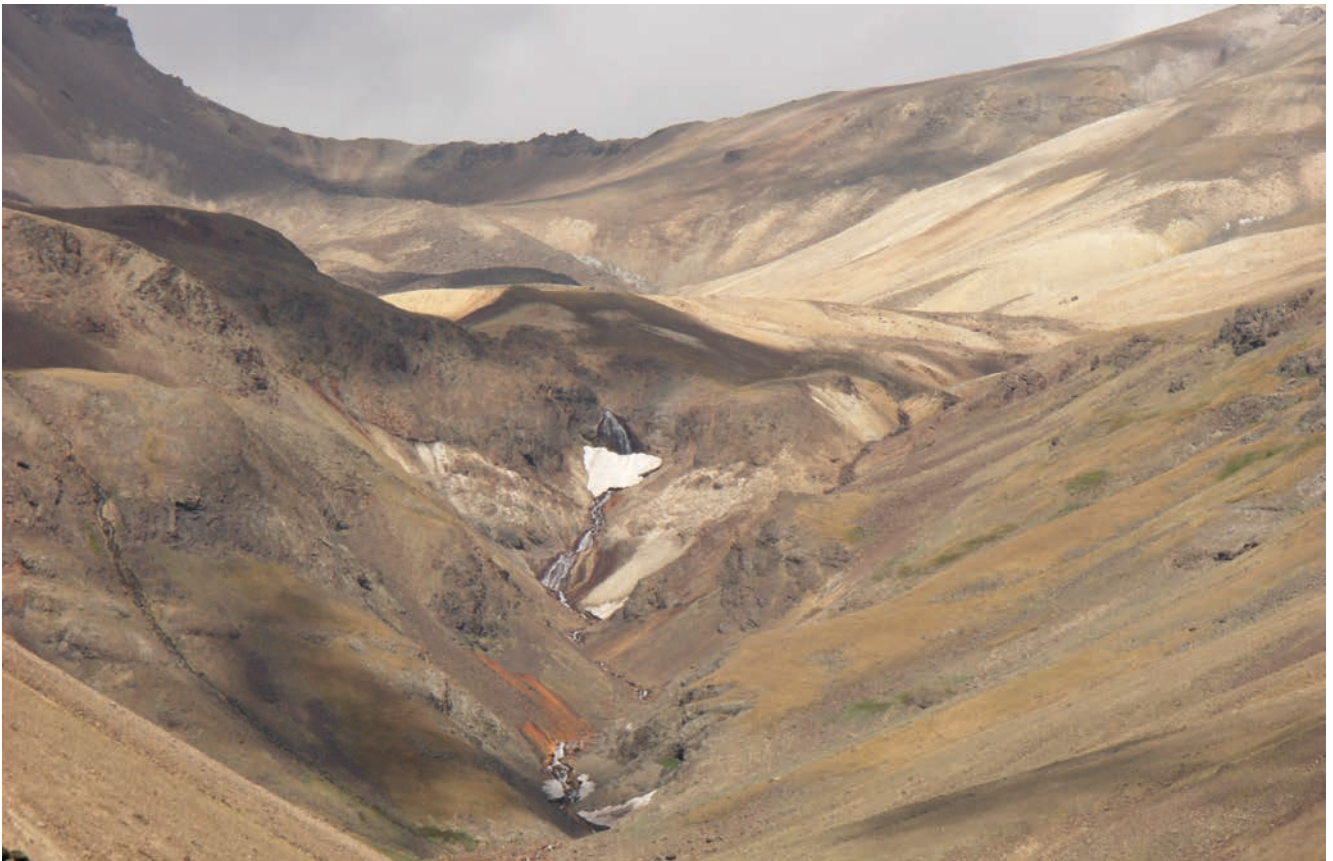






There are several detector systems on Mt. Aragats: the Aragats Solar Neutron Telescope, the Aragats Neutron Monitor, the Nor-Amberd Neutron Monitor, the Nor-Amberd Multidirectional Muon Telescope, and the Aragats Multidirectional Muon monitor, SEVAN detectors and other particle detectors. Recently the precise sensors measuring electrical and magnetic fields were added to particle detecting systems in Nor Amberd and Aragats. The Cosmic Ray Division in Armenia is a member of the neutron monitor and solar neutron telescope networks and Eurasian neutron monitor database (NMDB). The SEVAN particle detector network measuring secondary cosmic rays at middle-high latitudes has its nodes in Armenia, India, Croatia Bulgaria and Slovakia.



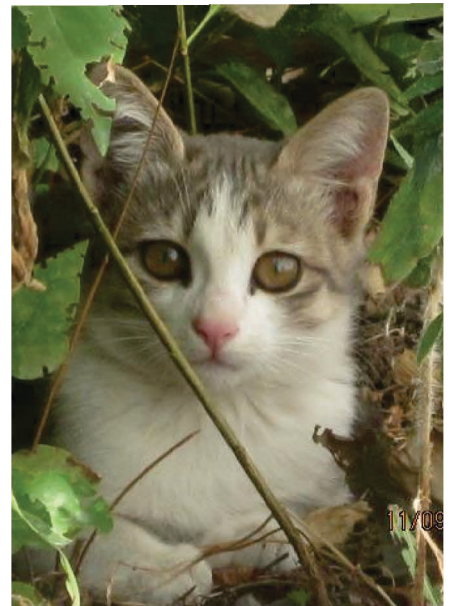
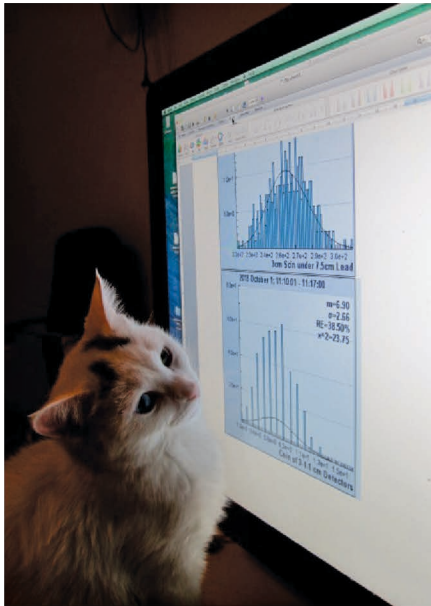






The massif of Mount Aragats is rich in alpine meadows around which fragrant flowers are all scattered. Among them are violets, wild lilies, poppies and bell-flowers. According to historians, Aragats used to be covered with exuberant forests where wild animals lived. At the height of 1800-2300 meters there is still a small forest. The main tree growing there is the Eastern oak. Hundreds of cool springs originate from the slopes of the mountain, which form the rivers of Kasakh, Gegharot, Amberd, Mantash, Geghadzor, Tsaghkahovit and so on. The springs coming out of the mountain's slopes nourish the Lake of Metsamor located in Ararat valley.



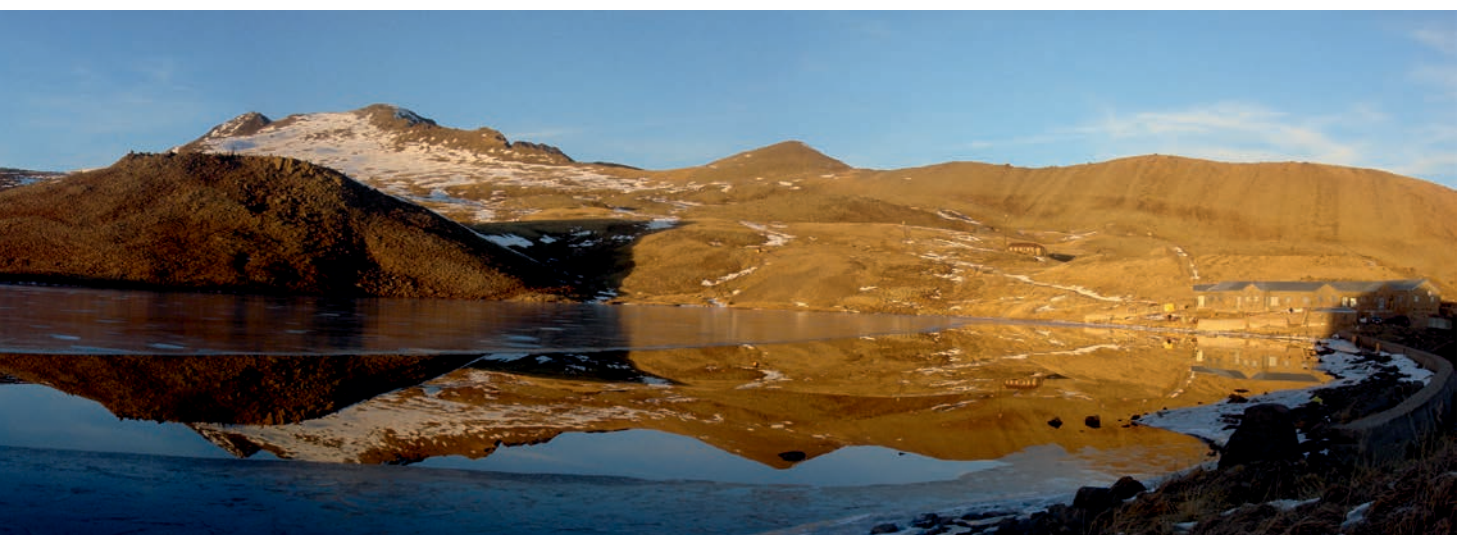


# ARAGATS





Formed by a volcano eruption in the distant past Mount Aragats is the highest peak in Armenia. It has four peaks the highest of which is the Northern with 4090 meters of height. Then come the Western peak (4080 meters), the Eastern (3916 meters) and the Southern (3879 meters). Traces of ancient culture as well as an ancient irrigation system were discovered on the slopes of the mountain. Also, fish-like monuments known as “dragons” and symbolizing cult of water were found. The slopes of the mountain are also known for some of the remarkable structures of medieval Armenian architecture that have been retained throughout the centuries, among them are the Fortress of Amberd, Tegher Monastery. Lake Kar (Stone Lake in English and Kari Lich in Armenian) is a small lake on the slopes of Mount Aragats. It is located 3,200 meters above sea level and is mostly formed by ice and snow.





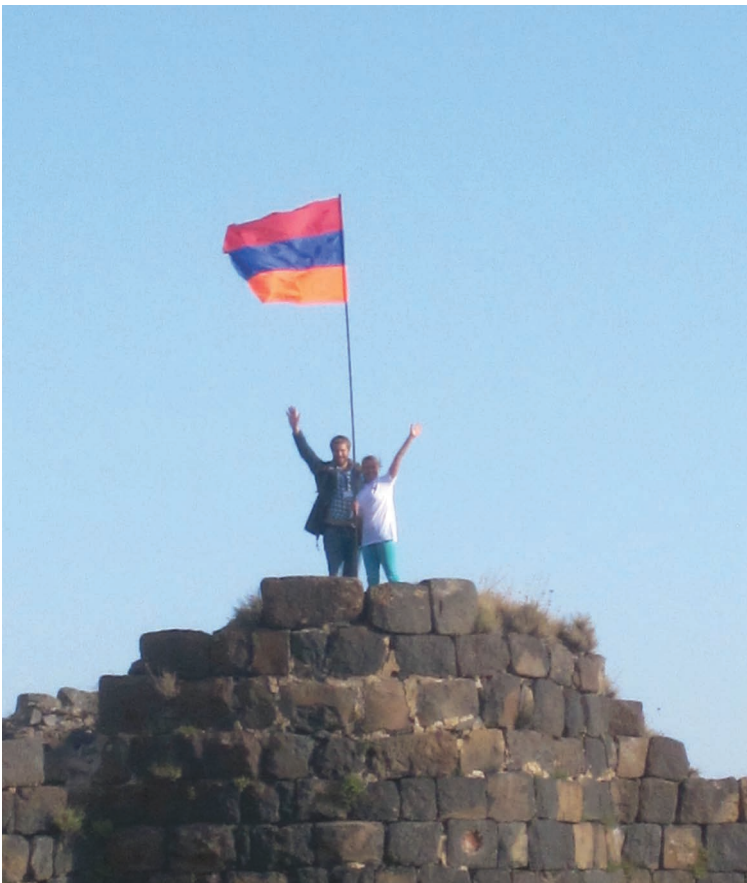


# ***CONFERENCES, VISITORS***



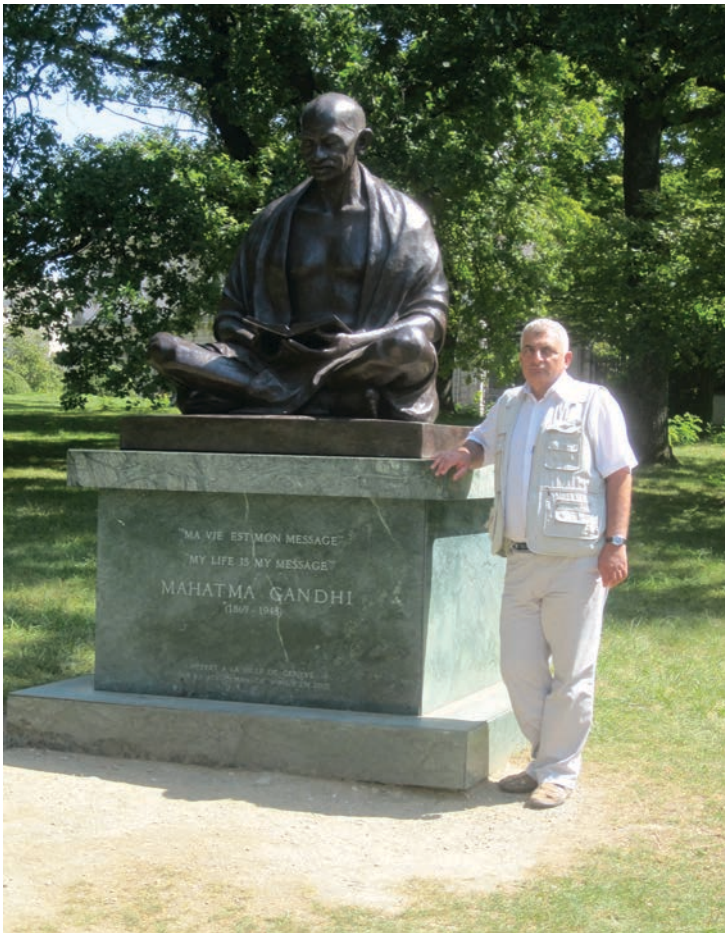
The Cosmic Ray Division and Skobeltsyn Institute of Nuclear Physics (SINP) of Moscow State University organized “The Thunderstorms and Elementary Particle Acceleration (TEPA-2013)” conference which was held from September 9 through 13, 2013 in the Nor Amberd international conference centre. 30 scientists and students from USA, Germany, Norway, Russia and Armenia attended the conference. Besides the scientific program an excursion was organized for the conference participants. Numerous scientists have paid visits to YerPhi and delivered lectures for young researchers of national lab, among them are professor emeritus of Physics at the University of Vienna Walter Kutschera and professor Thomas Ruth.































<http://crd.yerphi.am/Conferences/tepa2013/home>